Impacts of Dynamic U-values of Cross-laminated Timber (CLT) and Conventional Building Envelopes on Building Operational Energy Use

Jiaqi Yu

Thesis for the degree of Doctor of Philosophy (PhD)

University of Sheffield

School of Architecture and Landscape

2025

Abstract

Cross-laminated timber (CLT) buildings have recently received increasing attention owing to their lower carbon emissions. However, the question of whether CLT buildings demand less energy to operate compared with conventional buildings remains unanswered.

Building energy simulation is widely applied when studying building operational energy use. As a required input, the thermal transmittance (U-value) of building envelopes can significantly influence simulation results. Theoretical U-values have been employed in most related studies. However, the U-values of envelopes fluctuate owing to temperature and relative humidity (T/RH). This means that the dynamic U-values of building envelopes need to be considered in simulations.

In this study, the energy impacts of dynamic U-values were studied. The operational energy consumption of CLT and three conventional buildings was compared by considering dynamic U-values. First, in-situ U-value measurements of the CLT and three conventional envelopes were conducted. Second, different U-value calculation methods were applied to calculate dynamic and average U-values of the four tested envelopes. After validation, the optimal U-value calculation methods were proposed. Third, based on the calculated dynamic U-values, the U-value prediction models for the four tested envelopes were developed by linear and non-linear regression methods. The linear model was proven to be the optimal U-value prediction model. Finally, the theoretical U-values, predicted average U-values, and predicted dynamic U-values were used in operational energy simulations of CLT and three conventional buildings.

The results showed that the dynamic U-values had significant energy impacts in climate zone D. The dynamic U-values had more significant energy impacts in the CLT and masonry buildings than in the reinforced concrete (RC) and brick buildings. The CLT

building with insulation consumed the least operational energy in climate zone D, and conventional buildings consumed the least operational energy in climate zones A, B, and C.

Content

List of Figures

List of Tables

Acknowledgements

I have spent the past four years conducting my PhD research at the University of Sheffield. Throughout this journey, I have received tremendous support and guidance from many people, for which I am deeply grateful.

Firstly, I would like to express my deepest gratitude to my parents (Prof. Yuyan Wang and Mr. Lei Yu). Their love has been my constant source of strength throughout this journey. I would also like to express my heartfelt gratitude to my aunt (Ms. Yumiao Wang) and my uncle (Mr. Zhizeng Zhang) for their kind support and assistance during my experimental work.

Secondly, I am profoundly grateful to my supervisors, Prof. Wen-Shao Chang and Dr. Tsung-Hsien Wang, for their invaluable guidance, constructive feedback, and continuous support. Their expertise and dedication have been instrumental in the completion of my PhD research.

Thirdly, I would also like to extend my sincere thanks to Dr. Yu Dong and Prof. Jianhe Brad Wang for providing me with the necessary laboratory facilities and resources to conduct my in-situ measurements.

Finally, I am indebted to Dr. Ruichao Zhang for his support in providing the software tools (TRNSYS and TRNSYS 3D).

Chapter 1 Introduction

1.1 Background

According to the Global Status Report for Buildings and Construction, the building sector contributed 34% of global energy use (UNEP and GlobalABC 2024). Many researchers have paid attention to the building energy assessment and refinement of building energy management (Rayegan et al. 2024; Yang et al. 2025; Su et al. 2024; Sun et al. 2024; Khan et al. 2024). According to the life cycle assessment method, building life cycle energy includes two parts: (1) embodied energy, which refers to the energy use related to the building itself during the three stages of the life cycle (including the materialisation, operation and end-of-life stages); (2) operational energy, which refers to the energy used to run buildings during the operation stage of the life cycle (Sambataro et al. 2023; Duan et al. 2022). Detailed information on building life cycle energy is shown in Figure 1.1.

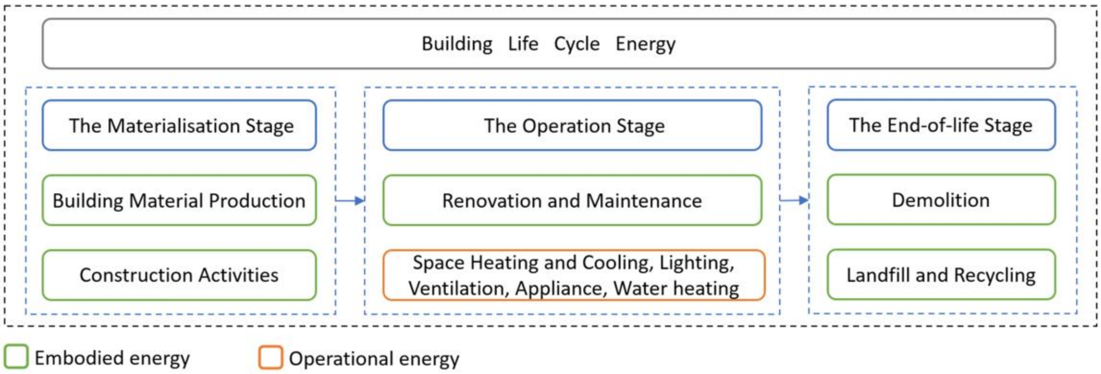

Figure 1.1 Detailed information on building life cycle energy

According to existing studies, building operational energy use accounts for 80%–90% of building life cycle energy (Ramesh, Prakash, and Shukla 2010). Therefore, studying building operational energy is valuable for improving building energy efficiency. Building energy simulation is an important method to study the building's operational energy use. Building energy simulation is also known as the physics-based or white-box model (Chen, Guo, et al. 2022). The building operational energy consumption of different types of buildings in many regions has been investigated through building energy simulation (Bruno and Bevilacqua 2022; Boyano, Hernandez, and Wolf 2013; Dong et al. 2019).

1.1.1 Operational Energy Simulation of Buildings with Different Envelopes

In recent decades, the operational energy of both conventional buildings and timber buildings has been studied in detail (Liu et al. 2016; Guo, Liu, Meng, et al. 2017; Shin et al. 2023; Duan et al. 2022; Chiniforush et al. 2018). In the conventional building sector, brick and reinforced concrete (RC) envelopes are the major building envelope types (Sartori and Hestnes 2007). Owing to the extensive use of these inorganic building envelopes, the conventional building sector has severe impacts on the environment, especially in energy consumption and carbon emissions (Zhou et al. 2023). To reduce the building sector's environmental impacts, timber that are more environmentally friendly than conventional inorganic materials has been widely used.

As a kind of timber material, cross-laminated timber (CLT) has been paid more attention owing to its low environmental impacts. Most CLT panels are made of odd-numbered layers (most are 3 or 5 layers) of timber panels glued together at a 90-degree angle. Each layer is glued to the adjacent layers on the broad side of each board, as shown in Figure 1.2 (Shan et al. 2022; Buck et al. 2016). The market size of CLT is increasing rapidly around the world. The global market size of CLT was $1,024.4 million in 2023 and is estimated to rise from $1,174.1 million in 2024 to $3,537.9 million in 2032 (Fortune Business Insights 2024).

Figure 1.2 CLT panels (Liu et al. 2016)

With the spread of CLT buildings, researchers have focused on comparing the operational energy use of CLT and conventional buildings by building energy simulations. However, a consensus has not been reached with regard to whether CLT buildings use less operational energy than conventional buildings (Duan et al. 2022; Yin and Bruno 2019; Dong et al. 2019; Guo, Liu, Chang, et al. 2017).

Some findings have shown that CLT buildings consume less operational energy. Guo et al. simulated the operational energy use in two seven-storey residential buildings, where the main construction materials were CLT and RC, respectively. The results showed that the CLT building consumed less operational energy than the RC building in temperate and continental climate zones (Guo, Liu, Chang, et al. 2017). Dong et al. simulated the operational energy use of both CLT and RC office buildings and also found that the CLT building consumed less operational energy than the RC building in temperate climate zones (Dong et al. 2019).

Conversely, a few findings have suggested that the operational energy use in CLT buildings is greater than that in conventional buildings. Yin and Bruno simulated the operational energy use of CLT and RC residential buildings in three cities in continental climate zones and found that the operational energy use in the CLT building was greater than that in the RC building (Yin and Bruno 2019). Duan et al. simulated the operational energy use of three residential buildings, including CLT, RC and hybrid CLT buildings. The results showed that both CLT and hybrid CLT buildings consumed more operational energy than the RC buildings in Tianjin, which is in the continental climate zone (Duan et al. 2022).

1.1.2 Uncertainties of Building Energy Simulation

To conduct accurate building energy simulations, many parameters need to be entered into the energy simulation software. This may cause uncertainties in building energy simulation because accurately entering all parameters is challenging (Yu, Chang, and Dong 2022). The parameters leading to uncertainties can be divided into three categories: weather, occupant and building parameters.

Weather parameters are necessary for building energy simulations. Numerous researchers have discussed the effects of different weather parameters on the operational energy simulation (Radhi 2009; Yan et al. 2022; Amoabeng et al. 2023; Li et al. 2022; Shi, Gao, et al. 2022; Bamdad et al. 2022; Li et al. 2018). For example, Roussac et al. proved that the air temperature could influence the cooling energy demand in the summer in Australia. The results showed that cooling energy increased by 6% when the average temperature increased by 1℃ (Roussac, Steinfeld, and de Dear 2011). This indicates that if the input of weather parameters differs from the actual weather conditions, the uncertainties in the simulation results could be caused by the weather parameters.

Many studies have focused on the uncertainties caused by occupant parameters in the simulation results of operational energy use (Zhao et al. 2021; Day et al. 2020; Uddin et al. 2022; Eguaras-Martínez, Vidaurre-Arbizu, and Martín-Gómez 2014; Silva, Ghisi, and Lamberts 2016; Fu and Miller 2022). According to existing studies, occupant parameters can lead to about 30% of the uncertainties in simulation results of operational energy use (Eguaras-Martínez, Vidaurre-Arbizu, and Martín-Gómez 2014).

In building energy simulations, considering the thermal comfort assessments and behaviours of all occupants is difficult, because thermal comfort assessments and human behaviours are stochastic. Thus, the simulation results showed uncertainties caused by human factors (Yu, Chang, and Dong 2022).

Building parameters can influence operational energy simulation. The uncertainties caused by building factors arise from two types of parameter inputs: HVAC system parameters and building envelope parameters. The HVAC system refers to heating, ventilation and air conditioning in a building (Sendra-Arranz and Gutiérrez 2020). Many researchers have focused on the uncertainties caused by HVAC systems in the operational energy simulation (Yoon et al. 2024; Gobinath et al. 2024; Ren, Kim, and Kim 2023). Some factors can contribute to the gap between the actual and simulated operational energy consumption of an HVAC system, such as ageing or substandard-quality equipment (Yoon et al. 2024).

The main building envelope parameters include U-value, density, specific heat capacity, thickness and thermal conductivity. Among these parameters, the U-value indicates the thermal insulation performance of the whole building envelope, and it is one of the most important parameters in building energy simulation (Kotsiris et al. 2012). The U-value can be affected by air temperature and relative humidity (T/RH). In actual situations, T/RH are constantly changing, which leads to fluctuations in the U-value. The existence of dynamic U-values has been realised in several studies (Kotsiris et al. 2012; Gagliano et al. 2014; Kontoleon and Giarma 2016; Yu, Chang, and Dong 2022; Byun et al. 2023). However, no study measured dynamic U-values.

Existing studies have confirmed the energy influence of dynamic U-values (Ficco et al. 2015; Yu, Chang, and Dong 2022; Kotsiris et al. 2012). However, only one study quantified the energy implications of dynamic U-values of conventional building envelopes (Bruno and Bevilacqua 2022). Bruno and Bevilacqua simulated operational energy in conventional buildings in the Mediterranean climate zone, considering both theoretical and simulated dynamic U-values. The heating energy use when the dynamic U-values were considered was 5.1%–9.2% more than those based on the theoretical U-values; this indicated that the effect of dynamic U-values on building operational energy consumption was not negligible. However, dynamic U-values have not been considered in most building operation energy simulations. Research gaps remain with regard to the impacts of dynamic U-values of different envelopes in different climatic zones on building operation energy simulations. To obtain U-values that reflect real-world conditions, the dynamic U-values of four envelope types were measured in this study. The measured data were subsequently incorporated into building operational energy simulations to examine the energy impacts of dynamic U-values.

1.2 Research Questions

The main research questions in existing studies are two:

1. How do the dynamic U-values affect the operational energy simulations of buildings made of different materials in different climate zones?

2. Do CLT buildings offer greater operational energy efficiency than conventional buildings when dynamic U-values are considered?

Four specific objectives answer the research questions:

1. Datasets used for calculating dynamic U-values of CLT and conventional building envelopes need to be obtained. To ensure the reliability of data, in-situ U-value measurements need to be conducted.

2. Dynamic U-values need to be calculated by suitable calculation methods, to prove that inputting dynamic U-values in building energy simulations can improve the accuracy of simulations compared to inputting the theoretical and average U-

values.

3. To obtain dynamic U-values in different climate zones, a U-value prediction model needs to be developed. The prediction model can be built based on measured datasets.

4. The operational energy use of CLT and conventional buildings needs to be simulated when the predicted dynamic U-values, predicted average U-values and theoretical U-values are considered. The impacts of dynamic U-values on building energy simulation can be studied in detail, and the operational energy use of CLT and conventional buildings can be compared in different climate zones.

1.3 Contributions to Knowledge

This study makes five contributions to knowledge:

1. The dynamic U-values of CLT and conventional building envelopes were obtained by the in-situ U-value measurements. The thermal properties of CLT and conventional building envelopes were recorded more accurately.

2. A calculation method of dynamic U-values was proposed. Inputting dynamic U-values calculated by this method into simulation software can ensure that the simulation's accuracy is improved without reducing its efficiency.

3. The prediction model of dynamic U-values was built by measured datasets. Dynamic U-values in various climate zones can be predicted by this model and environmental data. This model can improve the availability and universality of dynamic U-values.

4. The quantitative influence of the dynamic U-values on operational energy

simulation was obtained for different climate zones. It provided references for the suitable areas to apply the dynamic U-values.

5. The operational energy uses of CLT and conventional buildings were compared by considering the predicted dynamic U-values. Different conclusions were obtained in different climate zones. These findings inform the promotion of CLT buildings from an energy-consumption perspective.

1.4 Scope of the Research

The research subjects are CLT and conventional building envelopes. The conventional building envelopes included three types: RC, brick and masonry cavity envelopes. RC and bricks are the most common building materials in the conventional building sector, and RC and brick envelopes have been built widely in many countries globally (Biswas et al. 2024). Masonry cavity envelopes are made of concrete blocks and bricks and have been applied widely around the world, especially in Europe and the UK (Arslan et al. 2021).

The different climate zones are defined according to the Köppen climate classification, which divides the world into five main climate zones based on year-round weather characteristics: tropical zones (A), arid zones (B), temperate zones (C), continental zones (D) and polar zones (E). Among these zones, zones A–D contain most countries, and they are the scope of this study.

Building operational energy simulation was the main research method. Compared with existing studies related to building energy simulation, this study is innovative in that it considers the effects of dynamic U-values. As an important building thermal parameter, the U-value directly influences heating and cooling energy consumption during the building operation stage. To focus on the effects produced by dynamic U-values, the operational energy use in this study referred to heating and cooling energy consumption.

To reduce human interference, the operational energy use generated by human factors, such as ventilation, lighting and use of electrical appliances, is beyond the scope of this study.

1.5 Structure of the Thesis

The structure of this thesis is shown in Figure 1.3.

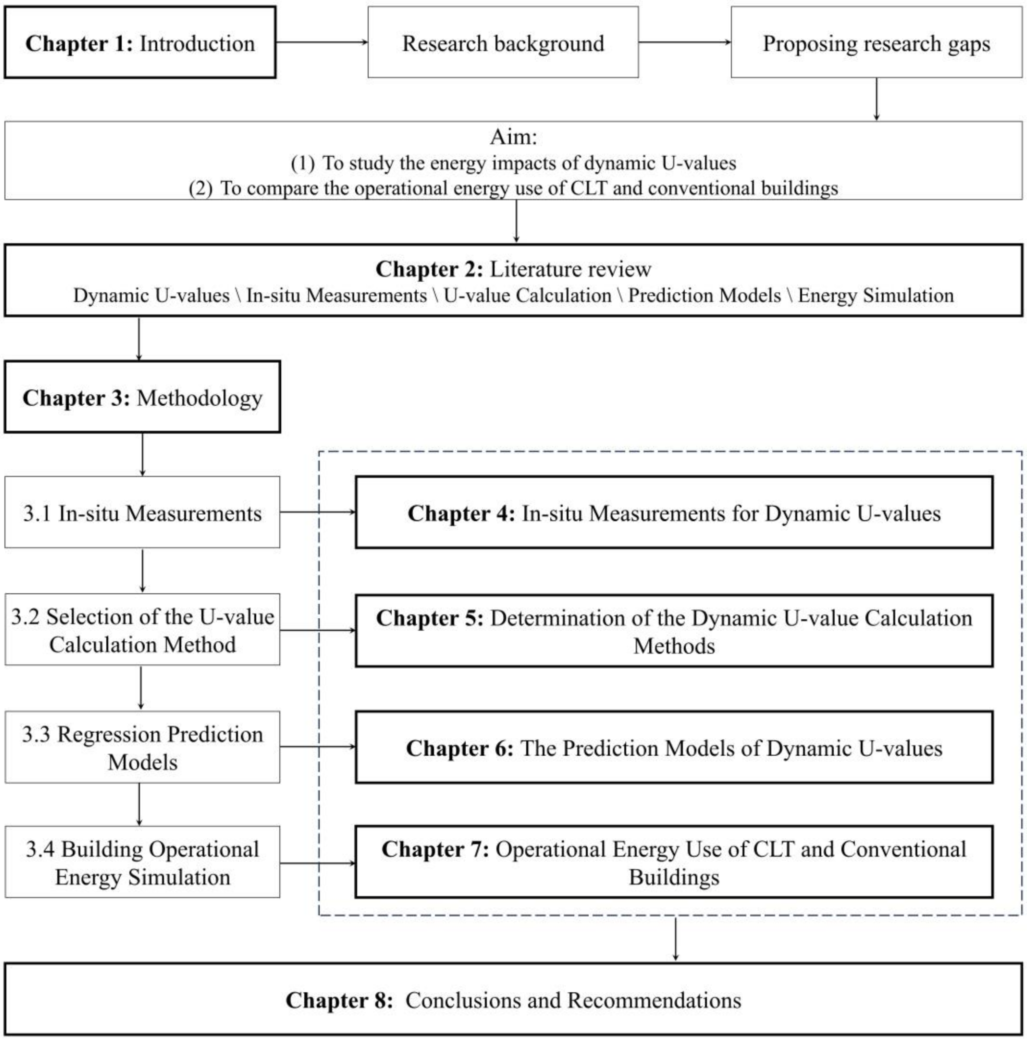

Figure 1.3 Logic of thesis

This thesis includes eight chapters. The background, research gaps and the aim of the research are described in Chapter 1.

Chapter 2 provides a comprehensive review of the existing literature on the U-values of building envelopes, including the causes and results of U-value fluctuations and the measurement and calculation of U-values. Then, studies related to regression prediction models and energy consumption simulation are reviewed and summarised.

Chapter 3 describes the methodology of this study. This includes four sections, including in-situ measurements, dynamic U-value calculation methods, U-value prediction models and operational energy simulations of CLT and conventional buildings in different climate zones.

Chapter 4 shows the in-situ measurements of the four tested envelopes. It provides detailed information on the four tested envelopes, including geographic information, climate zones, detailed construction and theoretical U-values. The measured data include indoor and outdoor T/RH of the four tested rooms, heat flux through the four tested envelopes and indoor T/RH of the neighbouring rooms.

In Chapter 5, dynamic U-values calculated by different methods are entered into the built environment simulation separately. Simulated indoor T/RH are compared with measured indoor T/RH to observe how every U-value calculation method changes the accuracy of simulation. Finally, an optimal method is determined for calculating dynamic U-values; this includes the optimal data pre-processing methods and optimal time interval.

In Chapter 6, the prediction models for dynamic U-values are built using linear and non-linear methods. The optimal data pre-processing methods are used to process data before building the prediction models. The dynamic U-values of the four envelopes in 11 case cities are predicted by the linear and non-linear models. Since the prediction results derived from the non-linear model do not match the physics, the linear model is chosen as the optimal U-value prediction model.

Chapter 7 presents the predicted dynamic U-values derived by the optimal U-value prediction model and optimal time interval. The operational energy use of CLT and three conventional buildings is simulated based on the theoretical U-values, predicted average U-values and predicted dynamic U-values in the 11 case cities. The influence of dynamic U-values on the operational energy simulations of CLT and conventional buildings in different climate zones is obtained. The operational energy uses of CLT and conventional buildings in different climate zones are also compared by considering dynamic U-values.

The important conclusions in this study and recommendations for the building sector are summarised in Chapter 8.

Chapter 2 Literature Review

This chapter reviews the literature in five aspects relevant to this study. Section 2.1 introduces dynamic U-values and discusses the causes and impacts of dynamic U-values. Section 2.2 introduces three methods for in-situ U-values measurements and describes the measurement method chosen for this study. Section 2.3 presents five methods for calculating U-values in different situations. Section 2.4 describes the regression prediction models applied in the building sector, including linear and non-linear models. Section 2.5 provides an overview of the strengths and disadvantages of existing building energy simulations and three common software for building energy simulations. The summary of this chapter is given in Section 2.6.

2.1 Dynamic U-values

The U-value of the building envelope is defined as the rate of heat transfer through a building envelope. The U-value is also named thermal transmittance (ISO 2007). The U-value of the building envelope can be illustrated by Equation (1):

$$U = \frac{\Phi}{A \times (T_1 - T_2)} \ [W/(m^2 \times K)] \qquad (1)$$

where $\boldsymbol{\Phi}$ is the heat transfer through the building envelope [W]; $\boldsymbol{T_1}$ and $\boldsymbol{T_2}$ are the air temperature on interior and exterior sides of the building envelope, respectively [K]; and $\boldsymbol{A}$ is the measured area $[\mathrm{m}^2]$.

The U-value responds to the thermal insulation properties of a building envelope in a real environment, and therefore, it is one of the most important thermal parameters of building envelopes (Calis 2024). Better-insulated building envelopes have lower U-values, while worse-insulated building envelopes have higher U-values.

The U-values of building envelopes are not fixed in real buildings because the U-values can be influenced by environmental factors (Wang, Zhang, et al. 2022; Wang, Liu, et al. 2022). According to existing studies, the fluctuations in T/RH contribute to the dynamic U-values of building envelopes, as shown in Figure 2.1 (Wang, Liu, et al. 2022; Nosrati and Berardi 2018; Kukk et al. 2022; Boukhattem et al. 2017; Wu et al. 2022; Bucklin et al. 2023; Mounir et al. 2024). Continuous fluctuations in T/RH change temperature and moisture content within building materials. It means that the hygrothermal behaviours of the building materials change (Lelievre, Colinart, and Glouannec 2014). A building material's hygrothermal behaviour is described as the change in physical characteristics caused by the absorption, storage and release of heat and liquid or gaseous moisture (Wu et al. 2022). The hygrothermal behaviours of building materials is influenced by their microstructures. Brick and concrete have inorganic porous structures (Okoh and Resources 2014), while timber features organic cellular structures composed of cell walls and lumens (Xin et al. 2022). Due to differences in porosity, changes in air temperature and relative humidity lead to varying thermal conductivities of building materials (Wang, Liu, et al. 2022; Wang, Zhang, et al. 2022; Eksi Kilicaslan and Kus 2024; de Serres-Lafontaine et al. 2024). A positive linear relationship exists between the thermal conductivities of building materials and the U-value of the building envelope. As a result, the U-value of the building envelope fluctuates.

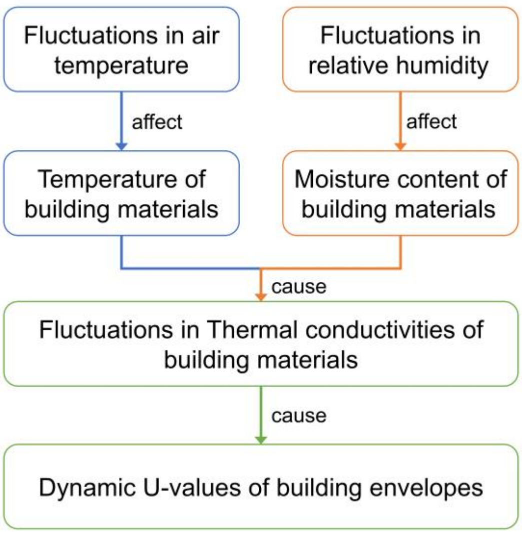

Figure 2.1 Generation of dynamic U-values

No researcher has measured the dynamic U-values of building envelopes in actual buildings. Only one study used simulation software to quantify dynamic U-values (Bruno and Bevilacqua 2022). Bruno and Bevilacqua simulated the dynamic U-values of conventional building envelopes, including brick and concrete envelopes. The dynamic U-values consisted of the average U-value for each month. In dynamic U-values of the brick envelope, the maximum value was 0.45 $\mathrm{W}/(m^2 \times \mathrm{K})$, and the minimum value was 0.27 $\mathrm{W}/(m^2 \times \mathrm{K})$. In dynamic U-values of the concrete envelope, the maximum value was 0.46 $\mathrm{W}/(m^2 \times \mathrm{K})$, and the minimum value was 0.28 $\mathrm{W}/(m^2 \times \mathrm{K})$.

No study has investigated the quantitative relationship between environmental factors (including T/RH) and the dynamic U-values of building envelopes. Only a few studies have researched the quantitative relationship between environmental factors and the building materials' thermal conductivities, which have a positive linear relationship with the U-values of building envelopes (Boukhattem et al. 2017; Wang, Liu, et al. 2022; Wang, Zhang, et al. 2022; Harb et al. 2024; Tlaiji et al. 2023; El Assaad, Colinart, and Lecompte 2023). For example, Wang et al. studied the thermal conductivities of eight common insulation materials by laboratory measurements. The insulation materials included glass wool (GW), rock wool (RW), silica aerogel blanket (SAB), expanded polystyrene (EPS), extruded polystyrene (XPS), phenolic foam (PF), foam ceramic (FC) and foam glass (FG). As shown in Figure 2.2, the thermal conductivities of the eight insulation materials rose between 9% and 21% when the temperature rose from 20℃ to 60℃. The thermal conductivities of the five insulation materials rose between 15% and 187% when the relative humidity rose from 0% to 100% (Wang, Liu, et al. 2022). Tlaiji et al. focused on the thermal conductivities of three straw bales with different densities, showing that they rose by around 6% when the temperature rose by 10%, and by around 7% when the relative humidity rose by 10% (Tlaiji et al. 2023). These findings showed fluctuations in the thermal conductivities of building materials due to changes in environmental factors. The influence of T/RH on the thermal performance of building materials was significant.

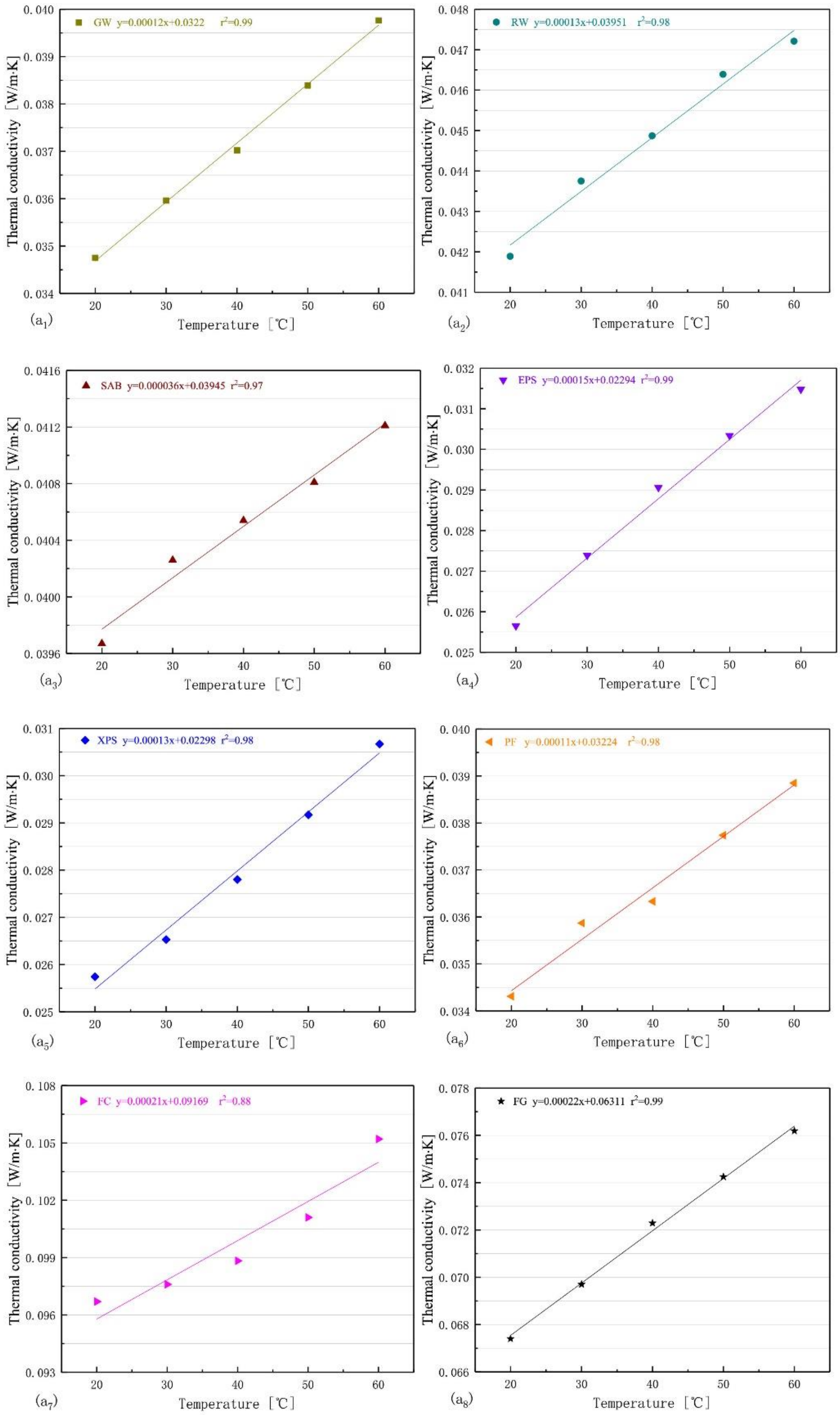

(a) Impact of temperature on the thermal conductivities of eight samples

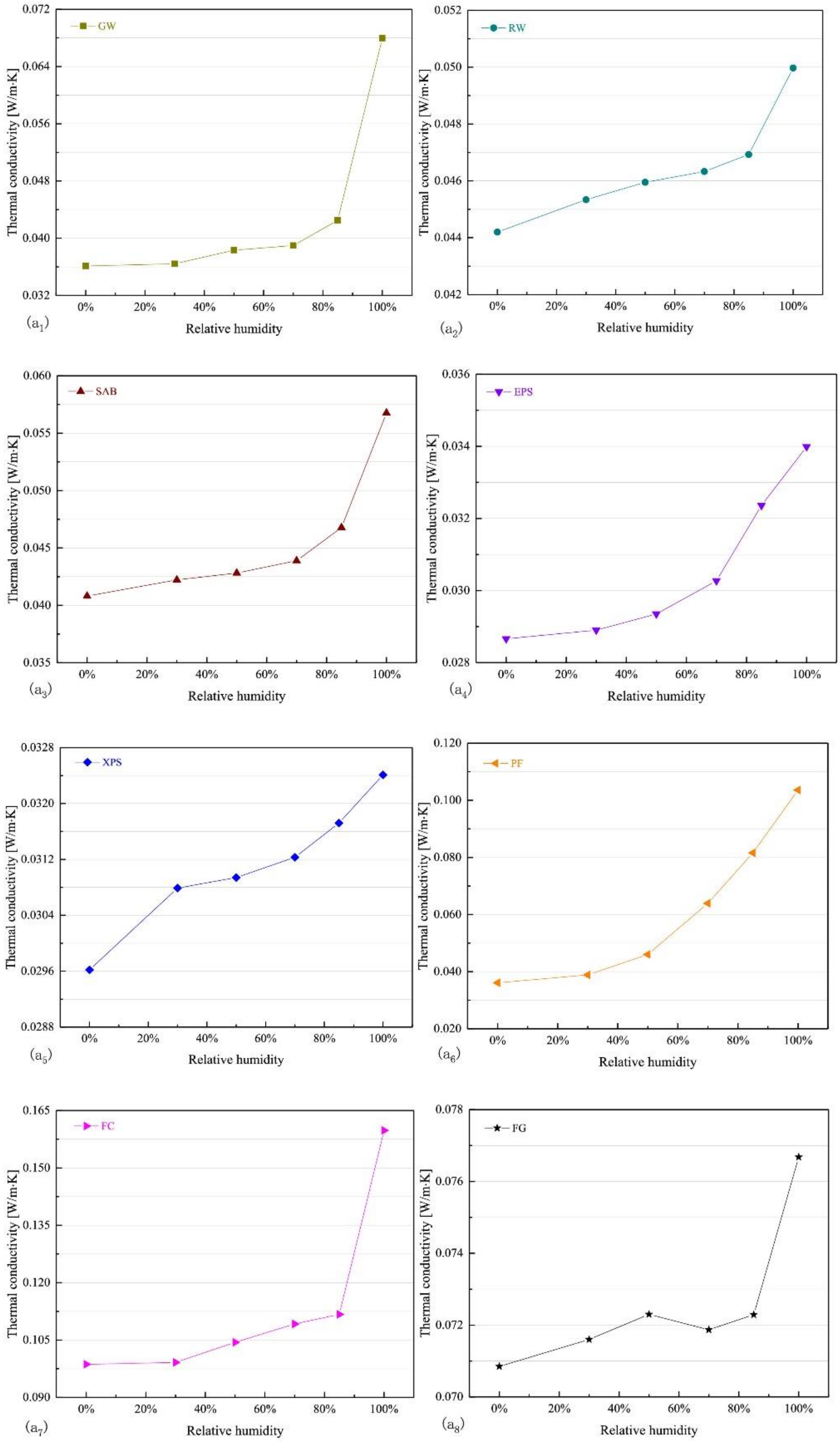

(b) Impact of relative humidity on the thermal conductivities of eight samples

Figure 2.2 Thermal conductivities of eight insulation materials (Wang, Zhang, et al. 2022)

The dynamic U-values suggest that the building envelope's thermal insulation is unstable. This instability directly influences the operational energy use of buildings. The only relevant quantitative study was conducted by Bruno and Bevilacqua (Bruno and Bevilacqua 2022). They simulated operational energy in brick and concrete buildings in the Climate zone C by both theoretical and simulated dynamic U-values. The heating energy use when the dynamic U-values were considered was 5.1%–9.2% more than those based on the theoretical U-values. The results showed that the energy impacts of dynamic U-values were significant.

In summary, studies on dynamic U-values have shown three research gaps. First, the dynamic U-values of both conventional and CLT building envelopes have not been measured in a real environment. Second, the quantitative relationship between dynamic U-values of both conventional and CLT building envelopes and environmental factors (including T/RH) has not been studied. Finally, the impacts of dynamic U-values of CLT building envelopes on operational building energy have not been focused on. Although a study researched the effect of dynamic U-values of conventional building envelopes on building operational energy consumption, simulated datasets were used rather than measured datasets. A gap still existed between the results of this research and the actual situation.

2.2 In-situ U-value Measurement Methods

In recent years, many studies have applied in-situ measurements to obtain U-values of various building envelopes (Walker and Pavía 2015; Samardzioska and Apostolska 2016; Gaspar, Casals, and Gangolells 2016; Pelsmakers et al. 2017; Tejedor et al. 2017; Teni, Krstić, and Kosiński 2019; Rahiminejad and Khovalyg 2021; Jung et al. 2024). The main measurement methods are the heat flow meter (HFM), simple hot box-heat flow meter (SHB-HFM) and thermometric (THM) methods, as shown in Figure 2.3.

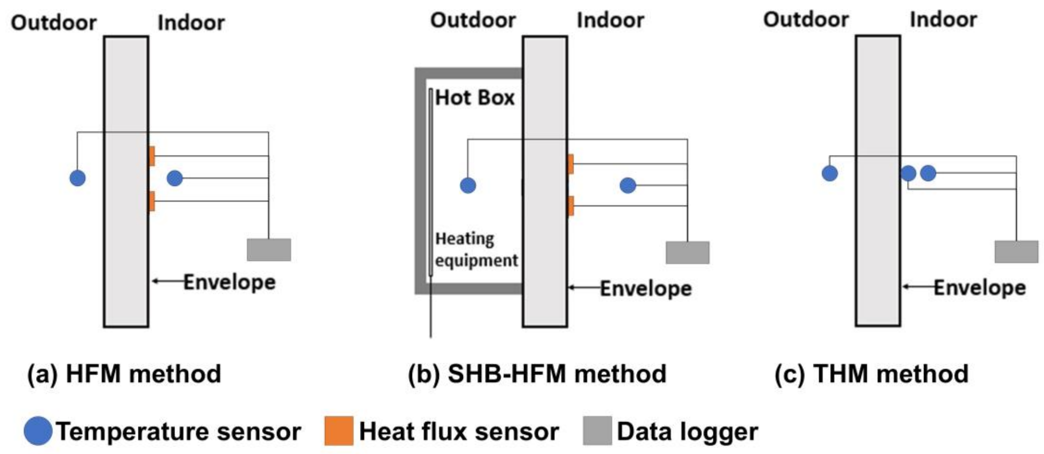

Figure 2.3 Schematic diagrams of in-situ U-value measurement methods

According to ISO 9869-1 and ASTM C1155 standards (ISO 2014; ASTM 2007), the HFM method is a standardised process to measure U-values of building envelopes in actual buildings. The principle of this method is based on Equation (1). The temperature difference between indoor and outdoor environments and the heat flux through the building envelope are necessary. As shown in Figure 2.1(a), a regular measurement system in the HFM method has three experimental apparatuses (O'Hegarty et al. 2021; Ficco et al. 2015; Jung et al. 2024; Nardi and Lucchi 2023). First, two heat flux sensors are attached to the internal surface of the building envelope. The heat flux sensor can produce electrical signals when heat fluxes occur through the building envelope. Second, two temperature sensors are needed for indoor and outdoor temperatures. The accuracy of the temperature sensor is at least 0.2℃. Third, a data logger is needed to store the temperature and heat flux datasets. The HFM method has three advantages: (1) the experimental apparatus is easy to install; (2) the surface of the envelope is not destroyed during the measurement; (3) a long-term measurement can be realised (Li et al. 2015; Bienvenido-Huertas et al. 2019; Teni, Krstić, and Kosiński 2019). It also has a shortcoming: when the temperature difference is unstable, it may produce errors in the measured results (Desogus et al. 2011).

The HFM has been the most widely used method over the last decade. Many researchers have adopted it to obtain average U-values of various building envelopes, as shown in

Table 2.1. Most of the tested envelopes are brick and concrete envelopes in residential buildings. A few the tested envelopes are bio-based envelopes, including timer and straw bale envelopes.

Table 2.1 Existing studies related to the HFM method

Reference	**Building type**	**Measured envelope**	**Research aim**
(Ficco et al. 2015)	Residential buildings	A tuff wall; a hollow brick and lightened concrete block wall; a double hollow brick wall with insulation	To estimate the energy consumption of conventional residential buildings by measured U-values
(Latif et al. 2015)	Residential buildings	A timber frame wall with wood-hemp insulation	To analyse the hygrothermal performance of the timber frame wall
(Miljan and Miljan 2015)	Office building	A straw bale wall with a timer frame	To study the embodied energy of walls when the U-values are considered
(Kim, Kim, et al. 2018)	Residential building	Brick and cement walls	To compare the HFM and air–surface temperature ratio method
(Fedorczak-Cisak et al. 2020)	Public building	Timber walls	To retrofit walls of historical timber buildings
(O'Hegarty et al. 2021)	Residential buildings	Concrete block walls with insulation; RC walls with insulation	To find the gaps between the theoretical and measured U-values of highly insulated building envelopes
(Mobaraki, Castilla Pascual, García, et al. 2023)	Residential buildings	A brick wall	To study the impacts of test conditions on the accuracy of the U-value measurement
(Lee et al. 2024)	Experimental building	An RC wall with insulation	To improve the accuracy of measured U-values of highly insulated walls

The SHB-HFM method has been developed from the HFM method with the aim to stabilise test conditions by controlling the temperature difference (Meng et al. 2015). The principle of the SHB-HFM method is the same as that of the HFM method. The differences between the two methods for instrument installation are shown in Figure 2.1(b). A box with a heating system is attached to the surface of the building envelope to control the temperature difference. The temperature sensor for the outdoor environment are placed in the hot box. This method allows for a more stable temperature difference. However, this method is not as widespread as the HFM method. As the heating system needs to work continuously, it increases the difficulty and cost of in-situ measurements. Several related studies are shown in Table 2.2.

Table 2.2 Existing studies related to the SHB-HFM method

Reference	Building type	Measured envelope	Research aim
(Meng et al. 2015)	Rural building	A self-insulation brick wall	To propose and validate the SHB-HFM method
(Meng et al. 2017)	Rural building	A sintered porous brick wall	To propose the determination method of the hot box size
(Roque et al. 2020)	Historical building	A timber frame wall filled with an earth-lime mortar	To study the thermal performance of a traditional wall of built heritage
(Xie et al. 2022)	NA	Hollow brick walls filled with agricultural wastes	To study the thermal performance enhancement of hollow brick walls
(Nicoletti, Antonio Cucumo, and Arcuri 2023)	Public building	Masonry walls with insulation	To compare the accuracy of different in-situ measurement methods

The THM method is also named the air–surface temperature ratio method. Compared with the other three methods, it is the most inexpensive. As shown in Figure 2.1(c), only three temperature sensors and a data logger are needed. The three temperature sensors are applied to obtain (1) the temperatures of the inner surface of the building envelope, (2) indoor temperature and (3) outdoor temperature. The principle of the THM method is shown in Equation (2), which is developed based on Equation (1) and Newton's law of convective cooling (Bienvenido-Huertas et al. 2019).

$$U = \frac{h_i(T_i - T_{si})}{T_i - T_e} \; [W/(m^2 \cdot K)] \qquad (2)$$

where $\boldsymbol{T_i}$ and $\boldsymbol{T_e}$ are the indoor and outdoor temperature, correspondingly [K]. $\boldsymbol{T_{si}}$ is the temperature of inner surface of the building envelope [K]. $\boldsymbol{h_i}$ is the heat transfer coefficient of the inner surface $[\mathrm{W}/(\mathrm{m}^2 \cdot \mathrm{K})]$.

Although this method is low-cost and easy to apply, it has high requirements for the conditions in-situ measurements. Bienvenido-Huertas et al. found that the THM method was reliable when the temperature difference between indoor and outdoor environments was stable and more than 10°C. Applying this method could lead to errors in the warm season. Because the temperature difference between indoor and outdoor environments is always less than 10°C in the warm season (Bienvenido-Huertas et al. 2018); this makes the application of this method limited. The relevant studies have focused on the feasibility of this method rather than its practical application, as shown in Table 2.3.

Table 2.3 Existing studies related to the THM method

Reference	Building type	Measured envelope	Research aim
(Andújar Márquez, Martínez Bohórquez, and Gómez Melgar 2017)	Residential building	NA	To invent and validate the THM method
(Kim, Lee, et al. 2018)	Residential building	Brick and cement walls	To improve the accuracy of the THM method
(Kim, Kim, et al. 2018)	Residential building	Brick and cement walls	To test the reliability of the THM method
(Bienvenido-Huertas et al. 2018)	Residential building	Brick cavity walls	To study the viability and limitations of the THM method
(Evangelisti, Guattari, and Asdrubali 2019)	NA	An assembled aluminium panel	To compare the HFM and THM methods

To comprehensively study dynamic U-values, the U-values of CLT and conventional building envelopes need to be measured under all seasonal conditions, including winter, transition season and summer. Thus, the THM method is not applicable. For observing U-values under free-running conditions of the building operation stage, the indoor environments during in-situ measurements should not be artificially controlled. Thus, the SHB-HFM method is also not applicable. Finally, the HFM method was chosen to measure dynamic U-values of CLT and conventional building envelopes. Firstly, the HFM allows for long-term continuous measurements, which is essential for capturing seasonal variations in dynamic U-values. Secondly, the HFM method does not damage the tested envelopes, which was critical for repeated and extended monitoring. Thirdly, compared to THM method, the HFM method has lower requirements for maintaining stable indoor-outdoor temperature differences, making it suitable for capturing data under real-world conditions where outdoor temperatures fluctuate significantly.

2.3 U-value Calculation Methods

Since the HFM method was used in this study, this section discusses how the U-value is calculated based on this method. In the HFM method, the measured average U-value can be calculated by Equation (3) according to ISO 9869-1 (ISO 2014). Equation (3) is the most widely used U-value calculation method in both industry and academia (Soares et al. 2019; Ficco et al. 2015; Lucchi 2017; Evangelisti et al. 2015; Bienvenido-Huertas et al. 2019; Mobaraki, Castilla Pascual, García, et al. 2023; O'Hegarty et al. 2021). This U-value calculation method is also known as the average method. In this study, the calculation of U-values is also based on the average method.

$$U = \frac{\sum_{j=1}^{n} q_j}{\sum_{j=1}^{n}(T_{ij} - T_{ej})} \; [W/(m^2 \cdot K)] \qquad (3)$$

Where $\boldsymbol{U}$ is the average U-value of the building envelope in the measuring process $[\mathrm{W}/(\mathrm{m}^2 \cdot \mathrm{K})]$. q_j is the heat flux density at time $\boldsymbol{j}$ $[\mathrm{W}/\mathrm{m}^2]$; $\boldsymbol{T_{ij}}$ and $\boldsymbol{T_{ej}}$ are the indoor and outdoor temperature at time $\boldsymbol{j}$, respectively [K], and $\boldsymbol{n}$ is the number of recorded samples in the measuring process.

In Equation (3), the directions of temperature difference and heat flux density are indicated by positive or negative values. Typically, the temperature difference and heat flux are positive when the indoor temperature is consistently higher than the outdoor temperature. When the direction of the temperature difference remains constant and the average temperature difference is greater than 3°C, the average method can be used to obtain reliable results without data cleaning or processing (Atsonios et al. 2017; O'Hegarty et al. 2021).

However, when in-situ U-value measurements are conducted in the summer, the direction of the temperature difference is not always stable as the indoor temperature is lower than the outdoor temperature at noon or in the afternoon and higher at night. This may lead to errors in U-value calculation because the change in the direction of the temperature difference leads to the change in the direction of heat flux, which occurs later than the change in the direction of the temperature difference owing to the building envelope's heat capacity. Conversely, when the temperature difference is in the opposite direction of heat flux, the U-value is negative according to Equation (3). The negative U-value is not in accordance with the principles of physics. Therefore, when the measurement conditions are unstable, the original data need to be processed before the average method is used. Some researchers (Pescari et al. 2022; Mobaraki, Castilla Pascual, Lozano-Galant, et al. 2023; Bienvenido-Huertas et al. 2018; Evangelisti, Guattari, and Asdrubali 2019; Evangelisti et al. 2020; Shi, Gong, et al. 2022; Ficco et al. 2015) have proposed data pre-processing methods as follows:

(1) Use of night-time data only

Pescari et al. measured the U-value of a RC envelope by the HFM method and calculated the U-value by the average method (Pescari et al. 2022). They conducted the in-situ measurement for 15 days. The measured results in this study are shown in Figure 2.4.

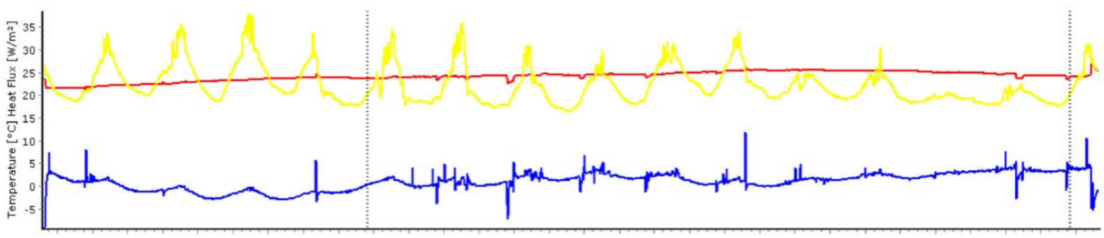

Figure 2.4 Measured data in the existing study (Pescari et al. 2022)

(yellow: outdoor temperature, red line: indoor temperature, blue: heat flux)

On some days during the measurement period, the direction of the temperature difference changed twice every day. When the temperature difference is in the opposite direction of the heat flux, it may lead to negative U-values. To remove abnormal values, Pescari et al. applied night-time data only because measurement conditions at nighttime were more stable than those in the daytime. Meanwhile, during the daytime, the measured outdoor temperature was higher than the actual outdoor air temperature owing to high solar radiation, which resulted in errors in the measured data. Finally, the results showed that this data pre-processing method had feasibility.

(2) Deletion of negative data

Evangelisti et al. used the HFM method to measure the U-values of north and south building envelopes in a new public building in both winter and summer. During the post-processing of summer data, the samples with negative heat flux or negative temperature difference were removed in the average method. The percentage differences between the measured and theoretical U-values for the north and south envelopes were 5.5% and 11.1%. Thus, this data pre-processing method was effective (Evangelisti et al. 2020).

(3) Adoption of absolute values of data

Evangelisti et al. measured the U-value of a new envelope in both winter and summer by the HFM method. To reduce the errors of calculated U-value in the summer measurement, the absolute values of heat flux and temperature difference were taken into account in the average method. The results showed that the U-values had good consistency between 0.40 $\mathrm{W/(m^2 \cdot K)}$ in the summer measurement and 0.39 $\mathrm{W/(m^2 \cdot K)}$ in the winter measurement (Evangelisti, Guattari, and Asdrubali 2019).

(4) Filtering data based on temperature difference

Mobaraki et al. measured the U-value of an RC envelope in an office. They filter the samples by temperature difference. The samples with a temperature difference of less than **X** °C were deleted, and then the U-value was calculated by the average method. **X** was an integer from 5 to 14. The results showed that when **X** increased from 5 to about 9, the calculated U-value became stable and close to the theoretical U-value. As **X** continued to rise, the U-value appeared unreasonably low (Mobaraki, Castilla Pascual, Lozano-Galant, et al. 2023). Some researchers have found that the average temperature difference should preferably not be less than 10°C to obtain reliable U-values by the HFM and average methods (Ficco et al. 2015; Desogus et al. 2011). Other have obtained reliable results with a temperature difference of 3°C (Evangelisti et al. 2020).

(5) Removing the heat storage effect and heat flow meter (RHS-HFM) method

To reduce the influence of unstable measurement conditions in summer, the RHS-HFM method was developed to measure the thermal resistance of clay brick envelopes (Shi, Gong, et al. 2022). Since the U-value can be approximated as the reciprocal of the thermal resistance, this method can also be used for U-value measurements (Bastos Porsani et al. 2023; Chen et al. 2023; Xing et al. 2023). In this method, the heat storage effect was considered and overcame seasonal limitations. The calculation formulae are described in Chapter 3. Shi et al. proved that the RHS-HFM method had good accuracy, and the measurement error was about 5% in the summer and transition season (Shi, Gong, et al. 2022).

Although all these data pre-processing methods can be applied before U-value calculation by the average method, no study has compared the accuracy of these data pre-processing methods. Thus, it is not clear which data pre-processing method is appropriate for this study. In this study, all these data pre-processing methods were applied, and the appropriate method was selected to calculate the dynamic U-values of CLT and conventional building envelopes.

2.4 Regression Prediction Models

The regression prediction models have been widely used in the building sector. Many researchers have applied regression prediction models to study buildings' thermal performance and energy efficiency (Sofuoglu 2008; Mba, Meukam, and Kemajou 2016; Ahmad, Mourshed, and Rezgui 2017; Yu, Chang, and Dong 2022). The kinds of regression prediction models are many and can be classified into linear and non-linear models. The most widely used linear model is multiple linear regression (MLR) (Chen, Zhou, et al. 2022). Most non-linear models are based on machine-learning methods (Zhang et al. 2021; Jraida et al. 2024; Li, Yin, and Chen 2024; Guo et al. 2024).

The MLR model has been applied in prediction issues in the last few decades to generate the linear relationship between several independent variables and one dependent variable. The formula of the MLR model is shown in Equation (4).

$$Y = a_1 \times x_1 + a_2 \times x_2 + a_3 \times x_3 + \cdots + a_n \times x_n + b \qquad (4)$$

Where $\boldsymbol{Y}$ is the dependent variable; $\boldsymbol{x_n}$ is the $\boldsymbol{n}$th independent variable; $\boldsymbol{a_n}$ is the coefficient of the $\boldsymbol{n}$th independent variable, and $\boldsymbol{b}$ is the constant term.

The MLR model has three advantages. First, it is relatively simple to understand and apply. Some statistical software can be helpful for building the MLR model, such as SPSS (Liu, Yu, et al. 2021). Second, the MLR model has interpretability. The coefficients of independent variables demonstrate the relationship between the independent and dependent variables. Positive or negative coefficients represent whether the correlation is positive or negative. A greater absolute value of the coefficient represents a greater effect of that independent variable on the dependent variable. Third, the MLR model can analyse datasets with fewer samples compared to machine-learning models.

Nevertheless, the MLR model still has some limitations. For example, if different independent variables show a high correlation, determining the individual influence of each independent variable is difficult. The predictive power of the MLR model decreases when the number of independent variables is excessively large or when a non-linear relationship exists between the independent and dependent variables.

According to related studies in the building sector, the MLR model can predict the building energy use and thermal performance of buildings by multiple related factors. Existing related studies are shown in Table 2.4.

Table 2.4 Existing studies using the MLR model

Reference	Predicted target	Influencing factors
(Catalina, Iordache, and Caracaleanu 2013)	Heating energy demand	Building global heat loss coefficient, the south equivalent surface, the difference between the indoor set point temperature and the sol-air temperature
(Qiang et al. 2015)	Cooling load	Dry-bulb temperature, wet-bulb temperature, solar radiation, relative humidity, occupants, equipment, lighting devices, the occupants' adjustment of HVAC systems
(Li et al. 2018)	Monthly and yearly cooling loads	Dry bulb temperature, solar radiation, wet bulb temperature, wind direction and wind speed
(Ciulla and D'Amico 2019)	Building energy performance	Cooling degree days, heating degree days, external temperature, glazed surface, opaque surface, internal gains
(Kim, Kim, and Srebric 2020)	Electricity consumption	Occupant number, Outdoor temperature, outdoor relative humidity, normal direct irradiance, cloud, wind speed

Table 2.4 (continued)

Reference	Predicted target	Influencing factors
(Chen, Zhou, et al. 2022)	Building's hourly cooling load	Outdoor temperature, outdoor relative humidity, outdoor wind speed, solar radiation, occupant, lighting power, equipment power
(Byun et al. 2023)	The U-value of building envelopes	The type, colour and finish of the exterior wall finishes, sources of pollution, exposure to the sea, existence of adjacent buildings
(Belpoliti et al. 2024)	Building energy consumption	Building age, floor area, roof area, form factor, number of students, number of classrooms and laboratories, availability of gymnasium and multi-purpose hall, use of digital technology

To overcome the limitations of the MLR model, some machine-learning models have been developed and applied over the past decade. These can be used to build more complex non-linear relationships between independent and dependent variables. Common machine-learning models include extreme gradient boosting (XGBoost), decision tree (DT), random forest (RF), K-nearest neighbours (KNN), support vector regression (SVR) and artificial neural network (ANN). These models are based on different mathematical principles (Yang, Sun, and Zhifeng 2024; Luo et al. 2024; Guo et al. 2024). The predictive accuracy of a machine-learning model is related to the specific research question. Therefore, no definitive conclusion exists as to which machine-learning model has the most effective prediction (Cakiroglu et al. 2024; Jraida et al. 2024; Li, Yin, and Chen 2024).

The machine-learning models for regression prediction have three advantages. First, they can capture more complex relationships between variables, whereas the MLR model can only deal with linear relationships. The machine-learning models are more effective in dealing with regression problems where high correlations exist between the independent variables. Second, some machine-learning models, such as ANN and SVR, are highly flexible and adaptable to different data patterns. Third, machine-learning models usually have higher prediction accuracy when handling big datasets. However, they have shortcomings. First, in contrast to the MLR model, explaining the prediction process of some models, such as ANN, is difficult. Second, machine-learning models are prone to overfitting the training data.

According to existing studies related to the building sector, many researchers have used machine-learning models to predict building energy use, indoor environment and the thermal performance of building envelopes. Some of these studies have applied one model, and the others have applied various models. Detailed information on the related research is shown in Table 2.5.

Table 2.5 Existing studies using machine-learning models

Reference	Model type	Predicted target	Influencing factors
(Mba, Meukam, and Kemajou 2016)	ANN	hourly indoor T/RH	Outdoor temperature, indoor temperature, outdoor relative humidity, indoor relative humidity
(Kim, Kim, and Srebric 2020)	ANN	electricity consumption	Occupant number, outdoor temperature, outdoor relative humidity, normal direct irradiance, cloud, wind speed
(Amasyali and El-Gohary 2021)	Regression trees, ensemble bagging trees, ANN, DNN	Cooling energy consumption	Occupant-behaviour features, building-size features, outdoor weather-condition features

Table 2.5 (continued)

Reference	Model type	Predicted target	Influencing factors
(Kristiansen et al. 2022)	ANN	Illuminance and indoor temperature	Glass parameters, window parameters, vertical view, horizontal view, view direction, distance to the window
(Olu-Ajayi et al. 2022)	ANN, SVR, RF, DT, KNN, Adaboost	Building energy performance	Outdoor temperature, wind speed, air pressure, postcode, floor area, property type, parameters of building envelopes and windows
(Xu et al. 2023)	ANN	Heat conduction flux inside the wall	Measured heat flux, temperature of inner surfaces
(Zhang et al. 2024)	ANN, KNN, SVR, XGBoost, RF	Embodied carbon emissions	Building height, construction form, seismic intensity, form of delivery, location, cost of materials
(Jung et al. 2024)	Tree, SVR, ensemble, ANN	Heat flux	Outdoor temperature, indoor temperature, surface temperature of building envelopes, temperature difference between indoor and outdoor air
(Cakiroglu et al. 2024)	Categorical Boosting, XGBoost, LightGBoost, RF	Cooling load	Building area, length-to-width ratio, height of ceilings, U-values of windows, walls and roofs, window-to-wall ratio, orientation, level shading overhangs

In this study, the U-value prediction model needs to be developed to obtain the dynamic

U-values of CLT and conventional building envelopes in different climate zones. The independent variables in the U-value prediction model are the type of building envelope, indoor temperature, indoor relative humidity, outdoor temperature and outdoor relative humidity. Since no study has proven whether these independent variables have linear or non-linear relationships with the U-values of building envelopes in actual buildings, both linear and non-linear methods were chosen for U-value prediction. The MLR model was used as the linear method and the ANN model as the non-linear method.

2.5 Building Energy Simulation

Owing to the availability and accessibility of relevant software, building energy simulation has been the most widespread method of predicting energy use in various types of buildings in recent years (Chen, Guo, et al. 2022). This method is also referred to as the physics-based or white-box approach as building energy simulations are built on the principles of physics to compute the energy use of the whole building. Building energy consumption is affected by many factors, such as weather conditions, thermal properties of the building materials, geometric building parameters and occupant behaviours. Therefore, to conduct an accurate building energy simulation, many parameters need to be collected and entered into the building simulation software (Marshall et al. 2017).

According to existing studies, using building energy simulation for predicting building energy use has three strengths. First, building energy simulation has interpretability. All building energy simulation software is developed based on thermodynamics. Thus, the simulation results can be explained by the principle of heat transfer (Boyano, Hernandez, and Wolf 2013). Second, existing building simulation software has been well developed, which means that the accuracy of the simulation result is high once all the important parameters have been gathered. Third, building energy simulation is widely available and can be used for different types of buildings, including residential and public buildings. It can also be used for buildings at different scales, from individual rooms to urban-scale building complexes (Malhotra et al. 2022).

However, the drawbacks are two. First, collecting all building parameters which are needed in building energy simulation is challenging. If the energy consumption of a building complex needs to be simulated, the number of parameters to enter is considerably higher. While remote sensing technology can provide detailed information on building geometry and visualise buildings' distribution, collecting the thermal parameters of the building materials remains particularly difficult (Dabirian, Panchabikesan, and Eicker 2022). Second, the actual situation of occupant behaviour in a building is often stochastic. Energy use by occupants can be influenced by many factors, including health status, subjective awareness of the environment, economic situations and weather conditions. However, a fixed schedule has been used to prescribe the behaviour of all occupants in many studies related to building energy consumption simulation, leading to a gap between actual and simulated building energy consumption (Alsharif et al. 2021).

Various software tools are available for building energy modelling. Some of the most used are EnergyPlus, TRNSYS and IDA ICE. All this software is based on the heat transfer principles, with slight differences between the principles. EnergyPlus applies a one-dimensional nodal method in which both weather information and building parameters are inputted as physical variables and the node can stand for figural or abstract building elements. For example, a room is a type of figural building element, and heating loads in a room are a type of abstract building element (Hamdaoui et al. 2021). TRNSYS applies a two-dimensional nodal method, simulating a complicated transient system with a modular structure. This software includes two parts: engine and component library. The engine can handle calculations and draw images to simulate the heat transfer in the buildings. The component library can provide models, including various building elements and HVAC equipment (Yu, Chang, and Dong 2022). IDA ICE applies the mathematical method, working with symbolic equations rather than variable assignments, and it is suitable to add the modelling function (Mazzeo et al.

2020).

In terms of accuracy, no building energy simulation software has an absolute higher accuracy than other software in various simulation scenarios (Catto Lucchino et al. 2021). For example, Mazzeo et al. compared the accuracy of EnergyPlus, TRNSYS and IDA ICE and found that all tools had high accuracy when simulating the indoor environment of the solar test box made of conventional materials. During the warm period, TRNSYS had the best accuracy; during the cold period, IDA ICE was the most accurate (Mazzeo et al. 2020). Gennaro et al. simulated the energy use of buildings with double skin façades by EnergyPlus, TRNSYS and IDA ICE. The results showed that no tool outperformed the others for all simulated results. EnergyPlus was the most accurate tool for simulating outdoor air curtains, and TRNSYS was the most accurate tool for simulating surface temperatures and transmitted solar radiation (Gennaro et al. 2023). Johari et al. simulated the energy use of residential multifamily buildings by these three software tools; the simulation results were similar when the simulated building model had enough details (Johari et al. 2022).

In recent years, building energy simulation software has also been employed in various scenarios. The objects being modelled included individual rooms, individual buildings and building complexes. The simulation result can be either the total energy consumption of the building or a certain type of energy consumption, such as cooling energy and heating energy. Related studies are as shown in Table 2.6.

Table 2.6 Existing studies related to building energy simulation

Tool	Reference	Simulated object	Simulation target
EnergyPlus	(Cetin et al. 2019)	Residential and commercial buildings	Development and validation of an on/off controller of HVAC systems
	(Yu, Kang, and Zhai 2020)	Underground building	Influence of different ground coupled heat transfer models on energy consumption
	(Ng, Dols, and Emmerich 2021)	Commercial building	Effects of infiltration correlations on HVAC operation
	(Feng et al. 2022)	Building envelope	Developing a model for the phase change materials used in the building envelope
	(Bastos Porsani et al. 2023)	Residential building	Evaluation of the infiltration model
	(Eid et al. 2024)	Supermarket	Building energy consumption and carbon emissions
	(Uribe, Vera, and Perino 2024)	Office	Building energy performance in different climates
TRNSYS	(Braas et al. 2020)	Residential building	Heating energy use by district heating systems
	(Kenai et al. 2021)	Brick masonry house	Influence of green walls on building energy use
	(M'Saouri El Bat et al. 2021)	Street	Influence of street canyon microclimate on building energy use
	(Rashad et al. 2022)	Residential building	Building energy use in 7 scenarios of heating and cooling demand

Table 2.6 (continued)

Tool	Reference	Simulated object	Simulation target
TRNSYS	(Sun et al. 2023)	Education building	Multi-objective optimisation of control strategies for a heating system in cold and arid regions
	(Wang et al. 2024)	Commercial office	Energy use by the HVAC system
	(Beaulac et al. 2024)	Greenhouse	Building energy consumption in a cold climate
	(Ethirveerasingham, Fung, and Kumar 2024)	Residential building	Use of a natural gas absorption heat pump for heating and cooling
IDA ICE	(Eriksson, Akander, and Moshfegh 2020)	Residential building	Development and validation of energy signature method
	(Yuan et al. 2021)	Ice and swimming hall	Use of the four possible waste heat sources
	(Hosamo et al. 2022)	Education building	Building energy consumption and thermal comfort
	(Fornari et al. 2023)	Hotel room	Development of a BLOCK zonal model to predict thermal stratification
	(Yin, Norouziasas, and Hamdy 2024)	Residential building	Influence of phase change materials on heating energy use

In this study, TRNSYS was chosen for the simulations of both the indoor environment of the tested rooms and the operational energy use of the reference building as it is more flexible than the other two software. For example, the initial indoor T/RH can be set for each simulation. It guarantees the continuity of the building energy simulation results based on dynamic U-values. When simulating the indoor T/RH of a thermal zone, the indoor T/RH of neighbouring thermal zones can be set to continuously varying values. These operations are essential in this study, and detailed information is shown in Chapter 3.

2.6 Summary

The literature review includes five aspects: introduction of dynamic U-values, in-situ U-value measurement methods, U-value calculation methods, regression prediction models and existing building energy simulations. According to the introduction of dynamic U-values (Section 2.1), research gaps exist in three terms of the quantitative studies related to dynamic U-values: (1) measured dynamic U-values of CLT and conventional envelopes; (2) relationship between environmental conditions and dynamic U-values; and (3) impacts of dynamic U-values on building operational energy simulation.

Sections 2.2, 2.3, 2.4 and 2.5 provided the theoretical basis and important reference for the selection of the research methods to investigate dynamic U-values quantitatively and comprehensively. First, the HFM method was chosen to measure dynamic U-values of CLT and conventional building envelopes. Second, the average method was applied to calculate dynamic U-values. The existing data pre-processing methods before the average method is used are five. Third, both the MLR and ANN models were used to build U-value prediction models. Fourth, TRNSYS was chosen to simulate the operational energy of CLT and conventional buildings.

Chapter 3 Methodology

The methodology in this study includes four stages: in-situ measurements, determination of the U-value calculation method, determination of the U-value prediction model and building operational energy simulation. The final simulation results were used to analyse the energy impacts of dynamic U-values. The operational energy use of CLT and conventional buildings were compared as well.

3.1 In-situ Measurements

During multiple measurements over a one-year period, four tested envelopes in three cities were measured. The masonry cavity envelope was measured in 2022 in Sheffield, UK. The CLT envelope was measured in 2023 in Ninghai, China. Both the RC and brick envelopes were measured in 2023 in Harbin, China. The detailed information and results of in-situ measurements are shown in Chapter 4.

Each in-situ measurement can be divided into two parts, as shown in Figure 3.1. The first part was the U-value measurement of the tested envelope, and it was conducted in the tested rooms. The collected data included heat flux, indoor T/RH and outdoor T/RH. These data were used for calculating the U-values in Chapter 5 and building the U-value prediction models in Chapter 6. The second part was the indoor environment measurements in the neighbouring rooms. The collected data included indoor T/RH and were used as boundary conditions for the indoor environment simulation in Chapter 5.

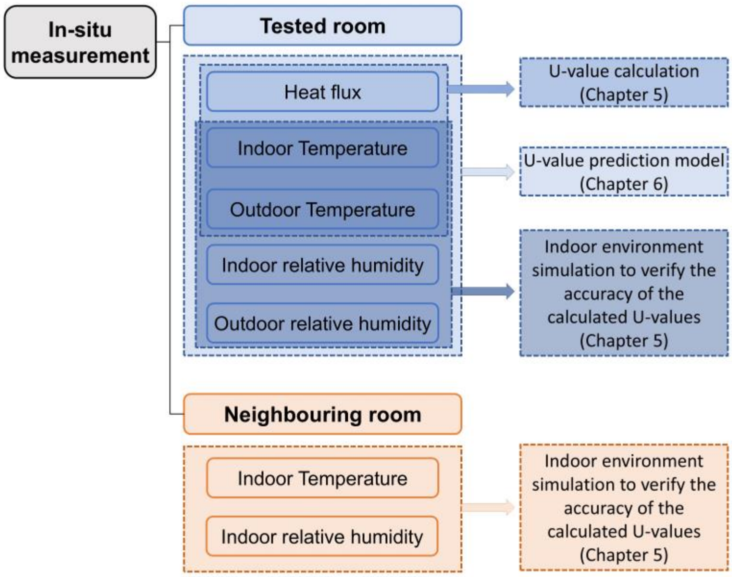

Figure 3.1 Types and purposes of measured data

3.2 Selection of the U-value Calculation Method

The measured heat flux and the indoor and outdoor temperature of the tested rooms were applied to calculate the dynamic U-values of the tested envelopes. Different U-value calculation methods were applied based on the average method and several data pre-processing methods with different time intervals. The accuracy of calculated U-values based on different methods was validated by the indoor T/RH simulations of the tested rooms, and the optimal dynamic U-value calculation methods were determined.

3.2.1 Different Dynamic U-value Calculation Methods

The U-value calculation methods were based on the average method according to ISO 9869-1 (ISO 2014). The calculation is shown in Equation (3) in Section 2.3. To reduce the impacts of outliers, five methods were applied to process data before using the average method. The causes of outliers were detailed in Section 2.3. The five data pre-processing methods were developed from existing methods which were also detailed in Section 2.3.

(1) Night data (ND) method

The data from times with no or weak solar radiation can be used. This study uses the daily data from 8 p.m. to 6 a.m.

(2) Temperature difference (TD) method

The data with a temperature difference of less than **X** ℃ are deleted. **X** is a natural number (such as 0, 1, 2, 3 and so on). Thus, this approach can be subdivided into several scenarios abbreviated as TD0, TD1, TD2, TD3 and so on. Since the calculation of U-values using the average method may incur errors when the temperature difference is low, choosing a suitable critical value helps to filter out unreliable data and reduce the calculation bias. There is no evidence that a certain fixed critical value of temperature difference can lead to the most accurate U-value. Therefore, this study used different critical values of temperature difference and determined which one could lead to more accurate U-value results in subsequent studies.

(3) Positive value (PV) method

Only data with positive heat flux can be used. At the same time, the data with a temperature difference of less than **X** ℃ are deleted. **X** is a natural number (such as 0, 1, 2, 3 and so on). Thus, this approach can be subdivided into several scenarios abbreviated as PV0, PV1, PV2, PV3 and so on.

(4) Absolute value (AV) method

The absolute value of heat flux and temperature difference can be used. At the same time, the data with an absolute value of temperature difference which is less than **X** ℃ are deleted. **X** is a natural number (such as 0, 1, 2, 3 and so on). Thus, this approach can be subdivided into several scenarios abbreviated as AV0, AV1, AV2, AV3 and so on.

(5) Time lag (TL) method

This method is based on the RHS-HFM method, as shown in Equations (5) - (8). The indoor temperature changes later than the outdoor temperature owing to the heat storage properties of the envelope. To eliminate the effect of the time lag, the temperature difference for calculating the U-value is the average of the difference between the maximum values of indoor and outdoor temperature and the difference between the minimum values of indoor and outdoor temperature in one day; this is because one day is a minimum period of outdoor and indoor temperature fluctuation. It also indicates that the minimum time interval for calculating a U-value in this method is one day.

$$U = \frac{\overline{q_N}}{\overline{\Delta T_N}}\ [W/(m^2 \cdot K)] \qquad (5)$$

$$\overline{\Delta T_N} = \frac{\sum_{i=1}^{n} \overline{\Delta T_{period,i}}}{n}\ [K] \qquad (6)$$

$$\overline{\Delta T_{period,i}} \approx \frac{|T_{in,max} - T_{out,max}| + |T_{in,min} - T_{out,min}|}{2}\ [K] \qquad (7)$$

$$\overline{q_N} = \frac{\sum_{i=1}^{n} \overline{|q_{period,i}|}}{n}\ [W/m^2] \qquad (8)$$

Where $\boldsymbol{U}$ is the U-value of the building envelope during the measurements $[\mathrm{W/(m^2 \cdot K)}]$. $\overline{\boldsymbol{q_N}}$ and $\overline{\Delta \boldsymbol{T_N}}$ are the average heat flux and temperature difference during the measurement period, respectively $[\mathrm{W/m^2}]$ $[K]$. $\overline{\boldsymbol{q_{period,i}}}$ and $\overline{\Delta \boldsymbol{T_{period,i}}}$ are the average heat flux and temperature difference during a minimum period (one day), respectively $[\mathrm{W/m^2}]$ $[\mathrm{K}]$. $\boldsymbol{n}$ is the number of the minimum period during the measurements. $\boldsymbol{T_{in,max}}$ and $\boldsymbol{T_{out,max}}$ are the maximum indoor and outdoor temperature in a minimum period, respectively $[\mathrm{K}]$. $\boldsymbol{T_{in,min}}$ and $\boldsymbol{T_{out,min}}$ are the minimum indoor and outdoor temperature in a minimum period, respectively $[\mathrm{K}]$.

Based on the average method, the average U-value can be calculated if the time interval for calculating the U-value is the complete measurement period. When dynamic U-values are calculated, the time interval for calculating each U-value needs to be shortened. For example, when dynamic U-values with 3-day time intervals are calculated, they consist of all average U-values for every 3 days during the measurement. According to ISO 9869-1, a U-value can be obtained based on at least 3 days of measurement data when the average method is used (ISO 2014). In this study, the time intervals for calculating dynamic U-values were set to 3, 5, 7, 10, 14, 20, 30, 40 and 50 days. When the total duration of the measurement is not an integer multiple of the time interval, the last period for calculating the dynamic U-values is treated as a separate period if it is more than or equal to 3 days; if it is less than 3 days, it is combined with the previous period into a single period.

Theoretically, the dynamic U-value can contain an infinite number of values owing to the constant changes in T/RH. However, it is difficult to realise in a simulation. To reasonably simplify dynamic U-values, different time intervals were chosen to calculate dynamic U-values in this study. The calculated dynamic U-values of the four tested envelopes based on different data pre-processing methods with different time intervals are shown in Chapter 5.

3.2.2 Validation of Calculation Results

The indoor T/RH simulations of the four tested rooms were used to validate the accuracy of the calculated dynamic U-values based on different data pre-processing methods with different time intervals by TRNSYS. The logic diagram of indoor T/RH simulations and U-value validation is shown in Figure 3.2.

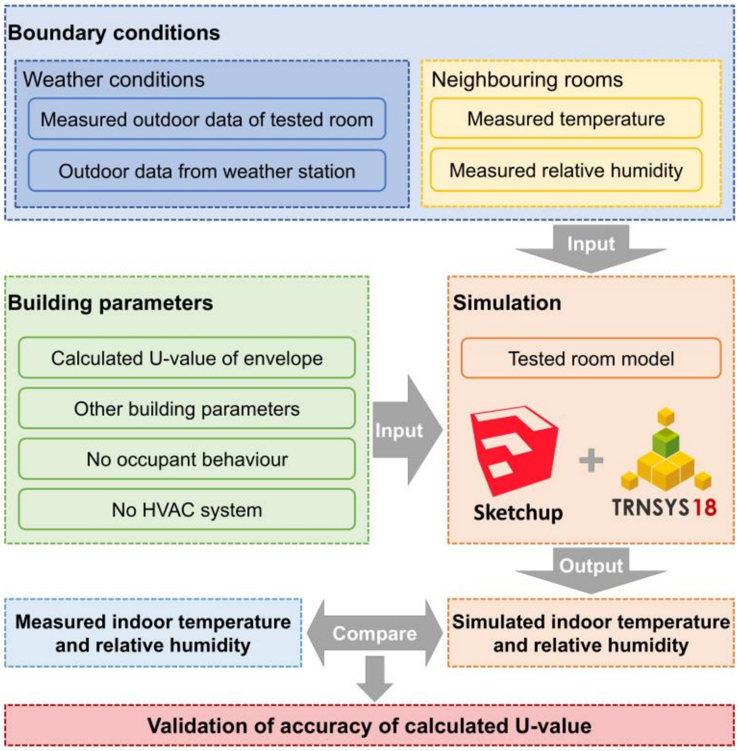

Figure 3.2 Logic diagram of indoor T/RH simulation

The steps to obtain the simulated indoor T/RH of the four tested rooms are as follows: (1) each tested room model was built by Sketchup and imported into TRNSYS by TRNSYS 3D. (2) The weather file was input into the simulation, including the measured outdoor T/RH of the tested room and other necessary data from the weather station. (3) As the indoor boundary conditions, the indoor T/RH of the neighbouring rooms were input into the simulation. (4) Building parameters of the model were set, especially the U-value of envelopes. The simulation included no occupant behaviours and HVAC systems. (5) The simulation was run, and the results were output.

The simulated indoor T/RH based on the different U-values were compared with the measured indoor T/RH of the tested rooms respectively, and the error rates of these simulated results were calculated. The U-value calculation method, which can calculate the simulation indoor T/RH with the lowest error rate, is the optimal dynamic U-value calculation method. It includes the optimal data pre-processing method with the optimal time interval. The optimal data pre-processing method will be applied before building the U-value prediction model in Chapter 6. It can reduce outliers in the data and improve the performance of the U-value prediction model. The optimal time interval will be applied to generate the predicted dynamic U-values for the operational energy consumption of buildings in different climatic zones in Chapter 7. It can improve the efficiency of the simulation by reasonably simplifying dynamic U-values.

3.3 Regression Prediction Models

Since the optimal dynamic U-values of the four tested envelopes were derived from specific climate zones and specific times, these U-values are not applicable universally. To increase the range of applicability of the dynamic U-values, U-value prediction models were developed. According to the literature review in Section 2.1, the factors that have large influences on the U-value are T/RH. Therefore, the independent variables in U-value prediction models were envelope type, indoor T/RH and outdoor T/RH. The dependent variable was the dynamic U-values of the envelope. The regression models have high applicability when they include only one dependent variable and several independent variables. Thus, the regression models were applied to U-value prediction.

The logic diagram for building the optimal model is shown in Figure 3.3. The measured indoor and outdoor T/RH of the four tested rooms and calculated U-values based on the optimal data pre-processing method were used to build the U-value prediction models. Since whether a linear relationship exists between dynamic U-values and T/RH in actual buildings is unclear, both linear and non-linear regression models were developed. These models were used in 11 case cities of different climate zones. The model that can provide reasonable results was chosen as the optimal model, and the predicted dynamic U-values by this model will be adopted for operational energy simulations of CLT and conventional buildings in Chapter 7.

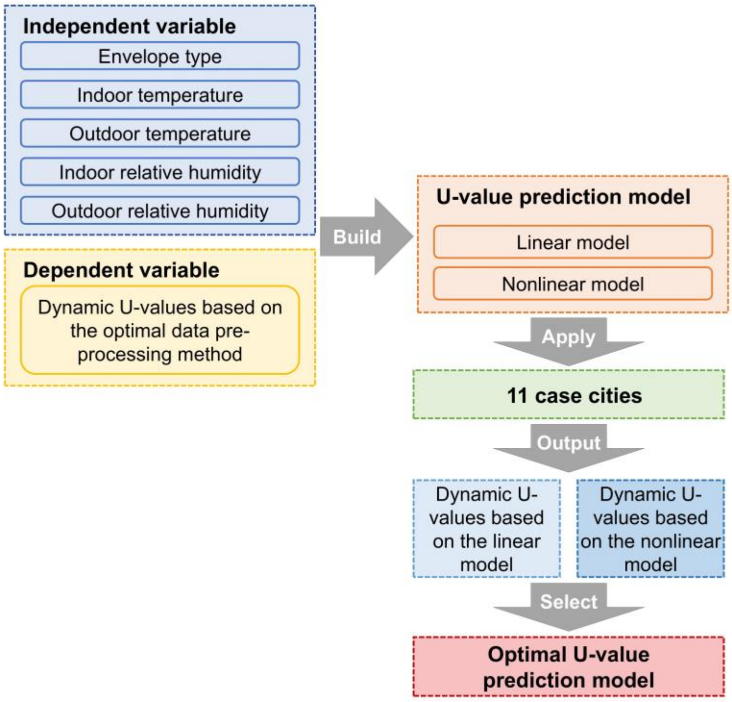

Figure 3.3 Building the optimal U-value prediction model

3.3.1 Linear Prediction Model

The linear prediction model was built by hierarchical linear regression (HLR), which is a multiple linear regression (MLR) method. In the HLR method, independent variables can be input into the model in order; this is beneficial for understanding the impact of each independent variable on the model's prediction performance. The order of inputting the independent variables can be decided based on the relevant theories of the study and the researchers' previous experience (Zhao et al. 2024; Chiriko 2023). This improves the interpretability of the linear prediction model.

In the linear U-value prediction model, independent variables included a categorical variable (the tested envelope type) and continuous variables (outdoor and indoor T/RH of the tested room), and the dependent variable was the dynamic U-values of the tested envelope. The specific steps for applying the HLR method to build the linear prediction model are shown in Chapter 6.

3.3.2 Non-linear Prediction Model

The non-linear prediction model was built by multi-layer perceptron (MLP), which is one of the most widely used types of artificial neural networks (ANN). The MLP is a black-box method that learns from datasets. It has three types of layers, including an input layer, one or more hidden layers and an output layer. The input layer can receive the raw input data, with each neuron representing an independent variable. The hidden layers have neurons which are linked to every neuron in both the input and output layers. The hidden layers can build complex non-linear relationships in data through activation functions. The neuron of the output layer can produce the final results based on the weighted sum of the activations from the last hidden layer. It has advantages in solving some complex practical problems. In this study, the MLP model's structure is shown in Figure 3.4. The specific steps for applying the MLP model to build the non-linear U-value prediction model are shown in Chapter 6.

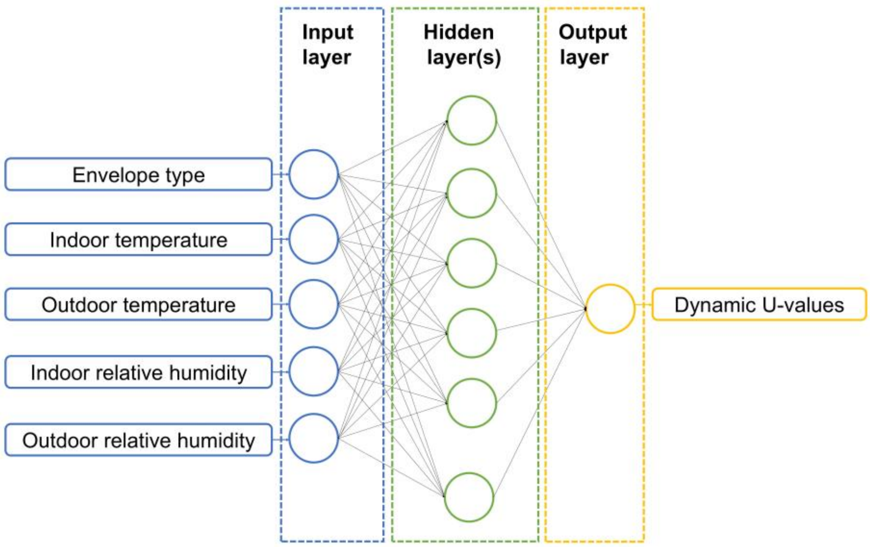

Figure 3.4 Structure of the MLP model

3.3.3 Selection of the U-value Prediction Model

Both the linear and non-linear U-value prediction models were applied in 11 case cities from different climate zones. The reasonableness of the two models' prediction results can be tested. Figure 3.5 and Table 3.1 show the geographic location and climate zones of the 11 case cities. The climate zones of the case cities can cover the main climate zones in which most countries and regions of the world are located, including tropical (A), arid (B), temperate (C) and continental (D) zones.

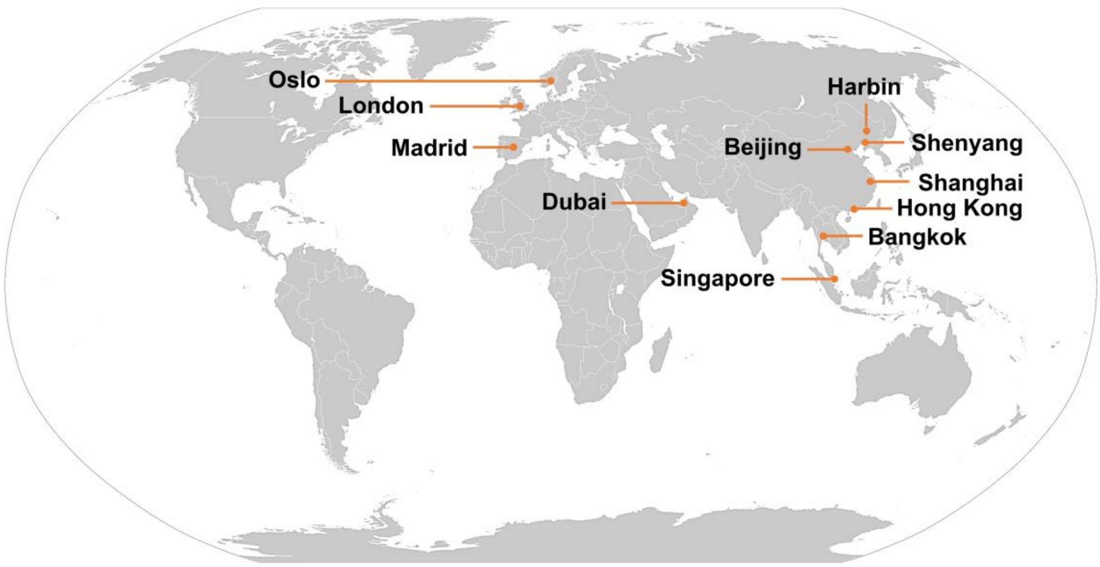

Figure 3.5 Geographic location of 11 case cities

Table 3.1 Geographic location and climate zones of 11 case cities

	Case city	Köppen climate classification		Longitude	Latitude
		Main zone	Sub-zone		
1	Singapore	Tropical (A)	Tropical wet (Af)	103°49'E	1°21'N
2	Bangkok	Tropical (A)	Tropical savanna (Aw)	100°30'E	13°45'N
3	Dubai	Arid (B)	Hot desert (BWh)	55°20'E	25°16'N

Table 3.1 (continued)

	Case city	Köppen climate classification		Longitude	Latitude
		Main zone	**Sub-zone**		
4	Hong Kong	Temperate (C)	Dry-winter humid subtropical (Cwa)	114°10'E	22°19'N
5	Shanghai	Temperate (C)	Humid subtropical (Cfa)	121°28'E	31°14'N
6	Madrid	Temperate (C)	Hot-summer mediterranean (Csa)	3°42'W	40°25'N
7	London	Temperate (C)	Temperate oceanic (Cfb)	0°08'W	51°31'N
8	Beijing	Continental (D)	Hot summer humid continental (Dwa)	116°24'E	39°54'N
9	Oslo	Continental (D)	Warm summer humid continental (Dfb)	10°45'E	59°55'N
10	Shenyang	Continental (D)	Hot summer humid continental (Dwa)	123°26'E	41°48'N
11	Harbin	Continental (D)	Hot summer humid continental (Dwa)	128°42'E	45°04'N

The hourly outdoor T/RH of 11 case cities were obtained from the weather station data. The outdoor T/RH datasets of 11 case cities were input into both the linear and non-linear U-value prediction models. The indoor T/RH were set to 22℃ and 50%. According to the American Society of Heating, Refrigerating, and Air-Conditioning Engineers (ASHRAE) recommendations, 22℃ and 50% are suitable indoor T/RH for living (Vaughn 2020). The envelope type was set in order as the CLT, masonry cavity, RC and brick. The reasonableness of predicted dynamic U-values needs to be verified based on physics. For example, the U-value of the common building envelope is usually between 0 and 2 $W/(m^2 \cdot K)$ and cannot change abruptly. The U-value prediction model, which can produce reasonable results, was chosen as the optimal U-value prediction model. Owing to the dependent variables being hourly datasets, the predicted dynamic U-values based on the optimal model consisted of hourly U-values.

3.4 Building Operational Energy Simulation

The operational energy use of the reference building was simulated in 11 case cities in different years based on the theoretical U-values, predicted average U-values and predicted dynamic U-values of the four envelopes. The predicted dynamic U-values of the four envelopes needed to be simplified by the optimal time interval to improve the simulations' efficiency. According to the simulated results, the energy impacts of dynamic U-values can be analysed in different climate zones. The operational energy use of CLT and conventional buildings can be compared. The logic diagram of the building's operational energy simulation is shown in Figure 3.6.

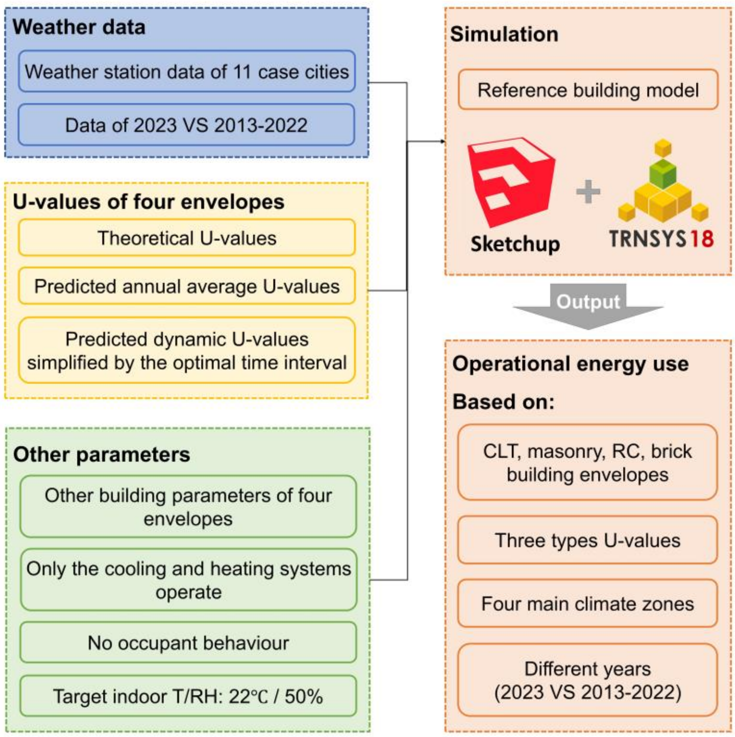

Figure 3.6 Logic diagram of the building operational energy simulation

The operational energy simulations of CLT and conventional buildings were achieved by varying the envelope parameters of the same reference building model. The weather data and building parameters were input into this model by TRNSYS. The weather files of 11 case cities in different years were obtained from the weather station data. The weather files for each city were two, one with hourly weather data for 2023 and the other with hourly weather data averaged over the 10 years (2013–2022). The theoretical, predicted annual average and predicted dynamic U-values of the four envelopes were input sequentially into the simulations.

In simulations based on theoretical U-values, material type, thickness, thermal conductivity, density, and specific heat capacity were input according to the construction specifications. For simulations based on average and dynamic U-values, adjustments to the U-values of external walls were necessary. As TRNSYS does not allow direct input of U-values, the thermal conductivities of the wall materials were modified to achieve the target U-values, while all other material parameters remained constant. When average U-values were applied, a single U-value was used throughout the entire simulation period. The initial indoor T/RH were set to the average values recorded during the first hour of in-situ measurements.

For dynamic U-value simulations, the entire simulation was divided into multiple simulations based on the time intervals used in the dynamic U-value calculation. The U-value was adjusted once for each simulation. The initial T/RH of the first simulation was based on the first hour of measured data, while for subsequent simulations, the initial indoor T/RH was set to the simulated indoor T/RH at the end of the previous simulation. This approach ensured the continuity and stability of indoor environmental simulation results.

Only the heating and cooling systems were on in the simulations, with no occupant behaviour. The indoor T/RH were set to 22°C and 50%, respectively. Finally, the simulated operational energy of CLT and conventional buildings in different years and climate zones based on three types of U-values were obtained. The simulation results are shown in Chapter 7.

3.5 Summary

Sections 3.1–3.4 describe the four phases of the methodology. First, in-situ measurements were conducted in the four tested rooms. Four tested envelopes were CLT, RC, brick and masonry cavity envelopes. Second, the U-value calculation method had to be selected. Based on the measured data, the dynamic U-values of the four tested envelopes were calculated by the average method based on different data pre-processing methods and different time intervals. The indoor T/RH simulation was used to verify which data pre-processing method and time interval could be used to obtain the optimal dynamic U-values. Third, the U-value prediction models were built based on the measured data and calculated dynamic U-values based on the optimal data pre-processing method. These models were applied to predict dynamic U-values in different climate zones. Based on the reasonableness of the prediction results, the optimal U-value prediction model was selected. Finally, the predicted dynamic U-values were reasonably simplified by the optimal time interval. The theoretical, average and dynamic U-values were used for simulating the operational energy use of CLT, masonry cavity, RC and brick buildings in different climate zones and years. The energy impacts of dynamic U-values can be analysed based on the simulation results, and the operational energy use of CLT and conventional buildings can be compared.

Chapter 4 In-situ Measurements for Dynamic U-values

In-situ measurements were conducted to collect the required datasets for calculating dynamic U-values of the CLT, masonry cavity, RC and brick envelopes. The detailed information of tested cities and tested envelopes are introduced in Sections 4.1 and 4.2, respectively. The measurement duration and equipment are introduced in Section 4.3. The measurement process is introduced in Section 4.4. The results of in-situ measurements, including indoor and outdoor T/RH and heat flux, are shown in Section 4.5.

4.1 Tested Cities

According to the literature review, the dynamic U-value is related to the T/RH. In an ideal situation, in-situ measurements should be conducted in all climate zones to comprehensively capture the fluctuation characteristics of dynamic U-values under different T/RH conditions. However, due to limitations in time, budget, and available resources, in-situ measurements in this study were restricted to buildings located in three cities, covering climate zones C and D. Compared with climate zones A, B and E, climate zones C and D have greater variations in year-round temperature and relative humidity, as shown in Table 4.1. In subsequent stages of this research, U-value prediction models were developed using T/RH as independent variables, allowing dynamic U-values in other climate zones to be predicted and thereby compensating for the lack of direct measurements in those regions.

Three tested cities (Sheffield, Ninghai and Harbin) were selected in the C and D zones. Figure 4.1 and Table 4.1 show the geographic location and meteorological information of the three tested cities. The meteorological data in Table 4.1 refer to the weather station data of the year in which the measurement was taken. In the Köppen climate classification, Sheffield is under the Cfb category with temperate oceanic climate;

Ninghai is under the Cfa category with a humid subtropical climate, and Harbin is under the Dwa category with a monsoon-influenced humid continental climate. The annual T/RH fluctuation in the three cities exceeded 40℃ and 80%, respectively. The difference between the highest and lowest temperatures in Harbin was even greater than 60℃. The significant environmental fluctuations in the three cities are beneficial for studying dynamic U-values under various conditions.

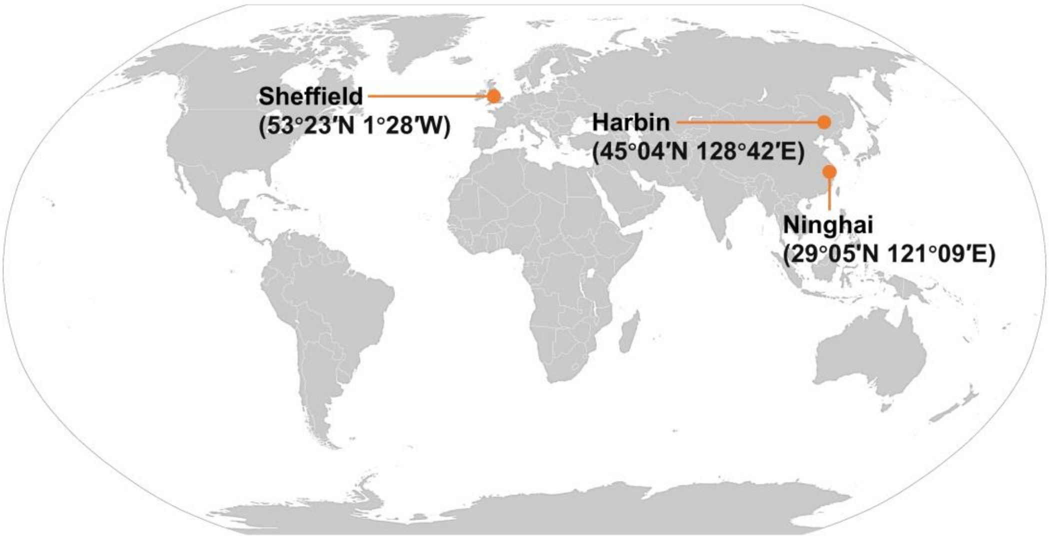

Figure 4.1 Geographic location of three tested cities

Table 4.1 Meteorological information of three tested cities

Parameter	Sheffield	Ninghai	Harbin
Köppen climate classification	Cfb	Cfa	Dwa
Average annual temperature	10.5℃	18.5℃	5.2℃
Annual maximum temperature	37.6℃	38.2℃	34.1℃
Annual minimum temperature	-5.3℃	-4.7℃	-32.2℃
Average annual RH	80.0%	76.7%	66.6%
Annual maximum RH	100.0%	100.0%	100.0%
Annual minimum RH	16.5%	19.9%	10.6%

Data source: weather station data for Sheffield in 2022 and for Ninghai and Harbin in 2023

4.2 Tested Envelopes

The in-situ measurements included one CLT tested envelope and three conventional tested envelopes consisting of a masonry cavity, an RC and a brick envelope. Table 4.2 and Figures 4.2–4.4 introduce the buildings and rooms where the tested envelopes are located. Table 4.2 shows the basic information of the four tested cases. Figure 4.2 shows the photos of the four tested buildings. Figure 4.3 shows the models of the four tested rooms. Figure 4.4 shows the floor plans and sections of the tested rooms and their adjoining rooms.

The CLT envelope is in a temporary bedroom in a demo building built in Ninghai in 2018. This CLT building was built by the Ningbo Sino-Canada Low-Carbon Technology Research Institute and is dedicated to empirical studies related to CLT. As shown in Figure 4.2 (a), the CLT building has two floors. The in-situ measurements for this study were conducted on the first floor. As shown in Figure 4.3 (a), the tested room has four external envelopes, and the tested envelope is the north envelope with an external window. As shown in Figure 4.4(a), the CLT tested room has only one neighbouring room, which is a warehouse for equipment on the ground floor.

The masonry cavity envelope is in a bedroom of a residential building built in Sheffield in the 1980s. As shown in Figure 4.2 (b), the building consists of four floors – three built above ground and one underground. The tested room is on the ground floor. As shown in Figure 4.3 (b), the tested room has only one external envelope, which was the tested envelope. As shown in Figure 4.4 (b), the tested room has an upstairs bedroom, a downstairs kitchen, two living rooms in the east and west adjacent spaces and a toilet in the south adjacent space.

The RC envelope is in a bedroom of a residential building built in Harbin in 2010. As shown in Figure 4.2 (c), the building consists of 12 floors, and the tested room is on the 9th floor. As shown in Figure 4.3 (c), the tested room has only one external envelope, which was the tested envelope. As shown in Figure 4.4 (c), the tested room has upstairs and downstairs bedrooms, a kitchen in the east adjacent spaces, a toilet in the south adjacent spaces and a bedroom in the west adjacent space.

The brick envelope is in a bedroom of a residential building built in Harbin in the 1980s. As shown in Figure 4.2 (d), the building consists of eight floors. The tested room is on the sixth floor. As shown in Figure 4.3 (d), the tested room has only one external envelope, which was the tested envelope. As shown in Figure 4.4 (d), the tested room has upstairs and downstairs bedrooms, a kitchen in the east adjacent spaces, a living room in the south adjacent spaces, and a bedroom in the west adjacent space.

Table 4.2 Basic information of the four tested cases

Case	**CLT**	**Masonry**	**RC**	**Brick**
Location	Ninghai	Sheffield	Harbin	Harbin
Year built	2018	1980s	2010	1980s
Tested building type	Demo building	Residential building	Residential building	Residential building
Tested room type	Temporary bedroom	Bedroom	Bedroom	Bedroom
Floor of tested room	1st floor	Ground floor	9th floor	6th floor

(a) CLT building

(b) Masonry building

(c) RC building

(d) Brick building

Figure 4.2 Photos of tested buildings

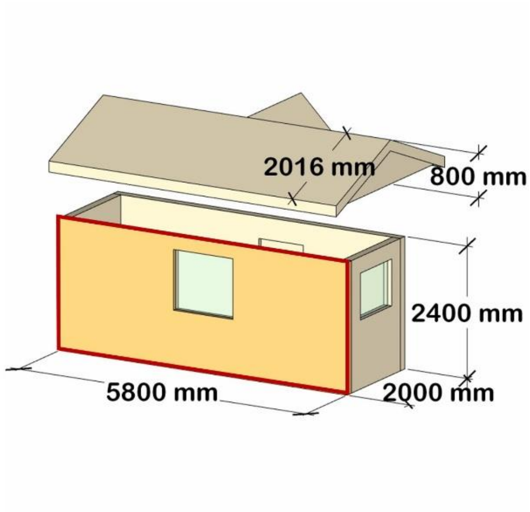

(a) CLT room

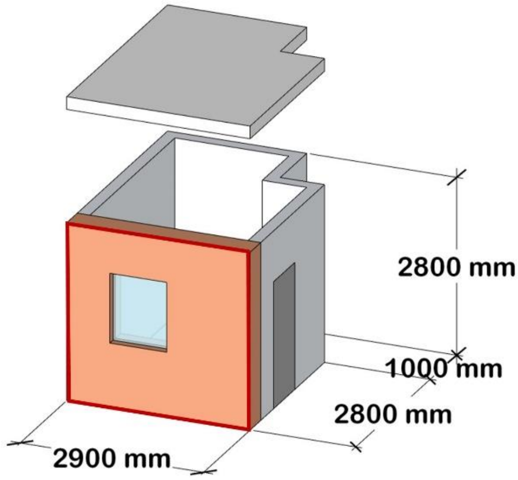

(b) Masonry room

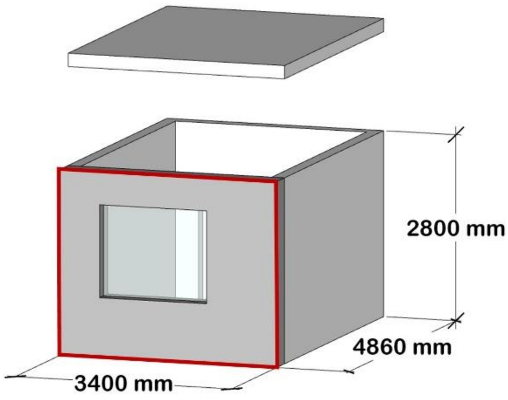

(c) RC room

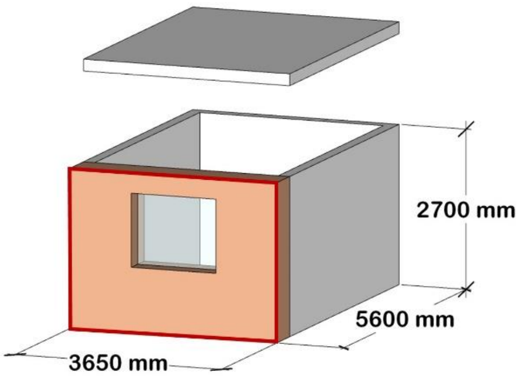

(d) Brick room

Figure 4.3 Models of tested rooms (red line: tested envelopes)

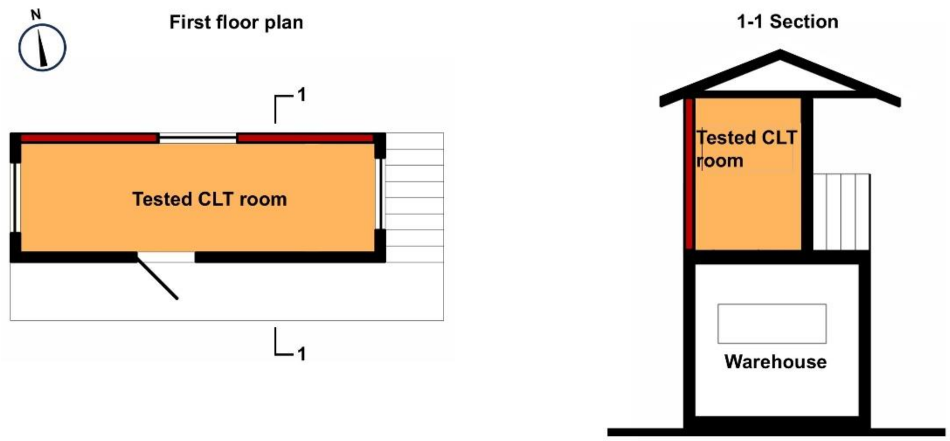

(a) CLT room

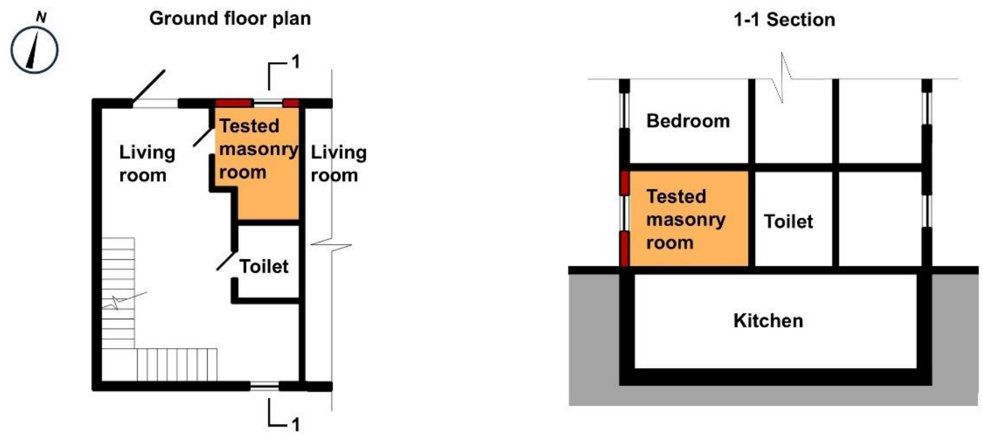

(b) Masonry room

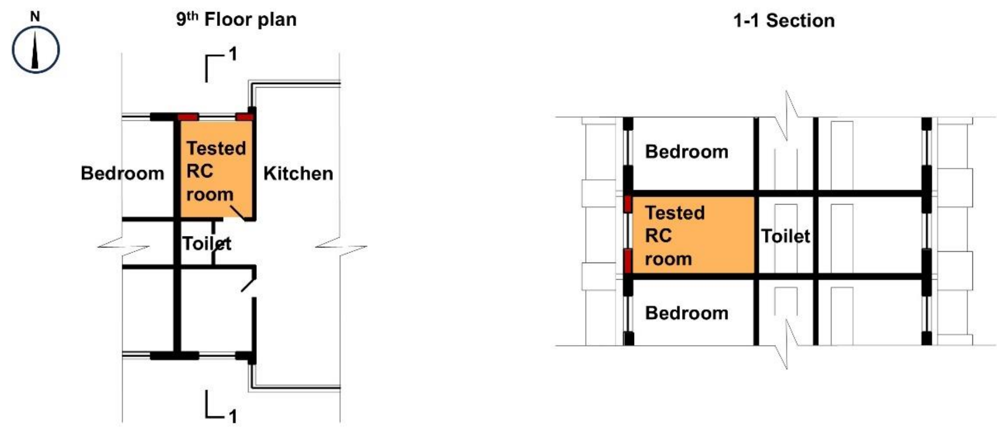

(c) RC room

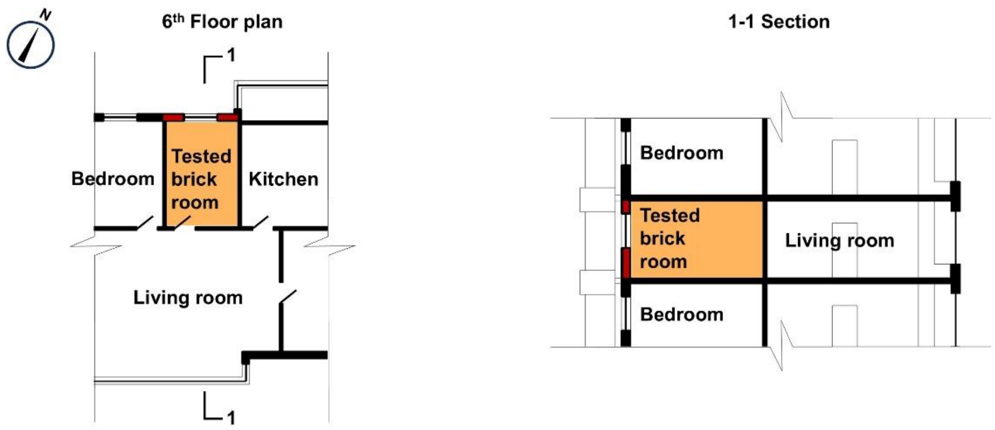

(d) Brick room

Figure 4.4 Floor plans and sections of tested rooms (red line: tested envelopes)

All tested envelopes are north exterior envelopes. According to ISO 9869-1, the preferred envelope for the U-value measurement is the north envelope (in the northern hemisphere), which can reduce the effect of solar radiation (ISO 2014). Excessive solar radiation may cause the outdoor temperature sensor to measure a higher temperature than the actual outdoor temperature. It may also cause a rapid increase in heat flux through the envelopes, resulting in an unreasonably high U-value.

Three tested rooms with conventional envelopes are bedrooms in residential buildings. All these rooms are not on the bottom or top floor and have only one north exterior envelope as the tested envelope. These consistent location conditions can reduce the influence of extraneous factors on U-values and are beneficial for comparing the dynamic U-values of different tested envelopes. Compared to conventional buildings, the extant CLT buildings are considerably fewer. Thus, finding a CLT room with the same location conditions as that of the other three rooms is difficult. Finally, this study chose to conduct the measurements in a demo building. Because this CLT room can be measured for a long period of time and has a north exterior envelope as the tested envelope, it meets the necessary requirements of this study.

The window-to-wall ratios and dimensions of the four test rooms are different.

According to the HFM method (ISO 2014), the measured U-values are calculated by the indoor and outdoor temperatures and heat flux. The window-to-wall ratios and the room dimensions are not considered in the U-value calculation, although it could influence indoor environment.

The detailed construction of the four tested envelopes is presented in Table 4.3. The tested CLT envelope is made of a five-layer CLT panel with exterior finishes. This type of CLT panel is one of the most common timber building materials. Masonry cavity envelopes have been the most common external envelopes in the UK since the 1920s. This type of envelope comprises two leaves with a cavity. The leaves of the tested envelope are made of bricks or concrete blocks. For better insulation, the cavity part of the tested envelope was filled with insulation materials; this practice is a common way of retrofitting old buildings in the UK (Vagtholm et al. 2023). Both the tested RC and brick envelopes are exterior insulated envelopes. RC and brick envelopes are used widely in the northeast of China. Clay brick envelopes were the most used before the 1990s; however, clay bricks were restricted in the 2000s because clay is obtained from arable land, which is an important but limited resource. Since then, RC envelopes have become the most important building envelope in China (NDRC 2011).

The theoretical U-values of the tested envelopes were calculated by Equations (9) and (10). This method is derived from ISO 6946 (ISO 2007).

$$U = 1/(R_{se} + R_{si} + R_1 + R_2 + R_3 + \cdots + R_N)\ [W/(m^2 \cdot K)] \tag{9}$$

$$R = D/\lambda\ [(m^2 \cdot K)/W] \tag{10}$$

where $\boldsymbol{R_{se}}$ and $\boldsymbol{R_{si}}$ are the thermal resistance of the exterior and interior surface, respectively; $\boldsymbol{R_1 + R_2 + R_3 + \cdots + R_N}$ is the sum of thermal resistance of all layers of the envelope $[(\mathrm{m}^2 \cdot \mathrm{K})/\mathrm{W}]$. $\boldsymbol{D}$ and $\boldsymbol{\lambda}$ are the thickness and thermal conductivity of the building material, respectively $[\mathrm{m}]$ $[\mathrm{W}/\mathrm{m} \cdot \mathrm{K})]$. According to ISO 6946, $\boldsymbol{R_{se}}$ and $\boldsymbol{R_{si}}$ are set to 0.04 $(\mathrm{m}^2 \cdot \mathrm{K})/\mathrm{W}$ and 0.13 $(\mathrm{m}^2 \cdot \mathrm{K})/\mathrm{W}$, respectively (ISO 2007).

Table 4.3 Detailed construction of the four tested envelopes

Test envelope		Material	Thickness [mm]	Conductivity [W/(m · K)]	Density [kg/(m^3)]	Specific Heat Capacity [J/(kg · K)]	Layering sketch
CLT	1	CLT panel	140	0.12	500	1500	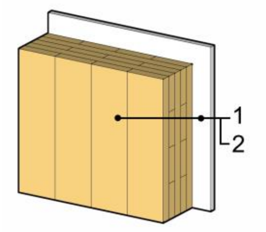
	2	Finishes	15	0.19	950	840	
Mas-onry cavity	1	Plaster broad	12.5	0.17	950	840	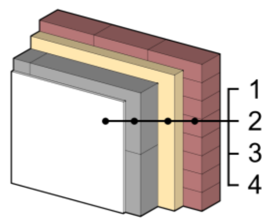
	2	Concrete block	100	1.10	1950	900	
	3	Mineral wool	50	0.04	130	850	
	4	Clay brick	102.5	0.78	1700	840	
RC	1	Cement mortar	10	0.93	1800	1050	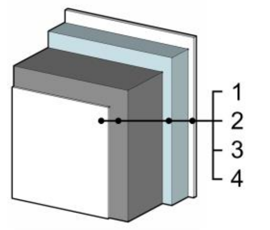
	2	RC	210	1.75	2500	920	
	3	EPS broad	100	0.03	28.5	1650	
	4	Cement mortar	15	0.93	1800	1050	

Table 4.3 (continued)

Test envelope		Material	Thickness [mm]	Conductivity $[W/(m \cdot K)]$	Density $[kg/(m^3)]$	Specific Heat Capacity $[J/(kg \cdot K)]$	Layering sketch
Brick	1	Cement mortar	10	0.93	1800	1050	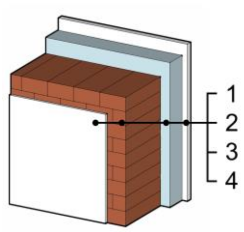
	2	Clay brick	240	0.78	1700	840	
	3	EPS broad	80	0.03	28.5	1650	
	4	Cement mortar	20	0.93	1800	1050	

Theoretical U-value:

CLT tested envelope: 0.71 $W/(m^2 \cdot K)$; Masonry cavity tested envelope: 0.39 $W/(m^2 \cdot K)$

RC tested envelope: 0.27 $W/(m^2 \cdot K)$; Brick tested envelope: 0.32 $W/(m^2 \cdot K)$

4.3 Measurement Duration and Equipment

The measurement duration of the four tested envelopes is shown in Table 4.4. To observe the fluctuation of U-values in different T/RH, all tested envelopes were measured for a long period, and the measurement duration of every tested envelope included the summer, transition season and winter. The CLT envelope was measured for 144 days, from 4 February to 27 June 2023. The masonry cavity envelope was measured for 150 days, from 17 July to 13 December 2022.

The total measurement period in China was limited to around six months. Only two sets of equipment were available. One set was used to continuously measure the CLT envelope in Ninghai. The other set was used to alternately measure the brick and RC envelopes from 16 January to 15 July 2023. Both RC and brick tested envelopes were measured six times separately. The duration of each measurement was around 2 weeks. According to ISO 9869-1, the in-situ U-value measurement should not be conducted in less than 3 days to obtain reliable results when the HFM and average methods are used to collect data and calculate the U-value, respectively (ISO 2014). At the same time, if the measurement duration for one envelope exceeded two weeks, significant fluctuations in outdoor T/RH could occur during this period. As a result, when switching to the other envelope, some outdoor T/RH data may no longer be captured, leading to gaps in the outdoor T/RH coverage for the other envelope.

Table 4.4. Measurement duration of the four tested envelopes

Tested envelope	Measurement duration	
CLT envelope	2023.02.04 – 2023.06.27 (144D)	
Masonry cavity envelope	2022.07.17 – 2022.12.13 (150D)	
RC envelope	2023.02.02 – 2023.02.13 (12D)	2023.03.03 – 2023.03.14 (12D)
	2023.04.03 – 2023.04.14 (12D)	2023.05.01 – 2023.05.14 (14D)
	2023.06.02 – 2023.06.14 (13D)	2023.07.03 – 2023.07.15 (13D)
Brick envelope	2023.01.16 – 2023.01.29 (14D)	2023.02.15 – 2023.03.01 (15D)
	2023.03.16 – 2023.03.31 (16D)	2023.04.16 – 2023.04.29 (14D)
	2023.05.16 – 2023.05.31 (16D)	2023.06.16 – 2023.07.01 (16D)

The in-situ measurements included three types of equipment: heat flux meters, T/RH recorders and a data logger (shown in Figure 4.5). The parameters of this equipment are shown in Table 4.5. The data logger links to the heat flux meters for recording heat flux data. In Harbin, winter temperatures can drop below -20°C. Therefore, T/RH recorders with a wider measurement range than common T/RH recorders were selected to ensure accurate data collection under extreme conditions. To improve measurement precision, heat flux meters with higher accuracy than standard devices were used. In addition, two heat flux meters were installed in each measurement to reduce random errors. The data logger was configured to upload recorded data to a cloud platform in real-time, allowing continuous monitoring of data quality and minimising the risk of data loss.

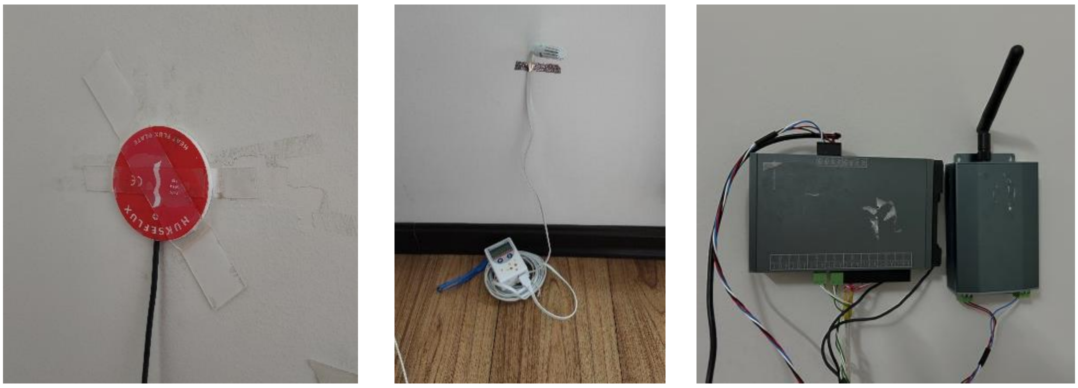

(a) Heat flux meter (b) T/RH recorder (c) Data logger

Figure 4.5 Photos of equipment

Table 4.5 Parameters of equipment

Equipment	Heat flux meter	T/RH recorder	Data logger
Brand	Hukseflux	JDRK	Yustek
Model	HFP01	COS-04	IUDAQ 256-8
Measuring range	-2000 to +2000 W/m^2	T: -40 to +80 ℃ RH: 0 to +100 %	NA
Accuracy	± 3 %	T: ±0.1 ℃ RH: ±1.5 %	NA
Resolution	0.001 W/m^2	T: 0.1 ℃ RH: 0.1 %	NA

4.4 Measurement Process

In tested rooms, the U-value measurement process referred to the HFM method in

ISO 9869-1 (ISO 2014). Before measurement, the four tested envelopes were checked with a thermal imager to ensure that the envelopes had uniform heat transfer and no thermal bridges in tested area, as shown in Figure 4.6.

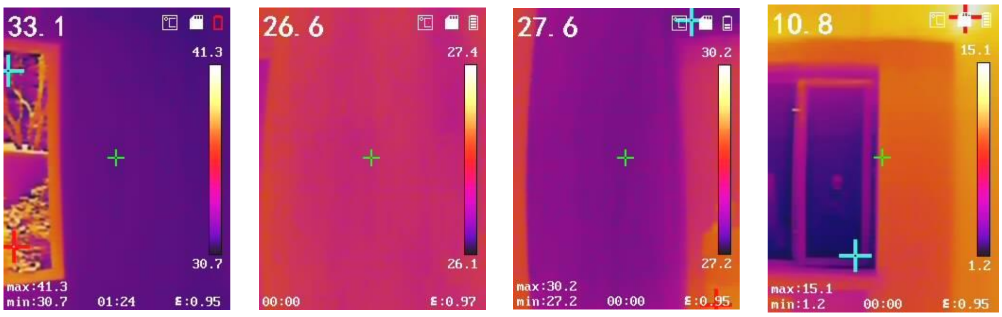

(a) CLT (b) Masonry cavity (c) RC (d) Brick

Figure 4.6 Thermal images of tested envelopes

The U-value measurement equipment included (1) two heat flux meters, (2) a heat flux data logger and (3) two T/RH recorders. All equipment was calibrated by the manufacturer before measurements. The two T/RH recorders and the heat flux data logger were used every 5 minutes during the measurement periods. The heat flux meters were installed at 1.5 m height from the floor and between windows and corners to avoid the impacts from thermal bridges of window-to-wall joints and wall-to-wall joints. In order to ensure that the heat flux meters can stay close to the inner surface of the envelope for a long period of time, nano tape and aluminium foil tape was used. The sketch of the tested envelope with all equipment is shown in Figure 4.7. The photographs of heat flux meters during the measurement periods are shown in Figure 4.8.

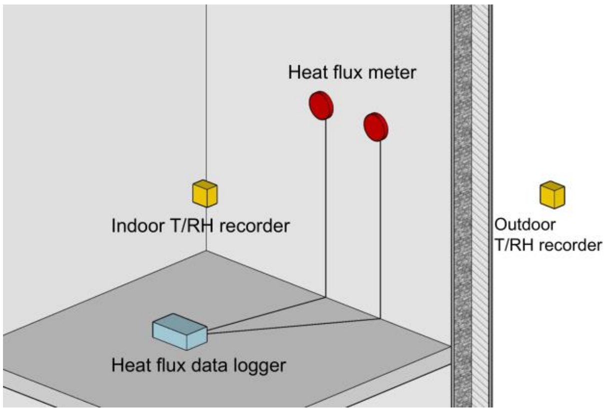

Figure 4.7 Sketch of the tested envelope with equipment

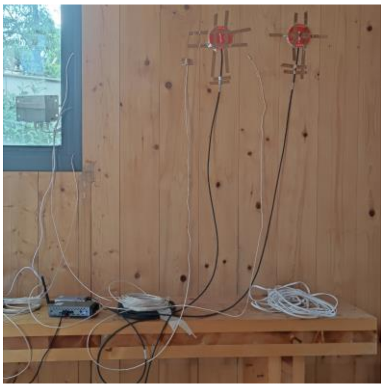

(a) CLT envelope

(b) Masonry cavity envelope

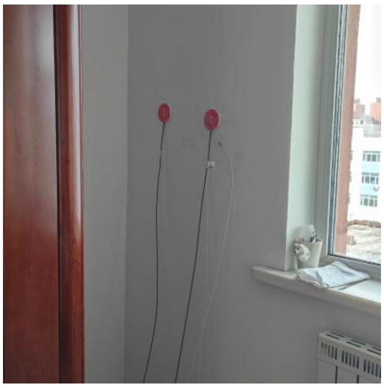

(c) RC envelope

(d) Brick envelope

Figure 4.8 Photographs of heat flux meters during measurements

During the measurements, the tested rooms were not occupied. The doors and windows were always closed, and no temperature control devices were switched on. The first reason for these operations is to reduce the impacts of human factors on heat flux through the envelopes. The second reason is for verifying the accuracy of the calculated

U-values (see Chapter 5 for details). The verification method involves inputting the calculated U-values into the indoor T/RH simulations of the tested rooms. The simulated T/RH are compared with the measured indoor T/RH to determine the accuracy of the calculated U-values. The indoor T/RH simulations require inputting the room operating conditions, such as the power and operating time of the heating system and occupant behaviours. Since three tested rooms (masonry cavity, RC and brick room) applied central heating systems, calculating their power was difficult. Occupant behaviours are random, and accurately recording occupant behaviours over a long time would be complicated. Therefore, to accurately conduct the indoor T/RH simulations of the tested rooms, all the effects of HVAC equipment and occupant behaviours were excluded.

The implementation of measurements in neighbouring rooms is shown in Table 4.6. The CLT tested room has only one neighbouring room, and each of the other three tested rooms has five neighbouring rooms. The indoor T/RH were measured in most neighbouring rooms. Five neighbouring rooms were not measured owing to the lack of permission from neighbours. In subsequent indoor T/RH simulations of each tested room, the indoor T/RH of the neighbouring rooms that were not measured were replaced by the indoor T/RH of other neighbouring rooms with the same function.

Table 4.6 Implementation of measurements in neighbouring rooms of the tested rooms

	CLT room	**Masonry room**	**RC room**	**Brick room**
Upstairs	NA	Yes (Bedroom)	Yes (Bedroom)	No (Bedroom)
Downstairs	Yes (Warehouse)	Yes (Kitchen)	No (Bedroom)	No (Bedroom)
South	NA	Yes (Toilet)	Yes (Toilet)	Yes (Living room)
East	NA	No (Living room)	Yes (Kitchen)	Yes (Kitchen)
West	NA	Yes (Living room)	No (Bedroom)	Yes (Bedroom)

(Note: NA: No neighbouring room in this direction; Yes: Measured; No: Unmeasured)

4.5 Results

Figures 4.9–4.12 show the measurement results of the four tested rooms, including indoor and outdoor T/RH in the tested rooms and heat flux through the tested envelopes. The heat flow data in Figures 4.9–4.12 are the average of the data measured by the two heat flux meters. The temperature difference in Figures 4.9–4.12 was the difference between the indoor temperature minus the outdoor temperature of the four tested rooms according to Equation (3).

The measured data in the CLT tested room are shown in Figure 4.9. During the measurement (04.02.2023–27.06.2023), the indoor temperature fluctuated from 5.5°C to 35.0°C, and the outdoor temperature fluctuated from 2.1°C to 36.0°C. The average indoor and outdoor temperatures were 19.5°C and 18.4°C, respectively. The indoor relative humidity fluctuated from 52% to 78%, and the outdoor relative humidity fluctuated from 14% to 99%. The average indoor and outdoor relative humidity was 68% and 74%, respectively. The heat flux through the CLT tested envelope fluctuated from -7.0 $\mathrm{W/m^2}$ to 8.3 $\mathrm{W/m^2}$. The average heat flux was -0.2 $\mathrm{W/m^2}$. The temperature difference fluctuated from -14.0°C to 8.3°C. The average temperature difference was 1.2°C. The measurement results showed that the indoor environment was influenced by the outdoor environment to a greater extent because the CLT tested room consisted of four external envelopes. The heat flux and temperature difference often reversed direction during the whole measurement period.

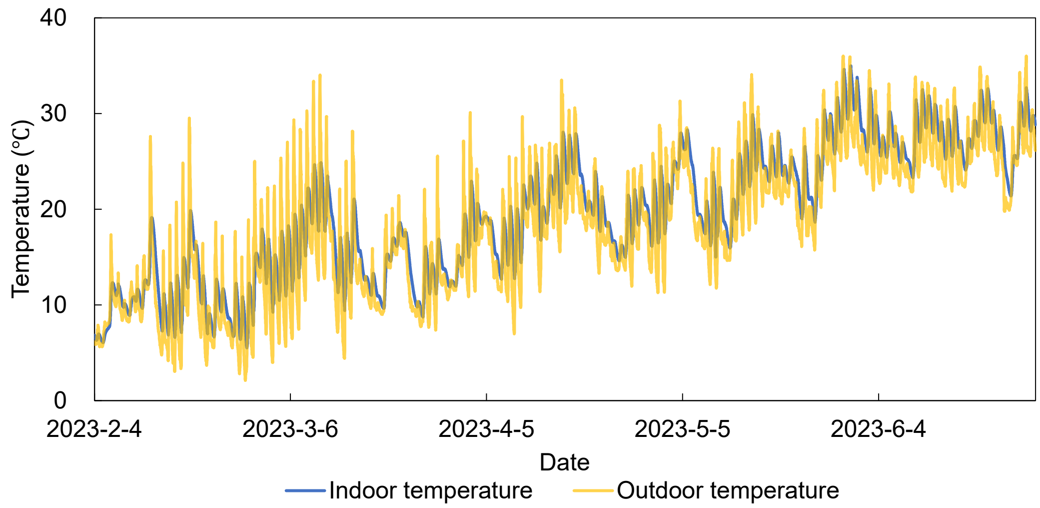

(a) Indoor and outdoor temperature

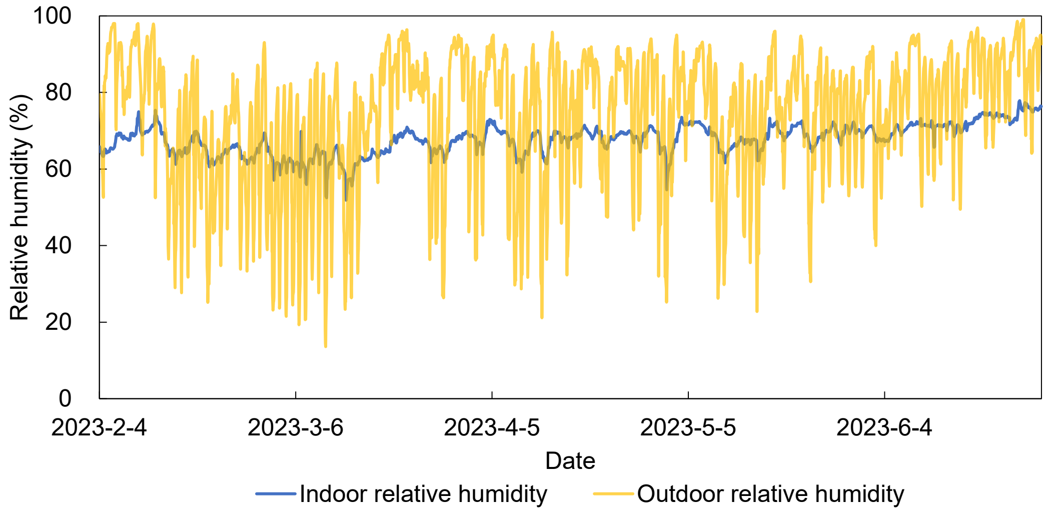

(b) Indoor and outdoor relative humidity

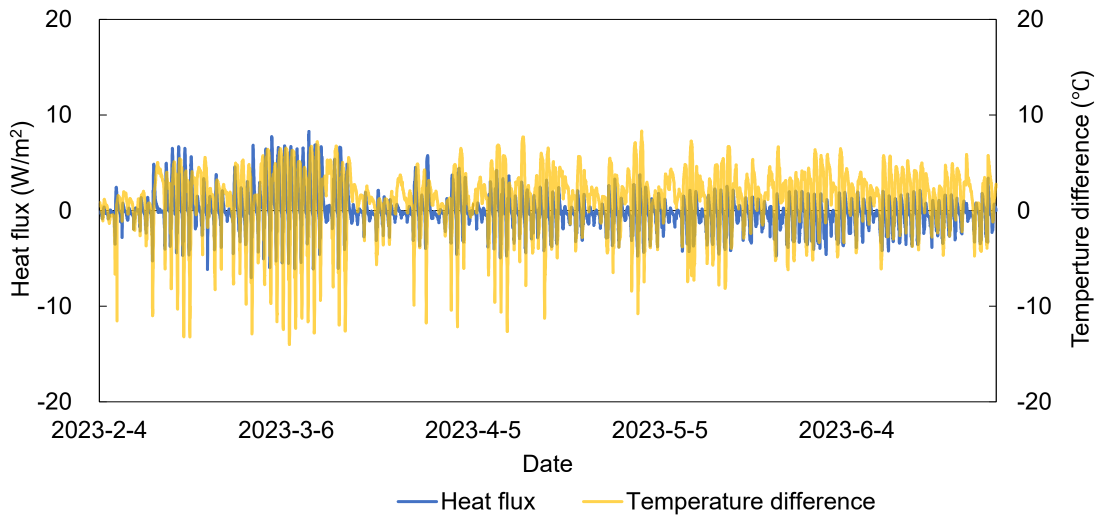

(c) Temperature difference and heat flux

Figure 4.9 Measured data of the CLT tested room

The measured data in the masonry tested room are shown in Figure 4.10. During the measurement (17.07.2022–13.12.2022), the indoor temperature fluctuated from 15.5℃ to 29.6℃, and the outdoor temperature fluctuated from -3.9℃ to 44.2℃. The average indoor and outdoor temperatures were 21.7℃ and 14.1°C, respectively. The indoor relative humidity fluctuated from 31% to 47%, and the outdoor relative humidity fluctuated from 12% to 100%. The average indoor and outdoor relative humidity was 47% and 78%, respectively. The heat flux through the masonry cavity tested envelope fluctuated from -7.1 W/m^2 to 16.5 W/m^2. The average heat flux was 4.5 W/m^2. The temperature difference fluctuated from -16.3℃ to 20.1℃. The average temperature difference was 7.6℃. The measurement results showed that the indoor environment of the masonry cavity tested room was relatively stable in winter because it was affected by the neighbouring rooms. The neighbouring rooms had heating systems during the winter. However, the heat flux and temperature difference always reversed direction during the summer.

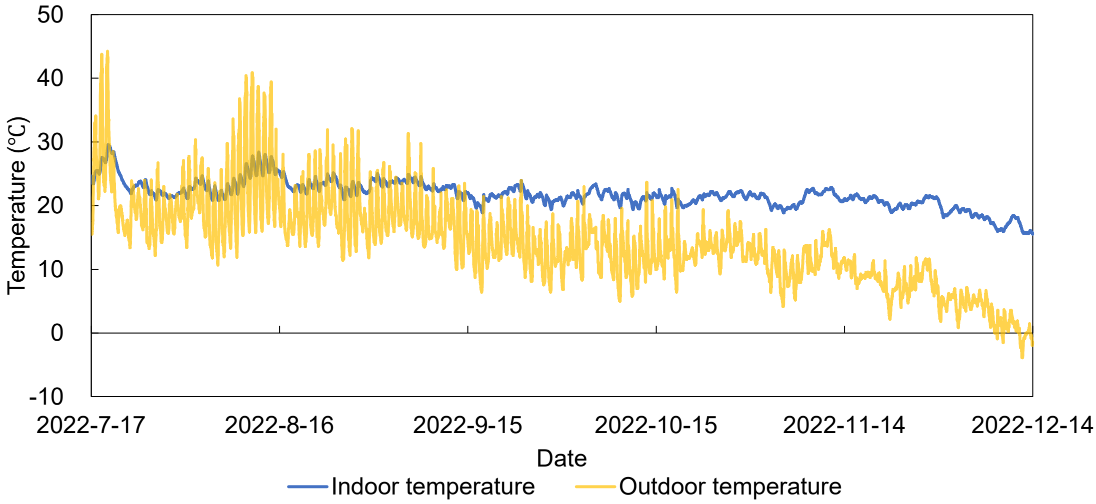

(a) Indoor and outdoor temperature

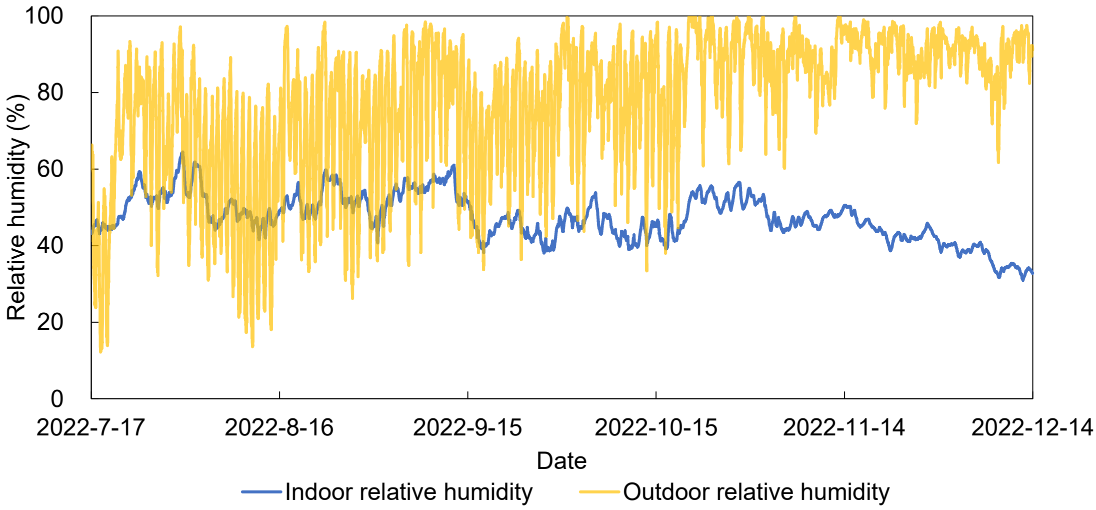

(b) Indoor and outdoor relative humidity

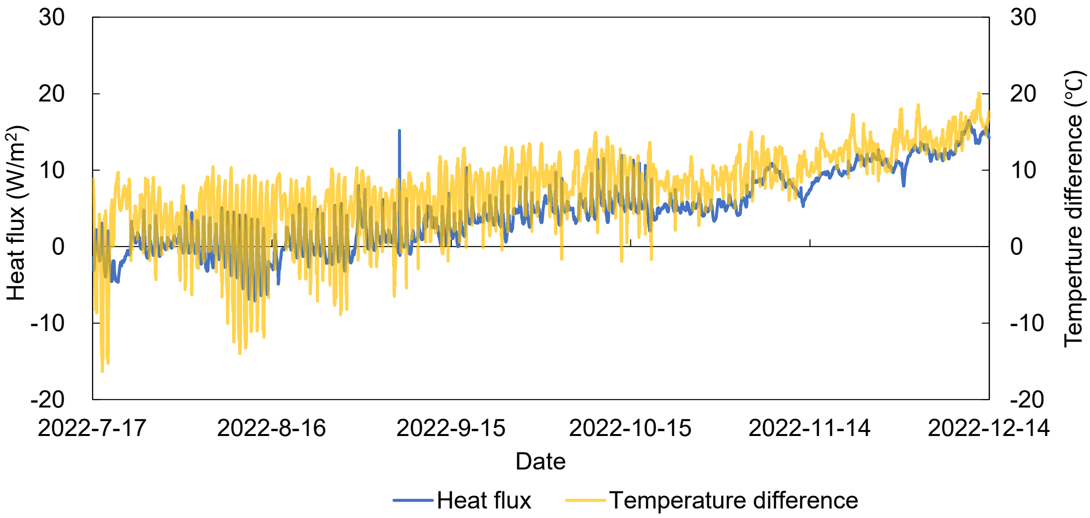

(c) Temperature difference and heat flux

Figure 4.10 Measured data of the masonry tested room

The measured data in the RC tested room are shown in Figure 4.11. During the six measurements from 02.02.2023 to 15.07.2023, the indoor temperature fluctuated from 20.2℃ to 28.9℃, and the outdoor temperature fluctuated from -17.8℃ to 34.6℃. The average indoor and outdoor temperatures were 23.9℃ and 10.9℃, respectively. The indoor relative humidity fluctuated from 17% to 51%, and the outdoor relative humidity fluctuated from 15% to 100%. The average indoor and outdoor relative humidity was 37% and 55%, respectively. The heat flux through the RC tested envelope fluctuated from -0.5 W/m^2 to 13.3 W/m^2. The average heat flux was 4.6 W/m^2. The temperature difference fluctuated from -6.3℃ to 38.9℃. The average temperature difference was 13.1℃. The characteristics of the measurement results of the RC tested room are similar to those of the masonry cavity tested room.

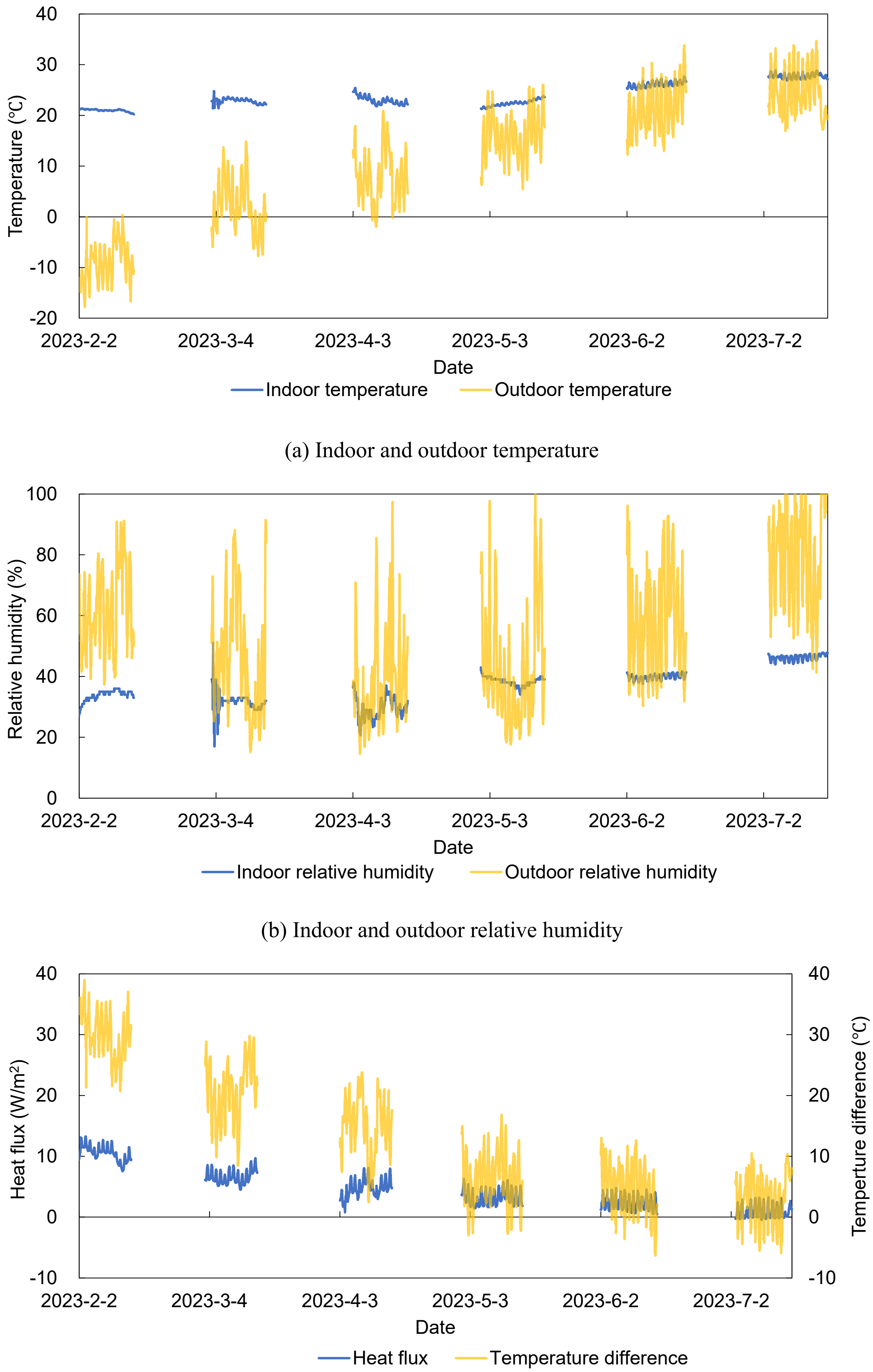

(a) Indoor and outdoor temperature

(b) Indoor and outdoor relative humidity

(c) Heat flux and temperature difference

Figure 4.11 Measured data of the RC tested room

The measured data in the brick tested room are shown in Figure 4.12. During the six measurements from 16.01.2023 to 01.07.2023, the indoor temperature fluctuated from 16.0℃ to 33.3℃, and the outdoor temperature fluctuated from -28.8℃ to 37.2℃. The average indoor and outdoor temperatures were 21.6℃ and 6.5℃, respectively. The indoor relative humidity fluctuated from 25% to 51%, and the outdoor relative humidity fluctuated from 11% to 100%. The average indoor and outdoor relative humidity was 36% and 50%, respectively. The heat flux through the brick tested envelope fluctuated from -1.7 W/m^2 to 28.9 W/m^2. The average heat flux was 7.9 W/m^2. The temperature difference fluctuated from -8.3℃ to 45.9℃. The average temperature difference was 15.1℃. The characteristics of the measurement results of the brick tested room are also similar to those of the masonry cavity and RC tested rooms.

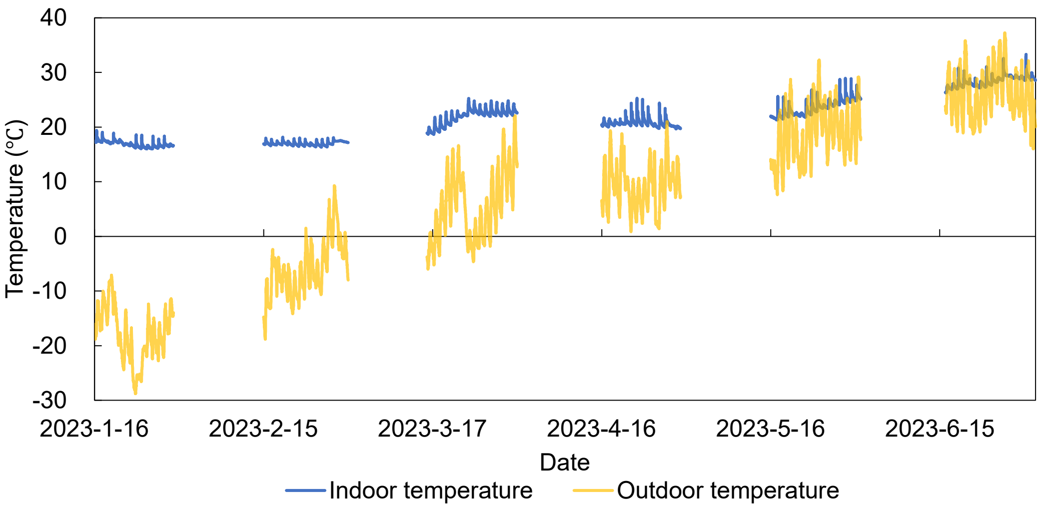

(a) Indoor and outdoor temperature

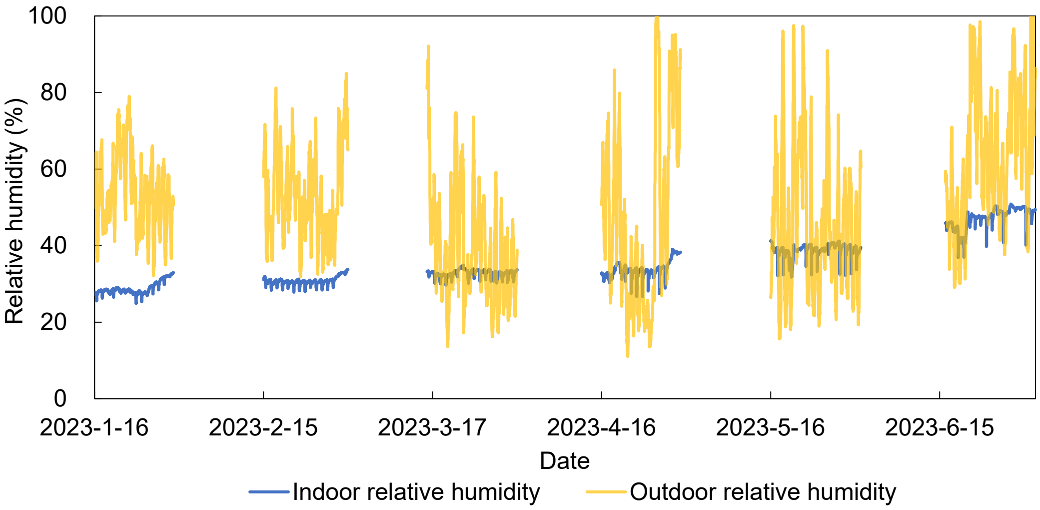

(b) Indoor and outdoor relative humidity

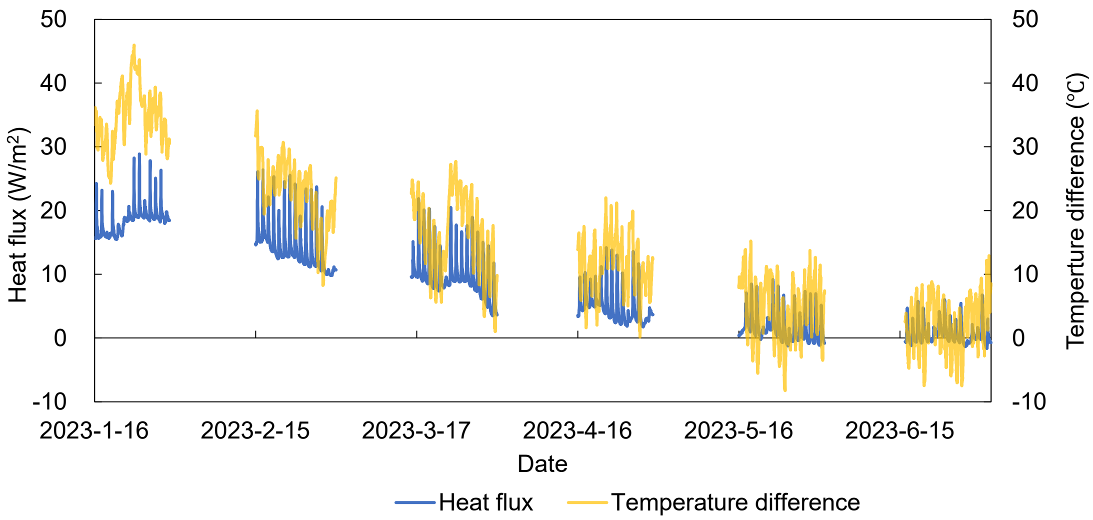

(c) Heat flux and temperature difference

Figure 4.12 Measured data of the brick tested room

The measured indoor T/RH of the neighbouring rooms of the four tested rooms are detailed in Appendix (A). These data only used as simulation boundary conditions in the indoor environment simulations in Chapter 5.

4.6 Summary

This chapter provided the key information on in-situ measurements. First, it introduced three tested cities (Sheffield in the UK and Ninghai and Harbin in China). Second, it showed the detailed information on four tested envelopes, including the tested buildings, tested rooms, neighbouring rooms and constructions and building parameters of the tested envelopes. Third, it introduced the measurement duration and equipment. Every tested envelope was measured in the summer, transition season and winter. The main equipment included T/RH recorders, heat flux meters and a data logger. Fourth, the specific measurement process was described in detail. The HFM method was used for measurements. Finally, the important measurement results were shown, including indoor and outdoor T/RH of the four tested rooms and heat flux through four tested envelopes.

Chapter 5 Determination of the Dynamic U-value Calculation Methods

After obtaining the measured indoor and outdoor T/RH of the four tested rooms and the measured heat flux through four tested envelopes, both dynamic and average U-values of the four tested envelopes were calculated by different data pre-processing methods and time intervals. All calculated dynamic and average U-values of the four tested envelopes are shown in Appendix (B). To verify the accuracy of different U-values, the indoor T/RH simulations of the four tested rooms were conducted by TRNSYS, as shown in Section 5.1. The theoretical U-values, average and dynamic U-values based on different methods were sequentially entered into the simulations. As shown in Section 5.2, the simulated indoor T/RH when different U-values were considered were compared with the measured indoor T/RH of the four tested rooms, and the accuracy of each type of U-value could be obtained. The methods that can calculate U-values with high accuracy can be considered the optimal dynamic U-value calculated methods.

5.1 Indoor Environment Simulation When Dynamic U-values were Considered

The indoor T/RH simulation included three stages: (1) making weather files; (2) building tested rooms' models; and (3) setting parameters.

(1) Making weather files

Four weather files were made for the simulations of the four tested rooms. Each weather file included the latitude and longitude of the tested city, time zone of the tested city, simulation time interval, start time, outdoor T/RH, solar radiation (including global horizontal irradiance [GHI] and diffuse horizontal irradiance [DHI]), wind direction and wind speed. The latitude and longitude of the three tested cities are shown in Figure 4.1. The time zone of Sheffield is Greenwich Mean Time (GMT), whose offset is

GMT+0. The time zone of Ninghai and Harbin is GMT+8. The simulation time interval was set to 1 hour. The start time was set to the start time of the in-situ measurement (as shown in Table 4.3). The outdoor T/RH were set to hourly averages of measured outdoor T/RH. Owing to the limitation of instrumentation, this study did not measure solar radiation, wind speed and direction. The hourly weather station data were chosen for making weather files (Solcast 2016). The hourly weather station data were collected at the same time and in the same city as the in-situ measurements.

(2) Building tested rooms' models

Four tested rooms' models were built by SketchUp and TRNSYS 3D, as shown in Figure 5.1. The dimensions and orientation of the tested rooms were consistent with the actual conditions. As boundary conditions for the simulations of the tested rooms, the neighbouring rooms were also modelled for inputting measured indoor T/RH data of the neighbouring rooms. The dimensions of the neighbouring rooms were not key information for the study and can be appropriately simplified. Each individual room was set up as a separate thermal zone, whether it was a tested room or a neighbouring room.

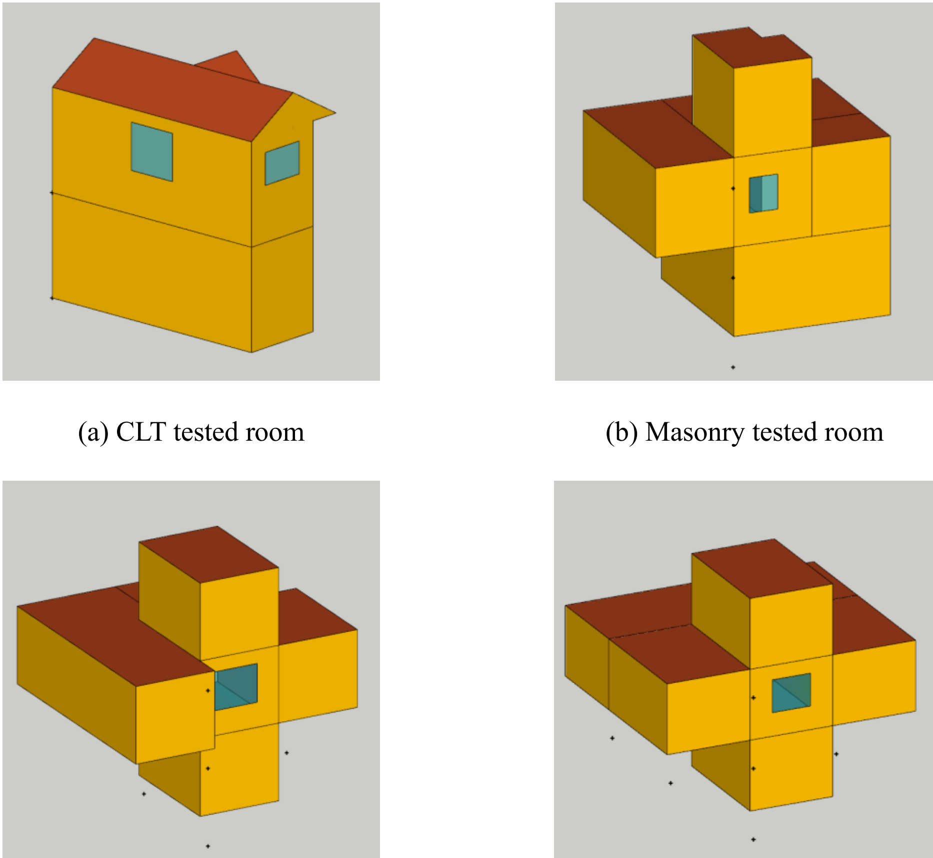

(a) CLT tested room

(b) Masonry tested room

(c) RC tested room

(d) Brick tested room

Figure 5.1 Models of the four tested rooms

(3) Setting parameters

When setting the spatial boundary conditions for the four tested rooms, the weather files were entered as external boundary conditions. Hourly averages of measured indoor T/RH of neighbouring rooms were entered as internal boundary conditions. This is one of the advantages of TRNSYS – it can control the hourly indoor T/RH in a particular thermal zone. When the time boundary conditions for the four tested rooms were set, the simulation time was consistent with the measurement time, and the simulation step was set to 1 hour.

When setting building operating parameters in the four tested rooms, occupancy and HVAC systems were set to none. Doors and windows were set to never operate. The air change rate of the CLT tested room was set to 0.9 h^{-1}, which was provided by the construction manufacturer. The air change rate of the other three tested rooms was set to 0.2 h^{-1}. These data referred to the existing literature. Several researchers tested the air change rate of bedrooms. These bedrooms were in an enclosed state with no occupancy or HVAC systems. The tested results were around 0.2 h^{-1} (Deshko et al. 2021; Sui et al. 2021).

When the building parameters of the four tested rooms were set, they were of four kinds: external wall, external window, door and other structure parameters (roof, floor slab, and interior wall). All data are from building manufacturers and homeowners. Setting external wall parameters involves the input of the different types of U-values, which is complex and lengthy. It is described at the end of this section.

The external window parameters of the four tested rooms are shown in Table 5.1. The G-value of the window is a parameter applied to show the transmittance of solar gain through the window; it is from 0 to 1. A higher G-value means that more solar heat is transmitted through the window. A window's frame factor is the proportion of the glass area to the entire window area. The door parameters of the four tested rooms are shown in Table 5.2. The CLT tested room has an exterior door, and the other three tested rooms each have an interior door. The parameters of other structures are shown in Table 5.3. The CLT tested room has a roof and a floor slab, and the other three tested rooms have interior walls and floor slabs. The size of these structures is shown in Figure 4.3.

Table 5.1 External window parameters of the tested rooms

Tested room	Window type	Width (mm)	Height (mm)	U-value $[W/(m^2 \cdot K)]$	G-value	Frame factor
CLT (North window)	Single-pane	1200	1100	5.7	0.8	0.83
CLT (West window)	Single-pane	1100	750	5.7	0.8	0.79
CLT (East window)	Single-pane	1100	500	5.7	0.8	0.73
Masonry	Double-pane	900	1100	1.0	0.6	0.76
RC	Triple-pane	1680	1500	1.0	0.4	0.78
Brick	Double-pane	1400	1250	1.7	0.7	0.79

Table 5.2 Door parameters of the tested rooms

Tested room	Door type	Material	Width (mm)	Height (mm)	Thickness (mm)	U-value $[W/(m^2 \cdot K)]$
CLT	Exterior door	Timber; insulation board	900	2000	60	2.5
Masonry	Interior door	Timber	762	1981	35	3.0
RC	Interior door	Timber	900	2100	40	2.4
Brick	Interior door	Timber	900	2100	35	2.8

Table 5.3 Parameters of other structures in the tested rooms

Tested envelope	Structure type	Material	Thickness [mm]	Conductivity $[W/(m \cdot K)]$	Density $[kg/(m^3)]$	Specific Heat Capacity $[J/(kg \cdot K)]$
CLT	Double-pitched roof	1 Steel sheet covering	0.5	50	7850	500
		2 CLT panel	120	0.12	500	1500
	Floor slab	1 Timber flooring	20	0.14	650	1700
		2 CLT panel	120	0.12	500	1500
Masonry	Interior wall	1 Plaster broad	12.5	0.17	950	840
		2 Clay brick	205	0.78	1700	840
		3 Plaster broad	12.5	0.17	950	840
	Floor slab	1 Carpet	10	0.05	1500	1700
		2 Cement mortar	40	0.93	1800	1050
		3 Concrete slab	100	1.74	2500	920
RC	Interior wall	1 Cement mortar	10	0.93	1800	1050
		2 Light weight concrete	200	0.18	700	1050
		3 Cement mortar	10	0.93	1800	1050
	Floor slab	1 Timber flooring	15	0.14	650	1700
		2 Cement mortar	20	0.93	1800	1050
		3 Concrete slab	100	1.74	2500	920

Table 5.3 (continued)

Tested envelope	Structure type	Material	Thickness [mm]	Conductivity $[W/(m \cdot K)]$	Density $[kg/(m^3)]$	Specific Heat Capacity $[J/(kg \cdot K)]$
Brick	Interior wall	1 Cement mortar	10	0.93	1800	1050
		2 Clay brick	240	0.78	1700	840
		3 Cement mortar	10	0.93	1800	1050
	Floor slab	1 Timber flooring	15	0.14	650	1700
		2 Cement mortar	20	0.93	1800	1050
		3 Concrete slab	100	1.74	2500	920

The most important input is the parameters of the external walls of tested rooms, especially U-values of the external walls. When simulations considering the theoretical U-values of external walls were conducted, the parameters of external walls were set based on Table 4.2, including building material types and the thickness, thermal conductivity, density and specific heat capacity of each building material. When simulations considering the average and dynamic U-values were conducted, the U-values of external walls needed to be changed. However, the U-value cannot be changed directly in TRNSYS. In this study, the thermal conductivities of building materials were changed to adjust the U-values of external walls, and other parameters were not changed. Since outdoor T/RH varies to a higher extent than indoor T/RH, the main material of the outer layer of the building wall is more susceptible to the effects of T/RH. The final decision was to adjust the U-value by changing the thermal conductivity of the four materials in four external walls: (1) the CLT panel in CLT wall, (2) clay brick in masonry cavity wall, (3) EPS broad in RC wall and (4) EPS broad in brick wall.

When simulations considering the average U-values were conducted, simulations covering the entire simulation time could be done using a single U-value. The initial T/RH of the simulation was set to the average T/RH of the first hour of in-situ measurement. These are consistent with the simulations considering the theoretical U-values.

Since only one U-value can be set in a single simulation, when conducting simulations that consider dynamic U-values, multiple simulations were performed to complete the simulation that covered the entire simulation time. The U-value was adjusted once for each simulation. The number of simulations corresponded to the number of time intervals used to calculate dynamic U-values. The duration of each simulation was consistent with the time interval for calculating dynamic U-values. The initial T/RH of the first simulation was set to the average T/RH of the first hour of in-situ measurement. To ensure the continuity of the simulated indoor T/RH of the tested rooms, the initial indoor T/RH for the second and subsequent simulations were set to the simulated indoor T/RH of the last hour of the previous simulation.

Figures 5.2–5.21 show the part of the calculated dynamic U-values and calculated average U-values of the four tested envelopes, including the results based on five data pre-processing methods with two different time intervals. According to the results of the U-value calculation, three types of U-values could not be set in the simulation:

(1) The dynamic U-values contained negative values. This situation was mostly found in the ND and TD methods.

(2) The data in some time intervals in the dynamic U-values were all deleted after data pre-processing. This situation occurred because the temperature difference for screening data in the data pre-processing method was large.

(3) The U-value was abnormally low. When the U value was less than 0.08 $W/(m^2 \cdot K)$, TRYSYS reported an error because it did not comply with the heat transfer principles.

Figures 5.2–5.6 show the calculated dynamic and average U-values of the CLT tested envelope. Regardless of the U-value calculation method, the calculated dynamic and average U-values were lower than the theoretical U-value. It showed that the CLT envelope was better insulated than expected. The dynamic U-values had a low amplitude fluctuation, with fluctuations of about 0.2 $W/(m^2 \cdot K)$. The dynamic U-values based on the TL method showed the characteristic of low U-values in winter and high U-values in summer, while the dynamic U-values based on the other four methods had the opposite characteristics. The accuracy of the different U-value calculation methods will be discussed in the next section.

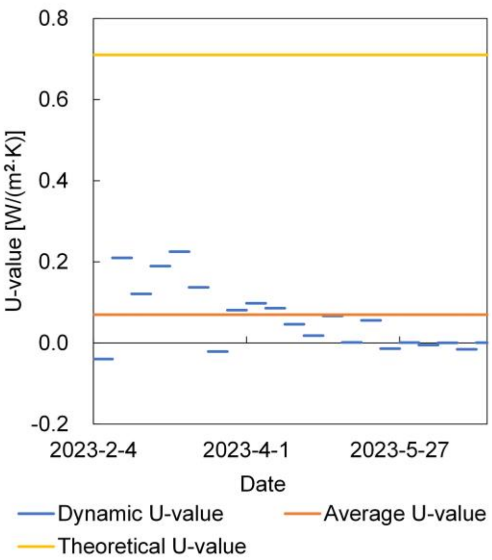

(a) ND (7-day interval)

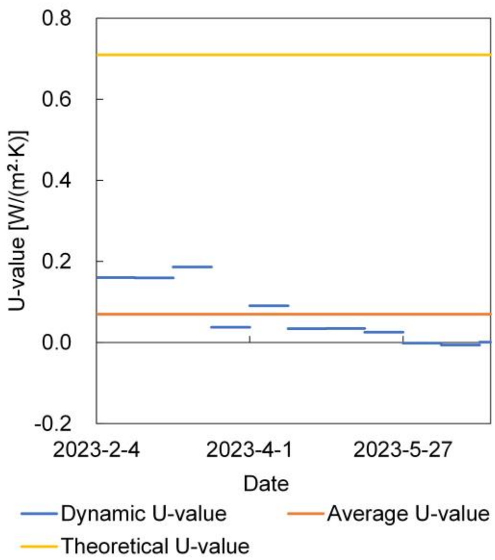

(b) ND (14-day interval)

Figure 5.2 U-values of the CLT tested envelope calculated by the ND method

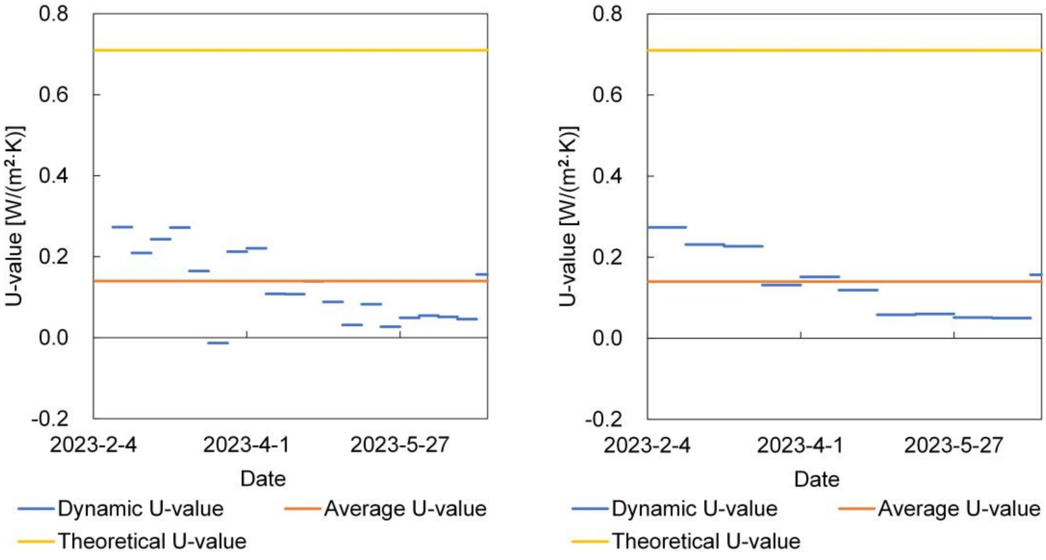

(c) TD3 (7-day interval) (d) TD3 (14-day interval)

Figure 5.3 U-values of the CLT tested envelope calculated by the TD3 method

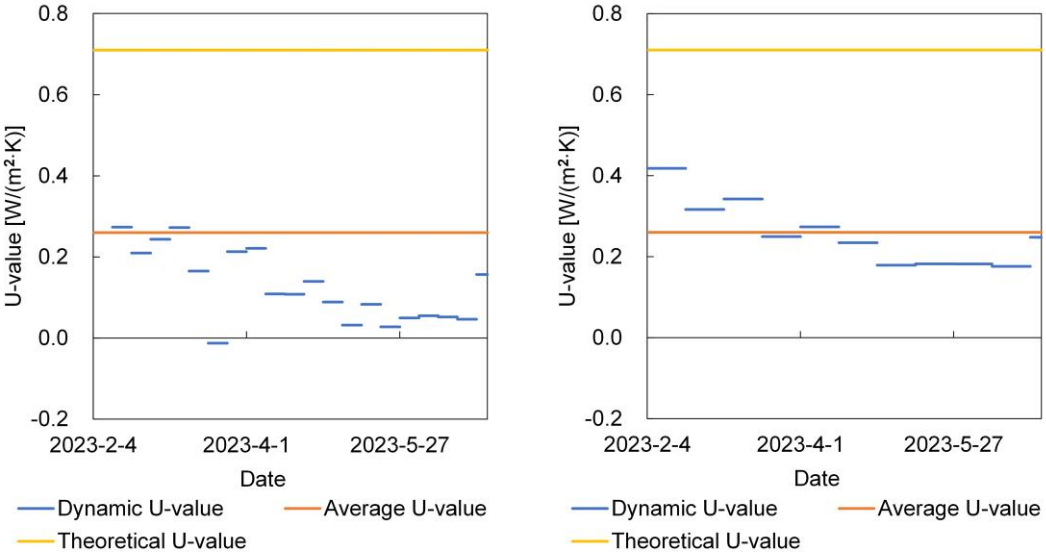

(e) PV3 (7-day interval) (f) PV3 (14-day interval)

Figure 5.4 U-values of the CLT tested envelope calculated by the PV3 method

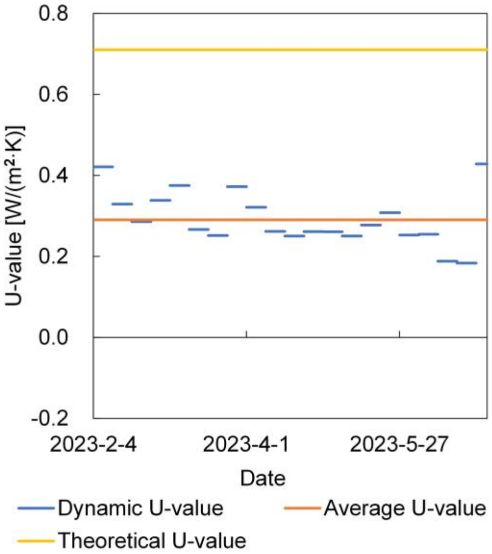

(g) AV3 (7-day interval)

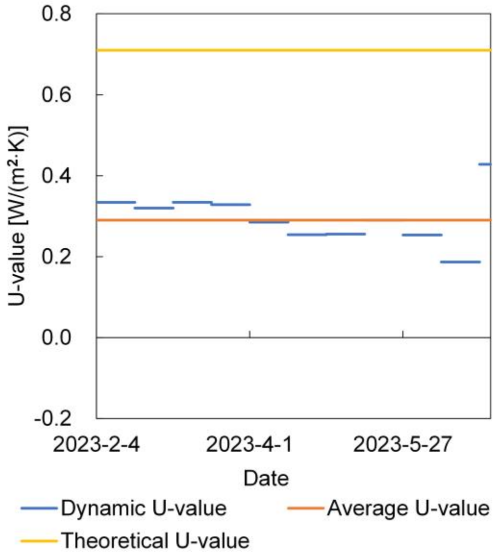

(h) AV3 (14-day interval)

Figure 5.5 U-values of the CLT tested envelope calculated by the AV3 method

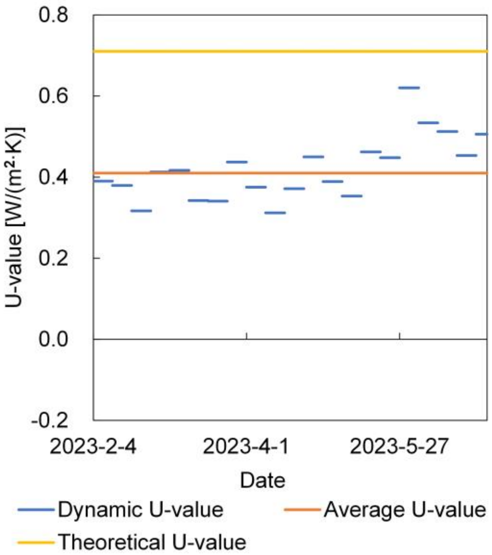

(i) TL (7-day interval)

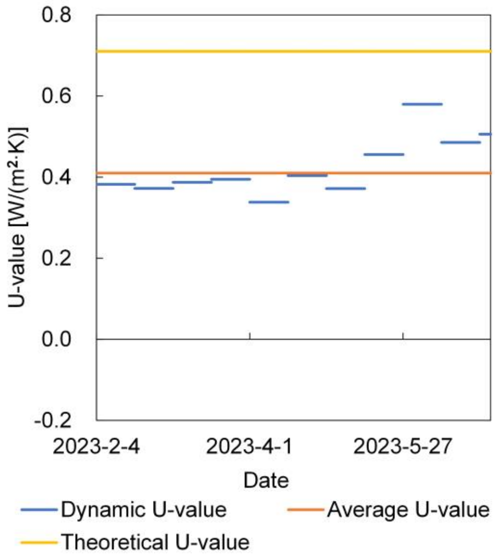

(j) TL (14-day interval)

Figure 5.6 U-values of the CLT tested envelope calculated by the TL method

Figures 5.7–5.11 show the calculated dynamic and average U-values of the masonry cavity tested envelope. Except for the ND method, the average U-values were higher than the theoretical U-value in the other four methods. In all methods, the dynamic U-values fluctuated widely by about 1.0 $W/(m^2 \cdot K)$. They showed a pronounced characteristic of higher U-values in winter and lower U-values in summer, compared with the average and theoretical U-values. This may indicate that the masonry cavity tested envelope was weakly insulated in winter.

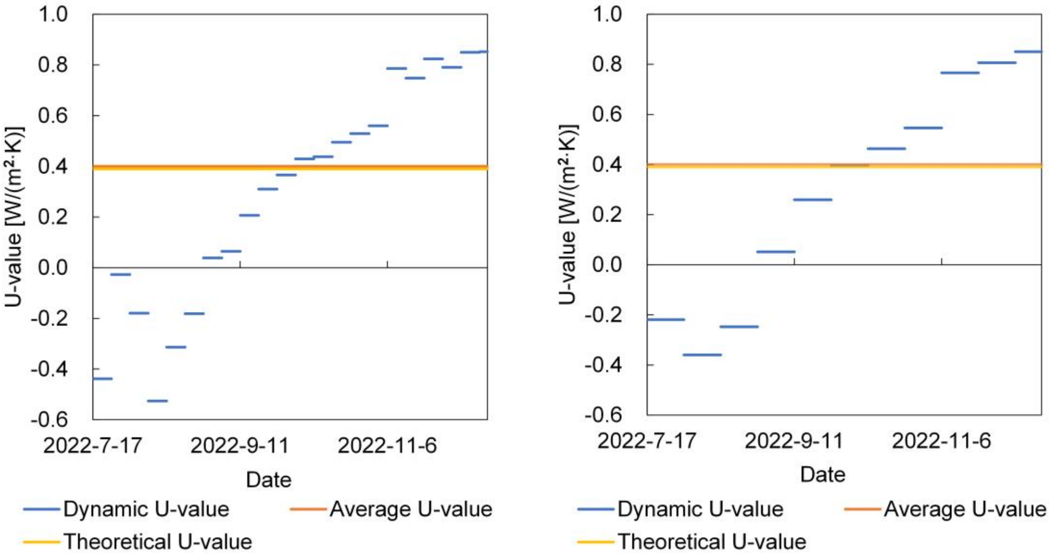

(a) ND (7-day interval) (b) ND (14-day interval)

Figure 5.7 U-values of the masonry tested envelope calculated by the ND method

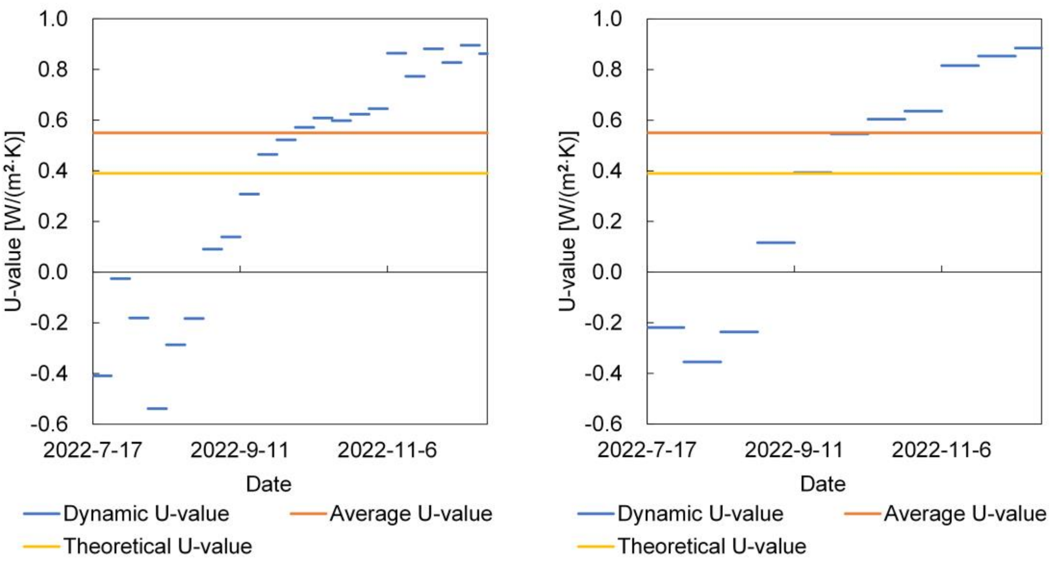

(c) TD3 (7-day interval) (d) TD3 (14-day interval)

Figure 5.8 U-values of the masonry tested envelope calculated by the TD3 method

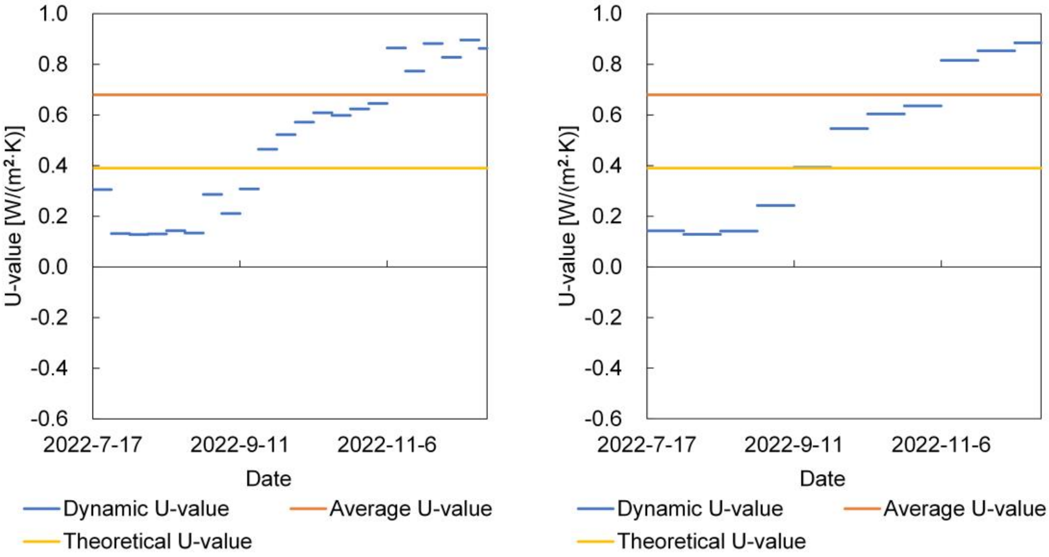

(e) PV3 (7-day interval)

(f) PV3 (14-day interval)

Figure 5.9 U-values of the masonry tested envelope calculated by the PV3 method

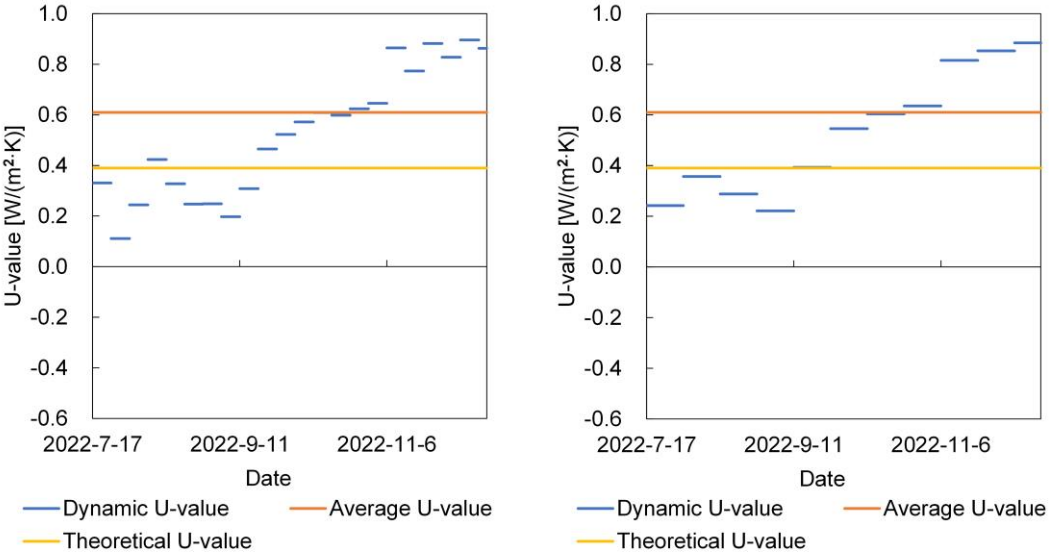

(g) AV3 (7-day interval)

(h) AV3 (14-day interval)

Figure 5.10 U-values of the masonry tested envelope calculated by the AV3 method

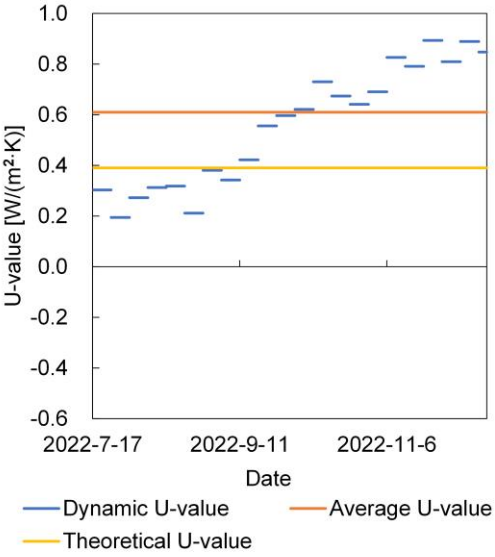

(i) TL (7-day interval)

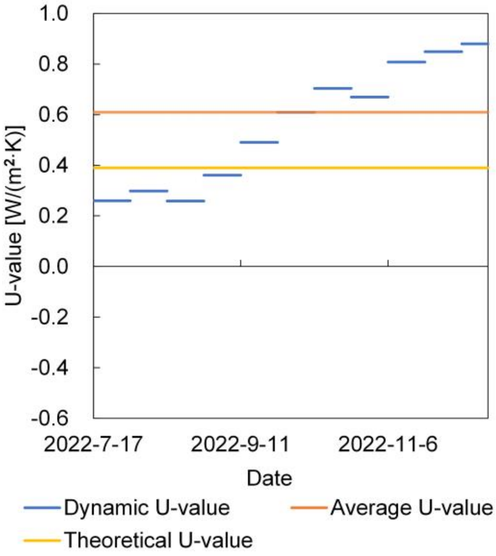

(j) TL (14-day interval)

Figure 5.11 U-values of the masonry tested envelope calculated by the TL method

Figures 5.12–5.16 show the calculated dynamic U-values and calculated average U-values of the RC tested envelope. In the ND method, the average U-values were lower than the theoretical U-value, while the average U-values had the opposite characteristics in the other four methods. Dynamic U-values were stable in winter and spring and became lower in summer. The fluctuations of dynamic U-values were smaller than those of the masonry cavity envelope, with fluctuations of about 0.3 $\mathrm{W/(m^2 \cdot K)}$.

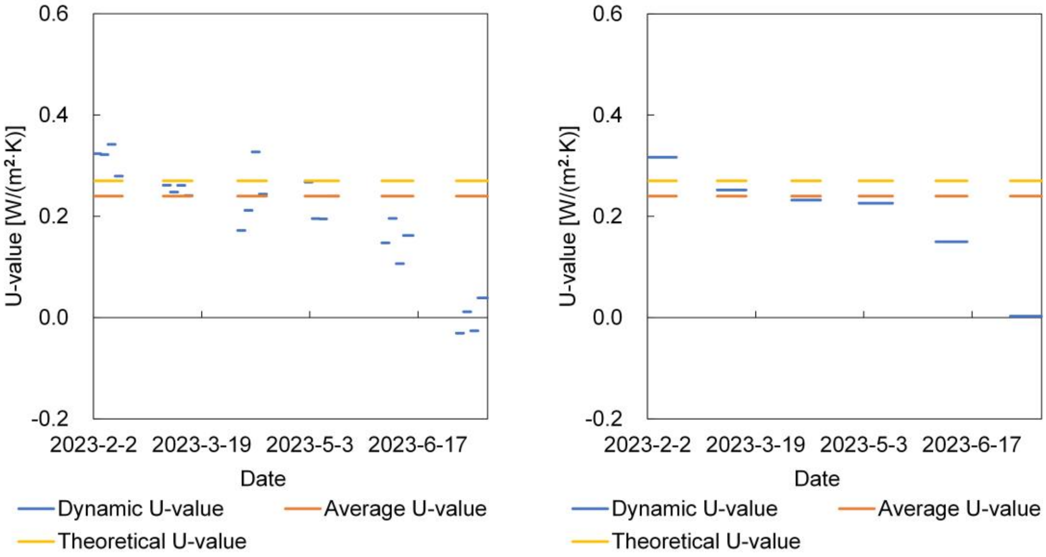

(a) ND (7-day interval)

(b) ND (14-day interval)

Figure 5.12 U-values of the RC tested envelope calculated by the ND method

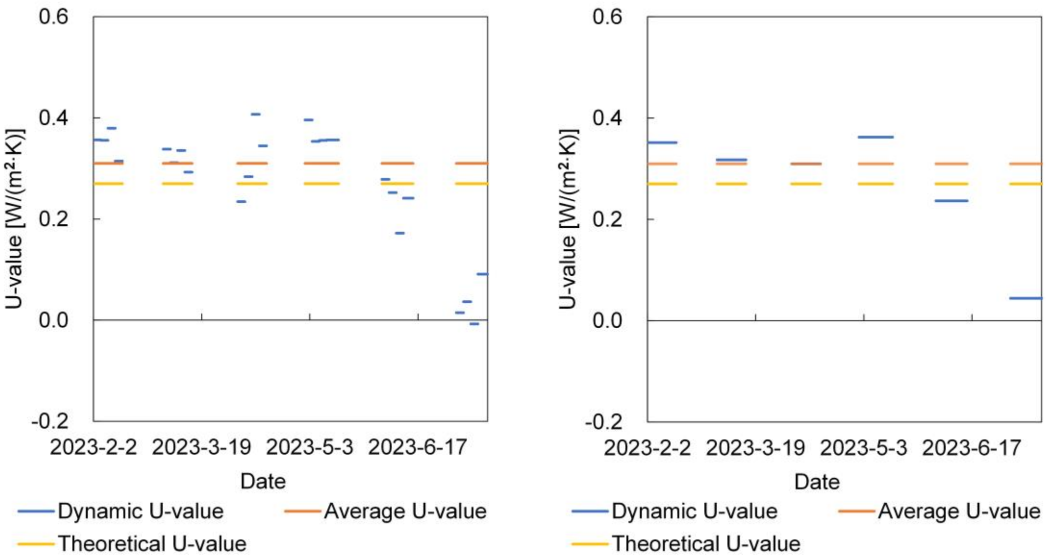

(c) TD3 (7-day interval)

(d) TD3 (14-day interval)

Figure 5.13 U-values of the RC tested envelope calculated by the TD3 method

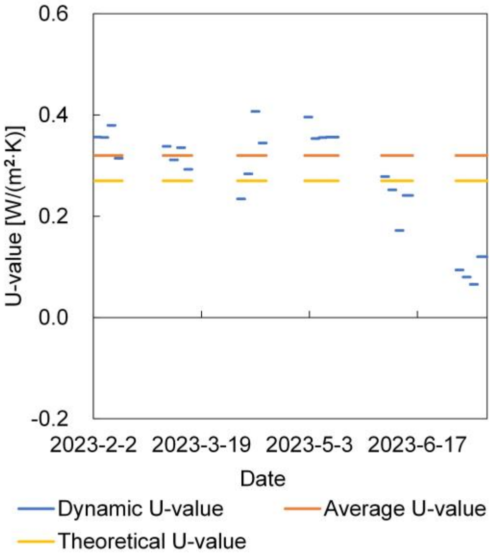

(e) PV3 (7-day interval)

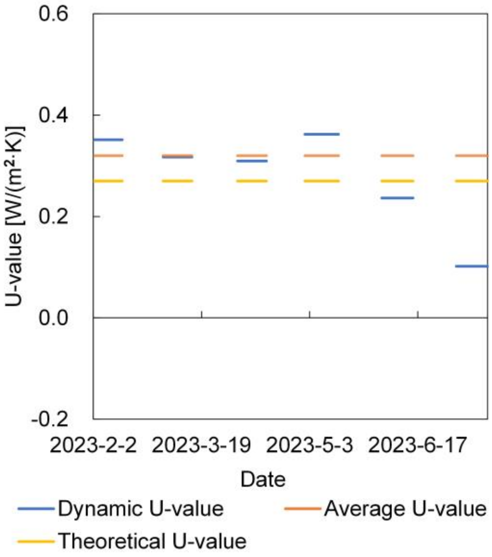

(f) PV3 (14-day interval)

Figure 5.14 U-values of the RC tested envelope calculated by the PV3 method

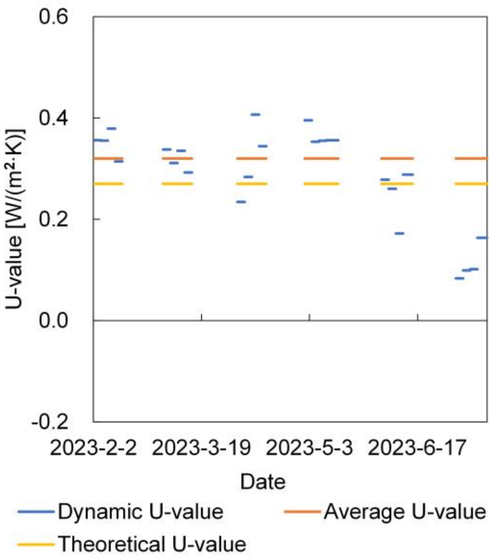

(g) AV3 (7-day interval)

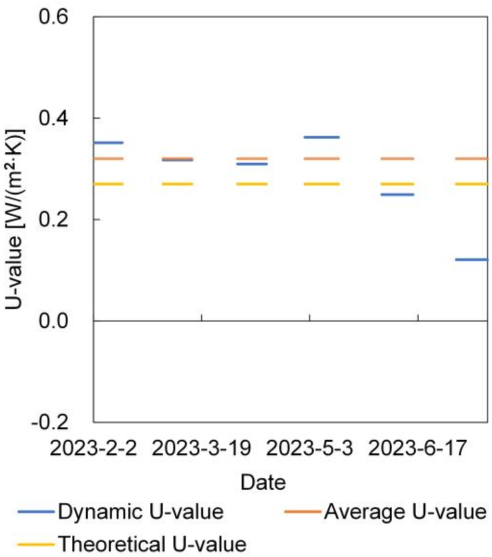

(h) AV3 (14-day interval)

Figure 5.15 U-values of the RC tested envelope calculated by the AV3 method

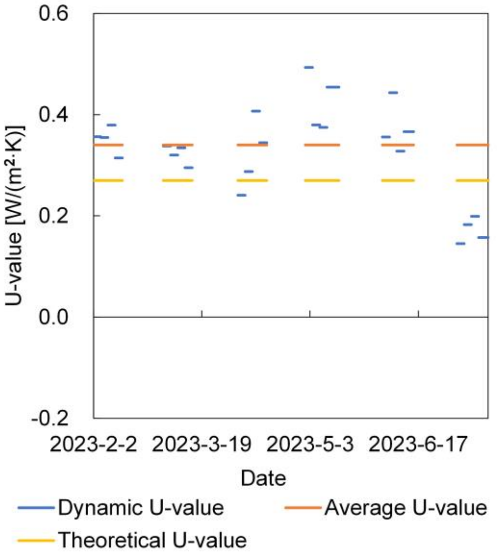

(i) TL (7-day interval)

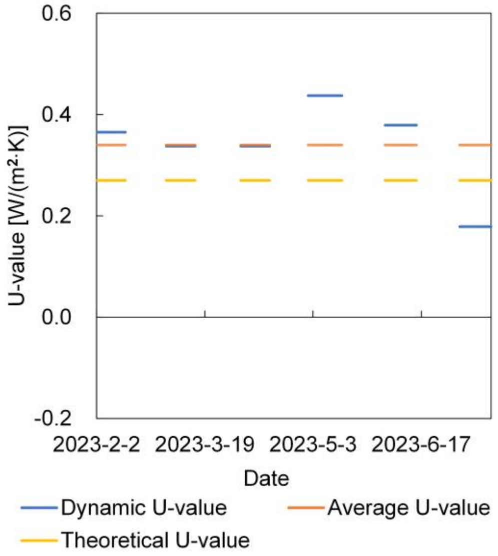

(j) TL (14-day interval)

Figure 5.16 U-values of the RC tested envelope calculated by the TL method

Figures 5.17–5.21 show the calculated dynamic and average U-values of the brick tested envelope. Regardless of the U-value calculation method, the calculated average U-values were higher than the theoretical U-value. Dynamic U-values were higher U-values in winter and lower U-values in summer. The magnitudes of the dynamic U-value fluctuations were between that of the masonry cavity and the RC tested envelope, with fluctuations of about 0.5 $\mathrm{W/(m^2 \cdot K)}$.

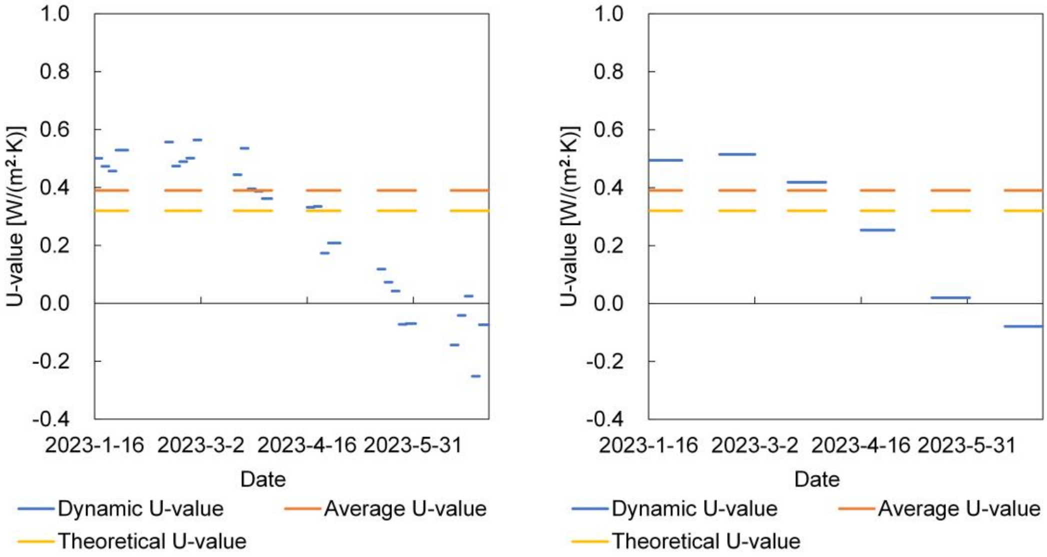

(a) ND (7-day interval) (b) ND (14-day interval)

Figure 5.17 U-values of the brick tested envelope calculated by the ND method

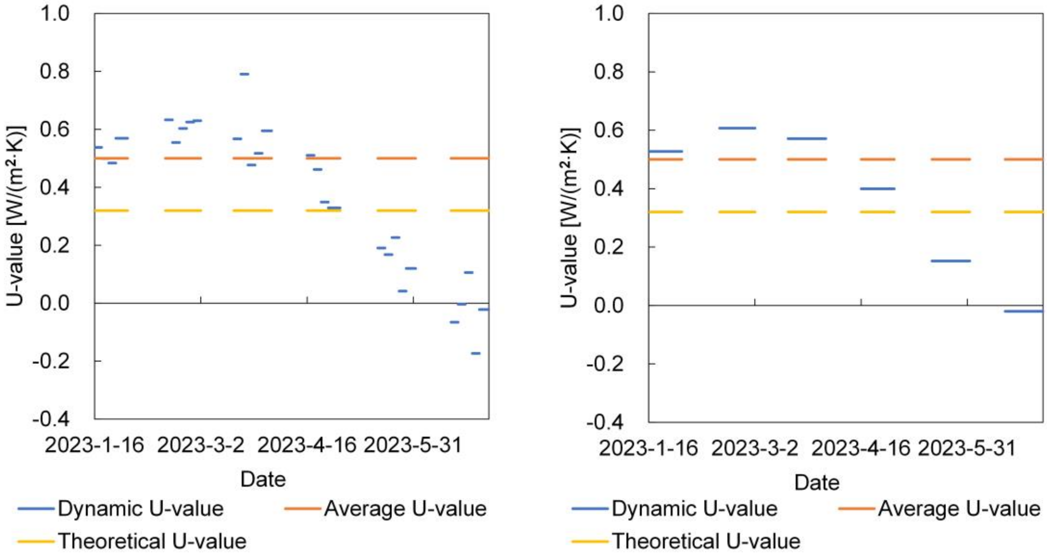

(c) TD3 (7-day interval) (d) TD3 (14-day interval)

Figure 5.18 U-values of the brick tested envelope calculated by the TD3 method

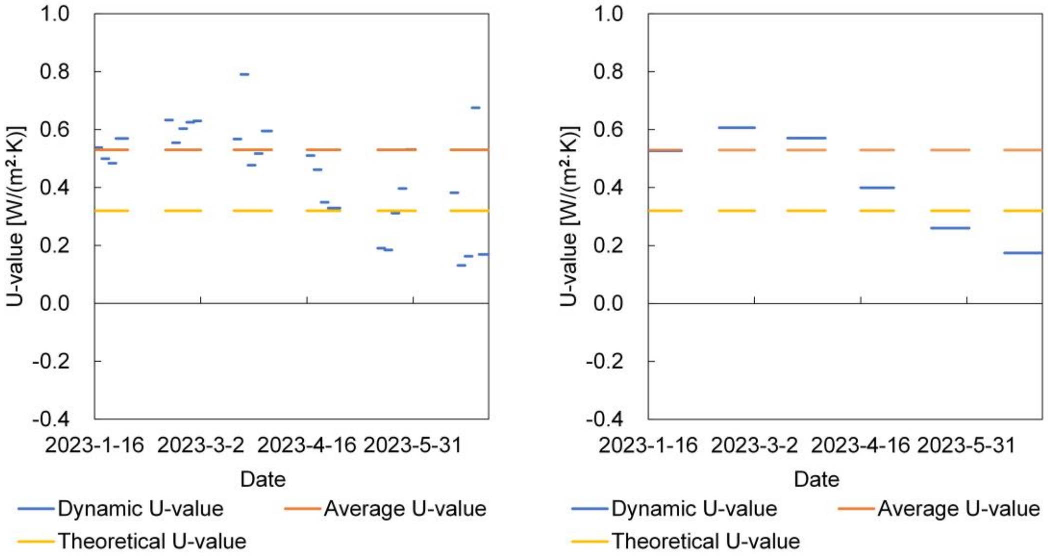

(e) PV3 (7-day interval) (f) PV3 (14-day interval)

Figure 5.19 U-values of the brick tested envelope calculated by the PV3 method

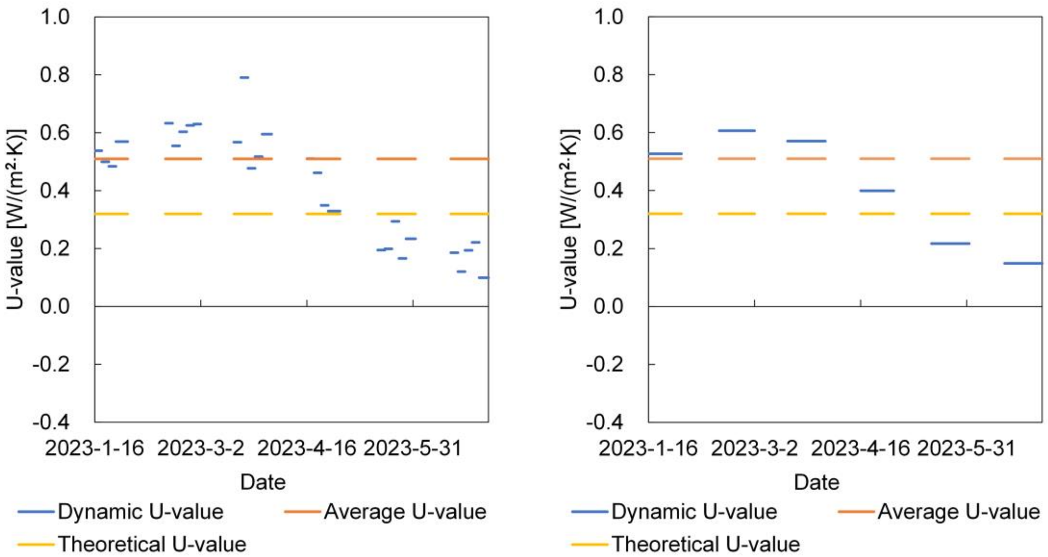

(g) AV3 (7-day interval) (h) AV3 (14-day interval)

Figure 5.20 U-values of the brick tested envelope calculated by the AV3 method

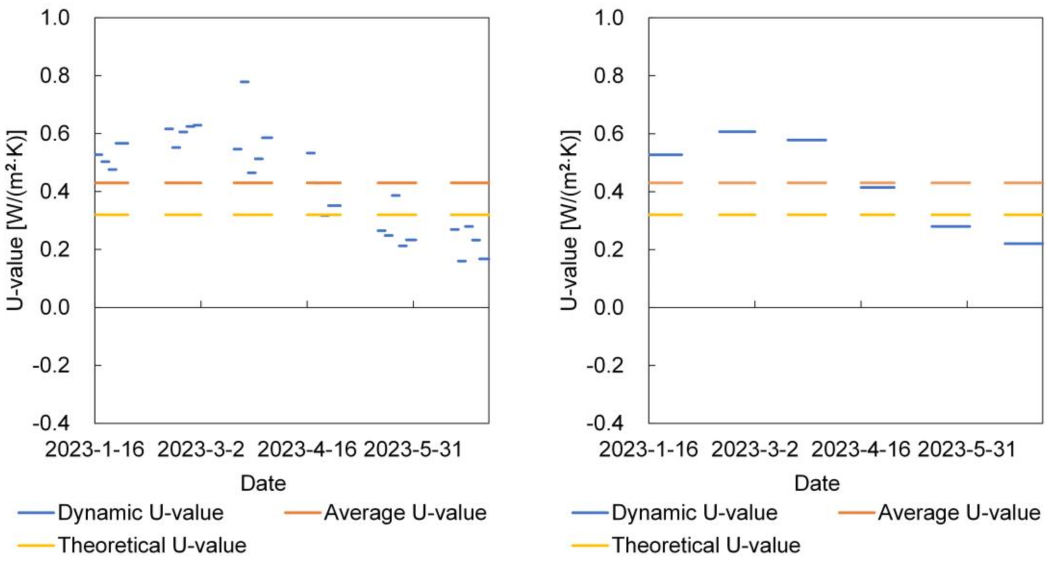

(i) TL (7-day interval) (j) TL (14-day interval)

Figure 5.21 U-values of the brick tested envelope calculated by the TL method

The dynamic U-values of masonry cavity and brick building envelopes showed an increasing trend from summer to winter. This phenomenon may be due to moisture within the envelopes frozen during the winter. During the winter measurement period in Harbin and Sheffield, the outdoor temperatures dropped below 0°C. Several researchers found that the thermal conductivity of ice was 2.22 $W/(m \cdot K)$ at –10℃, whereas that of water was 0.58 $W/(m \cdot K)$ at 10℃, 0.60 $W/(m \cdot K)$ at 20℃ and 0.61 $W/(m \cdot K)$ at 30℃ (Guo et al. 2013). The building materials of the masonry cavity and brick building envelopes are inorganic porous structures such as bricks, inorganic insulation boards and concrete blocks; these inorganic porous materials are absorbent. In actual situations, building envelopes constructed over 40 years ago are difficult to keep absolutely dry inside owing to precipitation, wall aging and other factors. When moisture within the envelopes was frozen, the building materials' thermal conductivity increased, resulting in an increase in the U-values of building envelopes. Some researchers have found similar phenomena in moisture-containing porous materials such as soil-rock mixture and sandy soils (Tang et al. 2023; Vu, Pereira, and Tang 2023).

The fluctuations in dynamic U-values of the brick and masonry cavity envelopes were wider than those of the RC envelope. The brick and masonry cavity envelopes had been built three decades before the RC envelope and may have more cracks owing to the aging of the building materials, which leads to higher moisture content. This may result in wider fluctuations in dynamic U-values.

The CLT tested envelope had more stable thermal characteristics. This might have been due to the CLT tested envelope being relatively new and well waterproofed. Meanwhile, the thermal properties of the CLT itself were dominant. Some researchers have found the thermal conductivity of the CLT panel to be highly stable at different temperatures and different moisture contents. The thermal conductivity of the CLT panel was 0.105 $W/(m \cdot K)$ at 10°C with 3.5% moisture content, 0.120 $W/(m \cdot K)$ at 10°C with 13.2% moisture content, 0.107 $W/(m \cdot K)$ at 30°C with 3.5% moisture content and 0.122 $W/(m \cdot K)$ at 30°C with 13.2% moisture content (Danovska et al. 2022).

Although the fluctuation trends of the dynamic U-values for the same tested envelopes based on different calculation methods were similar, the accuracy of the different U-values still needed to be verified for more accurate and efficient U-value prediction modelling and operational energy simulation.

5.2 Optimal Dynamic U-value Calculation Method

After the simulated indoor T/RH of the four tested rooms considering different U-values was obtained, the error rates of the simulation results were calculated. These error rates can indicate which U-value calculation methods are effective. The calculation method of the error rate is shown in Equations (11) and (12):

$$E(T) = \left(\sum_{i=1}^{n} \frac{|T_{sim,i} - T_{mea,i}|}{|T_{mea,i}|}\right) \times \frac{1}{n} \times 100\% \tag{11}$$

$$E(RH) = \left(\sum_{i=1}^{n} \frac{|RH_{sim,i} - RH_{mea,i}|}{|RH_{mea,i}|}\right) \times \frac{1}{n} \times 100\% \tag{12}$$

Where $\boldsymbol{E}$ is the error rate [%]. $\boldsymbol{T}$ is temperature [°C]. $\boldsymbol{RH}$ is relative humidity [%]. $\boldsymbol{T_{sim,i}}$ is the simulated indoor temperature at hour $\boldsymbol{i}$ [°C]. $\boldsymbol{T_{mea,i}}$ is the measure average indoor temperature at hour $\boldsymbol{i}$ [°C]. $\boldsymbol{RH_{sim,i}}$ is the simulated indoor relative humidity at hour $\boldsymbol{i}$ [%]. $\boldsymbol{RH_{mea,i}}$ is the measure average indoor relative humidity at hour $\boldsymbol{i}$ [%]. $\boldsymbol{n}$ is the number of hours during measurement.

The error rates of simulated indoor T/RH of the four tested rooms based on different U-values are shown in Tables 5.4–5.7. In these tables, when the time interval was all time, the U-value used for the simulation was the average U-value obtained based on the data pre-processing method. The error rates of simulated results based on the theoretical U-values were at the end of the tables. The results showed that the ND and TD methods did not effectively remove negative U-values and abnormally low U-values. The most dynamic U-values based on these two data pre-processing methods could not be used for indoor T/RH simulations. Because the U-value cannot be set to the negative value in TRNSYS. Negative U-values have no physical significance. The U-values cannot be abnormally small either. When the U value was less than 0.08 $\mathrm{W/(m^2 \cdot K)}$, TRYSYS reported an error because it did not comply with the heat transfer principles.

Table 5.4 shows the error rates of simulated indoor T/RH when different U-values in the CLT tested room are considered. As shown in Figure 4.9(c), the temperature difference in the CLT tested room fluctuated from -14.0°C to 8.3°C. The average temperature difference was 1.2°C. When the TD, PV and AV methods were used and the temperature difference used for screening data exceeded 7°C, the data-retention rate was less than 10%. All data for most time intervals was deleted and dynamic U-values could not be calculated.

Therefore, the temperature difference used for screening data in these three data pre-processing methods was considered between 0°C and 7°C. The minimum error rates of T/RH were 7.0% and 15.9%, respectively. The U-value calculation method used to derive the minimum temperature error rate was the TL method with 20-day intervals, and the U-value calculation method used to derive the minimum relative humidity error rate was the TL method with 30-day intervals.

Table 5.4 Error rates of simulated indoor T/RH in the CLT tested room

Data pre-processing methods	T/RH	Error rate of simulated indoor T/RH based on different time intervals (%)									
		3D	5D	7D	10D	14D	20D	30D	40D	50D	All time
ND	T	-	-	-	-	-	-	-	-	-	-
	RH	-	-	-	-	-	-	-	-	-	-
TD0	T	-	-	-	-	-	-	-	-	-	24.6
	RH	-	-	-	-	-	-	-	-	-	24.5
TD1	T	-	-	-	-	-	-	-	-	-	22.4
	RH	-	-	-	-	-	-	-	-	-	23.3
TD2	T	-	-	-	-	-	-	-	-	-	20.5
	RH	-	-	-	-	-	-	-	-	-	22.3
TD3	T	-	-	-	-	-	-	-	-	-	19.8
	RH	-	-	-	-	-	-	-	-	-	22.0
TD4	T	-	-	-	-	-	-	-	-	-	19.8
	RH	-	-	-	-	-	-	-	-	-	22.0
TD5	T	-	-	-	-	-	-	-	-	19.1	19.8
	RH	-	-	-	-	-	-	-	-	22.2	22.0
TD6	T	-	-	-	-	-	-	-	-	-	20.5
	RH	-	-	-	-	-	-	-	-	-	22.3
TD7	T	-	-	-	-	-	-	-	-	-	23.6
	RH	-	-	-	-	-	-	-	-	-	23.9
PV0	T	10.7	10.5	10.4	10.0	9.7	9.5	9.8	9.9	9.8	9.7
	RH	18.8	19.1	19.1	19.0	18.9	18.4	18.5	18.9	18.1	18.0
PV1	T	9.3	9.1	9.0	9.0	8.5	8.5	8.8	8.5	8.3	11.0
	RH	17.5	17.7	17.4	17.3	17.3	17.1	17.7	17.0	17.2	18.2
PV2	T	-	-	-	10.1	9.7	9.6	9.6	9.6	9.3	11.7
	RH	-	-	-	17.6	17.5	17.4	17.9	17.3	17.5	18.5
PV3	T	-	-	-	11.5	11.5	11.5	11.3	11.4	11.1	12.7
	RH	-	-	-	18.3	18.3	18.2	18.5	18.0	18.1	18.8
PV4	T	-	-	-	-	14.7	14.3	13.9	14.0	13.8	14.7
	RH	-	-	-	-	19.6	19.4	19.6	19.3	19.3	19.6
PV5	T	-	-	-	-	-	15.4	14.5	14.9	14.7	15.9
	RH	-	-	-	-	-	20.2	20.1	19.8	19.7	20.1
PV6	T	-	-	-	-	-	-	-	-	15.6	17.5
	RH	-	-	-	-	-	-	-	-	20.1	20.9
PV7	T	-	-	-	-	-	-	-	-	-	21.3
	RH	-	-	-	-	-	-	-	-	-	22.7

(Note: red numbers are minimum error rates)

Table 5.4 (continued)

Data pre-processing methods	T/RH	Error rate of simulated indoor T/RH based on different time intervals (%)									
		3D	5D	7D	10D	14D	20D	30D	40D	50D	All time
AV0	T	16.1	16.0	15.9	15.6	15.6	15.3	15.1	15.3	15.5	8.5
	RH	19.6	19.2	19.5	19.3	19.7	19.3	19.4	19.1	19.2	17.9
AV1	T	8.9	8.7	8.5	8.4	8.1	8.3	8.3	8.2	8.4	9.7
	RH	17.7	17.4	17.4	17.3	17.3	17.4	17.8	17.4	17.8	18.0
AV2	T	10.2	10.0	10.0	9.7	9.2	9.3	9.1	9.1	9.1	11.0
	RH	17.8	17.7	17.7	17.5	17.6	17.5	18.0	17.3	17.6	18.2
AV3	T	-	11.7	11.5	10.8	10.6	10.7	10.4	10.5	10.3	11.7
	RH	-	18.4	18.3	17.8	18.0	17.9	18.0	17.7	17.9	18.5
AV4	T	-	-	13.0	12.9	12.9	12.9	12.6	12.6	12.4	13.1
	RH	-	-	18.7	19.1	19.0	18.7	18.7	18.5	18.7	18.9
AV5	T	-	-	13.5	13.5	13.4	13.4	13.2	13.6	13.3	13.5
	RH	-	-	19.6	19.5	19.6	19.4	19.2	19.1	19.0	19.1
AV6	T	-	-	-	-	-	-	15.2	15.1	15.3	14.7
	RH	-	-	-	-	-	-	20.0	19.7	19.9	19.6
AV7	T	-	-	-	-	-	-	-	-	14.3	14.7
	RH	-	-	-	-	-	-	-	-	19.8	19.6
TL	T	7.5	7.3	7.2	7.2	7.1	**7.0**	7.1	7.3	7.4	9.1
	RH	16.7	16.4	16.3	16.4	16.1	16.0	**15.9**	16.2	16.4	17.9
Theoretical U	T	8.7									
	RH	19.0									

(Note: red numbers are minimum error rates)

Table 5.5 shows the error rates of simulated indoor T/RH when different U-values in the masonry tested room are considered. The temperature difference in the masonry tested room fluctuated from -16.3°C to 20.1°C. The average temperature difference was 7.6°C. When the TD, PV and AV methods were used and the temperature difference used for screening data exceeded 13°C, the data-retention rate in the summer was less than 5%. All data for most time intervals was deleted and dynamic U-values could not be calculated. Therefore, the temperature difference used for screening data in these three data pre-processing methods was considered to be between 0°C and 13°C. The minimum error rates of T/RH were 4.2% and 6.6%, respectively. These two error rates were based on some dynamic and average U-values. The U-value calculation methods that could obtain both the minimum temperature error rate and minimum relative humidity error rate at the same time were the PV1 methods with 14-, 20-, 30- and 40-day intervals; the AV1 methods with 14-, 20-, 30- and 40-day intervals; and the TL methods with 30- and 40-day intervals.

Table 5.5 Error rates of simulated indoor T/RH in the masonry tested room

Data pre-processing methods	T/RH	Error rate of simulated indoor T/RH based on different time intervals (%)									
		3D	5D	7D	10D	14D	20D	30D	40D	50D	All time
ND	T	-	-	-	-	-	-	-	-	-	4.4
	RH	-	-	-	-	-	-	-	-	-	7.0
TD0	T	-	-	-	-	-	-	-	-	-	4.3
	RH	-	-	-	-	-	-	-	-	-	6.8
TD1	T	-	-	-	-	-	-	-	-	-	4.3
	RH	-	-	-	-	-	-	-	-	-	6.8
TD2	T	-	-	-	-	-	-	-	-	-	4.3
	RH	-	-	-	-	-	-	-	-	-	6.8
TD3	T	-	-	-	-	-	-	-	-	-	4.3
	RH	-	-	-	-	-	-	-	-	-	6.8
TD4	T	-	-	-	-	-	-	-	-	-	4.3
	RH	-	-	-	-	-	-	-	-	-	6.8
TD5	T	-	-	-	-	-	-	-	-	-	4.3
	RH	-	-	-	-	-	-	-	-	-	6.8
TD6	T	-	-	-	-	-	-	-	-	-	4.3
	RH	-	-	-	-	-	-	-	-	-	6.8
TD7	T	-	-	-	-	-	-	-	-	-	4.3
	RH	-	-	-	-	-	-	-	-	-	6.8
TD8	T	-	-	-	-	-	-	-	-	-	4.3
	RH	-	-	-	-	-	-	-	-	-	6.7
TD9	T	-	-	-	-	-	-	-	-	-	4.3
	RH	-	-	-	-	-	-	-	-	-	6.7
TD10	T	-	-	-	-	-	-	-	-	-	4.3
	RH	-	-	-	-	-	-	-	-	-	**6.6**
TD11	T	-	-	-	-	-	-	-	-	-	4.3
	RH	-	-	-	-	-	-	-	-	-	**6.6**
TD12	T	-	-	-	-	-	-	-	-	-	4.3
	RH	-	-	-	-	-	-	-	-	-	**6.6**
TD13	T	-	-	-	-	-	-	-	-	-	4.3
	RH	-	-	-	-	-	-	-	-	-	**6.6**

(Note: red numbers are minimum error rates)

Table 5.5 (continued)

Data pre-processing methods	T/RH	Error rate of simulated indoor T/RH based on different time intervals (%)									
		3D	5D	7D	10D	14D	20D	30D	40D	50D	All time
PV0	T	-	-	4.6	4.5	4.5	4.5	4.6	4.4	4.3	4.3
	RH	-	-	7.2	6.9	6.9	7.4	6.8	7.2	6.9	**6.6**
PV1	T	-	-	4.3	**4.2**	**4.2**	**4.2**	**4.2**	**4.2**	4.3	4.3
	RH	-	-	6.6	6.7	**6.6**	**6.6**	**6.6**	**6.6**	**6.6**	**6.6**
PV2	T	-	-	4.4	4.4	4.4	4.4	4.3	4.4	4.3	4.3
	RH	-	-	6.8	6.7	6.7	6.7	6.7	6.7	6.7	**6.6**
PV3	T	-	-	4.5	4.5	4.5	4.5	4.4	4.5	4.3	4.3
	RH	-	-	6.8	6.8	6.8	6.8	6.8	6.8	6.8	**6.6**
PV4	T	-	-	-	-	-	4.5	4.5	4.5	4.4	4.3
	RH	-	-	-	-	-	6.8	6.8	6.8	6.8	6.7
PV5	T	-	-	-	-	-	-	-	-	4.4	4.3
	RH	-	-	-	-	-	-	-	-	6.8	6.7
PV6	T	-	-	-	-	-	-	-	-	4.4	4.3
	RH	-	-	-	-	-	-	-	-	6.8	6.7
PV7	T	-	-	-	-	-	-	-	-	4.4	4.3
	RH	-	-	-	-	-	-	-	-	6.8	6.7
PV8	T	-	-	-	-	-	-	-	-	4.5	4.3
	RH	-	-	-	-	-	-	-	-	6.8	**6.6**
PV9	T	-	-	-	-	-	-	-	-	4.5	4.3
	RH	-	-	-	-	-	-	-	-	6.8	**6.6**
PV10	T	-	-	-	-	-	-	-	-	4.6	4.3
	RH	-	-	-	-	-	-	-	-	6.9	**6.6**
PV11	T	-	-	-	-	-	-	-	-	-	4.3
	RH	-	-	-	-	-	-	-	-	-	**6.6**
PV12	T	-	-	-	-	-	-	-	-	-	4.3
	RH	-	-	-	-	-	-	-	-	-	**6.6**
PV13	T	-	-	-	-	-	-	-	-	-	4.3
	RH	-	-	-	-	-	-	-	-	-	**6.6**

(Note: red numbers are minimum error rates)

Table 5.5 (continued)

Data pre-processing methods	T/RH	Error rate of simulated indoor T/RH based on different time intervals (%)									
		3D	5D	7D	10D	14D	20D	30D	40D	50D	All time
AV0	T	4.6	4.6	4.6	4.5	4.4	4.4	4.4	4.5	4.5	4.3
	RH	7.0	7.0	7.0	6.9	6.9	7.0	7.1	6.9	7.1	6.7
AV1	T	4.4	4.3	4.3	4.3	**4.2**	**4.2**	**4.2**	**4.2**	4.3	4.3
	RH	6.8	6.7	**6.6**	**6.6**	**6.6**	**6.6**	**6.6**	**6.6**	**6.6**	6.7
AV2	T	4.4	4.4	4.4	4.3	4.3	4.3	4.3	4.3	4.2	4.3
	RH	6.8	6.8	6.7	6.7	6.6	6.6	6.6	6.7	6.7	6.7
AV3	T	4.5	4.5	4.5	4.5	4.4	4.4	4.3	4.4	4.3	4.3
	RH	6.8	6.8	6.8	6.7	6.7	6.7	6.7	6.7	6.7	6.7
AV4	T	-	4.5	4.5	4.5	4.4	4.4	4.4	4.4	4.3	4.3
	RH	-	6.9	6.8	6.8	6.7	6.7	6.7	6.7	6.7	6.7
AV5	T	-	4.5	4.5	4.5	4.5	4.4	4.4	4.4	4.3	4.3
	RH	-	6.9	6.8	6.8	6.8	6.7	6.7	6.7	6.8	6.7
AV6	T	-	4.5	4.5	4.5	4.5	4.4	4.4	4.4	4.4	4.3
	RH	-	6.8	6.8	6.8	6.8	6.7	6.7	6.7	6.8	6.7
AV7	T	-	4.5	4.5	4.5	4.5	4.4	4.4	4.4	4.4	4.3
	RH	-	6.9	6.8	6.8	6.7	6.7	6.7	6.7	6.8	6.7
AV8	T	-	4.5	4.5	4.5	4.5	4.4	4.4	4.4	4.4	4.3
	RH	-	6.9	6.8	6.8	6.7	6.7	6.7	6.6	6.8	6.7
AV9	T	-	-	4.5	4.5	4.5	4.5	4.5	4.4	4.5	4.3
	RH	-	-	6.8	6.7	6.7	6.7	6.7	6.6	6.8	6.7
AV10	T	-	-	-	-	4.6	4.6	4.6	4.5	4.6	4.3
	RH	-	-	-	-	6.8	6.8	6.8	6.7	6.9	**6.6**
AV11	T	-	-	-	-	-	-	-	4.6	4.7	4.3
	RH	-	-	-	-	-	-	-	6.8	7.0	**6.6**
AV12	T	-	-	-	-	-	-	-	4.5	4.7	4.3
	RH	-	-	-	-	-	-	-	6.7	7.0	**6.6**
AV13	T	-	-	-	-	-	-	-	4.6	4.7	4.3
	RH	-	-	-	-	-	-	-	6.8	7.1	**6.6**
TL	T	4.4	4.4	4.4	4.3	4.3	4.3	**4.2**	**4.2**	4.3	4.3
	RH	6.8	6.7	6.8	6.7	**6.6**	**6.6**	**6.6**	**6.6**	6.7	6.7
Theoretical U	T	4.4									
	RH	7.0									

(Note: red numbers are minimum error rates)

Table 5.6 shows the error rates of simulated indoor T/RH when different U-values in the RC tested room are considered. In the TD, PV and AV methods, the temperature difference used for screening data was considered to be between 0℃ and 13℃; the reason was the same as that in the previous case. As each measurement in the RC and brick tested rooms was about two weeks, the time intervals in these two cases were set to 3, 5, 7 and 14 days. The minimum error rates of T/RH were 2.2% and 45.0%, respectively; these two error rates were based on some dynamic U-values. The U-value calculation methods that could obtain both the minimum temperature error rate and minimum relative humidity error rate at the same time were the PV1 methods with 7- and 14-day intervals, the PV2 methods with 7- and 14-day intervals, the AV0 method with 14-day interval, and the AV1 methods with 7- and 14-day intervals.

Table 5.6 Error rates of simulated indoor T/RH in the RC tested room

Data pre-processing methods	T/RH	Error rate of simulated indoor T/RH based on different time intervals (%)				
		3D	5D	7D	14D	All time
ND	T	-	-	-	-	2.6
	RH	-	-	-	-	45.5
TD0	T	-	-	-	2.3	2.4
	RH	-	-	-	**45.0**	45.3
TD1	T	-	-	-	-	2.4
	RH	-	-	-	-	45.3
TD2	T	-	-	-	-	2.4
	RH	-	-	-	-	45.3
TD3	T	-	-	-	-	2.5
	RH	-	-	-	-	45.4
TD4	T	-	-	-	-	2.5
	RH	-	-	-	-	45.4
TD5	T	-	-	-	-	2.5
	RH	-	-	-	-	45.4
TD6	T	-	-	-	-	2.5
	RH	-	-	-	-	45.4
TD7	T	-	-	-	-	2.5
	RH	-	-	-	-	45.4
TD8	T	-	-	-	-	2.5
	RH	-	-	-	-	45.4
TD9	T	-	-	-	-	2.5
	RH	-	-	-	-	45.4
TD10	T	-	-	-	-	2.4
	RH	-	-	-	-	45.3

(Note: red numbers are minimum error rates)

Table 5.6 (continued)

Data pre-processing methods	T/RH	Error rate of simulated indoor T/RH based on different time intervals (%)				
		3D	5D	7D	14D	All time
TD11	T	-	-	-	-	2.4
	RH	-	-	-	-	45.3
TD12	T	-	-	-	-	2.4
	RH	-	-	-	-	45.3
TD13	T	-	-	-	-	2.5
	RH	-	-	-	-	45.4
PV0	T	2.3	2.3	**2.2**	2.3	2.5
	RH	45.2	**45.0**	45.1	45.1	45.3
PV1	T	2.3	2.3	**2.2**	**2.2**	2.4
	RH	**45.0**	**45.0**	**45.0**	**45.0**	45.3
PV2	T	2.3	2.3	**2.2**	**2.2**	2.4
	RH	45.1	**45.0**	**45.0**	**45.0**	45.3
PV3	T	-	-	-	**2.2**	2.4
	RH	-	-	-	45.1	45.3
PV4	T	-	-	-	2.3	2.4
	RH	-	-	-	45.1	45.3
PV5	T	-	-	-	2.3	2.5
	RH	-	-	-	45.1	45.4
PV6	T	-	-	-	2.3	2.5
	RH	-	-	-	45.2	45.4
PV7	T	-	-	-	-	2.5
	RH	-	-	-	-	45.4
PV8	T	-	-	-	-	2.5
	RH	-	-	-	-	45.4
PV9	T	-	-	-	-	2.5
	RH	-	-	-	-	45.4
PV10	T	-	-	-	-	2.4
	RH	-	-	-	-	45.3
PV11	T	-	-	-	-	2.4
	RH	-	-	-	-	45.3
PV12	T	-	-	-	-	2.4
	RH	-	-	-	-	45.3
PV13	T	-	-	-	-	2.5
	RH	-	-	-	-	45.4

(Note: red numbers are minimum error rates)

Table 5.6 (continued)

Data pre-processing methods	T/RH	Error rate of simulated indoor T/RH based on different time intervals (%)				
		3D	5D	7D	14D	All time
AV0	T	2.3	2.3	**2.2**	**2.2**	2.4
	RH	45.2	45.1	45.1	**45.0**	45.3
AV1	T	2.3	2.3	**2.2**	**2.2**	2.4
	RH	**45.0**	**45.0**	**45.0**	**45.0**	45.3
AV2	T	2.3	2.3	**2.2**	**2.2**	2.4
	RH	**45.0**	**45.0**	45.1	45.1	45.3
AV3	T	-	-	**2.2**	**2.2**	2.4
	RH	-	-	45.1	45.1	45.3
AV4	T	-	-	-	2.3	2.5
	RH	-	-	-	45.1	45.4
AV5	T	-	-	-	-	2.5
	RH	-	-	-	-	45.4
AV6	T	-	-	-	-	2.5
	RH	-	-	-	-	45.4
AV7	T	-	-	-	-	2.5
	RH	-	-	-	-	45.4
AV8	T	-	-	-	-	2.5
	RH	-	-	-	-	45.4
AV9	T	-	-	-	-	2.5
	RH	-	-	-	-	45.4
AV10	T	-	-	-	-	2.4
	RH	-	-	-	-	45.3
AV11	T	-	-	-	-	2.4
	RH	-	-	-	-	45.3
AV12	T	-	-	-	-	2.4
	RH	-	-	-	-	45.3
AV13	T	-	-	-	-	2.5
	RH	-	-	-	-	45.4
TL	T	2.3	2.3	2.3	2.3	2.4
	RH	45.2	45.1	45.2	45.1	45.3
Theoretical U	T	2.5				
	RH	45.5				

(Note: red numbers are minimum error rates)

Table 5.7 shows the error rates of simulated indoor T/RH when different U-values in the brick tested room are considered. In the TD, PV and AV methods, the temperature difference used for screening data was also considered between 0°C and 13°C; the reason was the same as that in the previous case. The minimum error rates of T/RH were 3.1% and 45.5%, respectively. These two error rates were based on some dynamic U-values. The U-value calculation methods that could obtain both the minimum temperature error rate and minimum relative humidity error rate at the same time were the TL method with 14-day interval.

Table 5.7 Error rates of simulated indoor T/RH in the brick tested room

Data pre-processing methods	T/RH	Error rate of simulated indoor T/RH based on different time intervals (%)				
		3D	5D	7D	14D	All time
ND	T	-	-	-	-	3.7
	RH	-	-	-	-	46.2
TD0	T	-	-	-	-	3.3
	RH	-	-	-	-	46.1
TD1	T	-	-	-	-	3.3
	RH	-	-	-	-	46.1
TD2	T	-	-	-	-	3.3
	RH	-	-	-	-	46.1
TD3	T	-	-	-	-	3.3
	RH	-	-	-	-	46.1
TD4	T	-	-	-	-	3.3
	RH	-	-	-	-	46.1
TD5	T	-	-	-	-	3.3
	RH	-	-	-	-	46.1
TD6	T	-	-	-	-	3.3
	RH	-	-	-	-	46.1
TD7	T	-	-	-	-	3.3
	RH	-	-	-	-	46.1
TD8	T	-	-	-	-	3.3
	RH	-	-	-	-	46.1
TD9	T	-	-	-	-	3.3
	RH	-	-	-	-	46.1
TD10	T	-	-	-	-	3.3
	RH	-	-	-	-	46.1
TD11	T	-	-	-	-	3.3
	RH	-	-	-	-	46.1
TD12	T	-	-	-	-	3.4
	RH	-	-	-	-	45.9
TD13	T	-	-	-	-	3.4
	RH	-	-	-	-	45.9

(Note: red numbers are minimum error rates)

Table 5.7 (continued)

Data pre-processing methods	T/RH	Error rate of simulated indoor T/RH based on different time intervals (%)				
		3D	5D	7D	14D	All time
PV0	T	3.4	3.3	3.2	3.3	3.4
	RH	46.1	46.0	45.7	**45.5**	45.9
PV1	T	3.4	3.3	3.2	**3.1**	3.4
	RH	46.1	46.0	45.7	45.6	45.9
PV2	T	3.4	3.3	**3.1**	**3.1**	3.4
	RH	46.1	46.1	45.9	45.6	45.9
PV3	T	3.4	3.3	3.2	**3.1**	3.4
	RH	46.2	46.1	45.8	45.7	45.9
PV4	T	-	3.3	3.2	3.2	3.4
	RH	-	46.1	45.9	45.7	45.9
PV5	T	-	-	3.2	3.2	3.3
	RH	-	-	45.9	45.8	46.1
PV6	T	-	-	-	-	3.3
	RH	-	-	-	-	46.1
PV7	T	-	-	-	-	3.3
	RH	-	-	-	-	46.1
PV8	T	-	-	-	-	3.3
	RH	-	-	-	-	46.1
PV9	T	-	-	-	-	3.3
	RH	-	-	-	-	46.1
PV10	T	-	-	-	-	3.4
	RH	-	-	-	-	45.9
PV11	T	-	-	-	-	3.4
	RH	-	-	-	-	45.9
PV12	T	-	-	-	-	3.4
	RH	-	-	-	-	45.9
PV13	T	-	-	-	-	3.4
	RH	-	-	-	-	45.9

(Note: red numbers are minimum error rates)

Table 5.7 (continued)

Data pre-processing methods	T/RH	Error rate of simulated indoor T/RH based on different time intervals (%)				
		3D	5D	7D	14D	All time
AV0	T	3.3	3.2	3.2	3.3	3.3
	RH	46.3	46.0	45.7	**45.5**	46.1
AV1	T	3.4	3.2	3.2	**3.1**	3.3
	RH	46.4	46.1	45.8	45.6	46.1
AV2	T	3.4	3.3	**3.1**	**3.1**	3.3
	RH	46.4	46.1	45.8	45.6	46.1
AV3	T	3.4	3.3	**3.1**	**3.1**	3.3
	RH	46.4	46.1	45.9	45.7	46.1
AV4	T	3.4	3.3	3.2	**3.1**	3.3
	RH	46.5	46.2	45.9	45.7	46.1
AV5	T	3.4	3.3	3.2	3.2	3.3
	RH	46.5	46.2	46.0	45.8	46.1
AV6	T	-	-	-	3.2	3.3
	RH	-	-	-	45.8	46.1
AV7	T	-	-	-	-	3.3
	RH	-	-	-	-	46.1
AV8	T	-	-	-	-	3.3
	RH	-	-	-	-	46.1
AV9	T	-	-	-	-	3.3
	RH	-	-	-	-	46.1
AV10	T	-	-	-	-	3.3
	RH	-	-	-	-	46.1
AV11	T	-	-	-	-	3.3
	RH	-	-	-	-	46.1
AV12	T	-	-	-	-	3.4
	RH	-	-	-	-	45.9
AV13	T	-	-	-	-	3.4
	RH	-	-	-	-	45.9
TL	T	3.3	3.3	3.2	**3.1**	3.6
	RH	46.5	45.9	45.6	**45.5**	46.2
Theoretical U	T	4.6				
	RH	46.8				

(Note: red numbers are minimum error rates)

Considering the results of the four cases, the TL, PV1 and AV1 methods were chosen as the optimal data pre-processing methods. In particular, the TL method showed substantial strengths in the accuracy of simulated indoor T/RH in the CLT tested room.

The 14-day interval was chosen as the optimal time interval as each measurement in the RC and brick tested rooms was about two weeks. This was a shortcoming in the programme design phase of the in-situ measurements. If only the results of CLT and masonry tested rooms were considered, the 30-day interval was the optimal time interval.

The error rates of the simulated indoor temperature in the CLT tested rooms were the highest among four cases, and the error rates of the simulated indoor relative humidity in the CLT tested rooms were relatively high. This might have been due to the CLT tested room having four external envelopes, which are more than those of other three tested rooms. Some outdoor environment data, such as wind speed and direction, had a degree of uncertainty owing to the differences of weather conditions between weather stations and the tested rooms. The impacts of this uncertainty on the simulations of the CLT tested rooms were more significant than the impacts on the simulations of the other three tested rooms.

The error rates of the simulated indoor relative humidity in the RC and brick tested rooms were particularly high. It was related to extreme winter conditions in Harbin and the deficiencies of TRNSYS settings. In TRNSYS settings, the air change rates of the test rooms referred to the air exchange between indoor and outdoor environment. If the room only exchanges air with the outdoor environment, the absolute humidity (mass of water vapour in air) of the indoor and outdoor environments will converge. With a huge temperature difference between indoor and outdoor environment, the gap in relative humidity (the ratio of the absolute humidity phase to the maximum humidity at a given temperature) between indoor and outdoor environments will also be huge; this is because the maximum humidity, which is the humidity of the air when it is saturated with water vapour, is related to the air temperature.

For example, the outdoor temperature in Harbin can reach -30°C in winter. When relative humidity is 100% at -30°C, absolute humidity is 0.46 g/m^3. When absolute humidity is 0.46 g/m^3, relative humidity is lower than 10% at 20°C. In other words, in TRNSYS, the simulated indoor relative humidity of the RC and brick tested rooms was abnormally low in the winter owing to the air exchange only with the outdoor environment. However, the measured indoor relative humidity in Harbin in the winter was kept at about 30%; thus, the air exchange in the tested rooms was not entirely dependent on the outdoor environment, even though no one entered the tested rooms during the measurements, and the room door was always closed. The tested room still exchanged air with the neighbouring rooms owing to the influence of the gaps in the internal envelopes. However, setting the air change rate between different rooms in TRNSYS was not possible; this resulted in large errors in the simulated indoor relative humidity in winter in Harbin.

5.3 Summary

The dynamic and average U-values of the four tested envelopes were obtained based on different calculation methods. The dynamic U-values of the masonry cavity and brick envelopes had more significant seasonality, which showed lower U-values in summer and higher U-values in winter. After validation by indoor T/RH simulation, the dynamic U-values were more accurate than the theoretical and average U-values. The optimal dynamic U-value calculation methods were included in two parts: (1) the optimal data pre-processing methods were the TL, PV1 and AV1 methods; (2) the optimal time interval was 14 days. In Chapter 6, the optimal data pre-processing methods were used to obtain accurate dynamic U-values, which were the dependent variables in the U-value prediction models. In Chapter 7, the optimal time interval was used to simplify the predicted dynamic U-values for building operational energy simulations.

Chapter 6 The Prediction Models of Dynamic U-values

Based on the calculated dynamic U-values, the linear and non-linear U-value prediction models were built in Section 6.1 and 6.2, respectively. In Section 6.3, these two models were applied to predict the dynamic U-values of the CLT, masonry cavity, RC and brick envelopes in 11 case cities. The model that can offer reasonable results was chosen as the optimal U-value prediction model.

6.1 Linear U-value Prediction Model

The HLR method was applied to build the linear U-value prediction model through SPSS. Building the linear U-value prediction model involved three stages: selecting the suitable dataset, setting independent variables and determining the best model.

(1) Dataset

When the U-value prediction model was built, the dependent variable was the calculated dynamic U-values of the four envelopes. Three datasets could be employed, including the data pre-processed by the PV1, AV1 and TL methods, owing to the fact that the equipment recorded data every five minutes. The data pre-processed by the PV1 and AV1 methods included dynamic U-values with five-minute time intervals, indoor T/RH every five minutes and outdoor T/RH every five minutes. The sample sizes of the data pre-processed by the PV1 and AV1 methods were 83,133 and 121,215, respectively. Different from the first two methods, in the TL method, the minimum time interval at which a U-value can be calculated is 1 day. The data pre-processed by the TL method included dynamic U-values with 1-day time intervals, daily average indoor T/RH and daily average outdoor T/RH. The data sample size was 461.

The dynamic U-values with five-minute time interval obtained by the PV1 and AV1 methods contain a small number of extreme high and low values, as shown in Figures 6.1 and 6.2; this can affect the linear regression model's predictive ability. The dynamic U-values with 1-day time intervals obtained by the TL method have a more reasonable range, as shown in Figure 6.3. Therefore, the data pre-processed by the TL method were chosen for building the linear U-value prediction model.

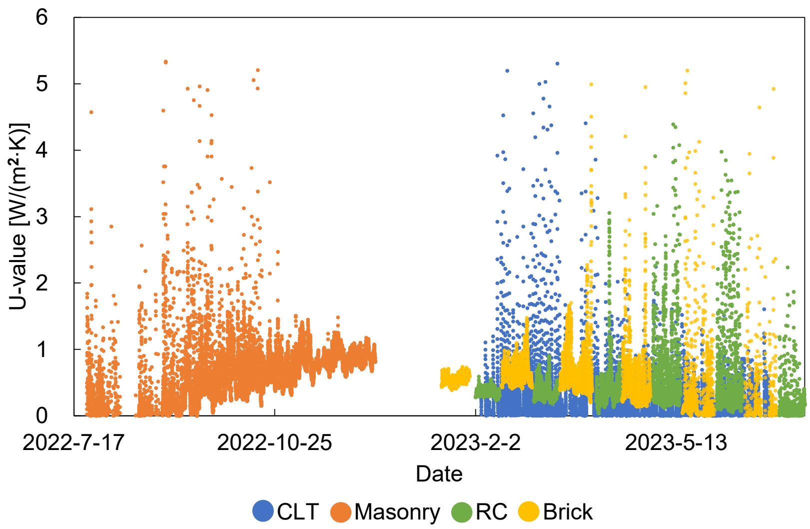

Figure 6.1 Dynamic U-values with 5-minute interval pre-processed by the PV1 method

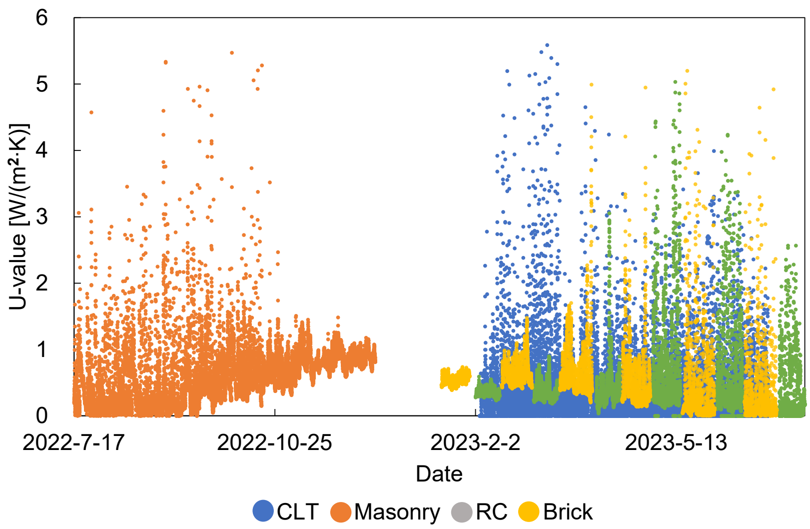

Figure 6.2 Dynamic U-values with 5-minute interval pre-processed by the AV1 method

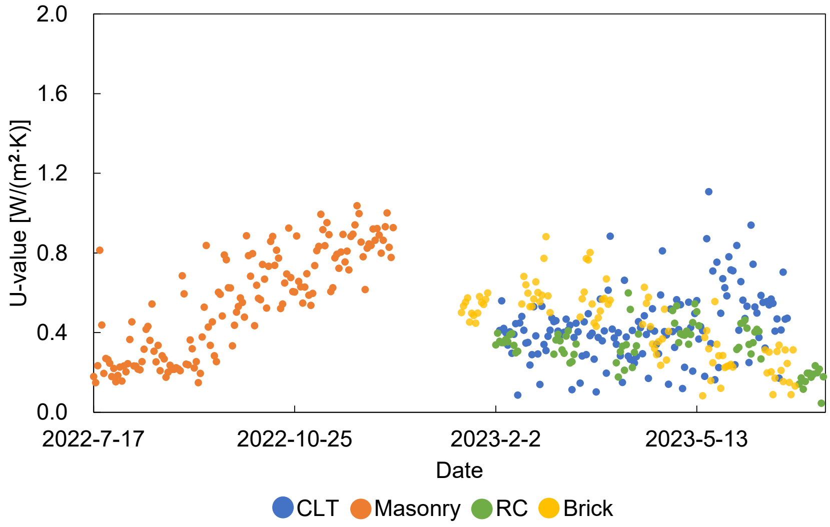

Figure 6.3 Dynamic U-values with one-day interval pre-processed by the TL method

(2) Independent variables

The independent variables included up to a categorical variable (the type of envelopes) and four continuous variables (including indoor T/RH and outdoor T/RH). In the HLR method, categorical variables cannot be entered directly into the model like continuous variables, and categorical variables need to be set as dummy variables. Whether or not it belongs to a category, a dummy variable is indicated by 1 or 0, with 1 indicating it belongs and 0 indicating it does not. The number of dummy variables corresponds to the number of categories in the categorical variables. In this study, the type of envelopes contained four categories (including CLT, masonry cavity, RC and brick envelopes). Four dummy variables were set as $\boldsymbol{A}$, $\boldsymbol{B}$, $\boldsymbol{C}$ and $\boldsymbol{D}$, as shown in Table 6.1. As shown in Table 6.2, four continuous independent variables – indoor temperature, indoor relative humidity, outdoor temperature and outdoor relative humidity – were set as $\mathbf{1}$, $\mathbf{2}$, $\mathbf{3}$ and $\mathbf{4}$, respectively. $\mathbf{1}$, $\mathbf{2}$, $\mathbf{3}$ and $\mathbf{4}$ contain the data of all measurements of the four tested envelopes. For the U-value prediction model to predict the dynamic U-values of the four envelopes separately, $\mathbf{1}$, $\mathbf{2}$, $\mathbf{3}$ and $\mathbf{4}$ could not be used to directly build the U-value prediction model. $\mathbf{1}$, $\mathbf{2}$, $\mathbf{3}$ and $\mathbf{4}$ needed to be multiplied with $\boldsymbol{A}$, $\boldsymbol{B}$, $\boldsymbol{C}$ and $\boldsymbol{D}$ separately to combine the new independent variables. For example, $\boldsymbol{A1}$

represents the indoor temperature in the measurement of the CLT envelope. All independent variables that may be applied are shown in Table 6.3.

Table 6.1 Dummy variables in the independent variables

Dummy variables	Meaning
$\boldsymbol{A}$	‘1’ indicates that these data belong to the CLT envelope category; ‘0’ indicates that they do not.
$\boldsymbol{B}$	‘1’ indicates that these data belong to the masonry cavity envelope category; ‘0’ indicates that they do not.
$\boldsymbol{C}$	‘1’ indicates that these data belong to the RC envelope category; ‘0’ indicates that they do not.
$\boldsymbol{D}$	‘1’ indicates that these data belong to the brick envelope category; ‘0’ indicates that they do not.

Table 6.2 Continuous variables in the independent variables

Continuous variables	Meaning
1	Indoor temperature
2	Indoor relative humidity
3	Outdoor temperature
4	Outdoor relative humidity

Table 6.3 Independent variables for the linear U-value prediction model

Independent variable	Meaning
$\boldsymbol{A1}$	Indoor temperature in the measurement of the CLT envelope
$\boldsymbol{A2}$	Indoor relative humidity in the measurement of the CLT envelope
$\boldsymbol{A3}$	Outdoor temperature in the measurement of the CLT envelope
$\boldsymbol{A4}$	Outdoor relative humidity in the measurement of the CLT envelope
$\boldsymbol{B1}$	Indoor temperature in the measurement of the masonry cavity envelope
$\boldsymbol{B2}$	Indoor relative humidity in the measurement of the masonry cavity envelope
$\boldsymbol{B3}$	Outdoor temperature in the measurement of the masonry cavity envelope
$\boldsymbol{B4}$	Outdoor relative humidity in the measurement of the masonry cavity envelope
$\boldsymbol{C1}$	Indoor temperature in the measurements of the RC envelope
$\boldsymbol{C2}$	Indoor relative humidity in the measurements of the RC envelope
$\boldsymbol{C3}$	Outdoor temperature in the measurements of the RC envelope
$\boldsymbol{C4}$	Outdoor relative humidity in the measurements of the RC envelope
$\boldsymbol{D1}$	Indoor temperature in the measurements of the brick envelope
$\boldsymbol{D2}$	Indoor relative humidity in the measurements of the brick envelope
$\boldsymbol{D3}$	Outdoor temperature in the measurements of the brick envelope
$\boldsymbol{D4}$	Outdoor relative humidity in the measurements of the brick envelope

(3) The best model

When the HLR method is used, independent variables are added to the model in order of importance. In this study, the outdoor T/RH of every measurement case was added as the more important independent variable before the indoor T/RH of every measurement case because the outdoor T/RH datasets of every measurement case are less affected by human factors and have higher objectivity. These datasets are strongly correlated with the climate zones in which the tested buildings are located.

When independent variables were added one by one, the three indicators of the prediction model needed to be observed to determine if the model was the best one. First, the variance inflation factor (VIF) of every independent variable was less than 10. VIF less than 10 is generally considered acceptable, which indicates that the multicollinearity of the independent variable is not significant in the model (Lyles 2006; Jeng 2023). Second, the P-value of every independent variable was less than 0.05. A P-value less than 0.05 suggests a statistically significant relationship, which shows that the independent variable may affect the dependent variable with great probability (Ciulla and D'Amico 2019). Third, the model's coefficient of determination (R^2) needed to be as large as possible when filling in the first two requirements. A large R^2 indicates a great predictive power of the linear regression model (Liu, Heuvelink, et al. 2021). The range of R^2 is between 0 to 1, and the formula of R^2 is shown in Equation (13).

$$R^2 = \frac{\sum_{i=1}^{n}(\hat{y_i}-\bar{y})^2}{\sum_{i=1}^{n}(y_i-\bar{y})^2} \tag{13}$$

Where $\boldsymbol{n}$ is the number of samples; $\boldsymbol{y_i}$ is the measured value for the **i**-th sample; $\boldsymbol{\hat{y_i}}$ is the predicted value for the **i**-th sample, and $\boldsymbol{\bar{y}}$ is the average value of measured values.

Finally, the best linear U-value prediction model was built, as shown in Table 6.4 and Equation (14). The R^2 of the best linear U-value prediction model was 0.456. According to Equation (14), the most important influences are different when U-values for different envelopes are predicted. Outdoor T/RH are the most important influences in predicting U-values for the CLT and masonry cavity envelopes. Outdoor relative humidity is the most important influence in predicting U-values for the RC envelope. Outdoor temperature is the most important influence in predicting U-values for the brick envelope.

Table 6.4 Detailed information of the best linear U-value prediction model

Output	Input	VIF	P-value	B (unstandardised coefficients)	R^2
U-value (CLT/masonry /RC/brick)	$\boldsymbol{A3}$	6.949	<0.001	0.011	0.456
	$\boldsymbol{A4}$	7.595	<0.001	-0.003	
	$\boldsymbol{B3}$	2.755	<0.001	-0.021	
	$\boldsymbol{B4}$	3.136	<0.001	0.005	
	$\boldsymbol{C4}$	1.516	<0.001	-0.003	
	$\boldsymbol{D3}$	1.128	<0.001	-0.007	
	(Constant)		<0.001	0.480	

$$U(CLT/Masonry/RC/Brick) = 0.011 \times T_{out}(CLT) - 0.003 \times RH_{out}(CLT) - 0.021 \times T_{out}(Masonry) + 0.005 \times RH_{out}(Masonry) - 0.003 \times RH_{out}(RC) - 0.007 \times T_{out}(Brick) + 0.48 \ \ [\mathrm{W/(m^2 \cdot K)}] \tag{14}$$

Where $\boldsymbol{U}$ is the U-value $[\mathrm{W/(m^2 \cdot K)}]$; $\boldsymbol{T_{out}}$ is outdoor temperature [°C]; $\boldsymbol{RH_{out}}$ is outdoor temperature [%]. $\boldsymbol{CLT/Masonry/RC/Brick}$ represent CLT, masonry cavity, RC and brick envelopes, respectively.

6.2 Non-linear U-value Prediction Model

The MLP model was applied to build the non-linear U-value prediction model through Python. The independent variables included a categorical variable (the type of envelopes) and four continuous variables (including indoor T/RH and outdoor T/RH). The dependent variable was the calculated dynamic U-values of the four envelopes. The stages to build the non-linear U-value prediction model were three: preparing the data, building and training model and determining the best model.

(1) Preparing the data

The data pre-processed by the AV1 method were chosen as their sample size was more adequate. The MLP model is a big data-based approach. Neural network methods have only been applied for prediction in studies with a sample size of at least 1,000 (Pino-Mejías et al. 2017; Yang et al. 2024). Although the range of the data pre-processed by the TL method was reasonable, the sample size was too small to be chosen. Compared to the data pre-processed by the AV1 method, the data pre-processed by the PV1 method had a significant lack of summer data, as shown in Figure 6.1. Thus, the data pre-processed by the PV1 method were not chosen. The min-max scaling technique, which can scale the range of the input data between 0 and 1, was applied to normalise different types of input data. The min-max scaling formula is shown in Equation (15) (Guo et al. 2024).

$$Data_{scaled} = \frac{Data - Data_{min}}{Data_{max} - Data_{min}} \qquad (15)$$

Where $\boldsymbol{Data_{scaled}}$ is the standardised input data; $\boldsymbol{Data_{max}}$ is the maximum value of input data; $\boldsymbol{Data_{min}}$ is the minimum value of input data, and $\boldsymbol{Data}$ is the input data.

(2) Building and training model

First, the input data were divided randomly into training and testing sets with a proportion of 7:3. Second, the ReLU activation function, Mean Squared Error (MSE) loss function and Adam optimizer were used to train the model. Third, Bayesian optimisation was applied to find optimal hyperparameters. All hyperparameter ranges were initially defined. Bayesian optimisation minimised the objective function, which was MSE, to obtain the optimal hyperparameter combination. MSE can measure the gap between a model's predicted and measured values; the lower the MSE, the stronger the prediction performance of a model. The formula of MSE is shown in Equation (16):

$$MSE = \frac{1}{n}\sum_{i=1}^{n}(y_i - \hat{y}_i)^2 \qquad (16)$$

Where $\boldsymbol{n}$ is the number of samples; $\boldsymbol{y_i}$ is the measured value for the **i**-th sample, and $\boldsymbol{\hat{y}_i}$ is the predicted value for the **i**-th sample.

(3) The best model

The prediction performance of the best non-linear U-value prediction model is shown in Figure 6.5. The R^2 and MSE of best non-linear U-value prediction model in the testing set were 0.637 and 0.038, respectively.

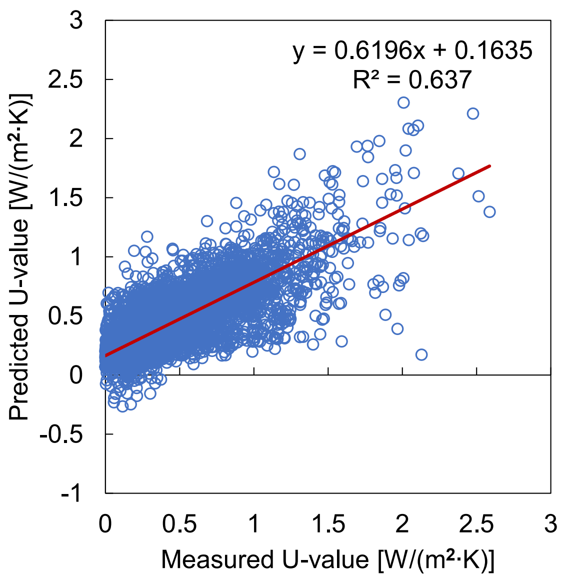

Figure 6.4 Predicted U-values and measured U-values for the testing set

6.3 Selection of the Optimal U-value Prediction Model

To compare the performance of the linear and non-linear models, both models were applied to predict the dynamic U-values of the four envelopes in 11 case cities. When independent variables were input into both the linear and non-linear models, the outdoor T/RH data in 11 case cities were obtained from weather-station data. The hourly outdoor T/RH in 2023 in 11 case cities and hourly average outdoor T/RH in 2013–2022 in 11 case cities are shown in Appendix C. Only T/RH data in 2023 were chosen for testing the performance of two U-value prediction models. Because the range and trend of outdoor T/RH fluctuations are similar in 2023 and in 2013–2022 in the same city. The indoor temperature was set to 22°C; the indoor relative humidity was set to 50%.

According to the optimal linear prediction model, indoor T/RH have no influence on U-value prediction, as these variables were not included as independent variables. In contrast, in the optimal nonlinear model, indoor T/RH were included as key independent variables and contributed to the U-value prediction. Therefore, fixing indoor T/RH values only affects the nonlinear model, while it has no impact on the linear model applied in this study.

The hourly dynamic U-values of the four envelopes predicted by both the linear and non-linear models are shown in Figures 6.5–6.15.

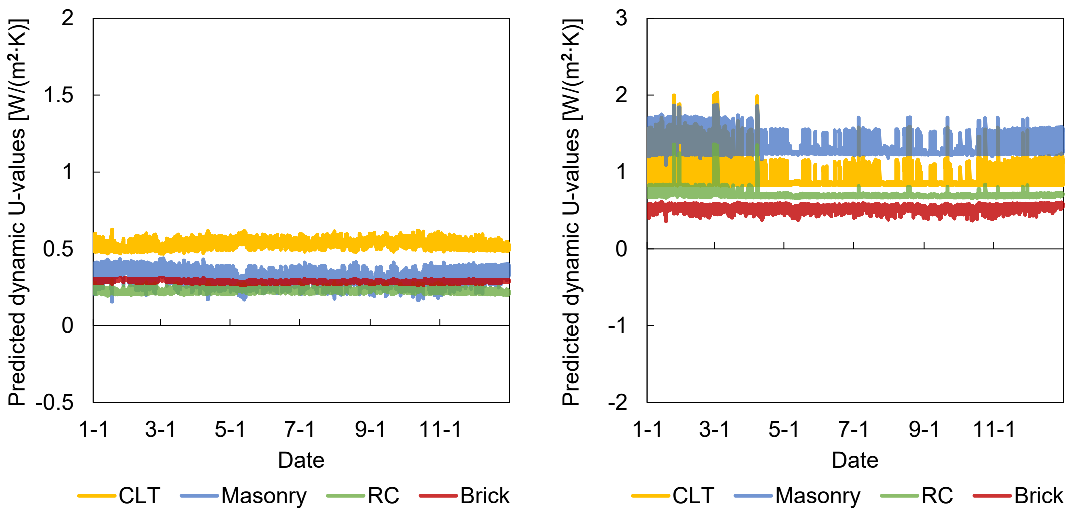

(a) Results based on the linear model (b) Results based on the non-linear model

Figure 6.5 Hourly predicted dynamic U-values of different envelopes in Singapore

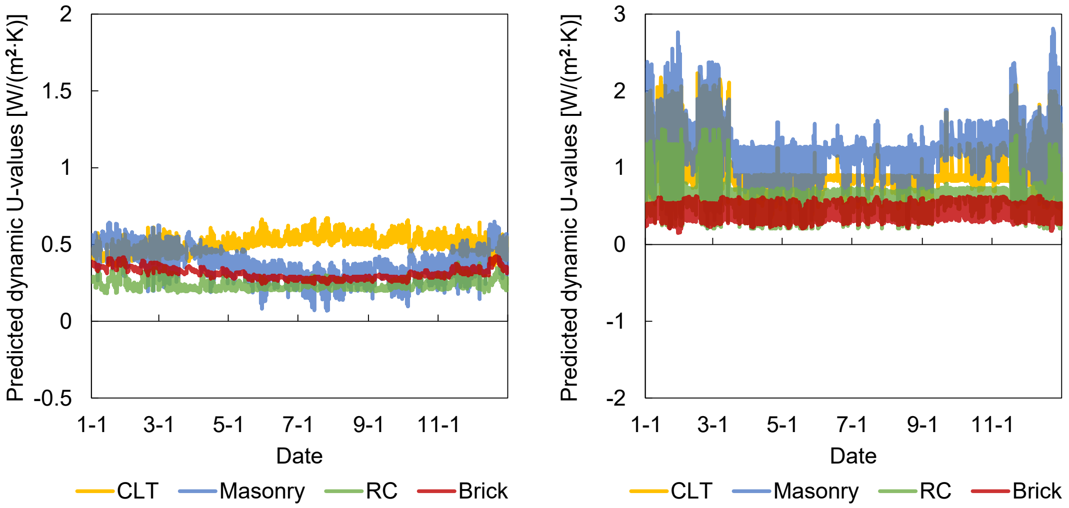

(a) Results based on the linear model (b) Results based on the non-linear model

Figure 6.6 Hourly predicted dynamic U-values of different envelopes in Bangkok

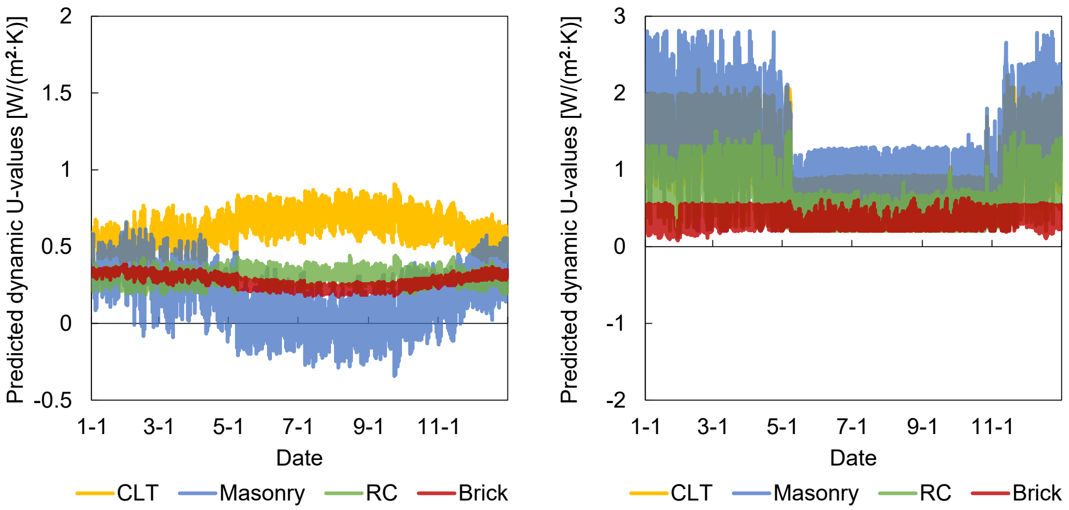

(a) Results based on the linear model (b) Results based on the non-linear model

Figure 6.7 Hourly predicted dynamic U-values of different envelopes in Dubai

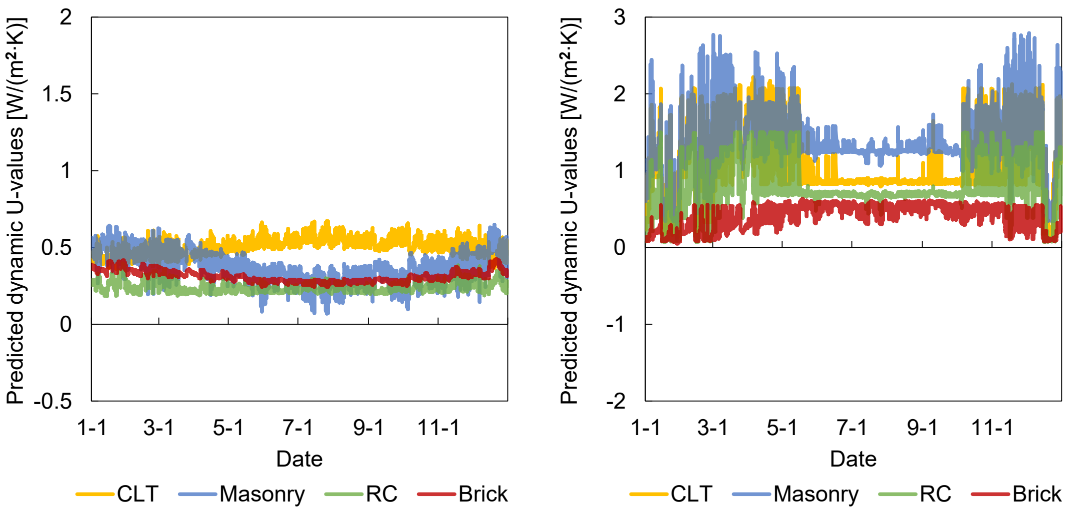

(a) Results based on the linear model (b) Results based on the non-linear model

Figure 6.8 Hourly predicted dynamic U-values of different envelopes in Hong Kong

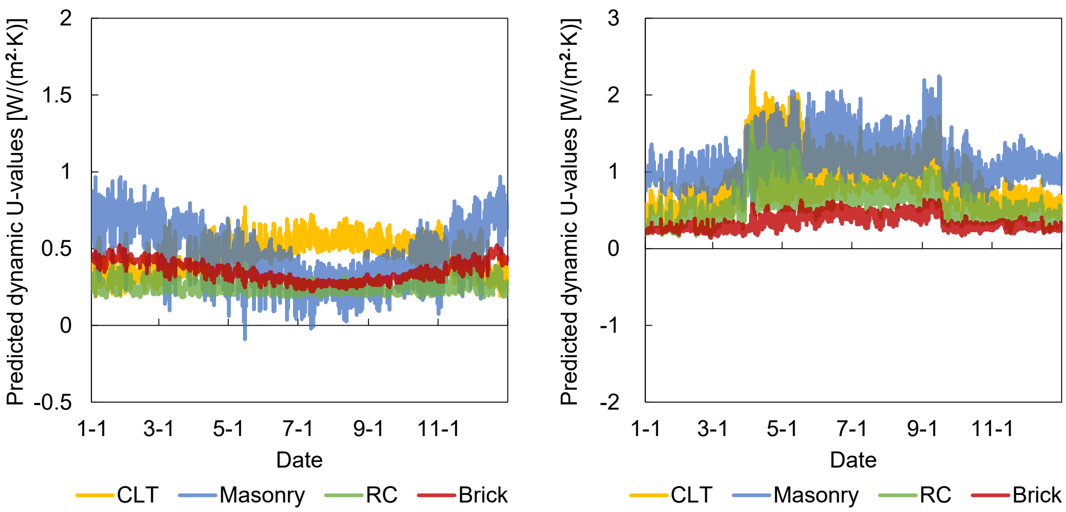

(a) Results based on the linear model (b) Results based on the non-linear model

Figure 6.9 Hourly predicted dynamic U-values of different envelopes in Shanghai

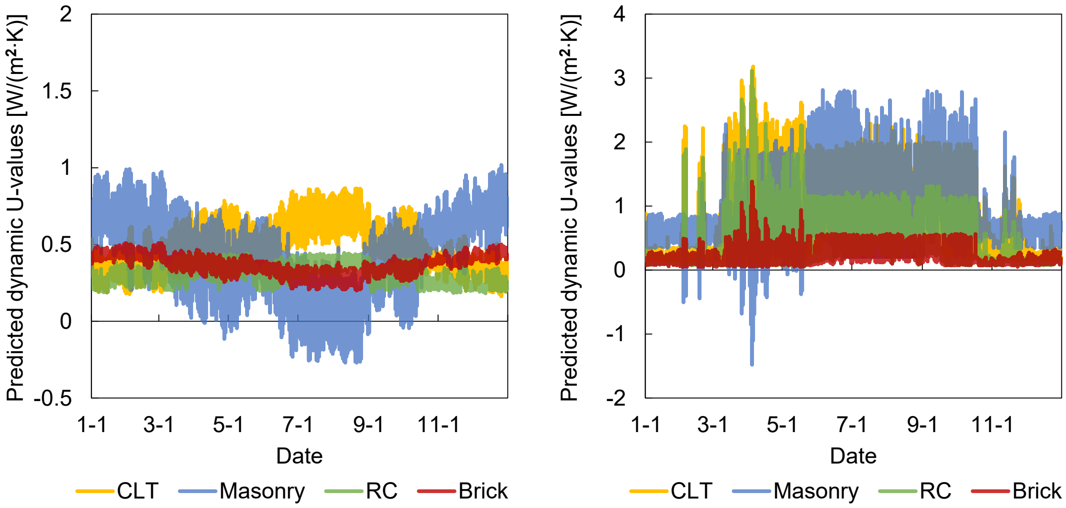

(a) Results based on the linear model (b) Results based on the non-linear model

Figure 6.10 Hourly predicted dynamic U-values of different envelopes in Madrid

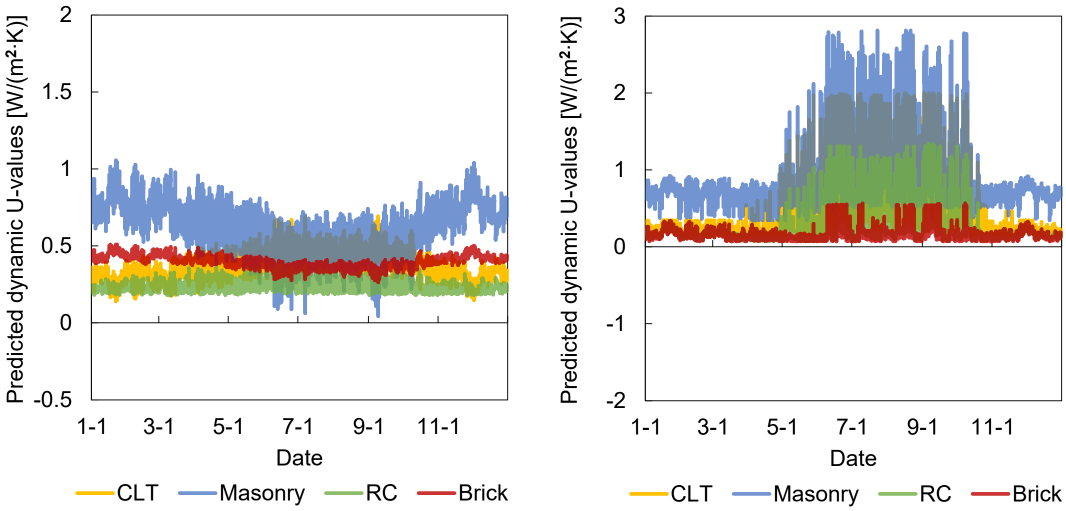

(a) Results based on the linear model (b) Results based on the non-linear model

Figure 6.11 Hourly predicted dynamic U-values of different envelopes in London

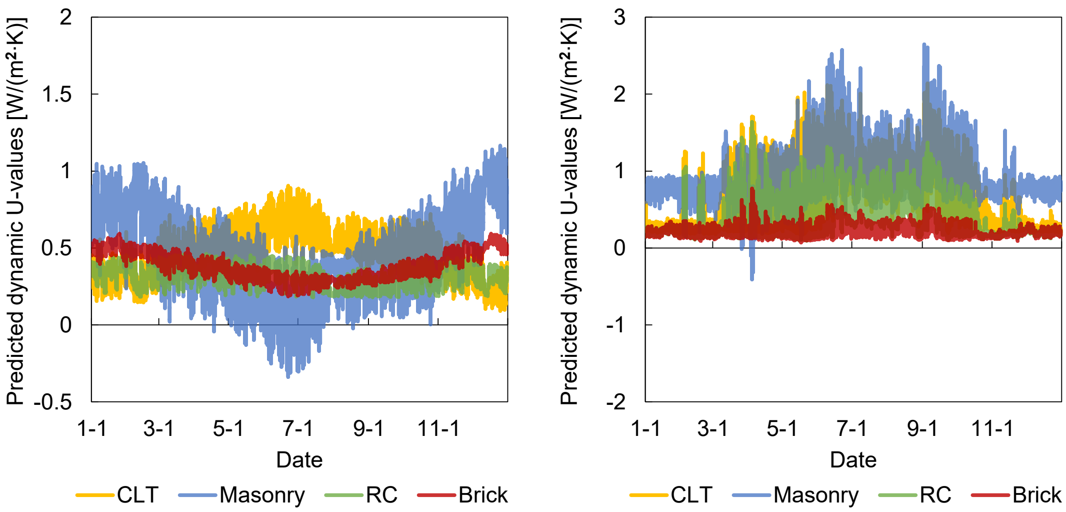

(a) Results based on the linear model (b) Results based on the non-linear model

Figure 6.12 Hourly predicted dynamic U-values of different envelopes in Beijing

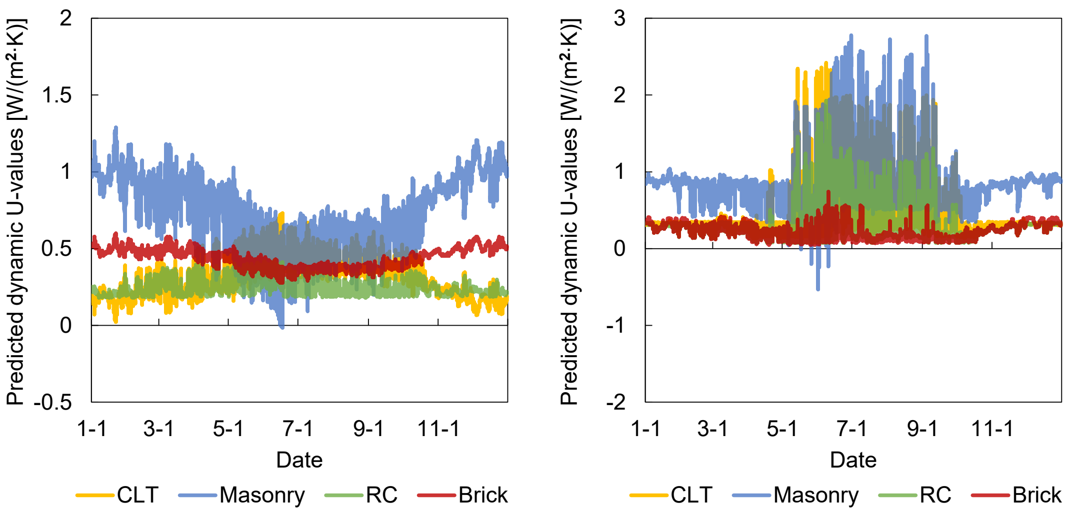

(a) Results based on the linear model (b) Results based on the non-linear model

Figure 6.13 Hourly predicted dynamic U-values of different envelopes in Oslo

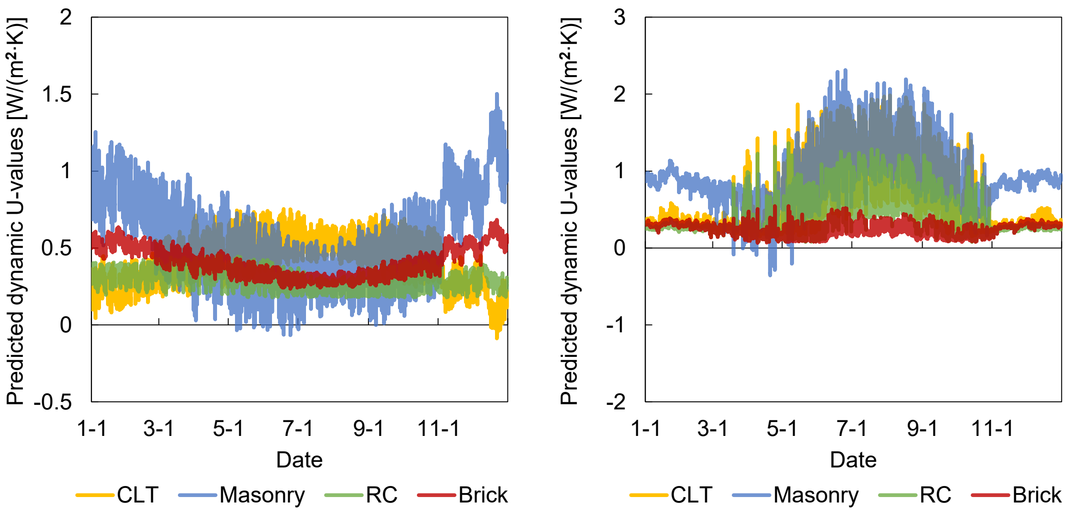

(a) Results based on the linear model (b) Results based on the non-linear model

Figure 6.14 Hourly predicted dynamic U-values of different envelopes in Shenyang

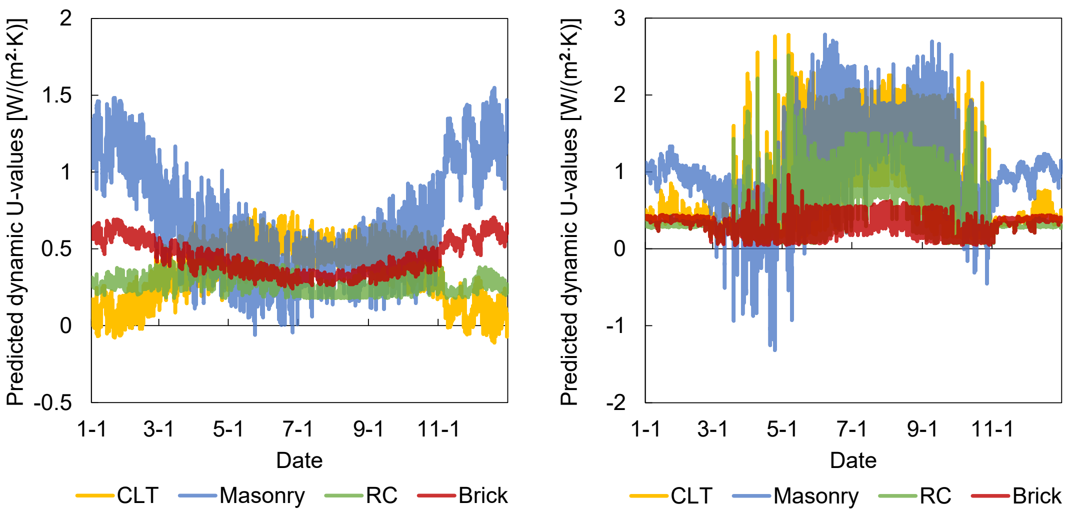

(a) Results based on the linear model (b) Results based on the non-linear model

Figure 6.15 Hourly predicted dynamic U-values of different envelopes in Harbin

To enhance the understanding of the prediction models developed, both uncertainty analysis and sensitivity analysis were conducted. In terms of uncertainty, several sources were identified. First, the measured datasets used for model training and validation may contain inherent measurement errors, particularly from sensors in in-situ U-value measurements. Second, the measured data were collected from only two climate zones, which do not represent the full range of climatic conditions in all eleven case cities. Third, the R^2 for both the linear and non-linear models were moderate rather than exceptionally high, indicating that there are limitations in the models' ability to fully capture the complexity of dynamic U-value fluctuations.

Sensitivity analysis revealed that the prediction results were significantly influenced by two factors: envelope type and climate zone. The models showed high sensitivity to envelope type, as evidenced by greater variations in predicted dynamic U-values for the masonry and CLT envelopes compared to the RC and brick envelopes. Additionally, climate zone had a notable impact on the predicted dynamic U-values. For example, predicted U-values in climate zone D exhibited larger fluctuations than those in climate zone A. These findings highlight that both material characteristics and environmental conditions play critical roles in determining dynamic U-values.

The hourly dynamic U-values predicted by the linear model are relatively reasonable. The characteristics of these predicted U-values matched those of the calculated dynamic U-values based on measured data. In case cities in climate zones C and D, most of these cities have warm summers and cold winters, including Harbin, London, Oslo, Shenyang, Beijing, Shanghai and Madrid. The dynamic U-values of the masonry cavity and brick envelopes in these cities increased from summer to winter. The dynamic U-values of the CLT envelope show an opposite trend. The dynamic U-values of the brick envelope were relatively flat throughout the year. The ranges of dynamic U-values of all envelopes in 11 case cities were almost between 0 $\mathrm{W/(m^2 \cdot K)}$ and 1.5 $\mathrm{W/(m^2 \cdot K)}$. The predicted results only had a few outliers, such as the negative U-values of the masonry cavity envelope in the summer in Madrid, Beijing and Dubai.

The hourly dynamic U-values predicted by the linear model point to another conclusion. In case cities where the outdoor T/RH were stable throughout the year (such as Hong Kong, Singapore and Bangkok), the dynamic U-values of all envelopes were flat. As the dynamic U-values are related to T/RH, this conclusion is reasonable in terms of physics, and it can be verified by in-situ measurements in future studies.

The hourly dynamic U-values predicted by the non-linear model are not totally reasonable. First, the trend of the predicted dynamic U-values did not follow physics. The predicted dynamic U-values of the CLT, masonry cavity and RC envelopes increased abruptly in the spring and decreased abruptly in autumn in Harbin, London, Oslo, Shenyang, Beijing, Shanghai and Madrid. The predicted dynamic U-values of the CLT, masonry cavity and RC envelopes decreased abruptly in the spring and increased abruptly in autumn in Hong Kong, Dubai and Bangkok. In the absence of abrupt changes in environmental conditions, the predicted dynamic U-values should not change abruptly in terms of physics. Second, the trend of the predicted dynamic U-values did not correspond to the results of in-situ measurements. In calculated dynamic U-values of the masonry cavity and brick envelopes based on measured data, the U-values in winter were higher the those in the summer in cold climate zones, such as Sheffield and Harbin. However, in the predicted dynamic U-values of the masonry cavity and brick envelopes, U-values in the winter were lower those in the summer in cold climate zones such as Harbin, London, Oslo and Shenyang.

The reasons why the dynamic U-values predicted by the non-linear model were not reasonable may be three. First, the sample size of the data may be inadequate for the MLP model. Neural network regression models require a higher sample size than linear regression models. This study only collected data from four envelopes in three cities of C and D climate zones, and data from other climate zones were not included. Moreover, the measurement period of each envelope did not exceed six months; thus, the data for the entire year were not obtained. Second, this research question may not suit the non-linear method. According to a literature review in Chapter 2, a linear relationship exists between T/RH and the thermal conductivities of some building materials. Meanwhile, a positive linear relationship exists between the U-values of building envelopes and the thermal conductivities of building materials. Thus, a linear relationship may be found between T/RH and the U-values of these four types of building envelopes. Compared with the non-linear method, the linear method may be more suitable for predicting the

U-values of building envelopes. Third, the difference in the characteristics of the measured indoor T/RH and the indoor T/RH entered into the prediction model resulted in anomalous prediction results. While measurements were conducted, the tested rooms contained no heating and cooling equipment, which resulted in greater fluctuations in measured indoor T/RH rather than in the fixed indoor T/RH input into the prediction model. If fluctuating indoor T/RH under normal use can be measured and applied in the non-linear model, it may be possible to improve the accuracy of the predicted dynamic U-values.

Finally, the linear U-value prediction model was chosen as the optimal U-value prediction model. It has three advantages. First, this model has universal applicability and can obtain reasonable dynamic U-values in different climate zones. Second, it requires a few parameters. As long as a city's outdoor T/RH is known, this model can predict the dynamic U-values of the four types of envelopes. Third, using this model requires only basic arithmetic without running complex code.

6.4 Summary

The linear U-value prediction model was developed by the HLR method. The non-linear U-value prediction model was developed by the MLP model. The dynamic U-values of the four envelopes in 11 case cities were predicted by both prediction models for comparing the performance of both prediction models. The results predicted by the linear model were more reasonable. Compared with the predicted U-values by the non-linear model, the predicted U-values by the linear model were more consistent with the characterisation of the measured results and with the principles of physics. Finally, the linear model was chosen as the optimal U-value prediction model.

Chapter 7 Operational Energy Use of CLT and Conventional Buildings

The operational energy use of CLT, masonry, RC and brick buildings in 11 case cities when the theoretical, average and dynamic U-values were considered was simulated by TRNSYS. The workflow of updating dynamic U-values for simulations are shown in Section 7.1. Section 7.2 introduces the settings in building energy simulations. Section 7.3 shows the predicted annual average U-values, the predicted dynamic U-values with 14-day intervals, and the simulated results. Sections 7.4 and 7.5 discussed the lowest-energy building types across different climate zones and the influence of dynamic U-values on energy use, respectively. Section 7.6 shows discussion about the uncertainty and sensitivity analysis, the energy use in the insulated CLT building, and building codes in different climate zones.

7.1 Workflow of Updating Dynamic U-values for Simulations

Before the operational energy use of CLT and conventional buildings was simulated, the dynamic U-values of the CLT and other three conventional envelopes with the optimal time interval in 11 case cities needed to be obtained. The workflow about how to obtain the updating dynamic U-values for simulations was shown in Figure 7.1.

Firstly, the measured data (obtained in Chapter 4) were pre-processed by the optimal method (obtained in Chapter 5). Secondly, the pre-processed data were used to build the U-value prediction model in Chapter 6. Thirdly, the predicted dynamic U-values were obtained based on both the U-value prediction model and the hourly weather data in 11 case cities in Chapter 6. Fourthly, in Chapter 7, the predicted dynamic U-values were simplified by the optimal time interval (obtained in Chapter 5). Finally, the updating dynamic U-values were obtained. The updating dynamic U-values with 14-day intervals included the average hourly U-values within each 14-day time interval.

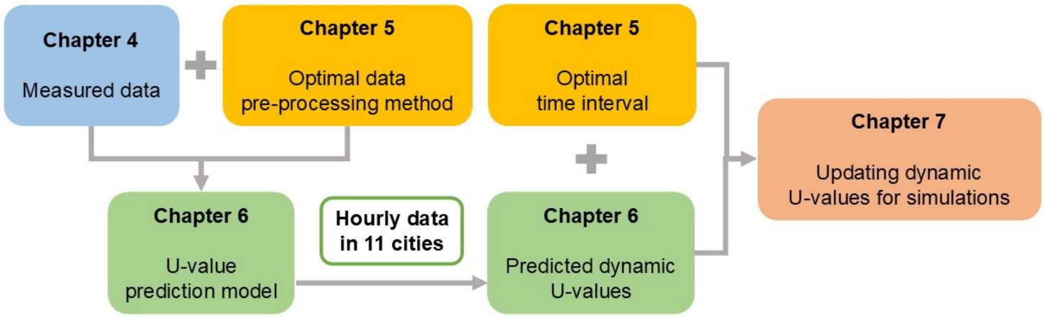

Figure 7.1 Workflow of updating dynamic U-values for simulations

7.2 Operational Energy Simulations by TRNSYS

The operational energy simulations of CLT and conventional buildings were conducted by TRNSYS. The theoretical, predicted annual average and predicted dynamic U-values of CLT, masonry cavity, RC and brick envelopes were sequentially entered into the simulations. The operational energy use of the CLT, masonry, RC and brick buildings in 11 case cities was obtained when three types of U-values were considered. The operational energy simulations included three stages: (1) making weather files, (2) modelling the reference building and (3) setting parameters.

(1) Making weather files

The hourly weather data of 11 case cities from 2013 to 2023 were obtained from the weather station (Solcast 2016) and included outdoor T/RH, solar radiation (GHI and DHI), wind direction and wind speed. The weather files of each case city also included latitude and longitude, time zone, simulation time interval and start time. The simulation time interval was set to 1 hour. The start time was set to the first hour on 1 January. Two weather files were produced for each case city. The first file included hourly weather data in 2023, and the second file included average hourly weather data from 2013 to 2022. The customised hourly weather data was created in Excel. A Type9c data reader module was used in TRNSYS to import this dataset. The outputs of the Type9c module were connected to the corresponding input nodes of the building model

(Type56), allowing simulations to be conducted under realistic and location-specific weather conditions.

(2) Modelling the reference building

The reference building model was built by SketchUp and TRNSYS 3D, as shown in Figure 7.2. Once the geometry and zoning were completed, the model was exported as a .idf file, which was then converted into a TRNSYS-compatible building input file (.bui). This .bui file was used in the Type56 module within TRNSYS for simulations. The dimensions of this building reference common multi-storey residential buildings. The reference building has six floors, each with an area of 520 m^2. Each floor has 24 windows, and the ground floor has an external door.

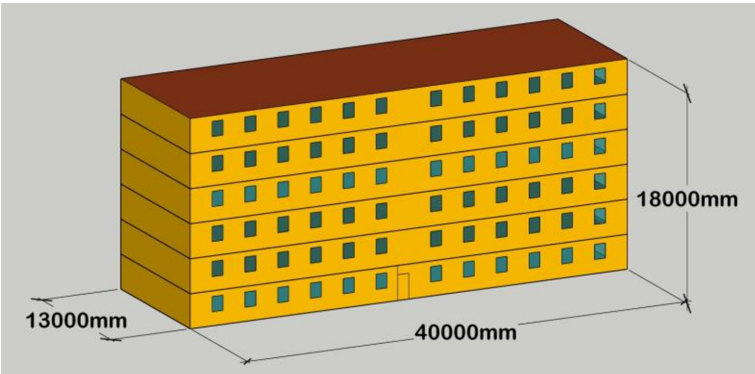

Figure 7.2 Reference building model

(3) Setting parameters

When the spatial boundary conditions for the reference building were set, the weather files of 11 case cities in 2023 and 2013–2022 were entered as external boundary conditions. When the time boundary conditions were set, the simulation time was from the first hour on 1 January to the last hour on 31 December, and the simulation step was set to 1 hour. The Simulation Control window in TRNSYS (accessed via the gear icon in Simulation Studio) is used to define the time boundary conditions.

When building operating parameters were set, occupancy was set to none; doors and windows were set to never operate, and the air change rate was set to 0.3 h^{-1}. The air change rate in unoccupied dwellings is around 0.3 h^{-1} (Nazaroff 2021; Bekö et al. 2016). The target indoor temperature was consistent with the indoor temperature set for predicting dynamic U-values, which was 22°C. Heating and cooling systems were activated when the indoor temperature was below 22°C or above 22.5°C. All building operating parameters were defined in TRNBuild, which is the graphical interface for configuring the Type56 model.

When building parameters were set, they were of four kinds: external wall, external window, external door and other structure parameters (roof, floor slab and ground floor slab). The building parameters were also defined within the TRNBuild interface. As the most important parameters, external wall parameters were set sequentially for the CLT, masonry, RC and brick walls when the theoretical, predicted annual average and predicted dynamic U-values were considered. The method for setting external wall parameters was the same as that in Chapter 5. The other building parameters referred to those in the RC-tested building, as shown in Tables 7.1–7.3.

Table 7.1 External window parameters in the reference building

Window type	**Width (mm)**	**Height (mm)**	**U-value** $[\mathbf{W/(m^2 \cdot K)}]$	**G-value**	**Frame factor**
Triple-pane window	1100	1400	1.0	0.4	0.78

Table 7.2 External door parameters in the reference building

Door type	**Width (mm)**	**Height (mm)**	**Thickness (mm)**	**U-value** $[\mathbf{W/(m^2 \cdot K)}]$
Insulated steel door	1000	2200	45	1.8

Table 7.3 Other structure parameters in the reference building

Structure type	Material	Thickness [mm]	Conductivity $[W/(m \cdot K)]$	Density $[kg/(m^3)]$	Specific Heat Capacity $[J/(kg \cdot K)]$
Roof	1 Concrete	40	1.51	2300	920
	2 Waterproof layer	1	0.23	900	1620
	3 Insulation layer	100	0.03	30	1650
	4 RC broad	100	1.74	920	2500
Floor slab	1 Timber flooring	15	0.14	650	1700
	2 Cement mortar	20	0.93	1800	1050
	3 Concrete slab	100	1.74	2500	920
Ground floor slab	1 Cement mortar	20	0.93	1800	1050
	2 Concrete slab	150	1.74	2500	920
	3 Insulation layer	100	0.03	30	1650
	4 Waterproof layer	1	0.23	900	1620
	5 Ground concrete floor	150	1.74	2500	920

7.3 Updating Predicted U-values and Simulation Results

The updating predicted U-values included both average and dynamic U-values. The predicted average U-values of the four envelopes are shown in Table 7.4. The predicted annual average U-values of each envelope can be calculated by taking the average of all values in the hourly dynamic U-values of each envelope. These average U-values were also entered into the building energy simulations. Except for Bangkok, a minimal difference was observed in the average U-values of the same envelope in the same city between 2023 and 2013–2022. In climate zones A and B, the average U-values of the CLT envelope were the highest, and the average U-values of the masonry or RC envelope were the lowest. In climate zone C, the average U-values of the CLT or masonry cavity envelope were the highest, and the average U-values of the RC envelope were the lowest. In climate zone D, the average U-values of the masonry cavity envelope were the highest, and the average U-values of the RC envelope were the lowest.

Table 7.4 The predicted annual average U-values of the four envelopes in 11 case cities

Climate zone	City	Annual average U-values of the four envelopes $[W/(m^2 \cdot K)]$							
		Based on weather data of 2023				Based on average weather data from 2013 to 2022			
		CLT	Masonry	RC	Brick	CLT	Masonry	RC	Brick
A	Singapore	0.53	0.32	0.23	0.29	0.53	0.32	0.23	0.29
	Bangkok	0.50	0.38	0.24	0.31	0.57	0.25	0.26	0.28
B	Dubai	0.62	0.17	0.30	0.28	0.62	0.17	0.31	0.28
C	Hong Kong	0.50	0.38	0.24	0.31	0.50	0.39	0.24	0.32
	Shanghai	0.45	0.49	0.25	0.36	0.44	0.49	0.26	0.36
	Madrid	0.48	0.44	0.31	0.37	0.48	0.44	0.31	0.37
	London	0.36	0.64	0.24	0.40	0.36	0.65	0.24	0.40
D	Beijing	0.47	0.47	0.32	0.39	0.46	0.47	0.32	0.39
	Oslo	0.31	0.75	0.25	0.44	0.31	0.74	0.24	0.44
	Shenyang	0.40	0.59	0.30	0.41	0.40	0.58	0.31	0.42
	Harbin	0.33	0.72	0.28	0.45	0.33	0.72	0.28	0.45

The updated predicted dynamic U-values of four envelopes and the operational energy use of all buildings are shown in Figures 7.3–7.24. Compared with hourly dynamic U-values, fewer outliers occurred in the dynamic U-values with 14-day intervals. The dynamic U-values in Dubai contain negative values, and those in Madrid contain extremely low values. These outliers cannot be entered directly into TRYSYS because TRYSYS reported an error when the U-value was less than 0.08 $W/(m^2 \cdot K)$. In the dynamic U-values with a 14-day interval, the values less than 0.08 $W/(m^2 \cdot K)$ were replaced by 0.08 $W/(m^2 \cdot K)$. The trend and range of the dynamic U-values of the four envelopes based on 2023 weather data are similar to those based on average weather data from 2013 to 2022 in each case city. This is because the fluctuations in the hourly outdoor T/RH in 2023 were similar to the average hourly outdoor T/RH from 2013 to 2022, as shown in Appendix C.

The simulated operational energy use in four types of buildings in 11 case cities when three types of U-values were considered includes the simulated results based on weather data of 2023 and average weather data from 2013 to 2022. The difference between the simulated results based on weather data of 2023 and average weather data from 2013 to 2022 is insignificant.

As shown in Figures 7.3 and 7.5, dynamic U-values for Singapore and Bangkok had similar features. The fluctuations of the four envelopes' dynamic U-values were small in Singapore and Bangkok in 2023 and 2013–2022 because the outdoor T/RH in these cities were stable throughout the year. These dynamic U-values influenced the operational energy use. As shown in Figures 7.4 and 7.6, the characteristics of operational energy use in Singapore and Bangkok were similar. In Singapore and Bangkok, the differences between the operational energy use of the four buildings were not significant when the three types of U-values were considered. Because the dynamic U-values of all envelopes exhibited small fluctuations and remained close to the theoretical and average U-values.

The dynamic U-values of the CLT envelope in these three cities throughout the year were around 0.5 $W/(m^2 \cdot K)$, which were higher than those of the other three envelopes during most of the year. In Singapore, the dynamic U-values of the CLT envelope were higher than those of the other three envelopes throughout the year. The dynamic U-values of the other three envelopes throughout the year were around 0.3 $W/(m^2 \cdot K)$. The characteristics of dynamic U-values in 2013–2022 in Bangkok are similar to those of dynamic U-values in 2013–2022 in Singapore. In Bangkok, in the winter of 2023, the dynamic U-values of the masonry cavity envelope were close to those of the CLT envelope. The dynamic U-values of the brick and RC envelopes were around 0.4 $W/(m^2 \cdot K)$ and 0.3 $W/(m^2 \cdot K)$, respectively. In Bangkok, in the summer of 2023, the dynamic U-values of the CLT envelope were higher than those of the other three envelopes. The dynamic U-values of the other three envelopes were around 0.3 $W/(m^2 \cdot K)$. The cooling energy accounted for more than 95% of the total operational energy in these cities. The ranges of annual operational energy use of different buildings when different types of U-values were considered in Singapore, Bangkok were 34–46 kWh/m^2 and 46–63 kWh/m^2, respectively.

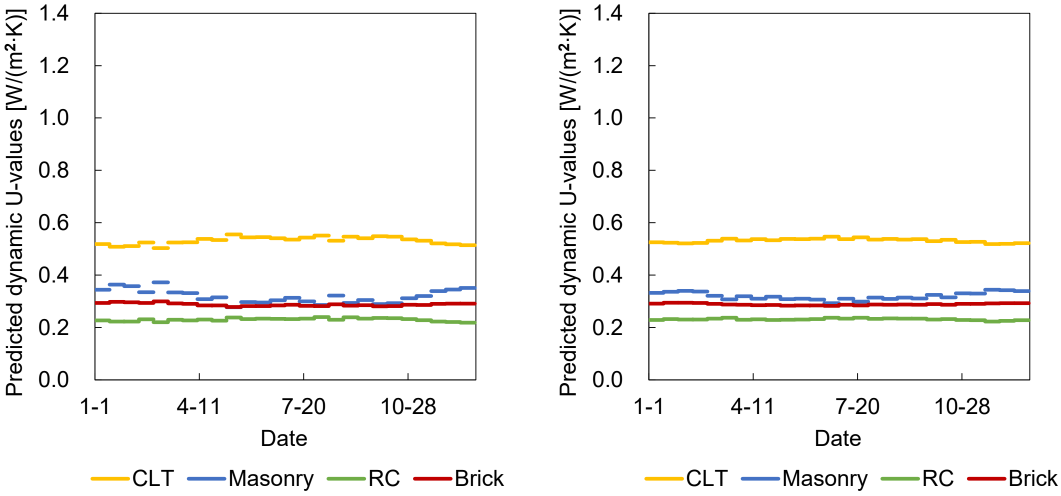

(a) Results based on weather data of 2023

(b) Results based on average weather data from 2013 to 2022

Figure 7.3 Predicted dynamic U-values of different envelopes in Singapore

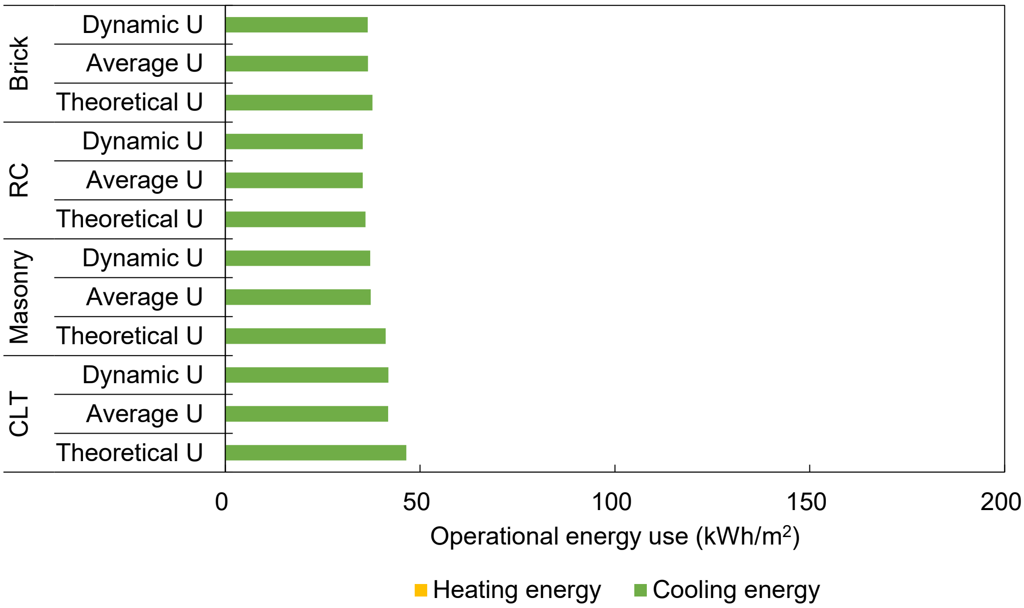

(a) Operational energy of different buildings based on weather data of 2023

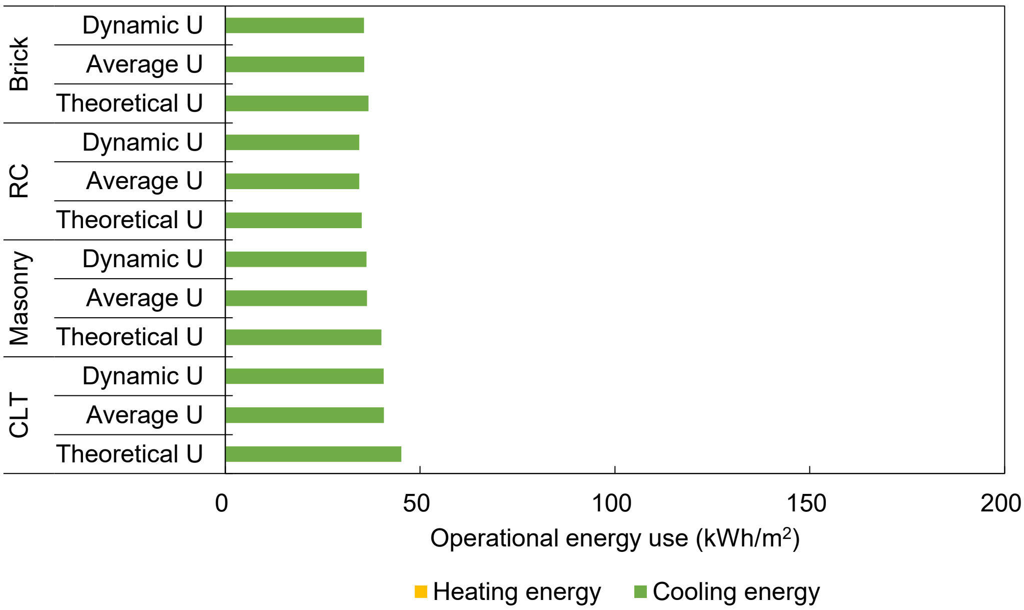

(b) Operational energy of different buildings based on average weather data from 2013 to 2022

Figure 7.4 Simulated operational energy use of different buildings in Singapore

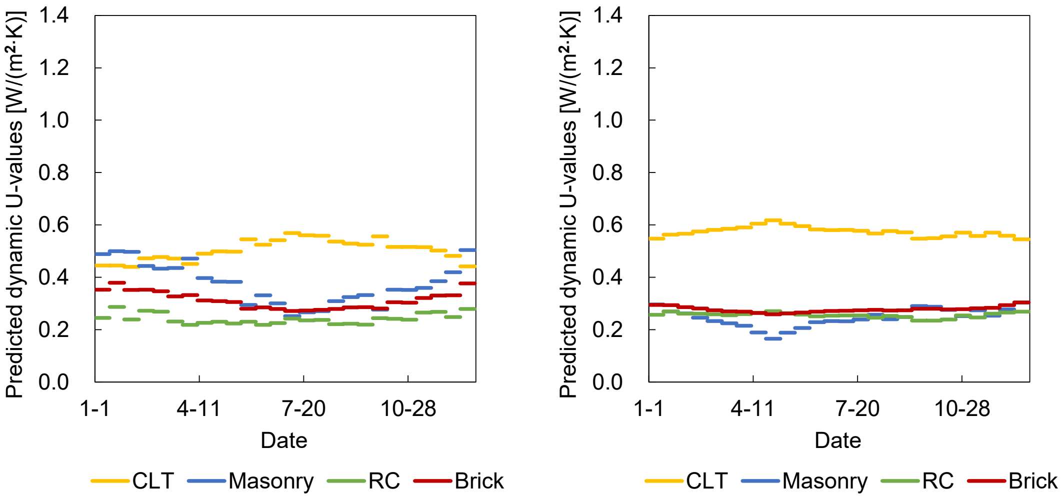

(a) Results based on weather data of 2023

(b) Results based on average weather data from 2013 to 2022

Figure 7.5 Predicted dynamic U-values of different envelopes in Bangkok

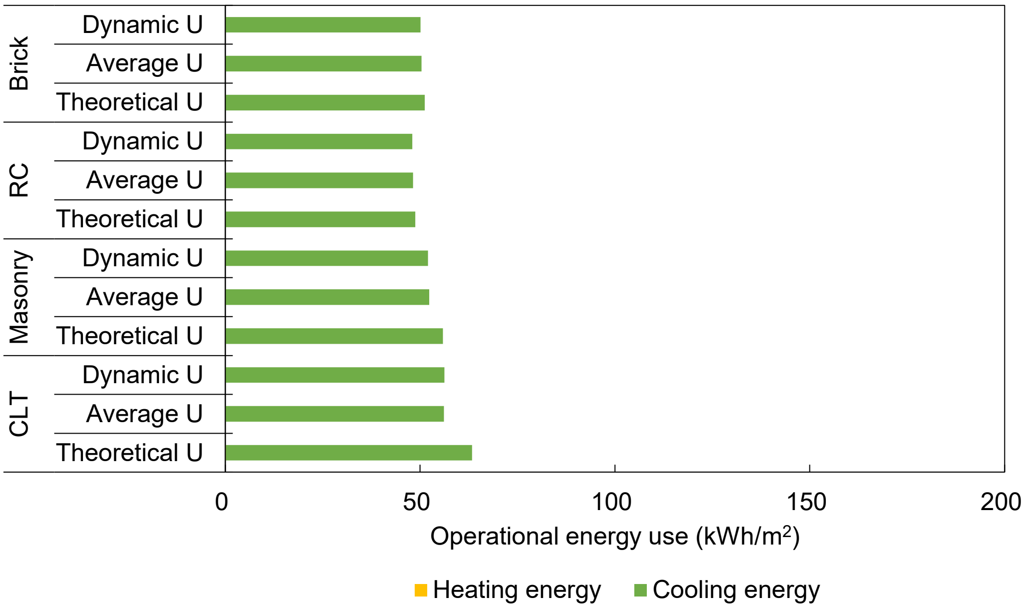

(a) Operational energy of different buildings based on weather data of 2023

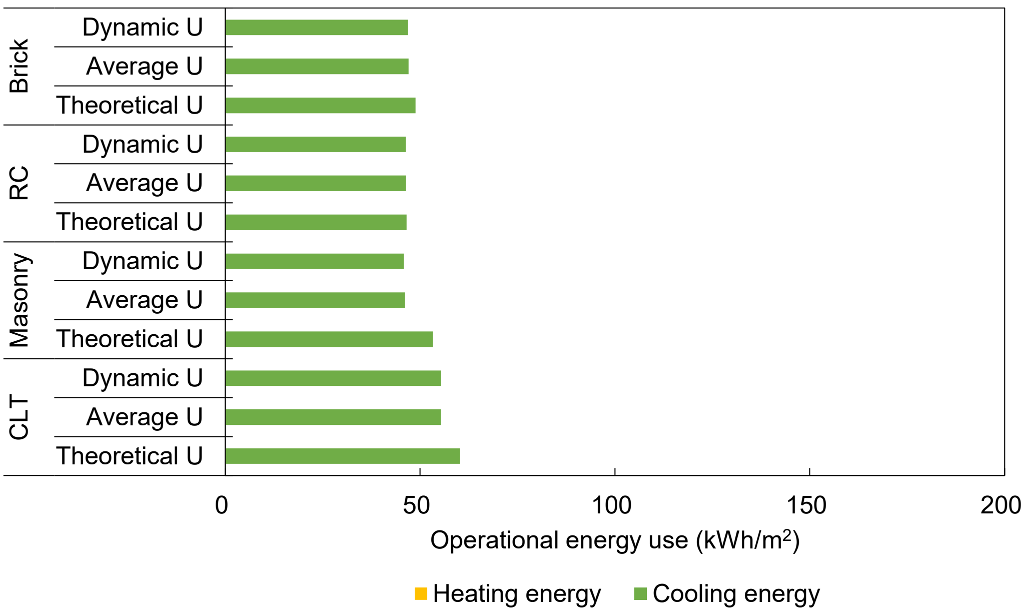

(b) Operational energy of different buildings based on average weather data from 2013 to 2022

Figure 7.6 Simulated operational energy use of different buildings in Bangkok

As shown in Figure 7.7, in Dubai during winter, the dynamic U-values of the CLT envelope were around 0.5 $W/(m^2 \cdot K)$ – higher than those of the other three envelopes. The dynamic U-values of the other three envelopes in winter were around 0.3 $W/(m^2 \cdot K)$. In summer in Dubai, the dynamic U-values of the CLT envelope were around 0.7

$W/(m^2 \cdot K)$ – considerably higher than those of the other three envelopes. The dynamic U-values of the brick and RC envelopes in summer were around 0.3 $W/(m^2 \cdot K)$. The dynamic U-values of the masonry cavity envelopes in summer were around 0.1 $W/(m^2 \cdot K)$. The dynamic U-values of the CLT envelope were higher than those of the other three envelopes throughout the year. As shown in Figure 7.8, the cooling energy accounted for more than 95% of the total operational energy in Dubai. The range of annual operational energy use of different buildings when different types of U-values were considered in Dubai was 43–66 kWh/m^2. In Dubai, the operational energy use when dynamic U-values were considered was lower than that when theoretical U-values in the masonry building were considered. The differences between the operational energy use of the other three buildings, when the three types of U-values were considered, were not significant. Because the dynamic U-values of the masonry envelope exhibited greater fluctuations compared to the other envelopes.

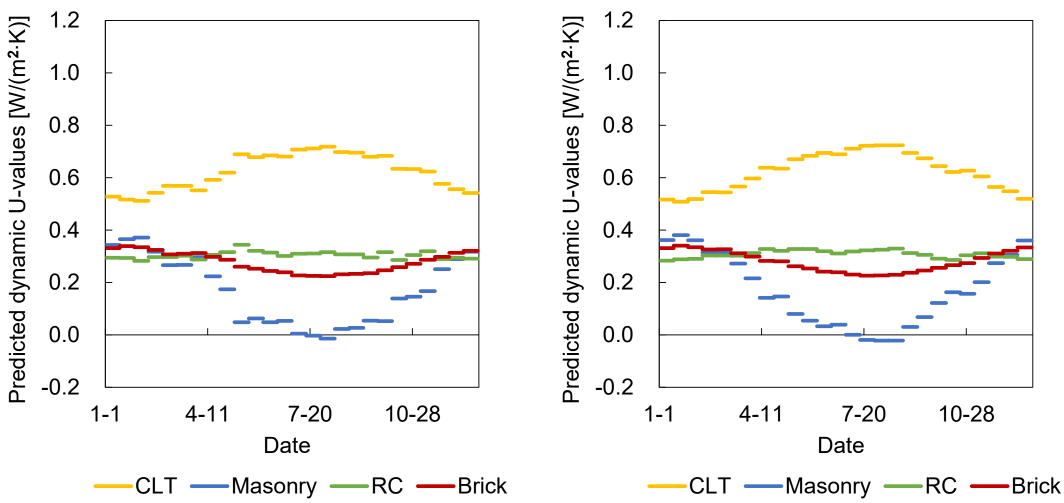

(a) Results based on weather data of 2023

(b) Results based on average weather data from 2013 to 2022

Figure 7.7 Predicted dynamic U-values of different envelopes in Dubai

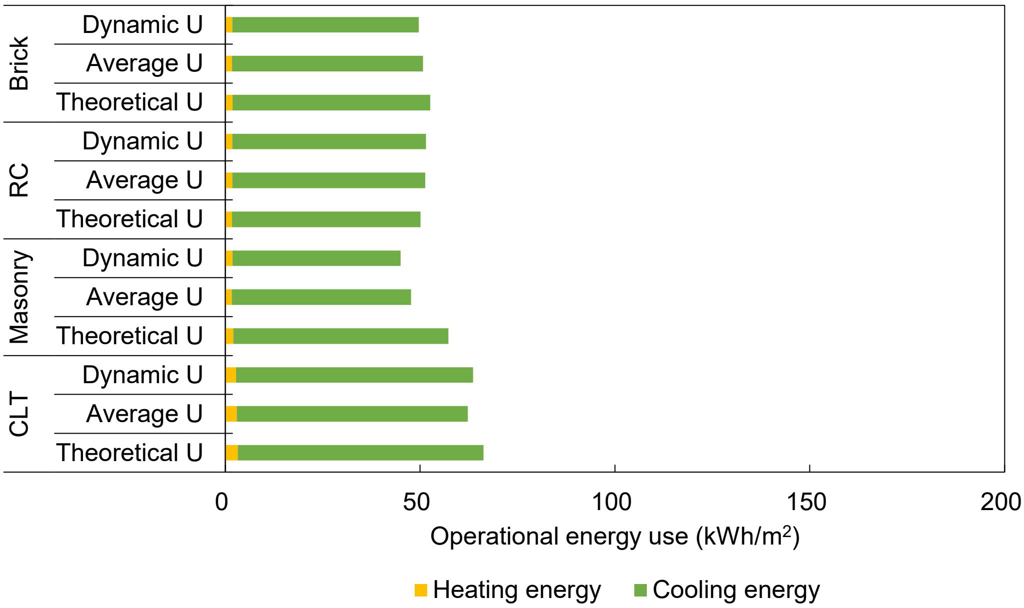

(a) Operational energy of different buildings based on weather data of 2023

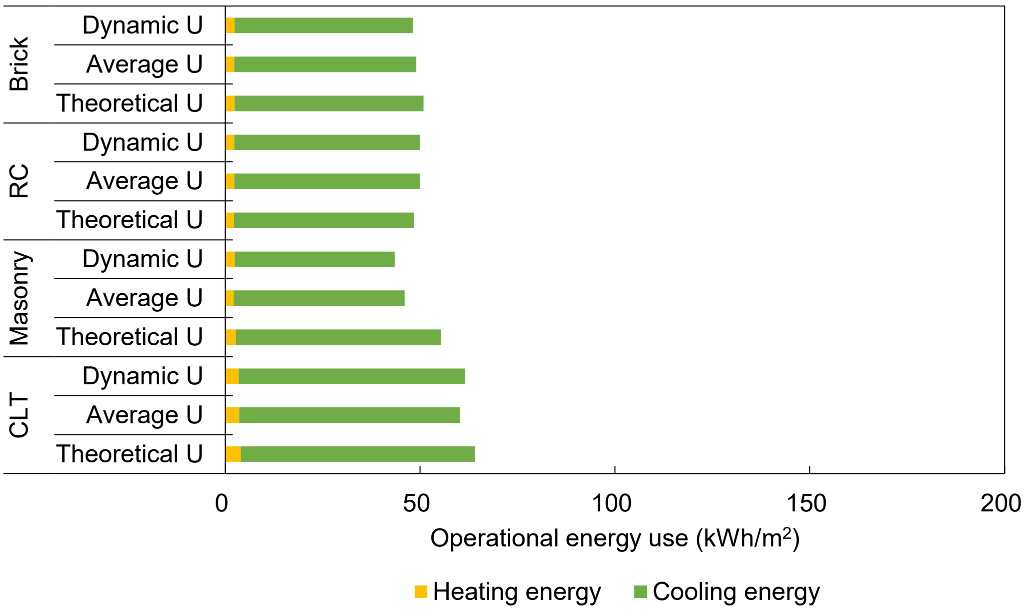

(b) Operational energy of different buildings based on average weather data from 2013 to 2022

Figure 7.8 Simulated operational energy use of different buildings in Dubai

As shown in Figure 7.9, in Hong Kong during winter, the dynamic U-values of the masonry cavity envelope were close to those of the CLT envelope, which was about 0.5 $W/(m^2 \cdot K)$. The dynamic U-values of the brick and RC envelopes were around 0.4 $W/(m^2 \cdot K)$ and 0.3 $W/(m^2 \cdot K)$, respectively. In the summer in Hong Kong, the dynamic U-values of the CLT envelope were about 0.6 $W/(m^2 \cdot K)$ – higher than those of the other three envelopes. The dynamic U-values of the other three envelopes were around 0.3 $W/(m^2 \cdot K)$. As shown in Figure 7.10, neither heating nor cooling energy accounted for more than 95% of total operational energy in these cities. The range of annual operational energy use of different buildings in Hong Kong when different types of U-values was considered were 28–40 kWh/m^2. In Hong Kong, the differences between the operational energy use of the four buildings when the three types of U-values were considered were not significant. This was because the fluctuations of dynamic U-values were not significant and the dynamic U-values were close to the theoretical and average U-values.

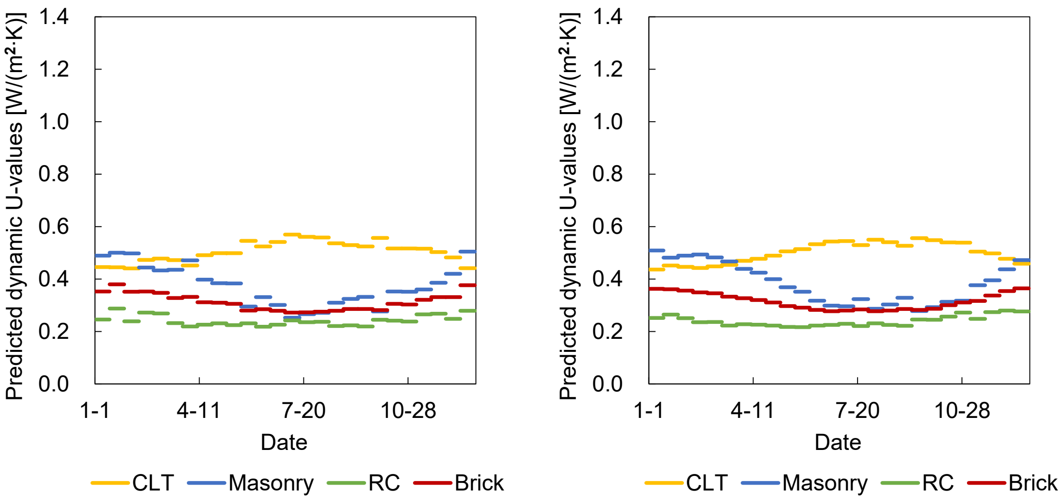

(a) Results based on weather data of 2023

(b) Results based on average weather data from 2013 to 2022

Figure 7.9 Predicted dynamic U-values of different envelopes in Hong Kong

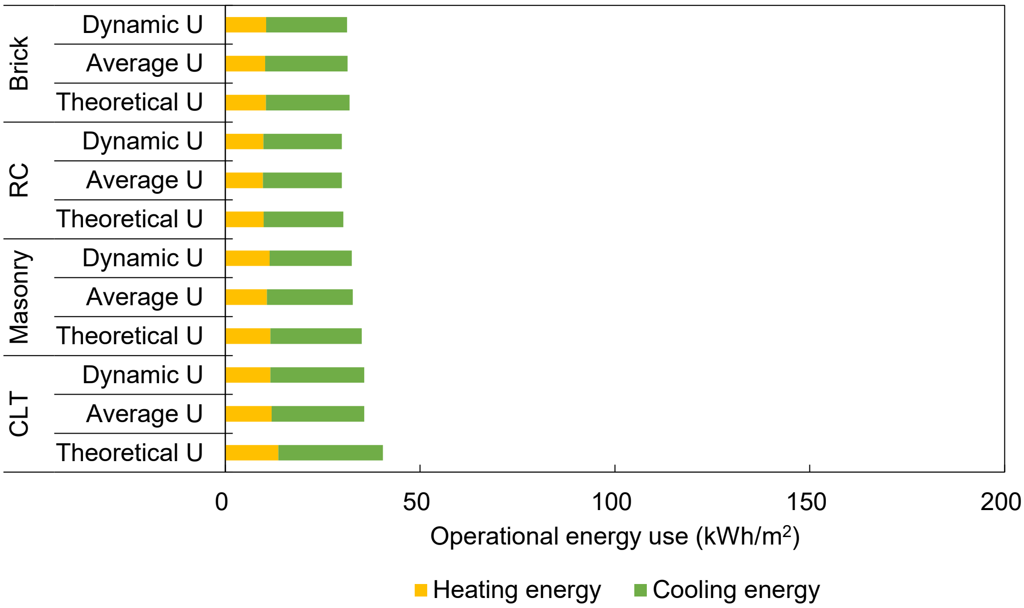

(a) Operational energy of different buildings based on weather data of 2023

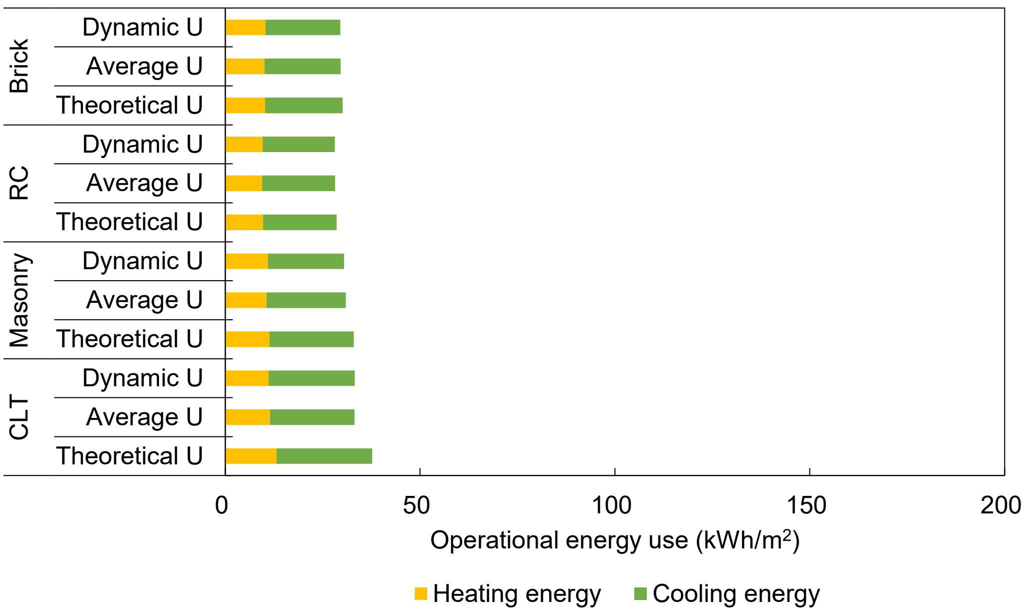

(b) Operational energy of different buildings based on average weather data from 2013 to 2022

Figure 7.10 Simulated operational energy use of different buildings in Hong Kong

As shown in Figures 7.11, 7.13, and 7.15, dynamic U-values in Shanghai, Madrid and Beijing had similar features. In the winter, in Shanghai, Madrid and Beijing, the dynamic U-values of the masonry cavity envelope were around 0.8 $W/(m^2 \cdot K)$ – considerably higher than those of the other three envelopes. The dynamic U-values of the brick envelope in winter were around 0.4 $W/(m^2 \cdot K)$, which were the second highest. The dynamic U-values of the CLT and RC envelopes in winter were around 0.3 $W/(m^2 \cdot K)$, which were relatively low. During the summer, in these three cities, the dynamic U-values of the CLT envelope were around 0.7 $W/(m^2 \cdot K)$ – considerably higher than those of the other three envelopes. The dynamic U-values of the brick and RC envelopes in the summer were around 0.3 $W/(m^2 \cdot K)$. The dynamic U-values of the masonry cavity envelopes in the summer were around 0.1–0.2 $W/(m^2 \cdot K)$.

As shown in Figures 7.12, 7.14, and 7.16, the characteristics of operational energy use in Shanghai, Madrid and Beijing were similar. Neither heating nor cooling energy accounted for more than 95% of total operational energy in these cities. The ranges of annual operational energy use of different buildings in Shanghai, Madrid and Beijing when different types of U-values were considered were $55-75$ kWh/m^2, $64-87$ kWh/m^2 and 84–115 kWh/m^2, respectively. In Shanghai, Madrid and Beijing, the operational energy use when dynamic U-values were considered was higher than that when theoretical U-values in the masonry building were considered. Due to the increase in the dynamic U-values of the masonry cavity envelope during winter, exceeding the theoretical U-value, the heating energy use was higher than expected. Further, the operational energy use when dynamic U-values were considered was lower than that when theoretical U-values in the CLT building were considered. As the dynamic U-values of the CLT envelope were lower than the theoretical U-value for most of the time, the resulting energy use was lower than expected. The differences between the operational energy use of the RC and brick buildings, when the three types of U-values were considered, were not significant. Because the dynamic U-values of the RC and brick envelopes exhibited small fluctuations and remained close to the theoretical U-values.

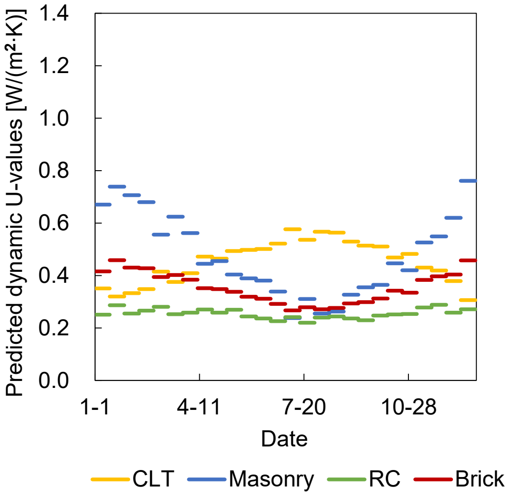

(a) Results based on weather data of 2023

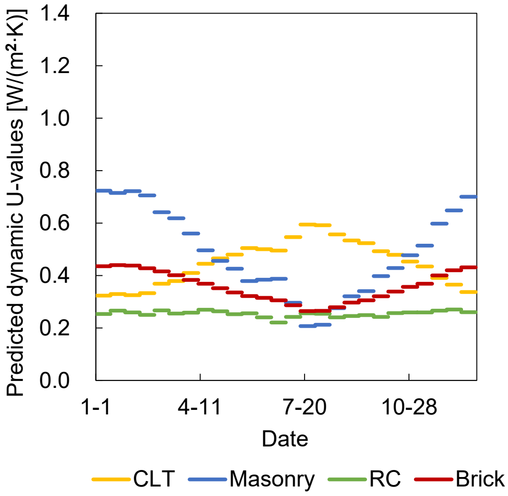

(b) Results based on average weather data from 2013 to 2022

Figure 7.11 Predicted dynamic U-values of different envelopes in Shanghai

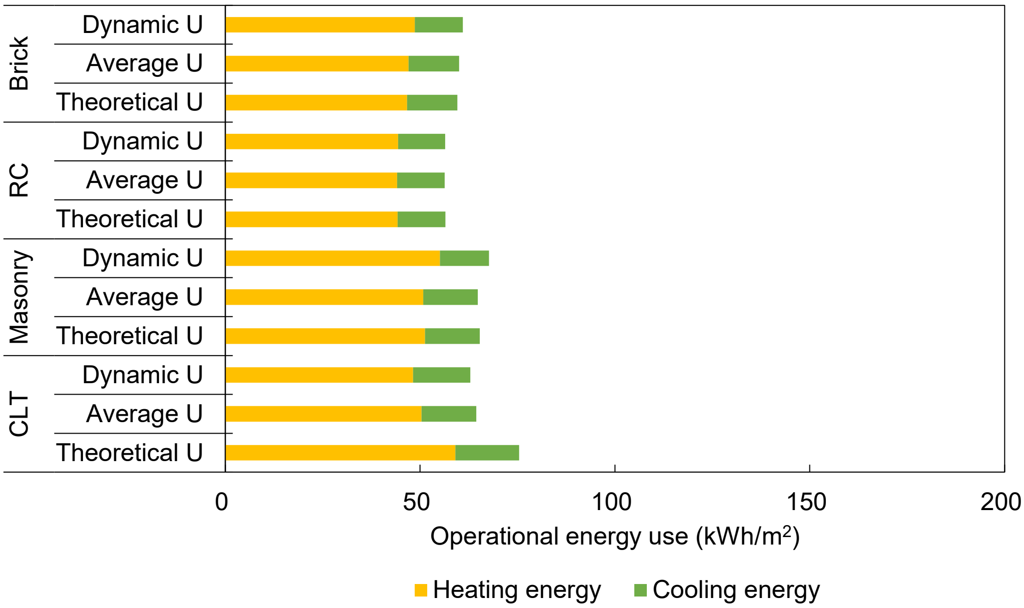

(a) Operational energy of different buildings based on weather data of 2023

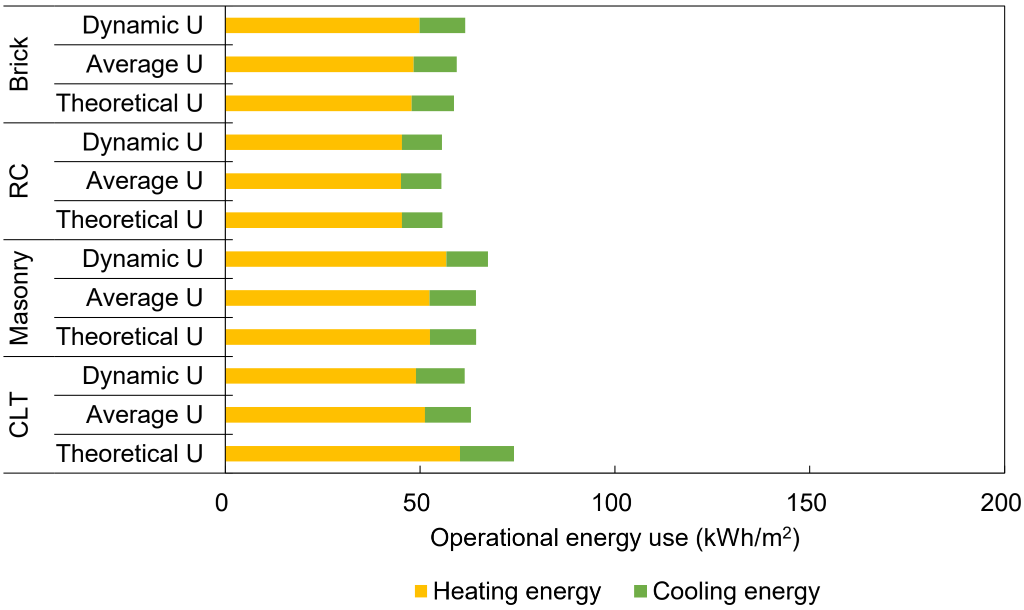

(b) Operational energy of different buildings based on average weather data from 2013 to 2022

Figure 7.12 Simulated operational energy use of different buildings in Shanghai

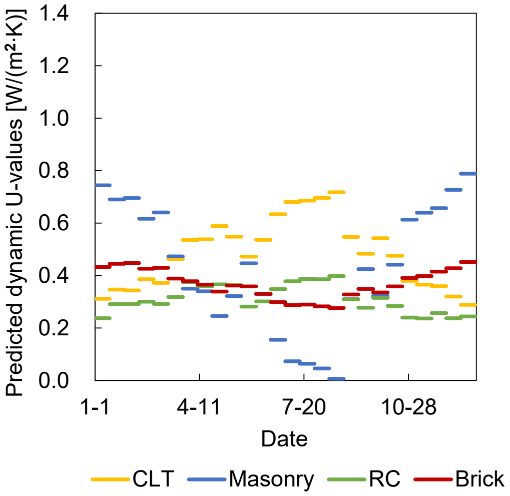

(a) Results based on weather data of 2023

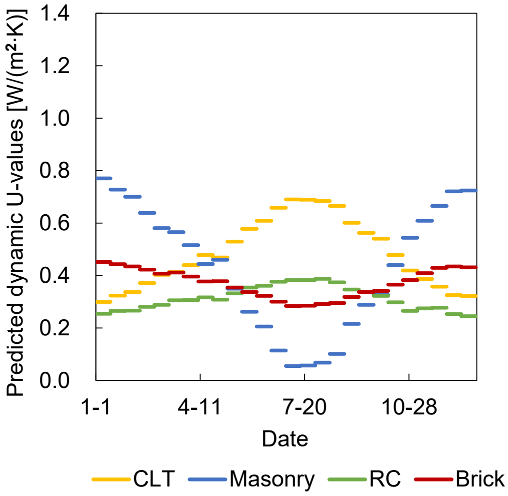

(b) Results based on average weather data from 2013 to 2022

Figure 7.13 Predicted dynamic U-values of different envelopes in Madrid

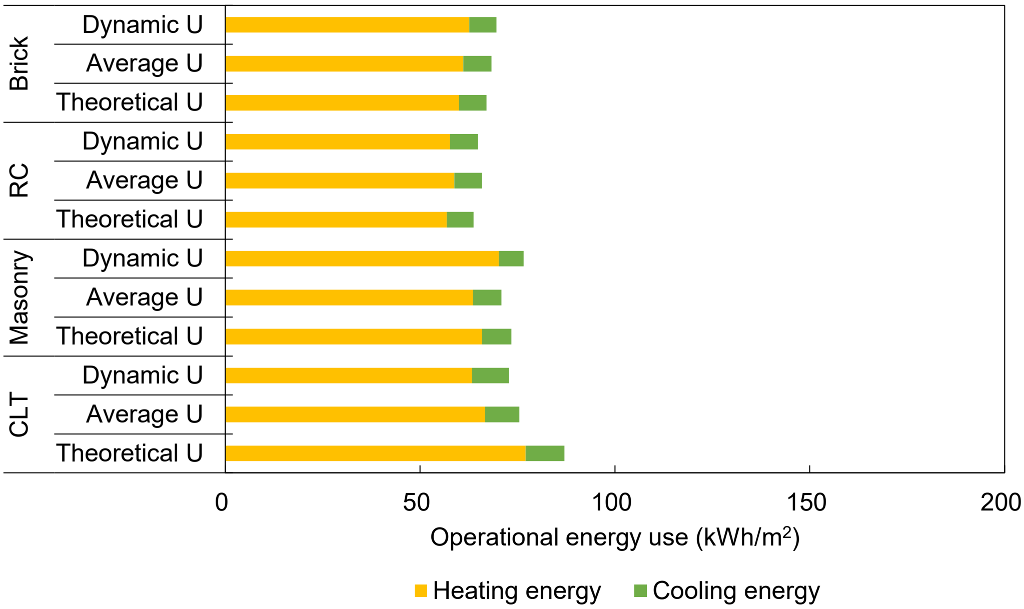

(a) Operational energy of different buildings based on weather data of 2023

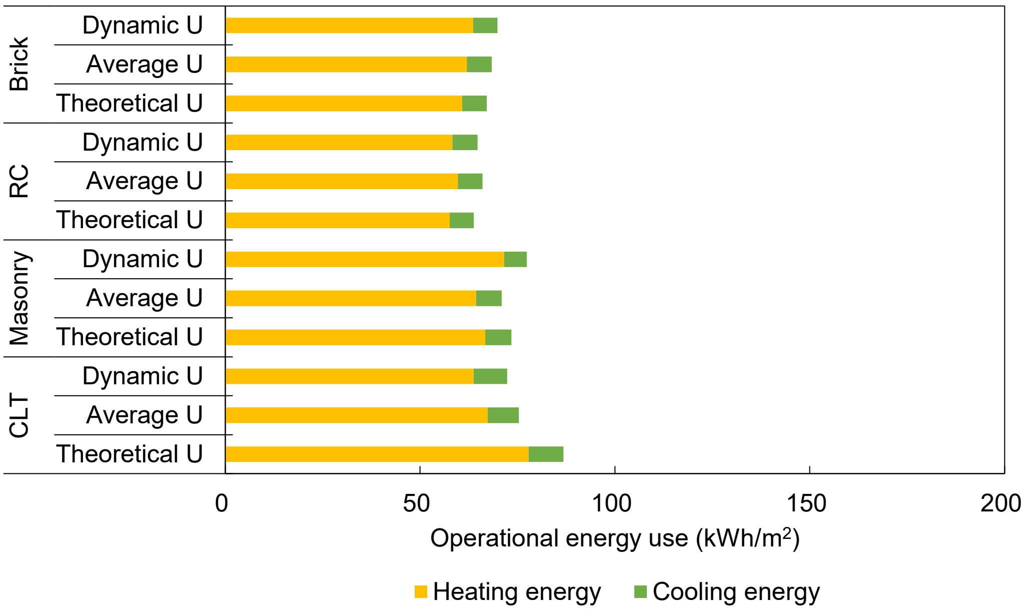

(b) Operational energy of different buildings based on average weather data from 2013 to 2022

Figure 7.14 Simulated operational energy use of different buildings in Madrid

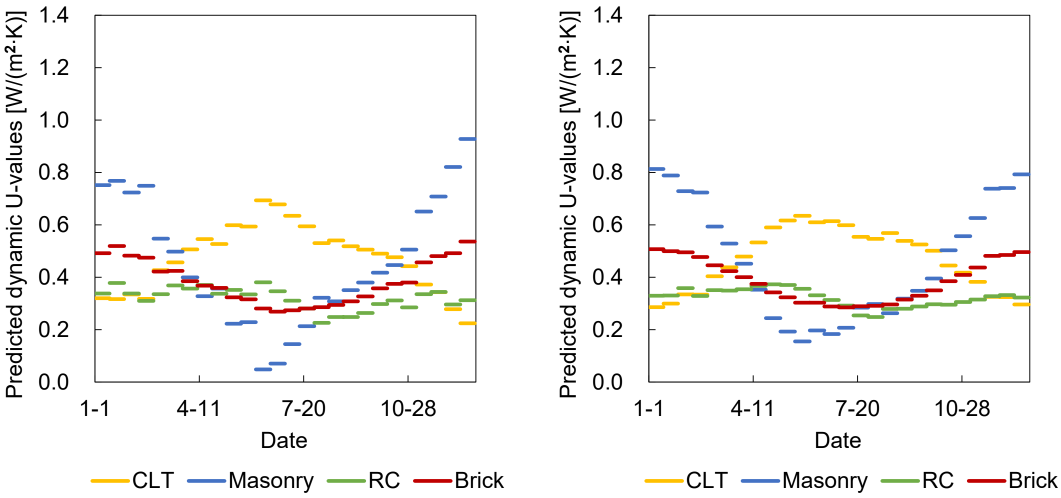

(a) Results based on weather data of 2023

(b) Results based on average weather data from 2013 to 2022

Figure 7.15 Predicted dynamic U-values of different envelopes in Beijing

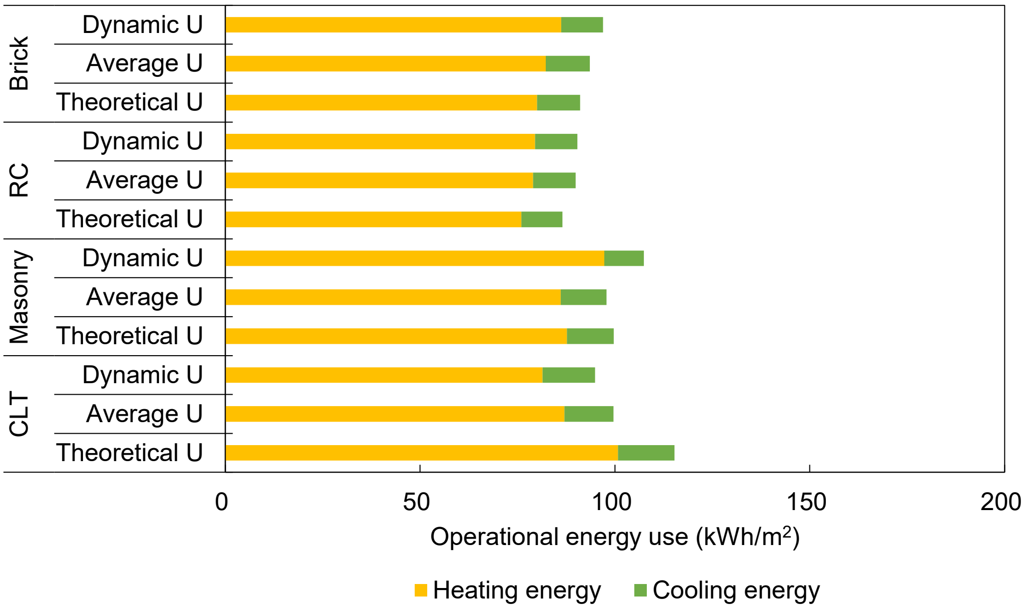

(a) Operational energy of different buildings based on weather data of 2023

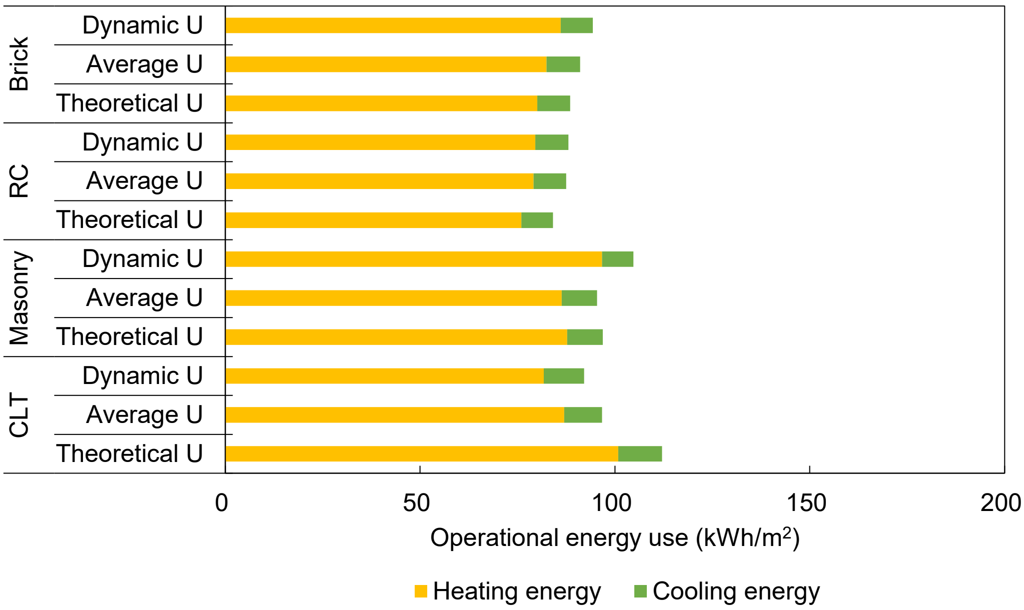

(b) Operational energy of different buildings based on average weather data from 2013 to 2022

Figure 7.16 Simulated operational energy use of different buildings in Beijing

As shown in Figures 7.17, 7.19, 7.21, and 7.23, dynamic U-values in London, Oslo, Shenyang and Harbin had similar features. During the winter, in London, Oslo, Shenyang and Harbin, the dynamic U-values of the masonry cavity envelope were around 1.0 $W/(m^2 \cdot K)$ – considerably higher than those of the other three envelopes.

The dynamic U-values of the brick envelope in the winter were around 0.5 $W/(m^2 \cdot K)$, which were the second highest. The dynamic U-values of the CLT and RC envelopes in the winter were around 0.2 $W/(m^2 \cdot K)$, which were relatively low. During the summer, in these four cities, the gaps between the dynamic U-values of the four envelopes narrowed. The dynamic U-values of the CLT and masonry cavity envelopes in summer were around 0.5 $W/(m^2 \cdot K)$ – higher than those of the other two envelopes. The dynamic U-values of the brick and RC envelopes in summer were around 0.4 $W/(m^2 \cdot K)$ and 0.3 $W/(m^2 \cdot K)$, respectively; this suggests that the thermal insulation of all four envelopes is similar in these cities in the summer.

As shown in Figures 7.18, 7.20, 7.22, and 7.24, the characteristics of operational energy use in London, Oslo, Shenyang and Harbin were similar. The heating energy accounted for more than 95% of total operational energy in these cities. The ranges of annual operational energy use of different buildings in London, Oslo, Shenyang and Harbin when different types of U-values were considered were 77–110 kWh/m^2, 116–168 kWh/m^2, 102–138 kWh/m^2 and 129–194 kWh/m^2, respectively. For these four cities, in the RC and brick buildings, the differences in operational energy use when three types of U-values were considered were not significant. Because the dynamic U-values of the RC and brick envelopes exhibited small fluctuations and remained close to the theoretical and average U-values. In the masonry building, the operational energy use when dynamic U-values were considered was higher than that when theoretical U-values were considered. Because of the increase in the dynamic U-values of the masonry envelope during winter, exceeding the theoretical U-value, the heating energy use was higher than expected. In the CLT building, the operational energy use when dynamic U-values were considered was lower than that when theoretical U-values were considered. As the dynamic U-values of the CLT wall were lower than the theoretical U-value for most of the time, the resulting energy consumption was lower than expected.

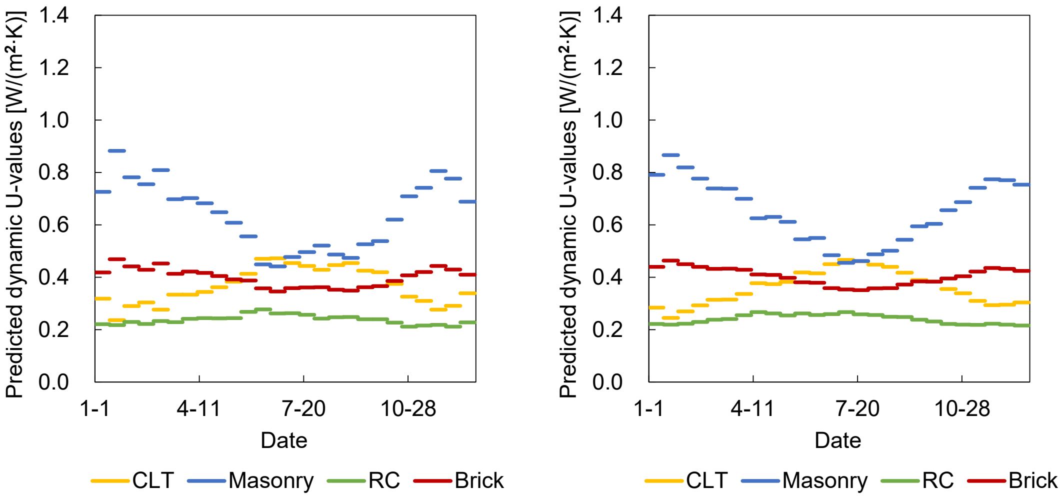

(a) Results based on weather data of 2023

(b) Results based on average weather data from 2013 to 2022

Figure 7.17 Predicted dynamic U-values of different envelopes in London

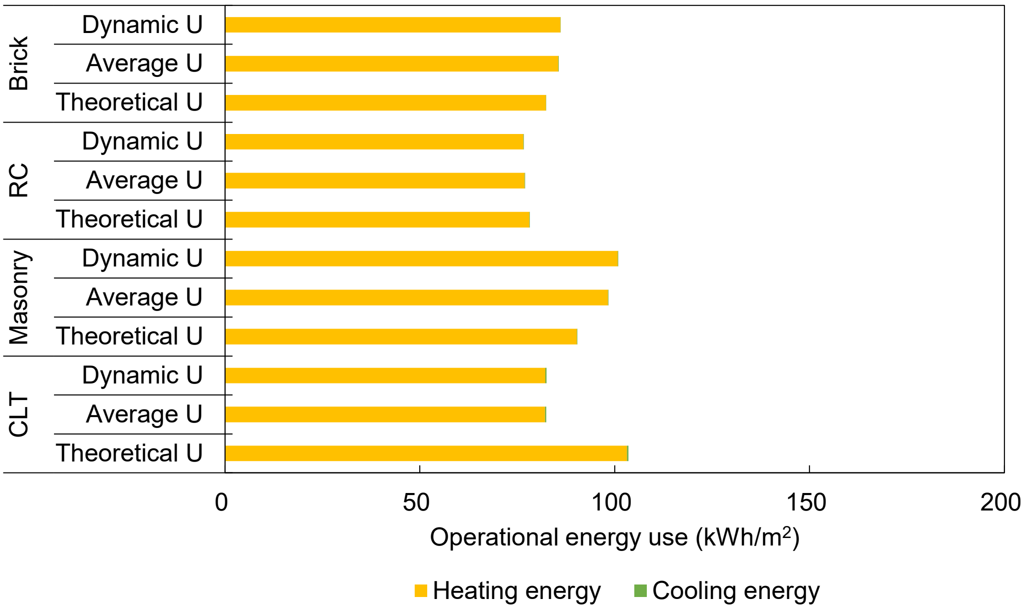

(a) Operational energy of different buildings based on weather data of 2023

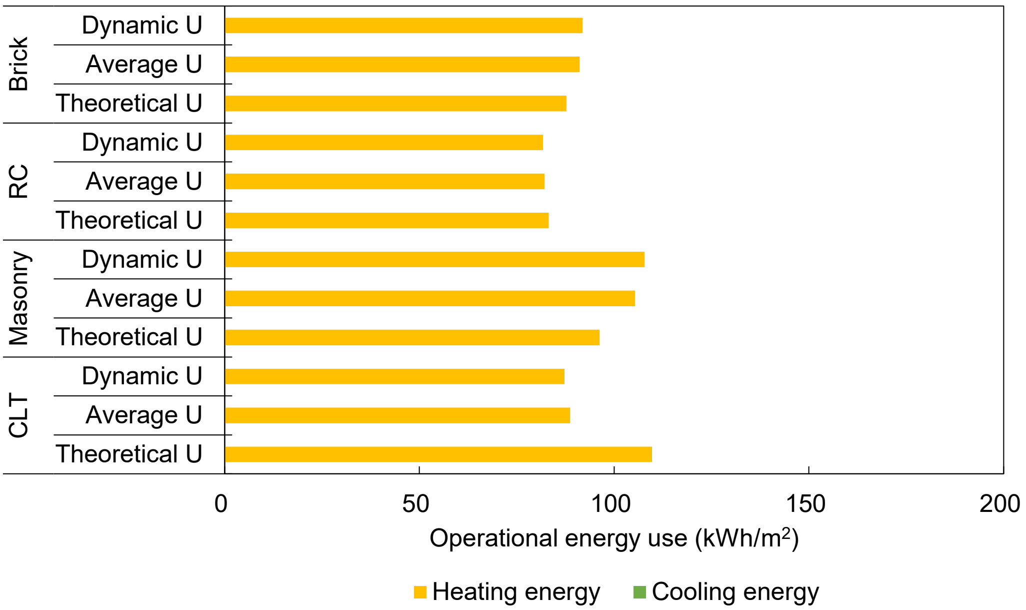

(b) Operational energy of different buildings based on average weather data from 2013 to 2022

Figure 7.18 Simulated operational energy use of different buildings in London

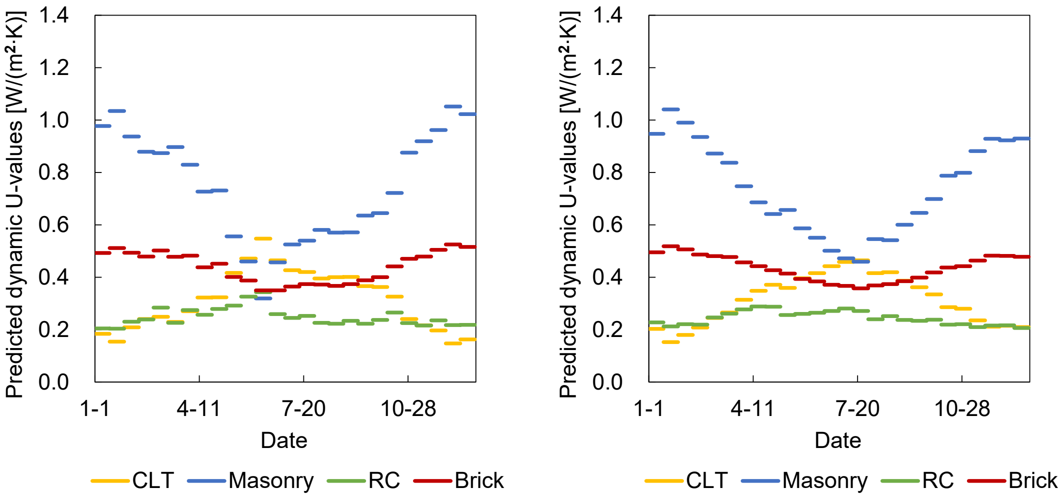

(a) Results based on weather data of 2023

(b) Results based on average weather data from 2013 to 2022

Figure 7.19 Predicted dynamic U-values of different envelopes in Oslo

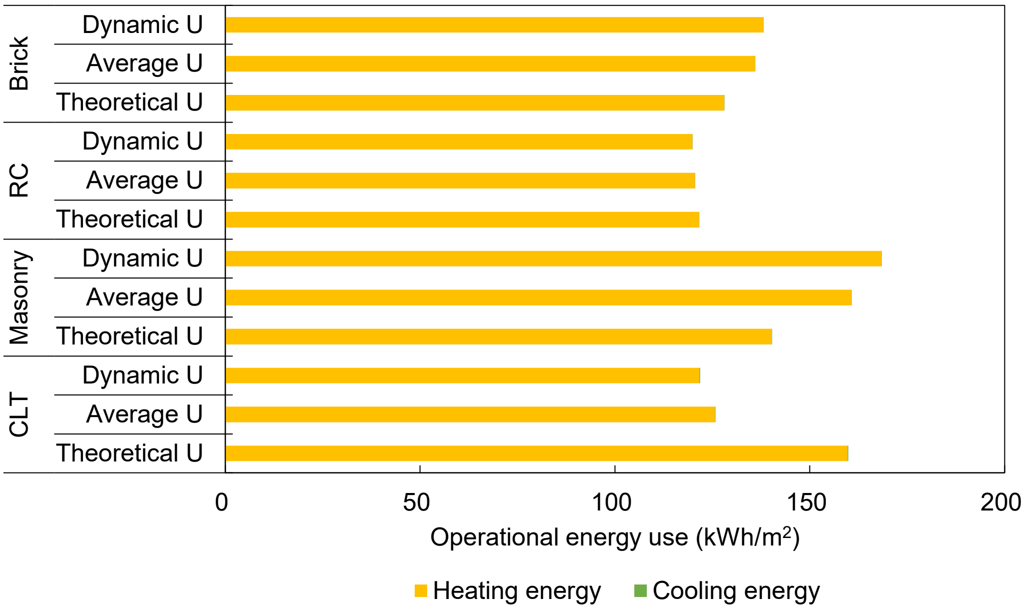

(a) Operational energy of different buildings based on weather data of 2023

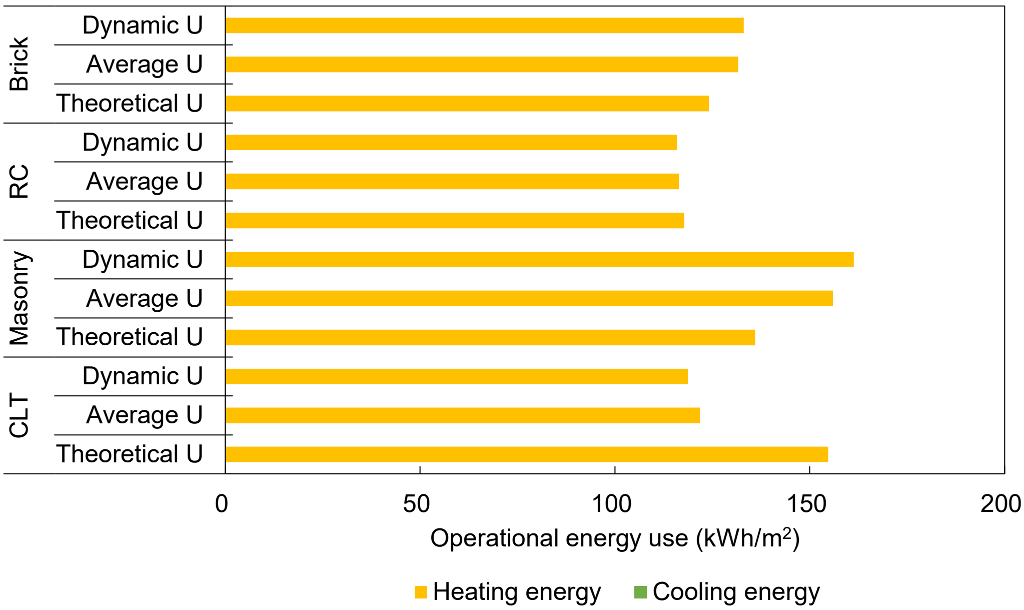

(b) Operational energy of different buildings based on average weather data from 2013 to 2022

Figure 7.20 Simulated operational energy use of different buildings in Oslo

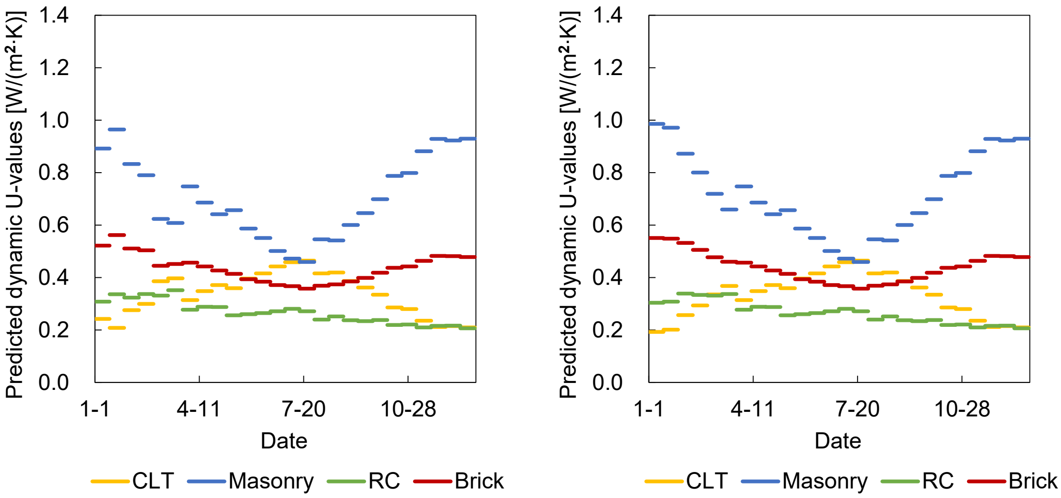

(a) Results based on weather data of 2023

(b) Results based on average weather data from 2013 to 2022

Figure 7.21 Predicted dynamic U-values of different envelopes in Shenyang

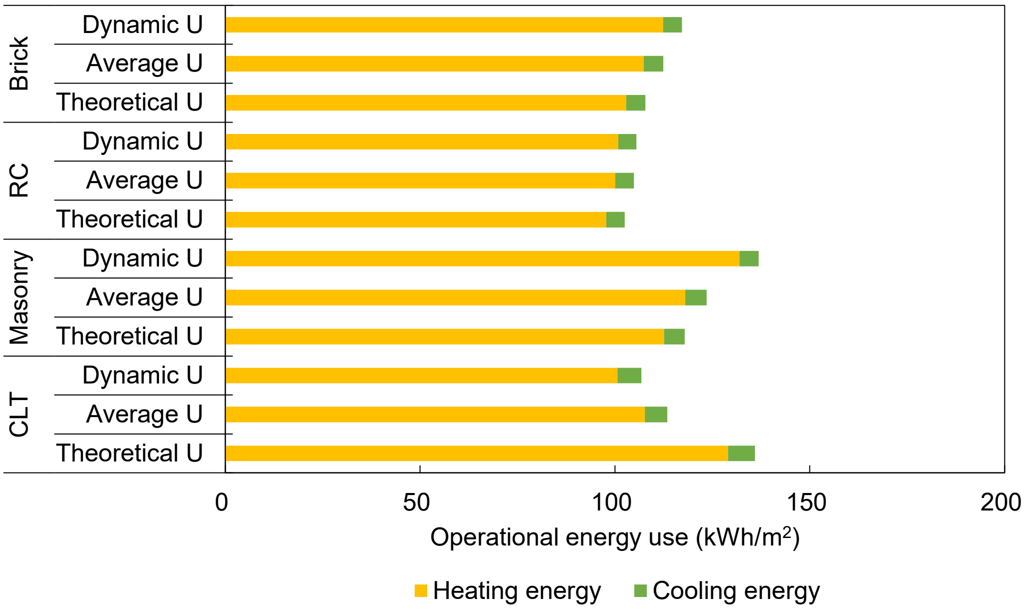

(a) Operational energy of different buildings based on weather data of 2023

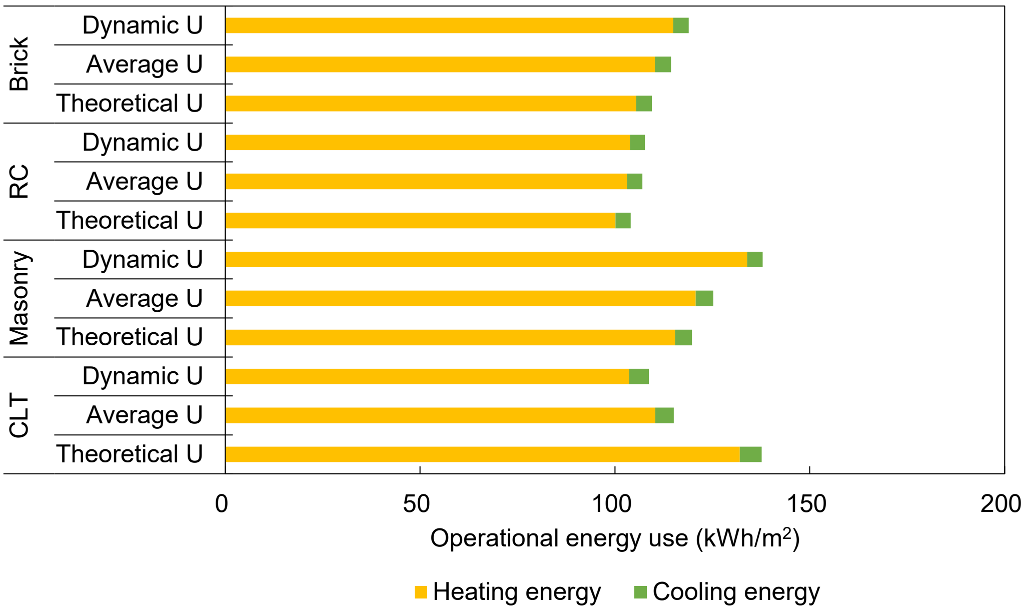

(b) Operational energy of different buildings based on average weather data from 2013 to 2022

Figure 7.22 Simulated operational energy use of different buildings in Shenyang

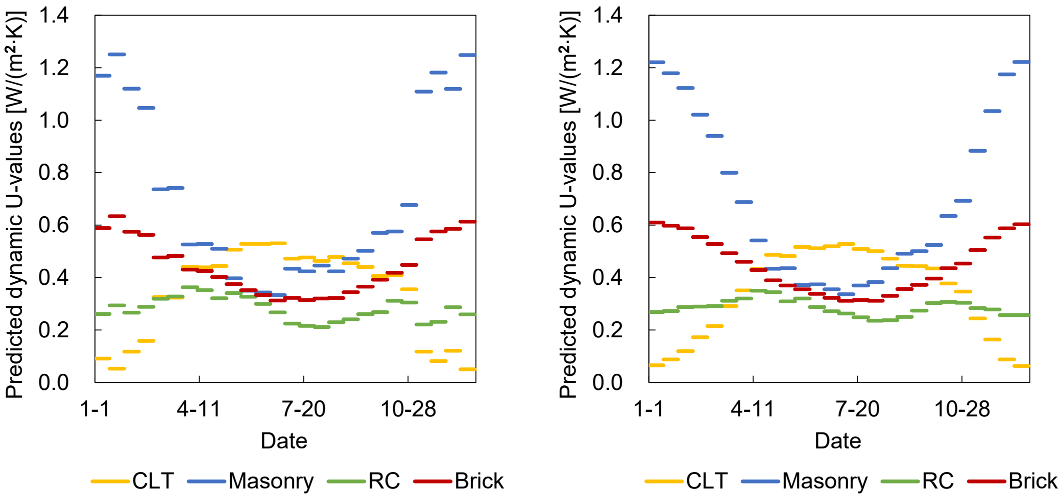

(a) Results based on weather data of 2023

(b) Results based on average weather data from 2013 to 2022

Figure 7.23 Predicted dynamic U-values of different envelopes in Harbin

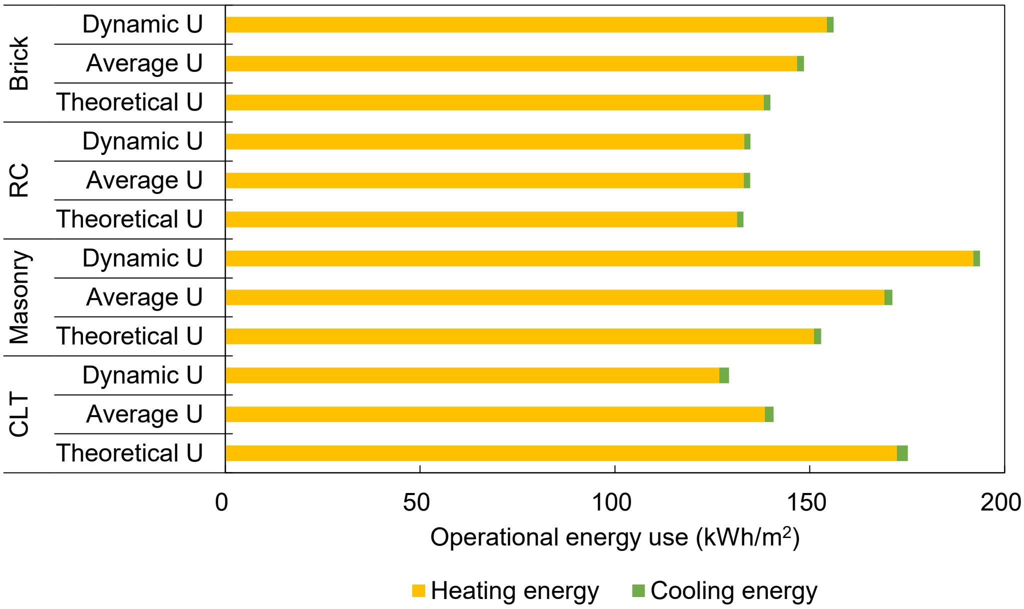

(a) Operational energy of different buildings based on weather data of 2023

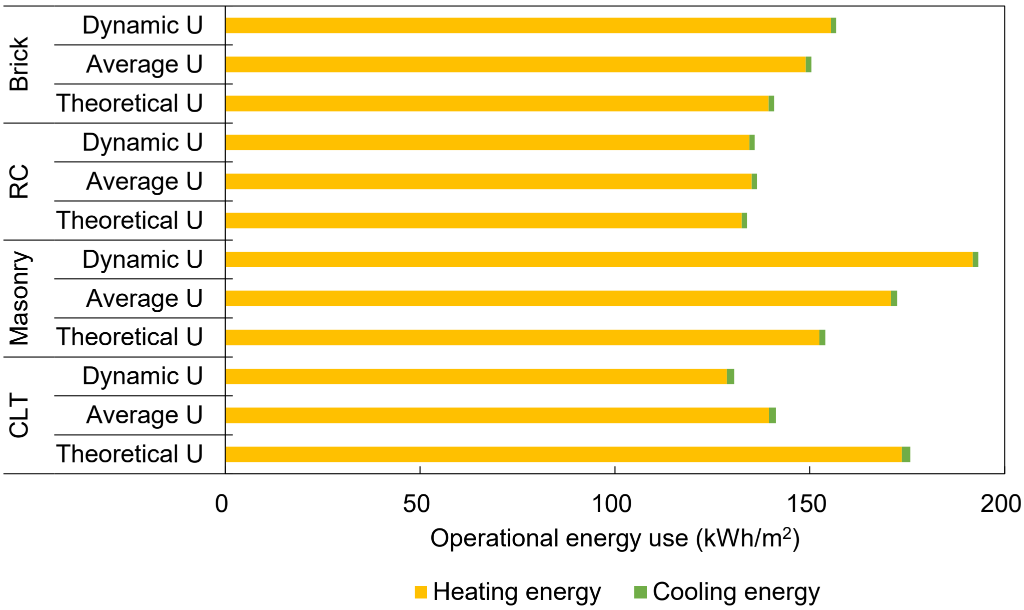

(b) Operational energy of different buildings based on average weather data from 2013 to 2022

Figure 7.24 Simulated operational energy use of different buildings in Harbin

7.4 Building Types with the Lowest Energy Use in Climate Zones

Tables 7.5–7.7 summarise the building types with the highest and lowest operational energy use in 11 case cities based on different years of weather data when theoretical, average and dynamic U-values were considered. The building types with the highest and lowest operational energy use were the same when the weather data of 2023 and average weather data from 2013 to 2022 were applied.

In climate zone A, the CLT building consumed the most operational energy and the RC building consumed the least operational energy, regardless of which type of U-values was considered. This illustrated that the CLT building may not be suitable, and the RC building may be suitable in climate zone A.

In climate zone B, the CLT building consumed the most operational energy, regardless of which type of U-values was considered. This illustrated that the CLT building may not be suitable in climate zone B. When the theoretical U-values were considered, the RC building consumed the least operational energy. When the predicted average and dynamic U-values were considered, the masonry building consumed the least operational energy. This illustrated the suitability of the masonry buildings for climate zone B.

In climate zone C, the RC building consumed the least operational energy, regardless of which type of U-values was considered. This illustrated that the RC building may be suitable in climate zone C. When the theoretical U-values were considered, the CLT building consumed the most operational energy. When the predicted average U-values were considered, the highest energy-consuming building type was changed to the masonry building in Shanghai and London. When the predicted dynamic U-values were considered, the highest energy-consuming building type was the masonry building in Madrid, Shanghai and London. The energy savings of the CLT building may be better than expected in climate zone C.

In climate zone D, when the theoretical U-values were considered, the CLT building consumed the most operational energy, and the RC building consumed the least operational energy. When the predicted average U-values were considered, the highest energy-consuming building type was changed to the masonry building in Oslo, Shenyang and Harbin, and the RC building consumed the least operational energy. When the predicted dynamic U-values were considered, the masonry building consumed the most operational energy in all case cities, and the lowest energy-consuming building type changed to the CLT building in Harbin. Thus, when the fluctuations in the U-values in the actual environment were taken into account, the CLT envelope might have been more energy efficient than expected. Moreover, the CLT envelope might have been even more energy efficient than some conventional envelopes with insulation, such as the masonry cavity envelope; this shows the suitability of CLT buildings for climate zone D. Among the three types of conventional buildings, the RC building offered the best energy savings regardless of which type of U-values was considered.

Table 7.5 Types of buildings with the highest and lowest operational energy use in 11 case cities based on different years of weather data when the theoretical U-values are considered

Climate zone	Case city	Building type with the highest operational energy use		Building type with the lowest operational energy use	
		2023	2013-2022	2023	2013-2022
A	Singapore	CLT	CLT	RC	RC
	Bangkok	CLT	CLT	RC	RC
B	Dubai	CLT	CLT	RC	RC
C	Hong Kong	CLT	CLT	RC	RC
	Shanghai	CLT	CLT	RC	RC
	Madrid	CLT	CLT	RC	RC
	London	CLT	CLT	RC	RC
D	Beijing	CLT	CLT	RC	RC
	Oslo	CLT	CLT	RC	RC
	Shenyang	CLT	CLT	RC	RC
	Harbin	CLT	CLT	RC	RC

Table 7.6 Types of buildings with the highest and lowest operational energy use in 11 case cities based on different years of weather data when the average U-values are considered

Climate zone	Case city	Building type with the highest operational energy use		Building type with the lowest operational energy use	
		2023	2013-2022	2023	2013-2022
A	Singapore	CLT	CLT	RC	RC
	Bangkok	CLT	CLT	RC	RC
B	Dubai	CLT	CLT	Masonry	Masonry
C	Hong Kong	CLT	CLT	RC	RC
	Shanghai	Masonry	Masonry	RC	RC
	Madrid	CLT	CLT	RC	RC
	London	Masonry	Masonry	RC	RC
D	Beijing	CLT	CLT	RC	RC
	Oslo	Masonry	Masonry	RC	RC
	Shenyang	Masonry	Masonry	RC	RC
	Harbin	Masonry	Masonry	RC	RC

Table 7.7 Types of buildings with the highest and lowest operational energy use in 11 case cities based on different years of weather data when the dynamic U-values are considered

Climate zone	Case city	Building type with the highest operational energy use		Building type with the lowest operational energy use	
		2023	2013-2022	2023	2013-2022
A	Singapore	CLT	CLT	RC	RC
	Bangkok	CLT	CLT	RC	RC
B	Dubai	CLT	CLT	Masonry	Masonry
C	Hong Kong	CLT	CLT	RC	RC
	Shanghai	Masonry	Masonry	RC	RC
	Madrid	Masonry	Masonry	RC	RC
	London	Masonry	Masonry	RC	RC
D	Beijing	Masonry	Masonry	RC	RC
	Oslo	Masonry	Masonry	RC	RC
	Shenyang	Masonry	Masonry	RC	RC
	Harbin	Masonry	Masonry	CLT	CLT

7.5 Energy influences of Dynamic U-values

The quantitative comparisons of operational energy use when the three types of U-values were considered are shown in Figures 7.25–7.27. The comparative results based on the weather data of 2023 were similar to those based on the average weather data from 2013 to 2022.

Figure 7.25 shows the differences in operational energy use of the four buildings in 11 case cities based on different weather data when the theoretical and average U-values were considered. The data in Figure 7.25 are calculated as Equation (17).

$$D_{T,A} = \frac{OE_{AVER} - OE_{THEO}}{OE_{THEO}} \times 100\% \qquad (17)$$

Where $\boldsymbol{D_{T,A}}$ is the difference of operational energy use when the theoretical and average U-values were considered [%]; $\boldsymbol{OE_{THEO}}$ is the operational energy use when the theoretical U-values were considered $[\mathrm{kWh/m^2}]$, and $\boldsymbol{OE_{AVER}}$ is the operational energy use when the average U-values were considered $[\mathrm{kWh/m^2}]$.

For the CLT building, the operational energy use when the dynamic U-values were considered was lower than that when the theoretical U-values were considered by 6.1% to 10.1% in climate zones A and B. The operational energy use when the dynamic U-values were considered was lower than that when the theoretical U-values were considered by 11.9% to 20.4% in climate zone C. The operational energy use when the dynamic U-values were considered was lower than that when the theoretical U-values were considered by 13.6% to 21.3% in climate zone D. Even when the dynamic U-values were excluded and only the average U-values were considered, under the environmental impacts, the operational energy use of the CLT building was lower than expected, especially in climate zones C and D.

For the masonry building, in climate zones A and B, the operational energy use when the average U-values were considered was lower than that when the theoretical U-values were considered by 6.3–16.9%. In climate zone C, the operational energy use when the average U-values were considered was lower or higher by no more than 9.5% than that when the theoretical U-values were considered. In climate zone D, the operational energy use when the average U-values were considered was higher or lower by no more than 14.6% than that when the theoretical U-values were considered. When the average U-values were considered, the operational energy use of the masonry building was lower than expected in climate zones A and B.

For the RC building, the operational energy use when the average U-values were considered was similar to that when the theoretical U-values were considered – higher or lower by no more than 4.0% in all climate zones. Thus, when the average U-values were considered, the operational energy use of the RC building was about as expected in any climate zone.

For the brick building, in climate zones A and B, the operational energy use when the average U-values were considered was lower than that when the theoretical U-values were considered by 1.6–3.8%. In climate zone C, the operational energy use when the average U-values were considered was similar to that when the theoretical U-values were considered – higher or lower by no more than 3.9%. In climate zone D, the operational energy use when the average U-values were considered was higher than that when the theoretical U-values were considered by 2.7–6.8%. Thus, when the average U-values were considered, the operational energy use of the brick building was higher than expected in climate zone D.

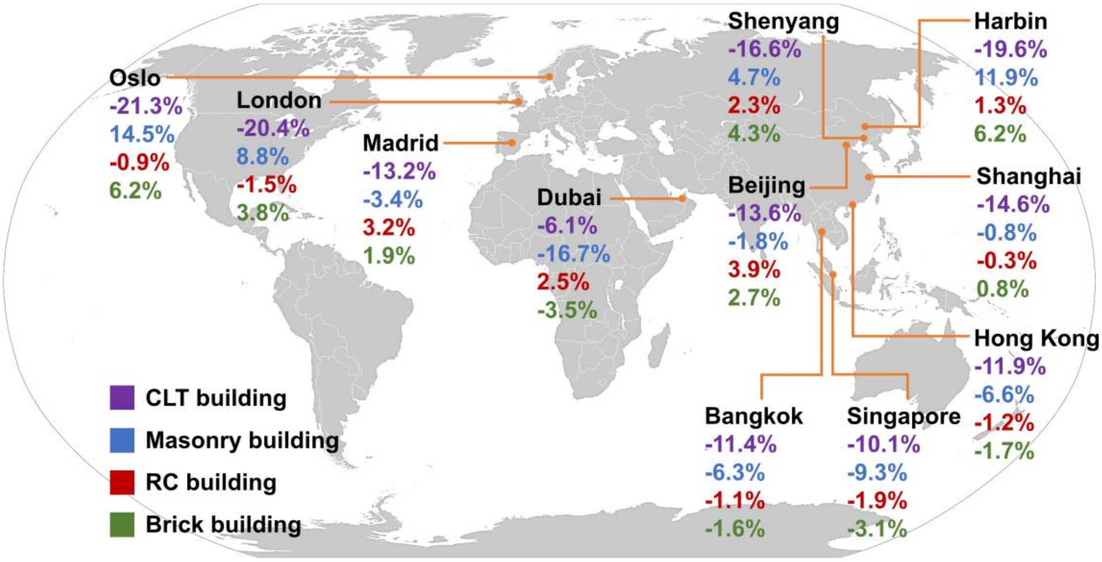

(a) Data based on the weather data of 2023

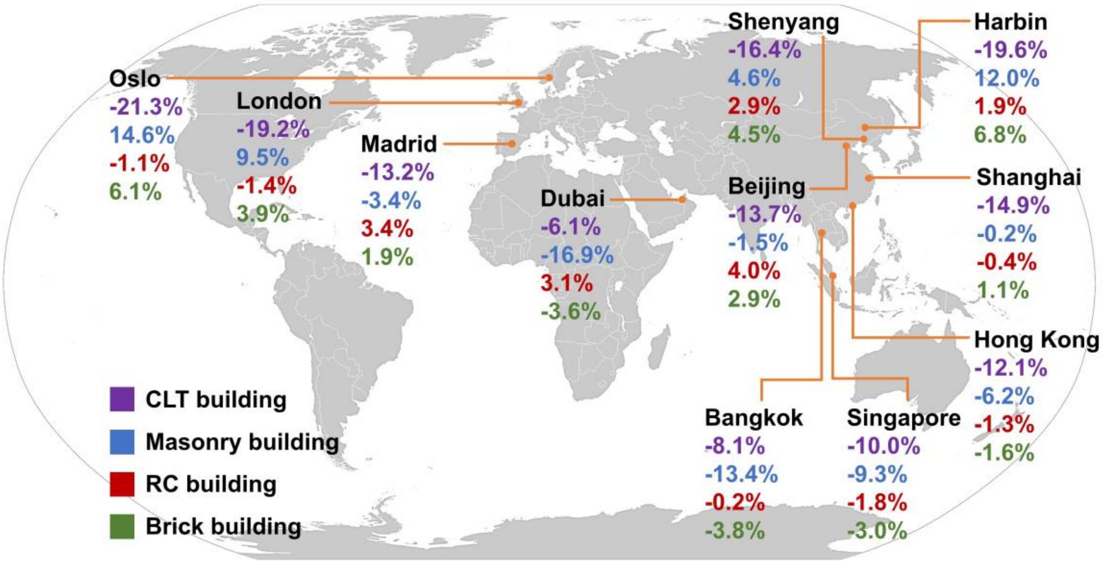

(b) Data based on the average weather data from 2013 to 2022

Figure 7.25 Comparisons of operational energy use when the theoretical and average U-values were considered

Figure 7.26 shows the differences in operational energy use of the four buildings in 11 case cities based on different weather data when the theoretical and dynamic U-values were considered. The data in Figure 7.26 are calculated as Equation (18).

$$D_{T,D} = \frac{OE_{DY}-OE_{THEO}}{OE_{THEO}} \times 100\% \qquad (18)$$

Where $\boldsymbol{D_{T,D}}$ is the difference of operational energy use when the theoretical and dynamic U-values were considered [%]; $\boldsymbol{OE_{THEO}}$ is the operational energy use when the theoretical U-values were considered $[\mathrm{kWh/m^2}]$, and $\boldsymbol{OE_{DY}}$ is the operational energy use when the dynamic U-values were considered $[\mathrm{kWh/m^2}]$.

For the CLT building, in climate zones A and B, the operational energy use when the dynamic U-values were considered was lower than that when the theoretical U-values were considered by 4.0–13.9%. In climate zone C, the operational energy use when the dynamic U-values were considered was lower than that when the theoretical U-values were considered by 11.8–20.5%. In climate zone D, the operational energy use when the dynamic U-values were considered was lower than that when the theoretical U-values were considered by 17.7–26.2%. When the dynamic U-values were considered, the operational energy use of the CLT building was lower than expected, especially in climate zone D. The impacts of dynamic U-values were the most significant in Harbin.

For the masonry building, in climate zones A and B, the operational energy use when the dynamic U-values were considered was lower than that when the theoretical U-values were considered by 6.9–21.6%. In climate zone C, the operational energy use when the dynamic U-values were considered was higher or lower than that when the theoretical U-values were considered by no more than 12.0%. In climate zone D, the operational energy use when the dynamic U-values were considered was higher than that when the theoretical U-values were considered by 7.7–26.7%. When the dynamic U-values were considered, the operational energy use of the masonry building was higher than expected in climate zone D and lower than expected in climate zones A and B. The impacts of dynamic U-values were the most significant in Harbin.

For the RC building, in all climate zones, the operational energy use when the dynamic

U-values were considered was similar to that when the theoretical U-values were considered – higher or lower by no more than 4.7%. Thus, when the dynamic U-values were considered, the operational energy use of the RC building was about as expected in any climate zone. The impacts of dynamic U-values were the most significant in Beijing.

For the brick building, in climate zones A and B, the operational energy use when the dynamic U-values were considered was lower than that when the theoretical U-values were considered by 2.1–5.5%. In climate zone C, the operational energy use when the dynamic U-values were considered was similar to that when the theoretical U-values were considered – higher or lower by no more than 4.9%. In climate zone D, the operational energy use when the dynamic U-values were considered was higher than that when the theoretical U-values were considered by 6.4–11.6%. Thus, when the dynamic U-values were considered, the operational energy use of the brick building was higher than expected in climate zone D and lower than expected in climate zones A and B. The impacts of dynamic U-values were the most significant in Harbin.

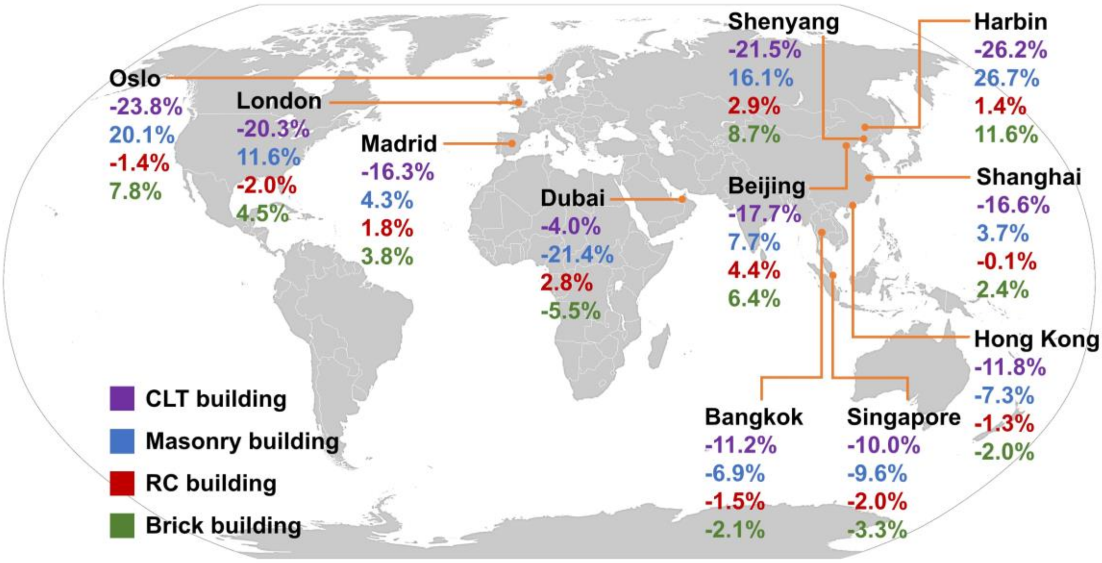

(a) Data based on the weather data of 2023

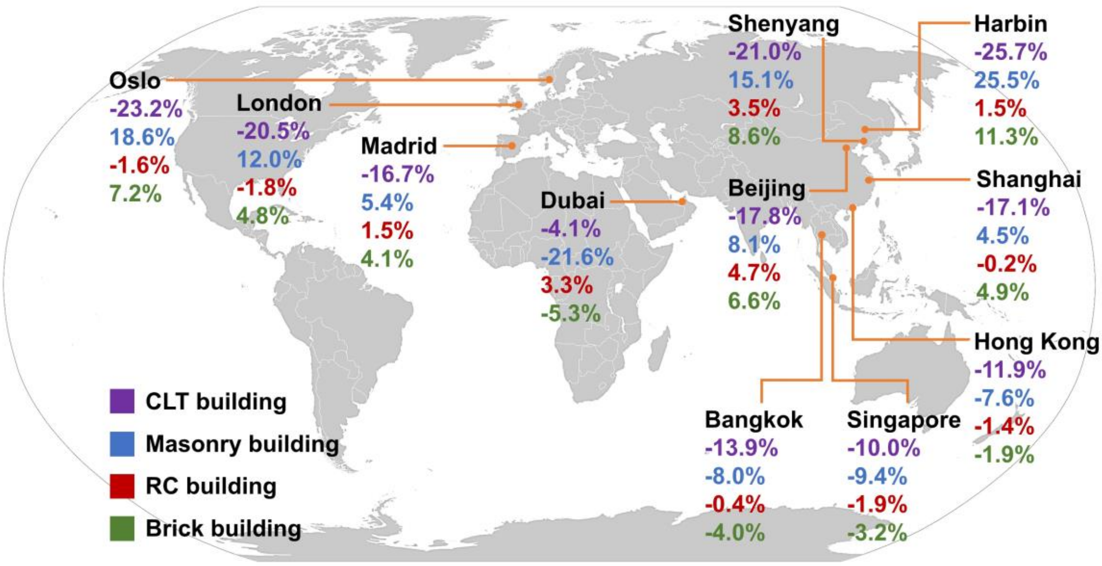

(b) Data based on the average weather data from 2013 to 2022

Figure 7.26 Comparisons of operational energy use when the theoretical and dynamic U-values were considered

Figure 7.27 shows the differences in operational energy use of the four buildings in 11 case cities based on different weather data when the average and dynamic U-values were considered. The data in Figure 7.27 are calculated as Equation (19).

$$D_{D,A} = D_{T,D} - D_{T,A} \ [\%] \qquad (19)$$

Where $\boldsymbol{D_{D,A}}$ is the difference of operational energy use when the average and dynamic U-values were considered [%]; $\boldsymbol{D_{T,D}}$ is the difference of operational energy use when the theoretical and dynamic U-values were considered [%]; $\boldsymbol{D_{T,A}}$ is the difference of operational energy use when the theoretical and average U-values were considered [%].

In this study, when the absolute value of $\boldsymbol{D_{D,A}}$ exceeded 5%, the operational energy use based on the dynamic U-values significantly differed from that based on average U-values. In this situation, average U-values cannot be substitute for dynamic U-values, and dynamic U-values must be considered for operational energy simulations of buildings.

For the CLT building, the absolute value of $\boldsymbol{D_{D,A}}$ only exceeded 5% in Harbin based on the weather data of 2023 and average weather data from 2013 to 2022. In these situations, the operational energy use when the dynamic U-values were considered was lower than that when the average U-values were considered. The minimum value of $\boldsymbol{D_{D,A}}$ was -6.6%.

For the masonry building, the absolute value of $\boldsymbol{D_{D,A}}$ exceeded 5% in Harbin, Shenyang, Madrid, Beijing and Oslo based on the weather data of 2023 and in Harbin, Shenyang, Madrid and Beijing based on the average weather data from 2013 to 2022. In these situations, the operational energy use when the dynamic U-values were considered was higher than that when the average U-values were considered. The maximum value of $\boldsymbol{D_{D,A}}$ was 14.7% in Harbin.

For the RC building, the absolute value of $\boldsymbol{D_{D,A}}$ did not exceed 5% in any case city based on any type of weather data. The operational energy use when the dynamic U-values were considered was similar to that when the average U-values were considered.

For the brick building, the absolute value of $\boldsymbol{D_{D,A}}$ only exceeded 5% in Harbin based on the weather data of 2023. In this situation, the operational energy use when the dynamic U-values were considered was higher than that when the average U-values were considered. The $\boldsymbol{D_{D,A}}$ was 5.4%.

Of the four types of buildings, the dynamic U-values needed to be considered most for operational energy simulations of the masonry building. Conversely, for the RC building, dynamic U-values did not need to be considered regardless of the T/RH conditions; this indicates that its thermal performance is not easily affected by the fluctuations of T/RH.

The case cities where dynamic U-values needed to be considered were Harbin, Oslo, Madrid, Beijing and Shenyang. Among the various climatic zones, the dynamic U-value had the most significant effect in climate zone D – especially in areas with extremely cold winters, such as Harbin.

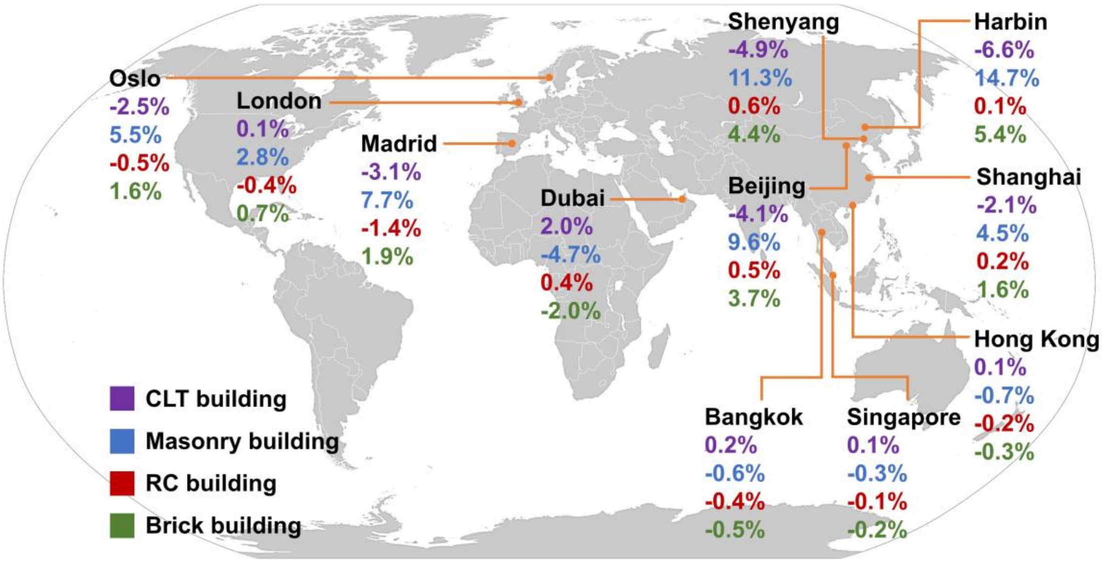

(a) Data based on the weather data of 2023

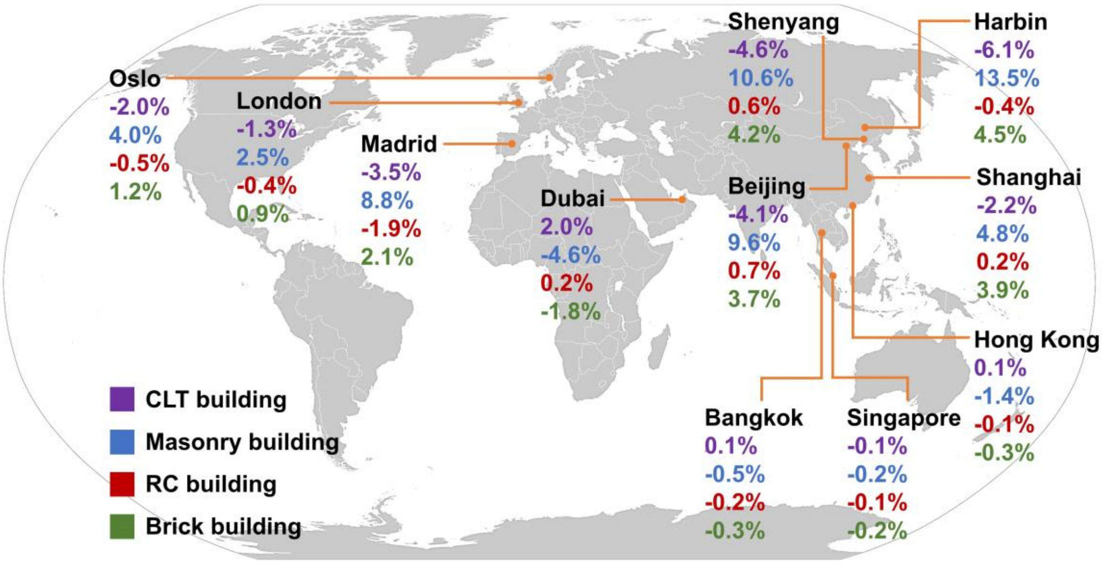

(b) Data based on the average weather data from 2013 to 2022

Figure 7.27 Comparisons of operational energy use when the average and dynamic U-values were considered

This study found that whether $\boldsymbol{D_{D,A}}$ is greater than 5% was related to the annual T/RH differences based on the monthly average T/RH in case cities. The annual T/RH differences in all case cities based on two types of weather data are shown in Figure 7.28. The annual T/RH differences in Figure 7.28 are calculated as Equations (20) and

(21).

$$\Delta T_{annual} = \bar{T}_{max,month} - \bar{T}_{min,month}\ [°C] \qquad (20)$$

$$\Delta RH_{annual} = \overline{RH}_{max,month} - \overline{RH}_{min,month}\ [\%] \qquad (21)$$

Where $\boldsymbol{\Delta T_{annual}}$ is the annual temperature difference based on the monthly average temperature [°C]; $\boldsymbol{\bar{T}_{max,month}}$ is the maximum monthly average temperature for the year [°C]; $\boldsymbol{\bar{T}_{max,month}}$ is the minimum monthly average temperature for the year [°C]; $\boldsymbol{\Delta RH_{annual}}$ is the annual relative humidity difference based on the monthly average relative humidity [%]; $\boldsymbol{\overline{RH}_{max,month}}$ is the maximum monthly average relative humidity for the year [%], and $\boldsymbol{\overline{RH}_{max,month}}$ is the minimum monthly average relative humidity for the year [%].

For the four types of buildings, the situations in which dynamic U-values need to be considered in building operational energy simulations are summarised as follows:

(1) For the CLT building, the dynamic U-values need to be considered in cities where the annual temperature difference based on the monthly average temperature is higher than 36°C and the annual relative humidity difference based on the monthly average relative humidity is higher than 37%.

(2) For the masonry building, the dynamic U-values need to be considered in cities where the annual temperature difference based on the monthly average temperature is higher than 22°C and the annual relative humidity difference based on the monthly average relative humidity is higher than 32%.

(3) For the RC building, the dynamic U-values do not need to be considered.

(4) For the brick building, the dynamic U-values need to be considered in cities where the annual temperature difference based on the monthly average temperature is higher than 40°C.

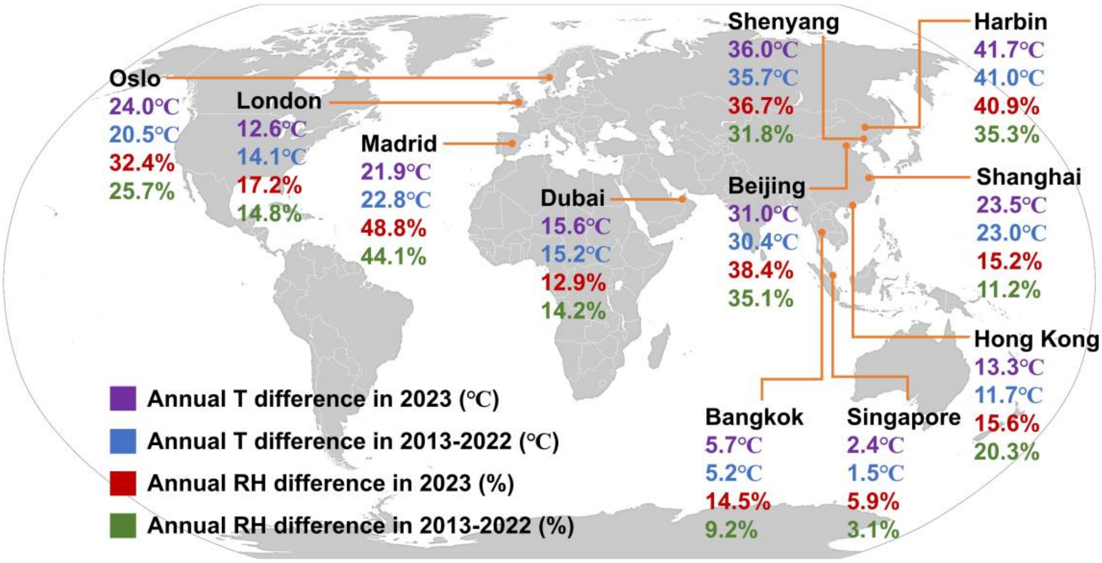

Figure 7.28 Annual T/RH differences in 11 case cities

7.6 Discussion

(1) The uncertainty analysis and sensitivity analysis of the simulation results

To better interpret the simulation results of building operational energy use, both uncertainty analysis and sensitivity analysis were carried out. In terms of uncertainty, three primary factors were identified. First, the dynamic U-values used in the simulations were based on 14-day average values, which may not fully capture the real-time heat transfer dynamics of building envelopes. Second, the simulations were conducted under idealised assumptions, where windows and doors remained closed, occupants were absent, and indoor temperature and humidity were kept constant. These assumptions simplify the model but may differ from actual building operation conditions. Third, the reference building was modeled as a typical six-story residential block with standard design parameters (excluding U-values), which may not represent the energy performance of other residential buildings with different configurations and usage patterns.

Sensitivity analysis of the simulation results indicated two key findings. First, operational energy use was highly sensitive to climate zones. For instance, buildings in climate zone D exhibited significantly higher energy consumption than those in climate zone A, mainly due to more extreme outdoor conditions. Second, the results showed that buildings with masonry and CLT envelopes were more sensitive to changes in U-values, leading to greater variations in energy use compared to RC and brick buildings. This suggests that building material selection and climatic zones play crucial roles in determining energy performance when dynamic U-values are considered.

(2) The operational energy simulation of the CLT building with exterior insulation

The CLT envelope has no insulation, while the other three conventional envelopes have insulation. This study tried to simulate the operational energy use of the CLT building with exterior insulation. The CLT envelope with exterior insulation is common CLT construction in existing buildings. According to the method of inputting dynamic U-values in this study, the thermal conductivity of the insulation layer should be changed for inputting dynamic U-values. However, no dynamic U-value data for the separate insulation layer were measured in this study; thus, the dynamic U-values of the CLT envelope with exterior insulation were entered by varying the thermal conductivity of the CLT panel. Figure 7.29 shows the logic of the operational energy simulations of the CLT building with exterior insulation.

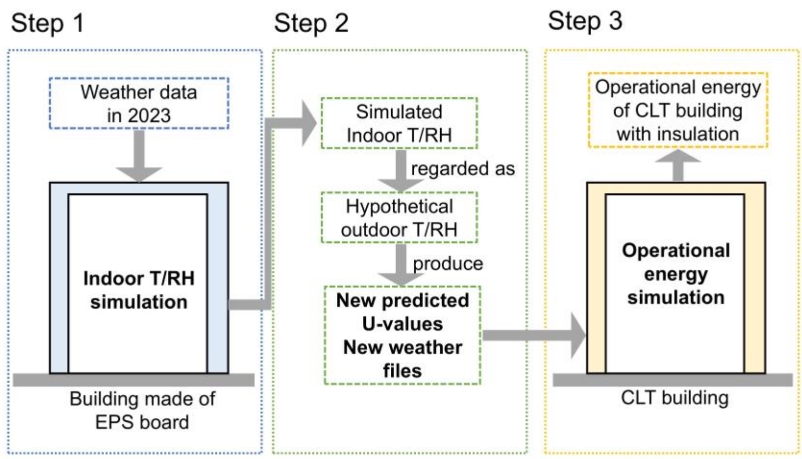

Figure 7.29 Logic of the operational energy simulations of the CLT building with exterior insulation

First, indoor T/RH in a building made of an EPS insulation board were simulated. A 13-cm-thick EPS insulation board was added in the setting of external wall parameters in indoor T/RH simulations. The building model and other building parameters were consistent with those in Section 7.2. The building included no HVAC system and occupant behaviours. The weather file for 11 case cities in 2023 was entered sequentially into indoor T/RH simulations. The simulated indoor T/RH of the building made of an EPS insulation board in 11 case cities in 2023 was obtained.

Second, the simulated indoor T/RH of the building made of an EPS insulation board was considered the hypothetical outdoor T/RH of the CLT building. The new predicted average and dynamic U-values of the CLT envelope were obtained based on the hypothetical outdoor T/RH. The original outdoor T/RH in the weather files were replaced with the hypothetical outdoor T/RH, and the new weather files of 11 case cities in 2023 were obtained.

Third, the operational energy use of the CLT building under the hypothetical outdoor T/RH was simulated. The new predicted average and dynamic U-values of the CLT envelope and new weather files of 11 case cities in 2023 were entered into the operational energy simulations of the CLT buildings. Other settings in the simulations were consistent with those in Section 7.2.

The operational energy use of the CLT building with exterior insulation of 11 case cities in 2023 is shown in Figure 7.30. Table 7.8 summarises the building types with the highest and lowest operational energy use in 11 case cities after the replacement of the original CLT building with the CLT building with exterior insulation.

After exterior insulation was added to the CLT building, the building types with the highest and lowest operational energy use did not change when the theoretical U-values were considered. The results changed when the average and dynamic U-values were considered. When the average U-values were considered, the building types with the highest operational energy use changed from the CLT building to the masonry building in Beijing and Madrid. When the dynamic U-values were considered, the CLT building was the building type with the lowest operational energy use in all case cities of climate zone D. Compared to the CLT building without exterior insulation, the CLT building with exterior insulation had higher potential for energy savings in climate zone D.

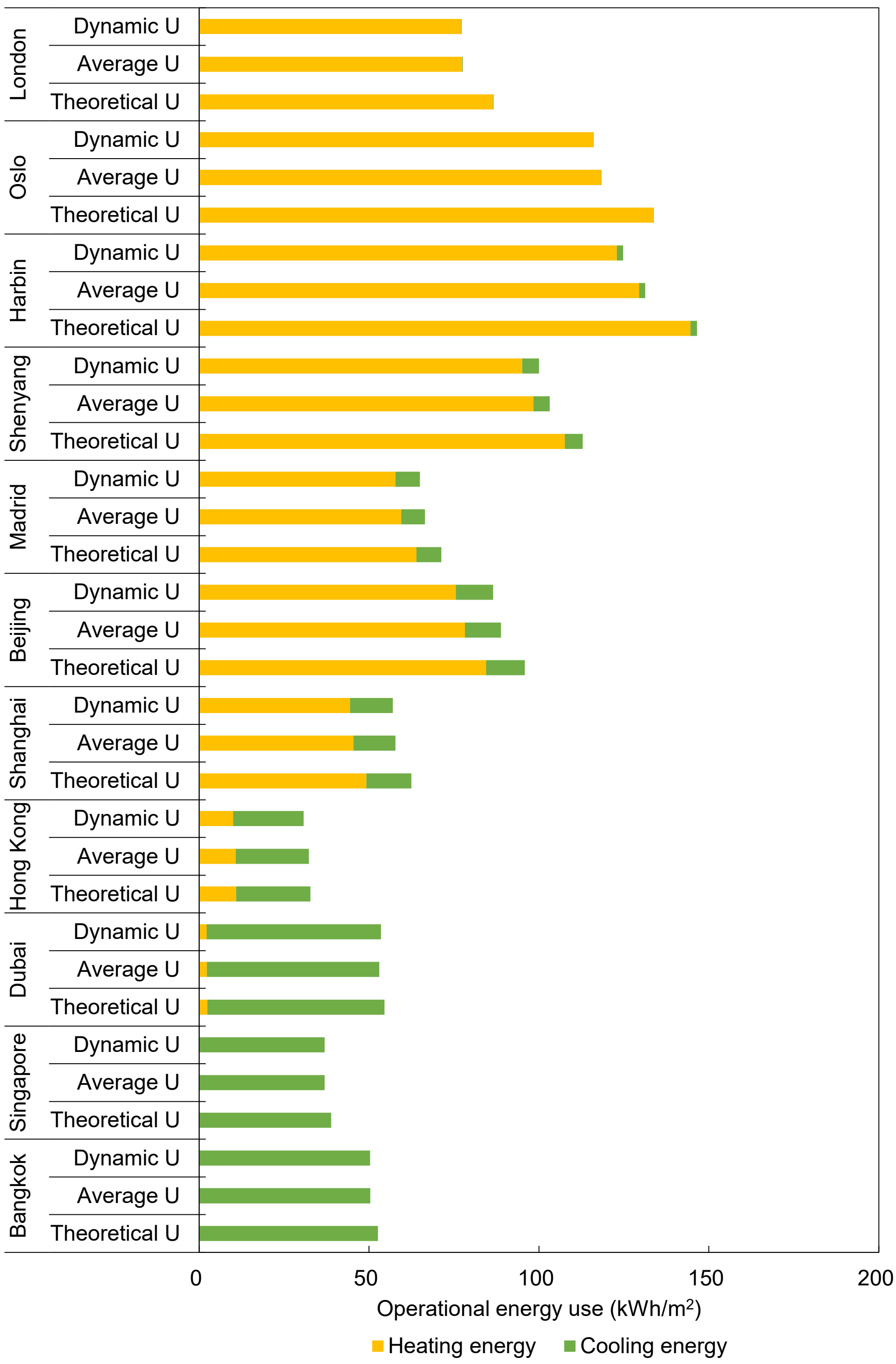

Figure 7.30 Operational energy use of the CLT building with exterior insulation

Table 7.8 Types of buildings with the highest and lowest operational energy use in 11 case cities based on 2023 weather data when the three types of U-values are considered

Climate zone	Case city	Theoretical U-values		Average U-values		Dynamic U-values	
		Highest	Lowest	Highest	Lowest	Highest	Lowest
A	Singapore	CLT	RC	CLT	RC	CLT	RC
	Bangkok	CLT	RC	CLT	RC	CLT	RC
B	Dubai	CLT	RC	CLT	Masonry	CLT	Masonry
C	Hong Kong	CLT	RC	CLT	RC	CLT	RC
	Shanghai	CLT	RC	Masonry	RC	Masonry	RC
	Madrid	CLT	RC	Masonry	RC	Masonry	RC
	London	CLT	RC	Masonry	RC	Masonry	RC
D	Beijing	CLT	RC	Masonry	RC	Masonry	CLT
	Oslo	CLT	RC	Masonry	RC	Masonry	CLT
	Shenyang	CLT	RC	Masonry	RC	Masonry	CLT
	Harbin	CLT	RC	Masonry	RC	Masonry	CLT

(Note: red: differences from Tables 7.5–7.7)

Figure 7.31 shows the $\boldsymbol{D_{T,A}}$, $\boldsymbol{D_{T,D}}$ and $\boldsymbol{D_{D,A}}$ of CLT building with exterior insulation. In all climate zones, the operational energy use when the average U-values were considered was lower than that when the theoretical U-values were considered by 4.6–16.9%. In all climate zones, the operational energy use when the dynamic U-values were considered was lower than that when the theoretical U-values were considered by 3.1–20.7%. The absolute value of $\boldsymbol{D_{D,A}}$ only exceeded 5% in Harbin. For the CLT building with exterior insulation, the dynamic U-values need to be considered in cities where the annual temperature difference based on the monthly average temperature is higher than 40°C and the annual relative humidity difference based on the monthly average relative humidity is higher than 40%. Compared with the CLT building without exterior insulation, the standards that need to consider the dynamic U-values in the CLT building with exterior insulation have been raised. This indicates that the thermal performance of the CLT building is more stable when the building has exterior insulation.

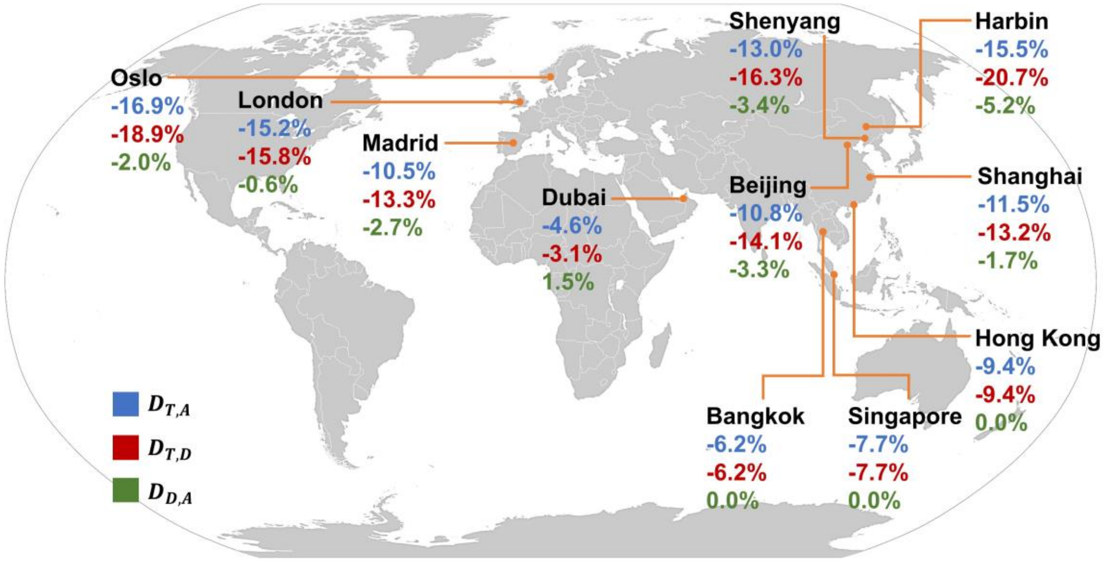

Figure 7.31 Comparisons of the operational energy use of the CLT building with exterior insulation when the three types of U-values are considered

(3) U-value requirements in building codes across different climate zones

To better examine the significance of dynamic U-values in real-world contexts, this section compared the theoretical and dynamic U-values with the maximum U-value limits specified in relevant building codes across 11 case cities, as shown in Tables 7.9 and 7.10, respectively. The theoretical U-values of the four tested wall types were presented in Table 4.3. The theoretical U-value of the CLT, masonry cavity, RC, and brick tested envelope is 0.71, 0.39, 0.27, and 0.32 W/(m^2·K), respectively.

Table 7.9 showed that the theoretical U-value of the CLT envelope met the code limits in climate zones A and some cities in climate zone C. The masonry cavity envelope met the code limits in most cities in climate zones A, B, and C. The RC and brick envelopes met the requirements in the majority of cities in all climate zones. In the previous section (Discussion (2)), to ensure that the CLT envelope better reflected a realistic construction and met the U-value requirements in each climate zone, an external insulation layer was added to the CLT envelope in the simulation, resulting in a revised theoretical U-value of 0.18 W/(m^2·K).

Table 7.9 Climate zone-based U-value requirements and theoretical U-value compliance

(√: The theoretical U-value meets the requirement; CLTI: CLT envelope with insulation)

Climate zone	**Case city**	**Building code**		**Theoretical U-value compliance**			
		U-value (max) (W/m²·K)	**Reference**	**CLT (0.71) CLTI (0.18)**	**Masonry (0.39)**	**RC (0.27)**	**Brick (0.32)**
A	Singapore	1.2	ETTV Code ((BCA) 2021)	√ √	√	√	√
	Bangkok	1.0	BEC ((DEDE) 2021)	√ √	√	√	√
B	Dubai	0.57	Al Sa'fat ((DM) 2023)	 √	√	√	√
C	Hong Kong	1.9	APP156 ((BD) 2014)	√ √	√	√	√
	Shanghai	0.80	GB 50176-2016 ((MOHURD) 2016)	√ √	√	√	√
	Madrid	0.41	CTE DB-HE (Ministerio de Transportes 2022)	 √	√	√	√
	London	0.30	ADL1 (Government 2021)	 √		√	

Table 7.9 (Continued)

Climate zone	Case city	Building code U-value (max) (W/m²·K)	Building code Reference	Theoretical U-value compliance CLT (0.71)	CLTI (0.18)	Masonry (0.39)	RC (0.27)	Brick (0.32)
D	Beijing	0.50	GB 50176-2016 ((MOHURD) 2016)		√	√	√	√
	Oslo	0.18	TEK17 ((DiBK) 2017)		√			
	Shenyang	0.35	GB 50176-2016 ((MOHURD) 2016)		√		√	√
	Harbin	0.35	GB 50176-2016 ((MOHURD) 2016)		√		√	√

Table 7.10 presented the maximum value in dynamic U-values of the five envelopes across 11 case cities, along with an assessment of whether these values complied with the respective local building code requirements. Compared to the theoretical U-value results shown in Table 7.9, it could be observed that in climate zones A and B, as well as in three cities in climate zone C and one city in climate zone D, the compliance results were consistent between the theoretical and dynamic U-values. However, in three cities in climate zone D and one city in climate zone C, although the theoretical U-values of conventional envelopes met the local building code, the peak values of the dynamic U-values exceeded the regulatory limits. This indicated that considering dynamic U-values was essential in cold climate regions. When exposed to fluctuating environmental conditions, some conventional envelopes performed worse than expected and may even fall below the minimum thermal performance required by regulations. This discrepancy could lead to significant underestimation of building

energy demand by policymakers or building owners, ultimately resulting in unnecessary energy waste.

Table 7.10 Maximum value in dynamic U-values and dynamic U-value compliance

(√: The dynamic U-values meet the requirement; CLTI: CLT envelope with insulation)

Climate zone	Case city	Maximum value in dynamic U-value				Dynamic U-value compliance			
		CLT CLTI	Masonry	RC	Brick	CLT CLTI	Masonry	RC	Brick
A	Singapore	0.56 0.17	0.37	0.24	0.30	√ √	√	√	√
	Bangkok	0.57 0.17	0.51	0.29	0.38	√ √	√	√	√
B	Dubai	0.72 0.19	0.37	0.34	0.34	 √	√	√	√
C	Hong Kong	0.57 0.17	0.51	0.29	0.38	√ √	√	√	√
	Shanghai	0.58 0.17	0.76	0.29	0.46	√ √	√	√	√
	Madrid	0.72 0.19	0.79	0.40	0.45	 √		√	
	London	0.47 0.16	0.88	0.28	0.47	 √		√	

Table 7.10 (continued)

Climate zone	Case city	Maximum value in dynamic U-value				Dynamic U-value compliance			
		CLT CLTI	Masonry	RC	Brick	CLT CLTI	Masonry	RC	Brick
D	Beijing	0.69	0.93	0.38	0.54			√	
		0.18				√			
	Oslo	0.55	1.05	0.34	0.53				
		0.17				√			
	Shenyang	0.4	0.96	0.35	0.56			√	
		0.16				√			
	Harbin	0.53	1.25	0.36	0.63				
		0.17				√			

7.7 Summary

According to the optimal U-value prediction model and the optimal time interval, the predicted average and dynamic U-values of CLT, masonry cavity, RC and brick envelopes were obtained. The operational energy use of the four types of buildings was simulated in 11 case cities based on the weather data of 2023 and 2013–2022 when the different types of U-values were considered. The influences of dynamic U-values on operational energy simulations were analysed, and the operational energy use of CLT and conventional buildings were compared. The operational energy use of the CLT building with exterior insulation was also analysed.

Chapter 8 Conclusions and Recommendations

8.1 Conclusions

The dynamic U-values of CLT and conventional envelopes were studied in detail. The operational energy use of the CLT and conventional buildings was simulated in different climate zones by considering dynamic U-values. The important conclusions are five:

(1) Optimal calculation methods and the optimal prediction model of dynamic U-values

The optimal calculation methods of dynamic U-values included the optimal data pre-processing methods and optimal time interval. The optimal data pre-processing methods were TL, PV1 and AV1. The optimal time interval was a 14-day interval. The optimal prediction model of dynamic U-values for the four envelopes was developed by the HLR method. In this model, outdoor T/RH were important factors.

(2) Characteristics of the dynamic U-values of CLT and three conventional envelopes

In climate zone A, no significant fluctuations were observed in the dynamic U-values of the four envelopes as outdoor T/RH are relatively stable throughout the year. In climate zones B, C and D, the dynamic U-values of the CLT envelope increased from winter to summer and decreased from summer to winter. The dynamic U-values of the masonry cavity and brick envelopes decreased from winter to summer and increased from summer to winter. The fluctuations in dynamic U-values for the masonry cavity envelope were greater than those for the CLT and brick envelopes. No significant fluctuations were observed in the dynamic U-values of the RC envelope throughout the year.

(3) Building type with the lowest operational energy use when dynamic U-values are considered

In climate zone A, the RC building consumed the least operational energy. In climate zone B, the masonry building consumed the least operational energy. In climate zone C, the RC building consumed the least operational energy. In climate zone D, the CLT building consumed the least operational energy in Harbin, and the RC building consumed the least operational energy in the other three case cities. If the CLT building with insulation was considered, the building types with the lowest operational energy use did not change in climate zones A, B and C. However, in climate zone D, the CLT building consumed the least operational energy in the four case cities.

(4) Influences of dynamic U-values on operational energy simulations

The impacts of dynamic U-values on energy simulations are caused by the hygrothermal behaviours of building materials. Changes in T/RH affect the hygrothermal behaviours of building materials, altering their thermal conductivities and leading to fluctuations in U-values. These fluctuations directly affect the heating and cooling energy, resulting in differences in simulated operational energy consumption compared to simulations using theoretical or average U-values.

For the four types of buildings, the energy influences of the dynamic U-values in the CLT and masonry buildings were more significant. In the CLT and masonry buildings, the simulated operational energy use when the dynamic U-values were considered can differ from that when the theoretical U-values were considered by up to 26.2% and 26.7%, respectively. If the CLT building with exterior insulation was considered, the simulated operational energy use when the dynamic U-values were considered differed from that when the theoretical U-values were considered by up to 20.8%. The energy influences of the dynamic U-values in the RC and brick buildings were less significant. In the RC and brick buildings, the simulated operational energy use when the dynamic

U-values were considered differed from that when the theoretical U-values were considered by up to 4.7% and 11.6%, respectively.

The energy influences of the dynamic U-values of the four building envelopes in climate zone D were the most significant, especially in Harbin. The energy influences of the dynamic U-values of the CLT, masonry cavity and brick envelopes were maximum in Harbin compared to other case cities.

(5) Situations that consider dynamic U-values

For the CLT building, the dynamic U-values need to be considered in cities where the annual T/RH difference based on the monthly average T/RH is higher than 36°C and 37%. If the CLT building with exterior insulation is considered, the dynamic U-values need to be considered in cities where the annual T/RH difference based on the monthly average T/RH is higher than 40°C and 40%. For the masonry building, the dynamic U-values need to be considered in cities where the annual T/RH difference based on the monthly average T/RH is higher than 22°C and 32%. For the RC building, the dynamic U-values do not need to be considered. For the brick building, the dynamic U-values need to be considered in cities where the annual temperature difference based on the monthly average temperature is higher than 40°C.

8.2 Recommendations for Practical Engineering

(1) Building energy simulation optimisation

Dynamic U-values can be used for optimisation of building parameter inputs when simulating the operational energy of CLT, masonry or brick buildings. The theoretical U-values of the envelope should be replaced by dynamic U-values when the climatic characteristics of the simulated city meet the standards that need to be taken into account for the dynamic U-values. Dynamic U-values can be calculated using the optimal U-value prediction model. This can narrow the gap between the heat transfer characteristics of the envelopes in actual conditions and those in the simulations.

(2) Application scope of CLT buildings

According to the results of the study, the CLT building had better energy efficiency in climatic zone D with cold winters. Conversely, the operational energy use of the CLT building was higher than that of the conventional buildings in climate zones A and B, which are warm throughout the year. This indicates that CLT buildings are more suitable for cold regions in terms of building operational energy use. The results of the study can inform the promotion of CLT buildings.

(3) Retrofit of old buildings

According to the measurement results in Sheffield and Harbin, where the minimum winter temperatures are below 0°C, the dynamic U-values of old envelopes (including the masonry cavity envelope and the brick envelope) were much higher than the theoretical U-values. High U-values can lead to high heating energy consumption in winter in climate zones C and D. Common retrofitting methods for old buildings include adding external insulation to the envelopes. The thickness of the insulation materials can be calculated with reference to the range of dynamic U-values in the winter.

8.3 Future Work

(1) Dynamic U-value database expansion

Owing to the limitation of measurement conditions, only four tested envelopes were selected in this study. Each tested envelope was only measured for a few months. In future studies, more types of envelopes can be measured, and the measurement time can last at least one year. More tested cities can be selected for each climate zone. A more comprehensive database can be used to build a more generalised U-value prediction model. A comprehensive dynamic U-value database can also provide a more reliable reference for optimising building energy simulations.

(2) Automated input of dynamic U-values

In TRNSYS, it is not possible to enter the dynamic U-values at once, because TRNSYS only allows one U-value to be entered in each simulation. Therefore, the entire simulation cycle was divided into multiple runs at 14-day intervals. For each run, the thermal conductivity of the outer layer of the envelope was manually adjusted to match the corresponding U-value. This process is highly repetitive and labour-intensive. It is a limitation of this study. In future research, methods for automating the input of dynamic U-values should be developed. For example, a customised TRNSYS plug-in could be created to import dynamic U-values from an Excel file directly into the simulation.

(3) Exploration of dynamic U-values inside the envelopes

In Chapter 7, the dynamic U-values of the insulated CLT envelope were obtained by adjusting the thermal conductivity of the CLT panel instead of the insulation panel. Because the dynamic U-values of the insulation panel were not measured. This is a limitation in the study. In future research, the dynamic U-values of each building material within the envelope should be studied in the real buildings to observe the change process of dynamic U-values in detail. Researchers can thus gain a deeper understanding of the principles of dynamic U-values.

Reference

(BCA), Building and Construction Authority. 2021. "Code on Envelope Thermal Performance for Buildings." In. Singapore: Building and Construction Authority.

(BD), Buildings Department. 2014. "APP-156: Design and Construction Requirements for Energy Efficiency of Residential Buildings." In. Hong Kong: Buildings Department.

(DEDE), Department of Alternative Energy Development and Efficiency. 2021. "Building Energy Code (BEC)." In. Bangkok: Ministry of Energy.

(DiBK), Direktoratet for Byggkvalitet. 2017. "Regulation on Technical Requirements for Construction Works (TEK17)." In. Oslo: Norwegian Building Authority.

(DM), Dubai Municipality. 2023. "Al Sa'fat-Dubai Green Building System-2nd edition." In. Dubai: Dubai Municipality.

(MOHURD), Ministry of Housing and Urban-Rural Development of the People's Republic of China. 2016. "Code for thermal design of civil building GB 50176-2016." In. Beijing: China Architecture & Building Press.

Ahmad, Muhammad Waseem, Monjur Mourshed, and Yacine Rezgui. 2017. 'Trees vs Neurons: Comparison between random forest and ANN for high-resolution prediction of building energy consumption', *Energy and Buildings*, 147: 77-89.

Alsharif, Rashed, Mehrdad Arashpour, Victor Chang, and Jenny Zhou. 2021. 'A review of building parameters' roles in conserving energy versus maintaining comfort', *Journal of Building Engineering*, 35: 102087.

Amasyali, Kadir, and Nora El-Gohary. 2021. 'Machine learning for occupant-behavior-sensitive cooling energy consumption prediction in office buildings', *Renewable and Sustainable Energy Reviews*, 142: 110714.

Amoabeng, Kofi Owura, Richard Opoku, Samuel Boahen, and George Yaw Obeng. 2023. 'Analysis of indoor set-point temperature of split-type ACs on thermal comfort and energy savings for office buildings in hot-humid climates', *Energy and Built Environment*, 4: 368-76.

Andújar Márquez, José M., Miguel Á Martínez Bohórquez, and Sergio Gómez Melgar. 2017. "A New Metre for Cheap, Quick, Reliable and Simple Thermal Transmittance (U-Value) Measurements in Buildings." In *Sensors*.

Arslan, O., F. Messali, E. Smyrou, İ E. Bal, and J. G. Rots. 2021. 'Mechanical modelling of the axial behaviour of traditional masonry wall metal tie connections in cavity walls', *Construction and Building Materials*, 310: 125205.

ASTM. 2007. "ASTM C1155-95 Standard, Standard Practice for Determining Thermal Resistance of Building Envelope Components from the In-situ Data." In.

Atsonios, Ioannis A, Ioannis D Mandilaras, Dimos A Kontogeorgos, Maria A %J Energy Founti, and Buildings. 2017. 'A comparative assessment of the standardized methods for the in–situ measurement of the thermal resistance of building walls', 154: 198-206.

Bamdad, Keivan, Soha Matour, Nima Izadyar, and Sara Omrani. 2022. 'Impact of climate change on energy saving potentials of natural ventilation and ceiling fans in mixed-mode buildings', *Building and Environment*, 209: 108662.

Bastos Porsani, Gabriela, Núria Casquero-Modrego, Juan Bautista Echeverria Trueba, and Carlos Fernández Bandera. 2023. 'Empirical evaluation of EnergyPlus infiltration model for a case study in a high-rise residential building', *Energy and Buildings*, 296: 113322.

Beaulac, Arnaud, Timothé Lalonde, Didier Haillot, and Danielle Monfet. 2024. 'Energy modeling, calibration, and validation of a small-scale greenhouse using TRNSYS', *Applied Thermal Engineering*, 248: 123195.

Bekö, Gabriel, Sine Gustavsen, Marie Frederiksen, Niels Christian Bergsøe, Barbara Kolarik, Lars Gunnarsen, Jørn Toftum, and Geo Clausen. 2016. 'Diurnal and seasonal variation in air exchange rates and interzonal airflows measured by active and passive tracer gas in homes', *Building and Environment*, 104: 178-87.

Belpoliti, Vittorino, Ahmed A. Saleem, Moohammed W. Yahia, and Reem Nassif. 2024. 'Energy consumption of UAE public schools. Mapping of a diversified sector assessing typology, conditions, and educational systems', *Energy and Buildings*, 320: 114599.

Bienvenido-Huertas, David, Juan Moyano, David Marín, and Rafael Fresco-Contreras. 2019. 'Review of in situ methods for assessing the thermal transmittance of walls', *Renewable and Sustainable Energy Reviews*, 102: 356-71.

Bienvenido-Huertas, David, Roberto Rodríguez-Álvaro, Juan J. Moyano, Fernando Rico, and David Marín. 2018. "Determining the U-Value of Façades Using the Thermometric Method: Potentials and Limitations." In *Energies*.

Biswas, Nisantika, Priyam Saha, Soumalya Mitra, Somnath Mitra, and Gautam Majumdar. 2024. '8.10 - Green building material (GBM) vs conventional building material (CBM) to reduce environmental impact.' in Saleem Hashmi (ed.), *Comprehensive Materials Processing (Second Edition)* (Elsevier: Oxford).

Boukhattem, Lahcen, Mustapha Boumhaout, Hassan Hamdi, Brahim Benhamou, and Fatima Ait Nouh. 2017. 'Moisture content influence on the thermal conductivity of insulating building materials made from date palm fibers mesh', *Construction and Building Materials*, 148: 811-23.

Boyano, A., P. Hernandez, and O. Wolf. 2013. 'Energy demands and potential savings in European office buildings: Case studies based on EnergyPlus simulations', *Energy and Buildings*, 65: 19-28.

Braas, Hagen, Ulrike Jordan, Isabelle Best, Janybek Orozaliev, and Klaus Vajen. 2020. 'District heating load profiles for domestic hot water preparation with realistic simultaneity using DHWcalc and TRNSYS', *Energy*, 201: 117552.

Bruno, Roberto, and Piero Bevilacqua. 2022. 'Heat and mass transfer for the U-value assessment of opaque walls in the Mediterranean climate: Energy implications', *Energy*, 261: 124894.

Buck, Dietrich, Xiaodong Wang, Olle Hagman, and Anders Gustafsson. 2016. "Further Development of Cross-Laminated Timber (CLT): Mechanical Tests on 45° Alternating Layers." In *World Conference on Timber Engineering (WCTE 2016)*. Vienna.

Bucklin, Oliver, Theresa Müller, Felix Amtsberg, Philip Leistner, and Achim Menges. 2023. 'Analysis of thermal Transmittance, air Permeability, and hygrothermal behavior of a solid timber building envelope', *Energy and Buildings*, 299: 113629.

Byun, Jiyeon, Jumi Baek, Jisoo Shim, Somin Park, and Doosam Song. 2023. 'Proposal of a correction factor for predicting the thermal transmittance of building envelopes in existing buildings accounting for aging and environmental conditions', *Building and Environment*, 243: 110658.

Cakiroglu, Celal, Yaren Aydın, Gebrail Bekdaş, Umit Isikdag, Aidin Nobahar Sadeghifam, and Laith

Abualigah. 2024. 'Cooling load prediction of a double-story terrace house using ensemble learning techniques and genetic programming with SHAP approach', *Energy and Buildings*, 313: 114254.

Calis, Metehan. 2024. 'Change of U-value with extreme temperatures on different types of block walls', *Journal of Building Engineering*, 85: 108653.

Catalina, Tiberiu, Vlad Iordache, and Bogdan Caracaleanu. 2013. 'Multiple regression model for fast prediction of the heating energy demand', *Energy and Buildings*, 57: 302-12.

Catto Lucchino, Elena, Adrienn Gelesz, Kristian Skeie, Giovanni Gennaro, András Reith, Valentina Serra, and Francesco Goia. 2021. 'Modelling double skin façades (DSFs) in whole-building energy simulation tools: Validation and inter-software comparison of a mechanically ventilated single-story DSF', *Building and Environment*, 199: 107906.

Cetin, Kristen S., Mohammad Hassan Fathollahzadeh, Niraj Kunwar, Huyen Do, and Paulo Cesar Tabares-Velasco. 2019. 'Development and validation of an HVAC on/off controller in EnergyPlus for energy simulation of residential and small commercial buildings', *Energy and Buildings*, 183: 467-83.

Chen, Lufang, Yun Zhang, Xin Zhou, Xing Shi, Liu Yang, and Xing Jin. 2023. 'A new method for measuring thermal resistance of building walls and analyses of influencing factors', *Construction and Building Materials*, 385: 131438.

Chen, Sihao, Xiaoqing Zhou, Guang Zhou, Chengliang Fan, Puxian Ding, and Qiliang Chen. 2022. 'An online physical-based multiple linear regression model for building's hourly cooling load prediction', *Energy and Buildings*, 254: 111574.

Chen, Yongbao, Mingyue Guo, Zhisen Chen, Zhe Chen, and Ying Ji. 2022. 'Physical energy and data-driven models in building energy prediction: A review', *Energy Reports*, 8: 2656-71.

Chiniforush, Alireza A., Ali Akbarnezhad, Hamid Valipour, and Jianzhuang Xiao. 2018. 'Energy implications of using steel-timber composite (STC) elements in buildings', *Energy and Buildings*, 176: 203-15.

Chiriko, Amare Yaekob. 2023. 'Supply side factors as determinants of Ethiopia's image as a destination', *Anatolia*, 34: 333-43.

Ciulla, G., and A. D'Amico. 2019. 'Building energy performance forecasting: A multiple linear regression approach', *Applied Energy*, 253: 113500.

Dabirian, Sanam, Karthik Panchabikesan, and Ursula Eicker. 2022. 'Occupant-centric urban building energy modeling: Approaches, inputs, and data sources - A review', *Energy and Buildings*, 257: 111809.

Danovska, Maja, Giovanni Pernigotto, Paolo Baggio, and Andrea Gasparella. 2022. 'Simulation uncertainty in heat transfer across timber building components in the Italian climates: The role of thermal conductivity', *Energy and Buildings*, 268: 112190.

Day, Julia K., Claire McIlvennie, Connor Brackley, Mariantonietta Tarantini, Cristina Piselli, Jakob Hahn, William O'Brien, Vinu Subashini Rajus, Marilena De Simone, Mikkel Baun Kjærgaard, Marco Pritoni, Arno Schlüter, Yuzhen Peng, Marcel Schweiker, Gianmarco Fajilla, Cristina Becchio, Valentina Fabi, Giorgia Spigliantini, Ghadeer Derbas, and Anna Laura Pisello. 2020. 'A review of select human-building interfaces and their relationship to human behavior, energy use and occupant comfort', *Building and Environment*, 178: 106920.

de Serres-Lafontaine, Célestin, Pierre Blanchet, Stéphane Charron, Laetitia Delem, and Lisa Wastiels. 2024. 'Bio-based innovations in cross-laminated timber (CLT) envelopes: A

hygrothermal and life cycle analysis (LCA) study', *Building and Environment*, 256: 111499.
Deshko, Valerii, Inna Bilous, Iryna Sukhodub, and Olena Yatsenko. 2021. 'Evaluation of energy use for heating in residential building under the influence of air exchange modes', *Journal of Building Engineering*, 42: 103020.
Desogus, Giuseppe, Salvatore Mura, Roberto %J Energy Ricciu, and Buildings. 2011. 'Comparing different approaches to in situ measurement of building components thermal resistance', 43: 2613-20.
Dong, Yu, Xue Cui, Xunzhi Yin, Yang Chen, and Haibo Guo. 2019. "Assessment of Energy Saving Potential by Replacing Conventional Materials by Cross Laminated Timber (CLT)—A Case Study of Office Buildings in China." In *Applied Sciences*.
Duan, Zhuocheng, Qiong Huang, Qiming Sun, and Qi Zhang. 2022. 'Comparative life cycle assessment of a reinforced concrete residential building with equivalent cross laminated timber alternatives in China', *Journal of Building Engineering*, 62: 105357.
Eguaras-Martínez, María, Marina Vidaurre-Arbizu, and César Martín-Gómez. 2014. 'Simulation and evaluation of Building Information Modeling in a real pilot site', *Applied Energy*, 114: 475-84.
Eid, Elias, Alan Foster, Graciela Alvarez, Fatou-Toutie Ndoye, Denis Leducq, and Judith Evans. 2024. 'Modelling energy consumption in a Paris supermarket to reduce energy use and greenhouse gas emissions using EnergyPlus', *International Journal of Refrigeration*, 168: 1-8.
Eksi Kilicaslan, Aysegül, and Hülya Kus. 2024. 'Hygrothermal performance of timber-framed walls in Turkey – Long-term monitoring', *Journal of Building Engineering*, 94: 109886.
El Assaad, M., T. Colinart, and T. Lecompte. 2023. 'Thermal conductivity assessment of moist building insulation material using a Heat Flow Meter apparatus', *Building and Environment*, 234: 110184.
Eriksson, Martin, Jan Akander, and Bahram Moshfegh. 2020. 'Development and validation of energy signature method – Case study on a multi-family building in Sweden before and after deep renovation', *Energy and Buildings*, 210: 109756.
Ethirveerasingham, Kajen, Alan S. Fung, and Rakesh Kumar. 2024. 'TRNSYS modelling and feasibility study of natural gas absorption heat pump (GAHP) for Canadian homes', *Applied Thermal Engineering*, 257: 124179.
Evangelisti, L., C. Guattari, and F. Asdrubali. 2019. 'Comparison between heat-flow meter and Air-Surface Temperature Ratio techniques for assembled panels thermal characterization', *Energy and Buildings*, 203: 109441.
Evangelisti, Luca, Claudia Guattari, Roberto De Lieto Vollaro, and Francesco Asdrubali. 2020. 'A methodological approach for heat-flow meter data post-processing under different climatic conditions and wall orientations', *Energy and Buildings*, 223: 110216.
Evangelisti, Luca, Claudia Guattari, Paola Gori, and Roberto D. Vollaro. 2015. "In Situ Thermal Transmittance Measurements for Investigating Differences between Wall Models and Actual Building Performance." In *Sustainability*, 10388-98.
Fedorczak-Cisak, Małgorzata, Elżbieta Radziszewska-Zielina, Bożena Orlik-Kożdoń, Tomasz Steidl, and Tadeusz Tatara. 2020. "Analysis of the Thermal Retrofitting Potential of the External Walls of Podhale's Historical Timber Buildings in the Aspect of the Non-Deterioration of Their Technical Condition." In *Energies*.

Feng, Fan, Yangyang Fu, Zhiyao Yang, and Zheng O'Neill. 2022. 'Enhancement of phase change material hysteresis model: A case study of modeling building envelope in EnergyPlus', *Energy and Buildings*, 276: 112511.

Ficco, Giorgio, Fabio Iannetta, Elvira Ianniello, Francesca Romana d'Ambrosio Alfano, and Marco Dell'Isola. 2015. 'U-value in situ measurement for energy diagnosis of existing buildings', *Energy and Buildings*, 104: 108-21.

Fornari, Walter, Grigori Grozman, Niklas Wikström, and Per Sahlin. 2023. 'Development of a BLOCK zonal model in a BPS software to predict thermal stratification and air flows', *Energy and Buildings*, 294: 113230.

Fortune Business Insights. 2024. "Cross Laminated Timber Market Size, Share & Industry Analysis, By Bonding Technology (Adhesive Bonded and Mechanically Fastened), By Application (Residential Buildings, Non-Residential Buildings, and Others), and Regional Forecast, 2024-2032." In. https://www.fortunebusinessinsights.com/cross-laminated-timber-clt-market-102884.

Fu, Chun, and Clayton Miller. 2022. 'Using Google Trends as a proxy for occupant behavior to predict building energy consumption', *Applied Energy*, 310: 118343.

Gagliano, A., F. Patania, F. Nocera, and C. Signorello. 2014. 'Assessment of the dynamic thermal performance of massive buildings', *Energy and Buildings*, 72: 361-70.

Gaspar, Katia, Miquel Casals, and Marta Gangolells. 2016. 'A comparison of standardized calculation methods for in situ measurements of façades U-value', *Energy and Buildings*, 130: 592-99.

Gennaro, Giovanni, Elena Catto Lucchino, Francesco Goia, and Fabio Favoino. 2023. 'Modelling double skin façades (DSFs) in whole-building energy simulation tools: Validation and inter-software comparison of naturally ventilated single-story DSFs', *Building and Environment*, 231: 110002.

Gobinath, Praddeep, Robert H. Crawford, Marzia Traverso, and Behzad Rismanchi. 2024. 'Comparing the life cycle costs of a traditional and a smart HVAC control system for Australian office buildings', *Journal of Building Engineering*, 91: 109686.

Government, HM. 2021. "Approved Document L: Conservation of Fuel and Power (Volume 1 – Dwellings)." In. London: Department for Levelling Up, Housing and Communities.

Guo, Haibo, Ying Liu, Wen-Shao Chang, Yu Shao, and Cheng Sun. 2017. 'Energy Saving and Carbon Reduction in the Operation Stage of Cross Laminated Timber Residential Buildings in China', 9: 292.

Guo, Haibo, Ying Liu, Yiping Meng, Haoyu Huang, Cheng Sun, and Yu Shao. 2017. 'A Comparison of the Energy Saving and Carbon Reduction Performance between Reinforced Concrete and Cross-Laminated Timber Structures in Residential Buildings in the Severe Cold Region of China', *Sustainability*, 9.

Guo, Ruiqi, Bin Yang, Yuyao Guo, He Li, Zhe Li, Bin Zhou, Bo Hong, and Faming Wang. 2024. 'Machine learning-based prediction of outdoor thermal comfort: Combining Bayesian optimization and the SHAP model', *Building and Environment*, 254: 111301.

Guo, S., W. Huang, Q. Jia, Z. Li, X. Liu, and H. Zhao. 2013. 'Effective thermal conductivity of reservoir freshwater ice with attention to high temperature', *Annals of Glaciology*, 54: 189-95.

Hamdaoui, Mohamed-Ali, Mohammed-Hichem Benzaama, Yassine El Mendili, and Daniel Chateigner. 2021. 'A review on physical and data-driven modeling of buildings hygrothermal behavior: Models, approaches and simulation tools', *Energy and Buildings*, 251: 111343.

Harb, Elias, Chadi Maalouf, Christophe Bliard, Elias Kinab, Mohammed Lachi, and Guillaume Polidori. 2024. 'Hygrothermal performance of multilayer wall assemblies incorporating starch/beet pulp in France', *Construction and Building Materials*, 445: 137773.

Hosamo, Haidar Hosamo, Merethe Solvang Tingstveit, Henrik Kofoed Nielsen, Paul Ragnar Svennevig, and Kjeld Svidt. 2022. 'Multiobjective optimization of building energy consumption and thermal comfort based on integrated BIM framework with machine learning-NSGA II', *Energy and Buildings*, 277: 112479.

ISO. 2007. "ISO 6946, Building components and building elements – Thermal resistance and thermal transmittance – Calculation method." In.

ISO. 2014. "ISO 9869-1, Thermal Insulation, Building Elements, In-Situ Measurement of Thermal Resistance and Thermal Transmittance-Part 1: Heat Flow Meter Method." In.

Jeng, Cheng-Chang. 2023. 'Why a Variance Inflation Factor of 10 Is Not an Ideal Cutoff for Multicollinearity Diagnostics', *教育研究學報*, 57: 67-93.

Johari, F., J. Munkhammar, F. Shadram, and J. Widén. 2022. 'Evaluation of simplified building energy models for urban-scale energy analysis of buildings', *Building and Environment*, 211: 108684.

Jraida, Kaoutar, Youness El Mghouchi, Amina Mourid, Chadia Haidar, and Mustapha El Alami. 2024. 'Machine learning-based predicting of PCM-integrated building thermal performance: An application under various weather conditions in Morocco', *Journal of Building Engineering*, 96: 110395.

Jung, Dong Eun, Dae Hwan Shin, Jihyun Seo, Kwang Ho Lee, and Jonghun Kim. 2024. 'In-situ virtual heat flow meter model for monitoring heat flux of existing building envelope', *Building and Environment*, 253: 111320.

Kenai, Mohamed-Amine, Laurent Libessart, Stéphane Lassue, and Didier Defer. 2021. 'Impact of green walls occultation on energy balance: Development of a TRNSYS model on a brick masonry house', *Journal of Building Engineering*, 44: 102634.

Khan, Abdul Mateen, Muhammad Abubakar Tariq, Zeshan Alam, Wesam Salah Alaloul, and Ahsan Waqar. 2024. 'Optimizing Energy Efficiency Through Building Orientation and Building Information Modelling (BIM) in Diverse Terrains: A Case Study in Pakistan', *Energy*: 133307.

Kim, Moon Keun, Yang-Seon Kim, and Jelena Srebric. 2020. 'Predictions of electricity consumption in a campus building using occupant rates and weather elements with sensitivity analysis: Artificial neural network vs. linear regression', *Sustainable Cities and Society*, 62: 102385.

Kim, Seo-Hoon, Jong-Hun Kim, Hak-Geun Jeong, and Kyoo-Dong Song. 2018. "Reliability Field Test of the Air–Surface Temperature Ratio Method for In Situ Measurement of U-Values." In *Energies*.

Kim, Seo-Hoon, Jung-Hun Lee, Jong-Hun Kim, Seung-Hwan Yoo, and Hak-Geun Jeong. 2018. "The Feasibility of Improving the Accuracy of In Situ Measurements in the Air-Surface Temperature Ratio Method." In *Energies*.

Kontoleon, K. J., and C. Giarma. 2016. 'Dynamic thermal response of building material layers in aspect of their moisture content', *Applied Energy*, 170: 76-91.

Kotsiris, G., A. Androutsopoulos, E. Polychroni, and P. A. Nektarios. 2012. 'Dynamic U-value estimation and energy simulation for green roofs', *Energy and Buildings*, 45: 240-49.

Kristiansen, Tobias, Faisal Jamil, Ibrahim A. Hameed, and Mohamed Hamdy. 2022. 'Predicting annual illuminance and operative temperature in residential buildings using artificial neural networks', *Building and Environment*, 217: 109031.

Kukk, Villu, Laura Kaljula, Jaan Kers, and Targo Kalamees. 2022. 'Designing highly insulated cross-laminated timber external walls in terms of hygrothermal performance: Field measurements and simulations', *Building and Environment*, 212: 108805.

Latif, Eshrar, Mihaela Anca Ciupala, Simon Tucker, Devapriya Chitral Wijeyesekera, and Darryl John Newport. 2015. 'Hygrothermal performance of wood-hemp insulation in timber frame wall panels with and without a vapour barrier', *Building and Environment*, 92: 122-34.

Lee, Ye-Ji, Ji-Hoon Moon, Doo-Sung Choi, and Myeong-Jin Ko. 2024. "Application of the Heat Flow Meter Method and Extended Average Method to Improve the Accuracy of In Situ U-Value Estimations of Highly Insulated Building Walls." In *Sustainability*.

Lelievre, D., T. Colinart, and P. Glouannec. 2014. 'Hygrothermal behavior of bio-based building materials including hysteresis effects: Experimental and numerical analyses', *Energy and Buildings*, 84: 617-27.

Li, Francis GN, AZP Smith, Phillip Biddulph, Ian G Hamilton, Robert Lowe, Anna Mavrogianni, Eleni Oikonomou, Rokia Raslan, Samuel Stamp, Andrew %J Building Research Stone, and Information. 2015. 'Solid-wall U-values: heat flux measurements compared with standard assumptions', 43: 238-52.

Li, Mingcai, Jingfu Cao, Mingming Xiong, Ji Li, Xiaomei Feng, and Fanchao Meng. 2018. 'Different responses of cooling energy consumption in office buildings to climatic change in major climate zones of China', *Energy and Buildings*, 173: 38-44.

Li, Xiao-Xu, Kai-Liang Huang, Guo-Hui Feng, Wan-Yu Li, and Jia-Xing Wei. 2022. 'Night ventilation scheme optimization for an Ultra-low energy consumption building in Shenyang, China', *Energy Reports*, 8: 8426-36.

Li, Yi, Peng-Kun Yin, and Fu-Bin Chen. 2024. 'Prediction of wind load power spectrum on high-rise buildings by various machine learning algorithms', *Structures*, 67: 107015.

Liu, Ying, Haibo Guo, Cheng Sun, and Wen-Shao Chang. 2016. "Assessing Cross Laminated Timber (CLT) as an Alternative Material for Mid-Rise Residential Buildings in Cold Regions in China—A Life-Cycle Assessment Approach." In *Sustainability*.

Liu, Ying, Jiaqi Yu, Qing Yin, Cheng Sun, and Ang Sun. 2021. 'Impacts of human factors on evacuation performance in university gymnasiums', *Physica A: Statistical Mechanics and its Applications*, 582: 126236.

Liu, Yingxia, Gerard B. M. Heuvelink, Zhanguo Bai, Ping He, Xinpeng Xu, Wencheng Ding, and Shaohui Huang. 2021. 'Analysis of spatio-temporal variation of crop yield in China using stepwise multiple linear regression', *Field Crops Research*, 264: 108098.

Lucchi, Elena. 2017. 'Thermal transmittance of historical brick masonries: A comparison among standard data, analytical calculation procedures, and in situ heat flow meter measurements', *Energy and Buildings*, 134: 171-84.

Luo, Zhaoyang, Xuanning Qi, Cheng Sun, Qi Dong, Jian Gu, and Xinting Gao. 2024. 'Investigation of influential variations among variables in daylighting glare metrics using machine learning and SHAP', *Building and Environment*, 254: 111394.

Lyles, Robert H. 2006. 'Regression Methods in Biostatistics: Linear, Logistic, Survival, and Repeated Measures Models', *Journal of the American Statistical Association*, 101: 403-04.

M'Saouri El Bat, Adnane, Zaid Romani, Emmanuel Bozonnet, and Abdeslam Draoui. 2021. 'Thermal impact of street canyon microclimate on building energy needs using TRNSYS: A case study of the city of Tangier in Morocco', *Case Studies in Thermal Engineering*, 24: 100834.

Malhotra, Avichal, Julian Bischof, Alexandru Nichersu, Karl-Heinz Häfele, Johannes Exenberger, Divyanshu Sood, James Allan, Jérôme Frisch, Christoph van Treeck, James O'Donnell, and Gerald Schweiger. 2022. 'Information modelling for urban building energy simulation—A taxonomic review', *Building and Environment*, 208: 108552.

Marshall, A., R. Fitton, W. Swan, D. Farmer, D. Johnston, M. Benjaber, and Y. Ji. 2017. 'Domestic building fabric performance: Closing the gap between the in situ measured and modelled performance', *Energy and Buildings*, 150: 307-17.

Mazzeo, Domenico, Nicoletta Matera, Cristina Cornaro, Giuseppe Oliveti, Piercarlo Romagnoni, and Livio De Santoli. 2020. 'EnergyPlus, IDA ICE and TRNSYS predictive simulation accuracy for building thermal behaviour evaluation by using an experimental campaign in solar test boxes with and without a PCM module', *Energy and Buildings*, 212: 109812.

Mba, Leopold, Pierre Meukam, and Alexis Kemajou. 2016. 'Application of artificial neural network for predicting hourly indoor air temperature and relative humidity in modern building in humid region', *Energy and Buildings*, 121: 32-42.

Meng, Xi, Yanna Gao, Yan Wang, Biao Yan, Wei Zhang, and Enshen Long. 2015. 'Feasibility experiment on the simple hot box-heat flow meter method and the optimization based on simulation reproduction', *Applied Thermal Engineering*, 83: 48-56.

Meng, Xi, Tao Luo, Yanna Gao, Lili Zhang, Qiong Shen, and Enshen Long. 2017. 'A new simple method to measure wall thermal transmittance in situ and its adaptability analysis', *Applied Thermal Engineering*, 122: 747-57.

Miljan, M., and J. Miljan. 2015. 'Thermal Transmittance and the Embodied Energy of Timber Frame Lightweight Walls Insulated with Straw and Reed', *IOP Conference Series: Materials Science and Engineering*, 96: 012076.

Ministerio de Transportes, Movilidad y Agenda Urbana (MITMA). 2022. "Documento Básico HE – Ahorro de Energía " In. Madrid: Boletín Oficial del Estado.

Mobaraki, Behnam, Francisco Javier Castilla Pascual, Arturo Martínez García, Miguel Ángel Mellado Mascaraque, Borja Frutos Vázquez, and Carmen Alonso. 2023. 'Studying the impacts of test condition and nonoptimal positioning of the sensors on the accuracy of the in-situ U-value measurement', *Heliyon*, 9.

Mobaraki, Behnam, Francisco Javier Castilla Pascual, Fidel Lozano-Galant, Jose Antonio Lozano-Galant, and Rocio Porras Soriano. 2023. 'In situ U-value measurement of building envelopes through continuous low-cost monitoring', *Case Studies in Thermal Engineering*, 43: 102778.

Mounir, Soumia, Miloudia Slaoui, Youssef Maaloufa, Fatima Zohra El Wardi, Yakubu Aminu Dodo, Sara Ibn-Elhaj, and Abdelhamid Khabbazi. 2024. 'Study of Hygrothermal Behavior of Bio-Sourced Material Treated Ecologically for Improving Thermal Performance of Buildings', *Journal of Renewable Materials*, 12: 1007-27.

Nardi, Iole, and Elena Lucchi. 2023. "In Situ Thermal Transmittance Assessment of the Building Envelope: Practical Advice and Outlooks for Standard and Innovative Procedures." In *Energies*.

Nazaroff, William W 2021. 'Residential air-change rates: A critical review', *Indoor Air*, 31: 282-313.

NDRC. 2011. 'Twelfth Five-Year Plan Guidance on Wall Materials Innovation ', https://zfxxgk.ndrc.gov.cn/web/iteminfo.jsp?id=19709.

Ng, Lisa C., W. Stuart Dols, and Steven J. Emmerich. 2021. 'Evaluating potential benefits of air barriers in commercial buildings using NIST infiltration correlations in EnergyPlus', *Building and Environment*, 196: 107783.

Nicoletti, Francesco, Mario Antonio Cucumo, and Natale Arcuri. 2023. 'Evaluating the accuracy of in-situ methods for measuring wall thermal conductance: A comparative numerical study', *Energy and Buildings*, 290: 113095.

Nosrati, Roya Hamideh, and Umberto Berardi. 2018. 'Hygrothermal characteristics of aerogel-enhanced insulating materials under different humidity and temperature conditions', *Energy and Buildings*, 158: 698-711.

O'Hegarty, R., O. Kinnane, D. Lennon, and S. Colclough. 2021. 'In-situ U-value monitoring of highly insulated building envelopes: Review and experimental investigation', *Energy and Buildings*, 252: 111447.

Okoh, Emmanuel Tete %J Journal of Energy, and Natural Resources. 2014. 'Water absorption properties of some tropical timber species', 3: 20-24.

Olu-Ajayi, Razak, Hafiz Alaka, Ismail Sulaimon, Funlade Sunmola, and Saheed Ajayi. 2022. 'Machine learning for energy performance prediction at the design stage of buildings', *Energy for Sustainable Development*, 66: 12-25.

Pelsmakers, S., R. Fitton, P. Biddulph, W. Swan, B. Croxford, S. Stamp, F. C. F. Calboli, D. Shipworth, R. Lowe, and C. A. Elwell. 2017. 'Heat-flow variability of suspended timber ground floors: Implications for in-situ heat-flux measuring', *Energy and Buildings*, 138: 396-405.

Pescari, Simon, Valeriu A. Stoian, Mircea Merea, and Alexandru Pitroaca. 2022. "Comparison Study of the Heating Energy Demand for a Multi-Storey Residential Building in Romania Using Steady-State and Dynamic Methods." In *Buildings*.

Pino-Mejías, Rafael, Alexis Pérez-Fargallo, Carlos Rubio-Bellido, and Jesús A. Pulido-Arcas. 2017. 'Comparison of linear regression and artificial neural networks models to predict heating and cooling energy demand, energy consumption and CO2 emissions', *Energy*, 118: 24-36.

Qiang, Guo, Tian Zhe, Ding Yan, and Zhu Neng. 2015. 'An improved office building cooling load prediction model based on multivariable linear regression', *Energy and Buildings*, 107: 445-55.

Radhi, Hassan. 2009. 'A comparison of the accuracy of building energy analysis in Bahrain using data from different weather periods', *Renewable Energy*, 34: 869-75.

Rahiminejad, M., and D. Khovalyg. 2021. 'In-situ measurements of the U-value of a ventilated wall assembly', *Journal of Physics: Conference Series*, 2069: 012212.

Ramesh, T., Ravi Prakash, and K. K. Shukla. 2010. 'Life cycle energy analysis of buildings: An overview', *Energy and Buildings*, 42: 1592-600.

Rashad, Magdi, Alina Żabnieńska-Góra, Les Norman, and Hussam Jouhara. 2022. 'Analysis of energy demand in a residential building using TRNSYS', *Energy*, 254: 124357.

Rayegan, Saeed, Ali Katal, Liangzhu Wang, Radu Zmeureanu, Ursula Eicker, Mohammad Mortezazadeh, and Sepehrdad Tahmasebi. 2024. 'Modeling building energy self-sufficiency of using rooftop photovoltaics on an urban scale', *Energy and Buildings*, 324: 114863.

Ren, Zhihao, Jung In Kim, and Jonghoon Kim. 2023. 'Assessment methodology for dynamic occupancy adaptive HVAC control in subway stations integrating passenger flow simulation into building energy modeling', *Energy and Buildings*, 300: 113667.

Roque, Eduardo, Romeu Vicente, Ricardo M. S. F. Almeida, J. Mendes da Silva, and Ana Vaz Ferreira. 2020. 'Thermal characterisation of traditional wall solution of built heritage using the simple hot box-heat flow meter method: In situ measurements and numerical simulation', *Applied Thermal Engineering*, 169: 114935.

Roussac, A. Craig, Jesse Steinfeld, and Richard de Dear. 2011. 'A preliminary evaluation of two strategies for raising indoor air temperature setpoints in office buildings', *Architectural Science Review*, 54: 148-56.

Samardzioska, Todorka, and Roberta Apostolska. 2016. "Measurement of Heat-Flux of New Type Façade Walls." In *Sustainability*.

Sambataro, Luciano, Agustin Laveglia, Neven Ukrainczyk, and Eddie Koenders. 2023. 'A performance-based approach for coupling cradle-to-use LCA with operational energy simulation for Calcium Silicate and Clay Bricks in masonry buildings', *Energy and Buildings*, 295: 113287.

Sartori, I., and A. G. Hestnes. 2007. 'Energy use in the life cycle of conventional and low-energy buildings: A review article', *Energy and Buildings*, 39: 249-57.

Sendra-Arranz, R., and A. Gutiérrez. 2020. 'A long short-term memory artificial neural network to predict daily HVAC consumption in buildings', *Energy and Buildings*, 216: 109952.

Shan, Bo, Bozhang Chen, Jie Wen, Yan %J Architectural Engineering Xiao, and Design Management. 2022. 'Thermal performance of cross-laminated timber (CLT) and cross-laminated bamboo and timber (CLBT) panels': 1-20.

Shi, Dachuan, Yafeng Gao, Peng Zeng, Baizhan Li, Pengyuan Shen, and Chaoqun Zhuang. 2022. 'Climate adaptive optimization of green roofs and natural night ventilation for lifespan energy performance improvement in office buildings', *Building and Environment*, 223: 109505.

Shi, Xing, Guangcai Gong, Pei Peng, and Yongchao Liu. 2022. 'Investigation of a new kind of in-situ measurement method of thermal resistance of building envelope', *Energy and Buildings*, 258: 111803.

Shin, Bigyeong, Seong Jin Chang, Seunghwan Wi, and Sumin Kim. 2023. 'Estimation of energy demand and greenhouse gas emission reduction effect of cross-laminated timber (CLT) hybrid wall using life cycle assessment for urban residential planning', *Renewable and Sustainable Energy Reviews*, 185: 113604.

Silva, Arthur Santos, Enedir Ghisi, and Roberto Lamberts. 2016. 'Performance evaluation of long-term thermal comfort indices in building simulation according to ASHRAE Standard 55', *Building and Environment*, 102: 95-115.

Soares, Nelson, Cláudio Martins, Margarida Gonçalves, Paulo Santos, Luís Simões da Silva, and José J. Costa. 2019. 'Laboratory and in-situ non-destructive methods to evaluate the thermal transmittance and behavior of walls, windows, and construction elements with innovative materials: A review', *Energy and Buildings*, 182: 88-110.

Sofuoglu, Sait C. 2008. 'Application of artificial neural networks to predict prevalence of building-related symptoms in office buildings', *Building and Environment*, 43: 1121-26.

Solcast. 2016. 'Historical Weather Data '.

Su, Shu, Ao Sun, Guozhi Li, Yujie Ding, and Ming Xu. 2024. 'A dynamic simulation model for building cooling and heating energy considering climate-building system-occupant interactions', *Case Studies in Thermal Engineering*, 61: 105145.

Sui, Xuemin, Zhongjie Tian, Huitao Liu, Hao Chen, and Dong Wang. 2021. 'Field measurements on indoor air quality of a residential building in Xi'an under different ventilation modes in winter', *Journal of Building Engineering*, 42: 103040.

Sun, Chang, Xiaolei Ju, Wengang Hao, and Yongfei Lu. 2023. 'Research on multi-objective optimization of control strategies and equipment parameters for a combined heating system of geothermal and solar energy in cold and arid regions based on TRNSYS', *Case Studies in Thermal Engineering*, 50: 103441.

Sun, Zhi, Yan Gao, Jingjing Yang, Yixing Chen, and Brian H. W. Guo. 2024. 'Development of urban building energy models for Wellington city in New Zealand with detailed survey data on envelope thermal characteristics', *Energy and Buildings*, 321: 114647.

Tang, Liyun, Shiyuan Sun, Juanjuan Zheng, Peiyong Qiu, and Ting Guo. 2023. 'Thermal conductivity changing mechanism of frozen soil-rock mixture and a prediction model', *International Journal of Heat and Mass Transfer*, 216: 124529.

Tejedor, Blanca, Miquel Casals, Marta Gangolells, and Xavier Roca. 2017. 'Quantitative internal infrared thermography for determining in-situ thermal behaviour of façades', *Energy and Buildings*, 151: 187-97.

Teni, Mihaela, Hrvoje Krstić, and Piotr Kosiński. 2019. 'Review and comparison of current experimental approaches for in-situ measurements of building walls thermal transmittance', *Energy and Buildings*, 203: 109417.

Tlaiji, Ghadie, Pascal Biwole, Salah Ouldboukhitine, and Fabienne Pennec. 2023. 'Effective thermal conductivity model of straw bales based on microstructure and hygrothermal characterization', *Construction and Building Materials*, 387: 131601.

Uddin, Mohammad Nyme, Hung-Lin Chi, His-Hsien Wei, Minhyun Lee, and Meng Ni. 2022. 'Influence of interior layouts on occupant energy-saving behaviour in buildings: An integrated approach using Agent-Based Modelling, System Dynamics and Building Information Modelling', *Renewable and Sustainable Energy Reviews*, 161: 112382.

UNEP, and GlobalABC. 2024. "Global Status Report for Buildings and Construction." In.

Uribe, Daniel, Sergio Vera, and Marco Perino. 2024. 'Development and validation of a numerical heat transfer model for PCM glazing: Integration to EnergyPlus for office building energy performance applications', *Journal of Energy Storage*, 91: 112121.

Vagtholm, Rune, Amy Matteo, Behrang Vand, and Laura Tupenaite. 2023. "Evolution and Current State of Building Materials, Construction Methods, and Building Regulations in the U.K.: Implications for Sustainable Building Practices." In *Buildings*.

Vaughn, Michael 2020. 'ASHRAE Research Report: 2019-2020', *ASHRAE Journal*, 62: 73-89.

Vu, Quoc Hung, Jean-Michel Pereira, and Anh Minh Tang. 2023. 'Effect of clay content on the thermal conductivity of unfrozen and frozen sandy soils', *International Journal of Heat and Mass Transfer*, 206: 123923.

Walker, Rosanne, and Sara Pavía. 2015. 'Thermal performance of a selection of insulation materials suitable for historic buildings', *Building and Environment*, 94: 155-65.

Wang, Xing, Tao Li, Yingying Yu, Qingxia Liu, Lei Shi, Jingtao Xia, and Qianjun Mao. 2024. 'Performance simulation and energy efficiency analysis of multi-energy complementary

HVAC system based on TRNSYS', *Applied Thermal Engineering*, 257: 124378.

Wang, Yingying, Kang Liu, Yanfeng Liu, Dengjia Wang, and Jiaping Liu. 2022. 'The impact of temperature and relative humidity dependent thermal conductivity of insulation materials on heat transfer through the building envelope', *Journal of Building Engineering*, 46: 103700.

Wang, Yingying, Sudan Zhang, Dengjia Wang, and Yanfeng Liu. 2022. 'Experimental study on the influence of temperature and humidity on the thermal conductivity of building insulation materials', *Energy and Built Environment*.

Wu, Dongxia, Mourad Rahim, Mohammed El Ganaoui, Rachid Bennacer, Rabah Djedjig, and Bin Liu. 2022. 'Dynamic hygrothermal behavior and energy performance analysis of a novel multilayer building envelope based on PCM and hemp concrete', *Construction and Building Materials*, 341: 127739.

Xie, Xudong, Wenquan Zhang, Xuezhen Luan, Weijun Gao, Xiaoyu Geng, and Ying Xue. 2022. 'Thermal performance enhancement of hollow brick by agricultural wastes', *Case Studies in Construction Materials*, 16: e01047.

Xin, Zhenbo, Ruiyun Fu, Yuanyuan Zong, Dongfang Ke, Houjiang Zhang, Yongzhu Yu, and Wenbo Zhang. 2022. 'Effects of natural ageing on macroscopic physical and mechanical properties, chemical components and microscopic cell wall structure of ancient timber members', *Construction and Building Materials*, 359: 129476.

Xing, Luyi, Kaihua Xie, Yihua Zheng, Benzhi Hou, and Liuyijie Huang. 2023. 'A thermal balance method for measuring thermal conductivity by compensation of electric cooling or heating based on thermoelectric modules', *International Journal of Thermal Sciences*, 189: 108264.

Xu, Bin, Yuan-xia Cheng, Xing-ni Chen, Xing Xie, Jie Ji, and Dong-sheng Jiao. 2023. 'Error correction method for heat flux and a new algorithm employed in inverting wall thermal resistance using an artificial neural network: Based on IN-SITU heat flux measurements', *Energy*, 282: 128896.

Yan, Haiyan, Fangning Shi, Zhen Sun, Guodong Yuan, Minli Wang, and Mengru Dong. 2022. 'Thermal adaptation of different set point temperature modes and energy saving potential in split air-conditioned office buildings during summer', *Building and Environment*, 225: 109565.

Yang, Hao, Maoyu Ran, Haibo Feng, and Danlin Hou. 2025. 'K-PCD: A new clustering algorithm for building energy consumption time series analysis and predicting model accuracy improvement', *Applied Energy*, 377: 124584.

Yang, Senwen, Dongxue Zhan, Theodore Stathopoulos, Jiwei Zou, Chang Shu, and Liangzhu Leon Wang. 2024. 'Urban microclimate prediction based on weather station data and artificial neural network', *Energy and Buildings*, 314: 114283.

Yang, Suhang, Jingsong Sun, and Xu Zhifeng. 2024. 'Prediction on compressive strength of recycled aggregate self-compacting concrete by machine learning method', *Journal of Building Engineering*, 88: 109055.

Yin, Hang, Alireza Norouziasas, and Mohamed Hamdy. 2024. 'PCM as an energy flexibility asset: How design and operation can be optimized for heating in residential buildings?', *Energy and Buildings*, 322: 114721.

Yin, Li, and Lee Bruno. 2019. ''Simulation-based building performance comparison between CLT-concrete hybrid, CLT, and reinforced concrete structures in Canada." In *CSCE Annual Conference*. Laval, QC, Canada.

Yoon, Yeobeom, Piljae Im, Jon Winkler, and Jeffrey Munk. 2024. 'Impact of refrigerant undercharge faults on building indoor conditions and HVAC system operation in residential Buildings: A simulation study', *Energy and Buildings*, 321: 114667.

Yu, Jia, Yanming Kang, and Zhiqiang Zhai. 2020. 'Comparison of ground coupled heat transfer models for predicting underground building energy consumption', *Journal of Building Engineering*, 32: 101808.

Yu, Jiaqi, Wen-Shao Chang, and Yu Dong. 2022. "Building Energy Prediction Models and Related Uncertainties: A Review." In *Buildings*.

Yuan, Xiaolei, Leo Lindroos, Juha Jokisalo, Risto Kosonen, and Yiqun Pan. 2021. 'Study on waste heat recoveries and energy saving in combined energy system of ice and swimming halls in Finland', *Energy and Buildings*, 231: 110620.

Zhang, Liang, Jin Wen, Yanfei Li, Jianli Chen, Yunyang Ye, Yangyang Fu, and William Livingood. 2021. 'A review of machine learning in building load prediction', *Applied Energy*, 285: 116452.

Zhang, Xiaocun, Hailiang Chen, Jiayue Sun, and Xueqi Zhang. 2024. 'Predictive models of embodied carbon emissions in building design phases: Machine learning approaches based on residential buildings in China', *Building and Environment*, 258: 111595.

Zhao, Tianyi, Chengyu Zhang, Jingwen Xu, Yifan Wu, and Liangdong Ma. 2021. 'Data-driven correlation model between human behavior and energy consumption for college teaching buildings in cold regions of China', *Journal of Building Engineering*, 38: 102093.

Zhao, Yifei, Shiliang Liu, Hua Liu, Fangfang Wang, Yuhong Dong, Gang Wu, and Yetong Li. 2024. 'Multilevel driving mechanism of ecosystem multidimensional stability in the Yangtze River Economic Belt: A hierarchical linear model approach', *Journal of Cleaner Production*, 449: 141513.

Zhou, Yijun, Mingxue Ma, Vivian W. Y. Tam, and Khoa N. Le. 2023. 'Design variables affecting the environmental impacts of buildings: A critical review', *Journal of Cleaner Production*, 387: 135921.

Appendix (A) Hourly Measured Indoor Temperature and Relative Humidity of the Neighbouring Rooms of Four Tested Rooms

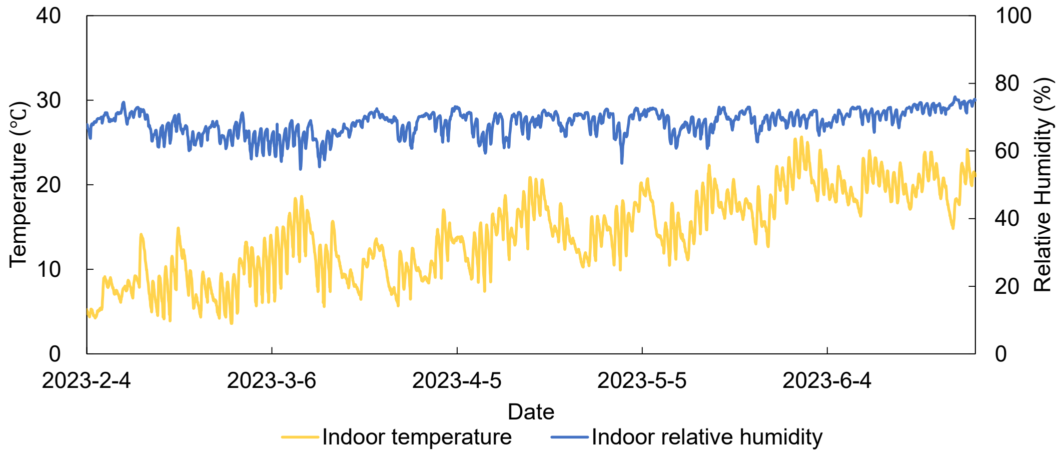

Figure A1 Indoor T/RH in the downstairs room of the CLT tested room

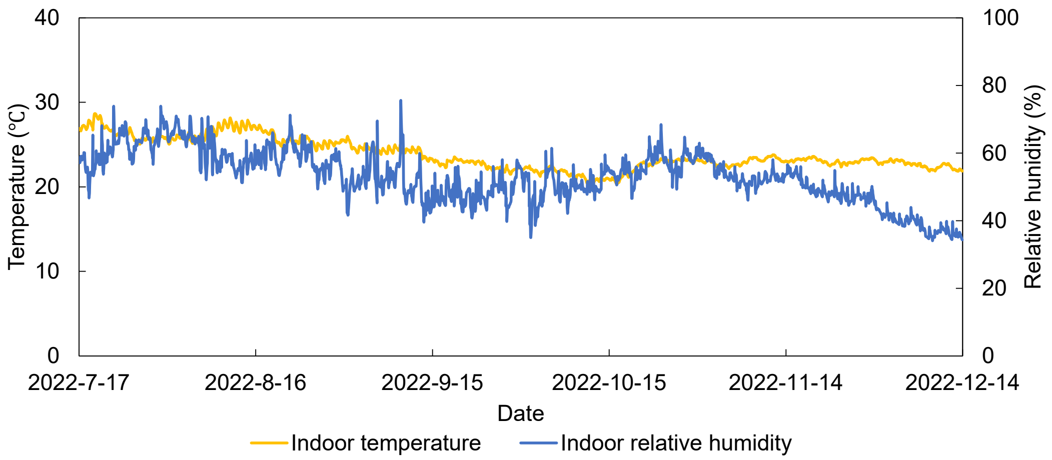

Figure A2 Indoor T/RH in the upstairs room of the masonry tested room

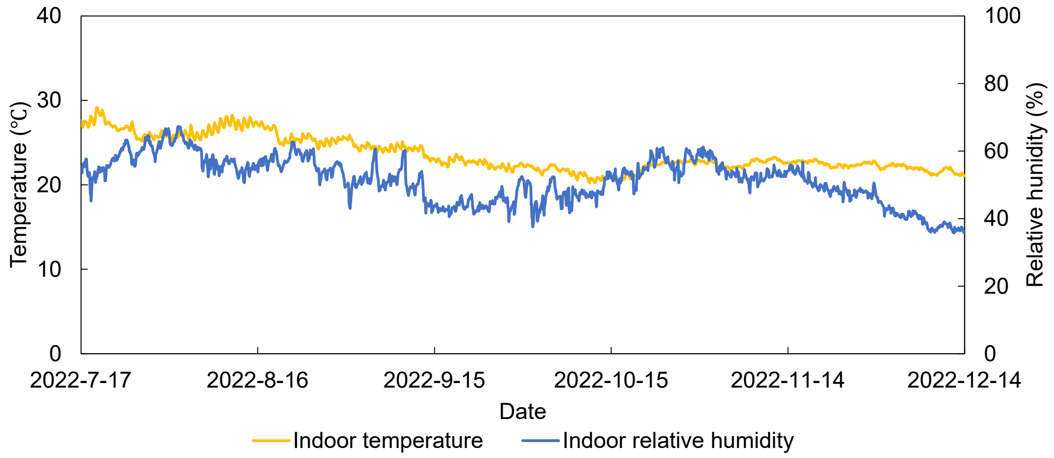

Figure A3 Indoor T/RH in the downstairs room of the masonry tested room

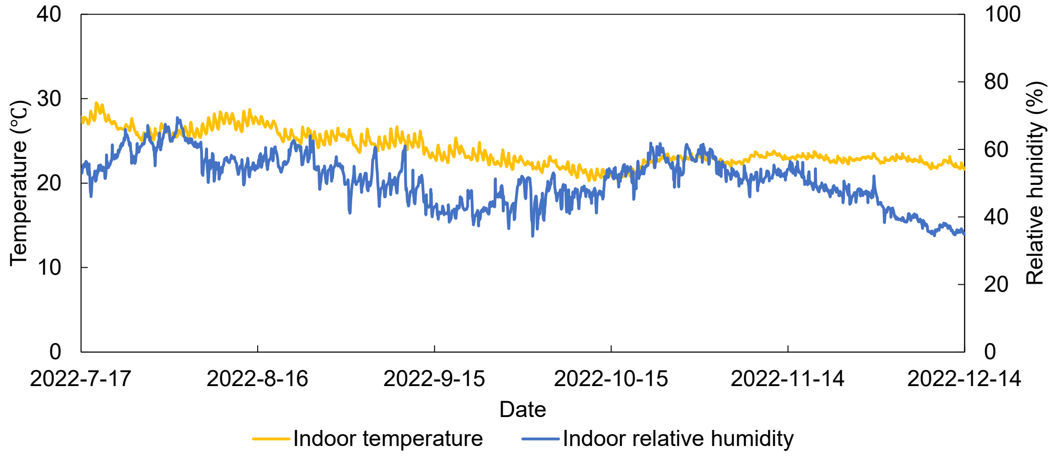

Figure A4 Indoor T/RH in the southern room of the masonry tested room

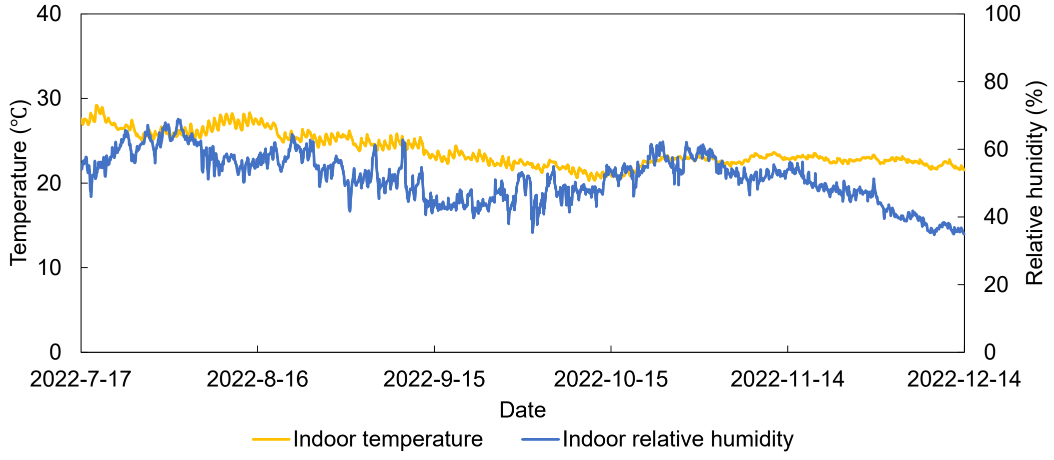

Figure A5 Indoor T/RH in the western room of the masonry tested room

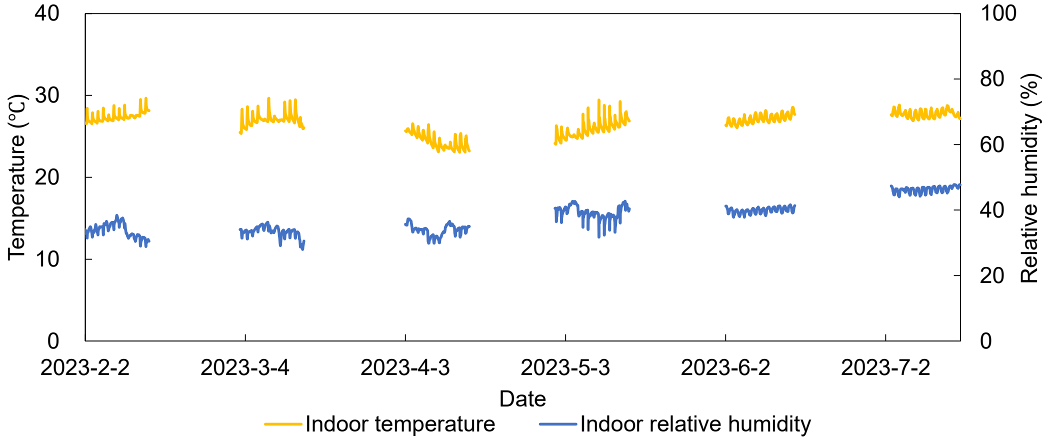

Figure A6 Indoor T/RH in the upstairs room of the RC tested room

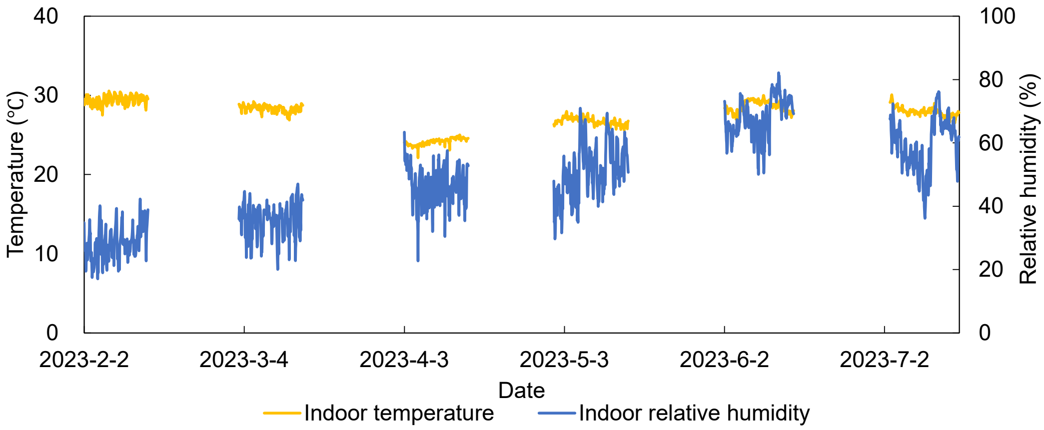

Figure A7 Indoor T/RH in the southern room of the RC tested room

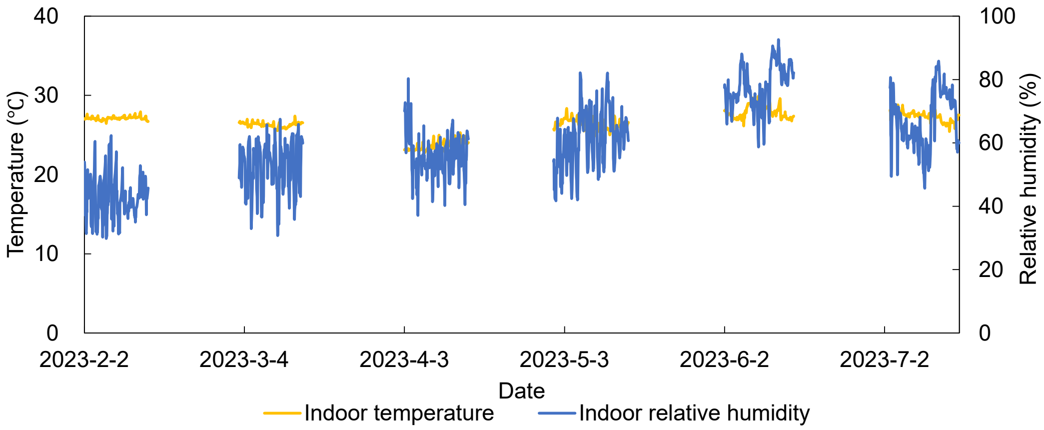

Figure A8 Indoor T/RH in the eastern room of the RC tested room

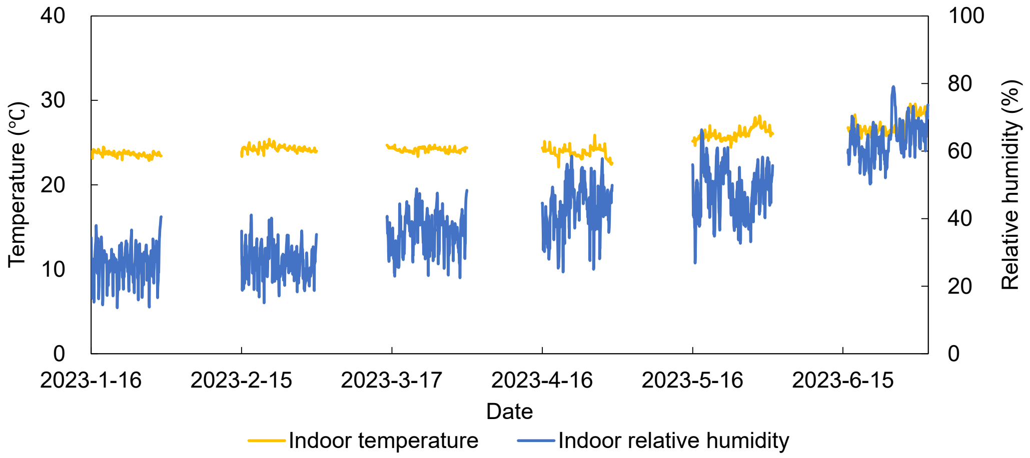

Figure A9 Indoor T/RH in the southern room of the brick tested room

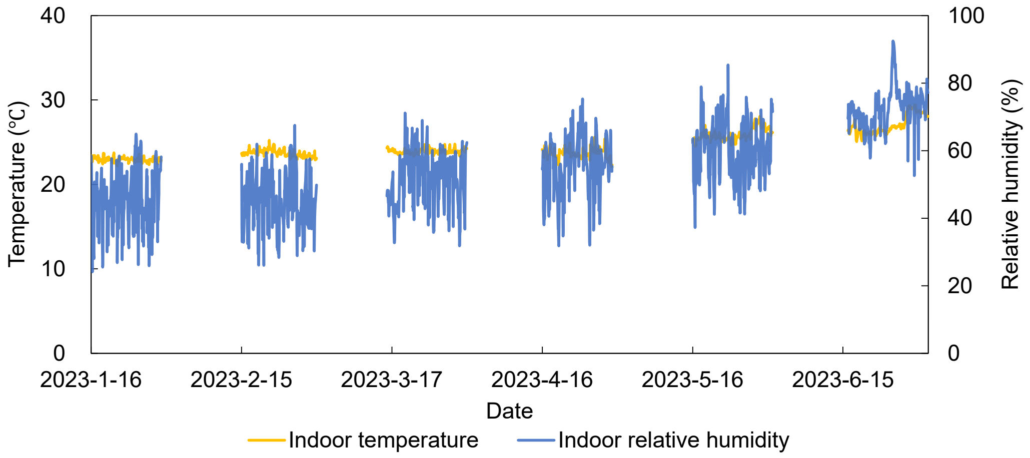

Figure A10 Indoor T/RH in the eastern room of the brick tested room

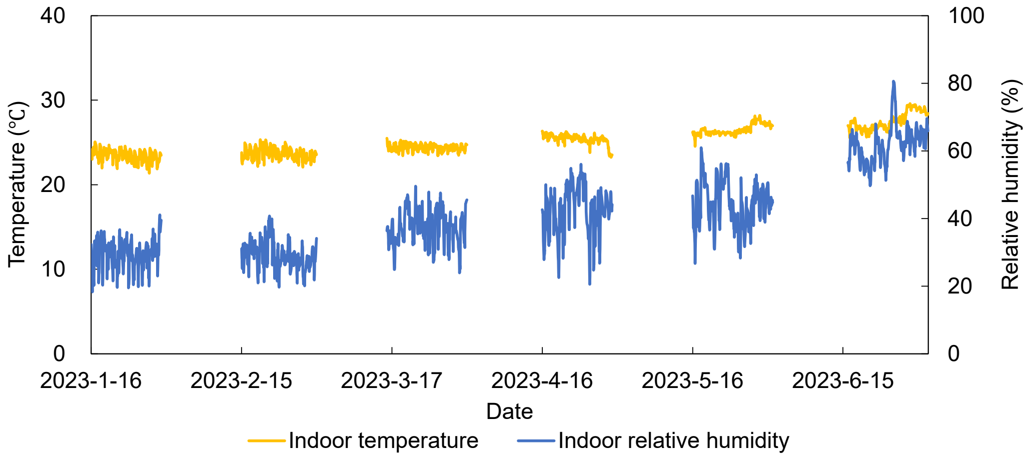

Figure A11 Indoor T/RH in the western room of the brick tested room

Appendix (B) Dynamic and Average U-values Calculated by Different Methods

Tables B1-B4 show all dynamic U-values of the four tested envelopes calculated by different data pre-processing methods with different time intervals. Table B5 shows all average U-values of the four tested envelopes calculated by different data pre-processing methods. Black numbers are positive and red numbers are negative in all tables in this appendix. **NA** indicates that all data were deleted in this time interval after data preprocessing.

Table B1(1) Dynamic U-values of the CLT tested envelope with 3-day time intervals

Start date of 3-day interval	Dynamic U-values calculated by data pre-processing methods [$W/(m^2 \cdot K)$]												
	ND	TD0	TD1	TD2	TD3	TD4	TD5	TD6	TD7	PV0	PV1	PV2	PV3
2023-2-4	0.24	0.10	0.41	NA	NA	NA	NA	NA	NA	0.80	0.42	NA	NA
2023-2-7	0.02	0.13	0.00	NA	NA	NA	NA	NA	NA	0.23	0.20	NA	NA
2023-2-10	0.23	0.41	0.41	0.77	NA	NA	NA	NA	NA	0.79	0.67	0.81	NA
2023-2-13	0.17	0.28	0.27	0.24	0.23	0.14	0.19	NA	NA	0.47	0.43	0.38	0.36
2023-2-16	0.25	0.45	0.41	0.37	0.38	0.34	0.34	NA	NA	0.69	0.61	0.55	0.53
2023-2-19	0.09	0.13	0.14	0.15	0.13	0.10	0.18	NA	NA	0.28	0.27	0.25	0.21
2023-2-22	0.09	0.12	0.14	0.25	0.43	NA	NA	NA	NA	0.52	0.43	0.40	0.43
2023-2-25	0.14	0.26	0.26	0.26	0.23	0.21	0.09	NA	NA	0.43	0.40	0.35	0.29
2023-2-28	0.23	0.42	0.32	0.30	0.25	0.24	0.27	0.26	NA	0.60	0.46	0.41	0.33
2023-3-3	0.24	0.40	0.38	0.34	0.30	0.22	0.22	0.17	NA	0.57	0.53	0.48	0.41
2023-3-6	0.22	0.37	0.33	0.28	0.22	0.20	0.14	0.14	NA	0.55	0.50	0.41	0.33
2023-3-9	0.20	0.38	0.34	0.31	0.26	0.24	0.23	0.22	0.28	0.61	0.54	0.48	0.42
2023-3-12	0.15	0.22	0.20	0.18	0.17	0.12	0.13	0.17	NA	0.39	0.36	0.32	0.26
2023-3-15	0.11	0.05	0.07	0.12	0.16	0.13	0.14	NA	NA	0.29	0.27	0.27	0.26
2023-3-18	0.03	0.01	0.03	0.14	NA	NA	NA	NA	NA	0.70	0.54	0.22	NA
2023-3-21	0.00	0.05	0.06	0.16	0.09	NA	NA	NA	NA	0.34	0.19	0.16	0.09
2023-3-24	0.04	0.06	0.10	0.14	0.18	0.40	NA	NA	NA	0.54	0.50	0.52	0.42
2023-3-27	0.13	0.14	0.15	0.19	0.09	0.06	NA	NA	NA	0.43	0.36	0.30	0.16
2023-3-30	0.06	0.12	0.22	0.49	0.45	0.35	NA	NA	NA	0.68	0.59	0.52	0.45
2023-4-2	0.11	0.14	0.18	0.19	0.18	0.12	0.15	0.09	NA	0.41	0.38	0.34	0.31
2023-4-5	0.03	0.01	0.06	0.15	0.22	0.32	0.20	NA	NA	0.27	0.25	0.23	0.27
2023-4-8	0.11	0.16	0.17	0.17	0.13	0.13	0.13	0.13	NA	0.35	0.34	0.33	0.26

Table B1(1) (continued)

Start date of 3-day interval	Dynamic U-values calculated by data pre-processing methods $[W/(m^2 \cdot K)]$												
	ND	TD0	TD1	TD2	TD3	TD4	TD5	TD6	TD7	PV0	PV1	PV2	PV3
2023-4-11	0.07	0.09	0.09	0.09	0.08	0.13	0.13	0.12	0.10	0.31	0.28	0.25	0.21
2023-4-14	0.08	0.11	0.13	0.14	0.14	0.16	0.14	0.13	NA	0.36	0.33	0.29	0.28
2023-4-17	0.01	0.03	0.01	0.01	0.04	0.05	0.05	0.06	NA	0.22	0.21	0.19	0.18
2023-4-20	0.05	0.01	0.03	0.09	0.16	0.14	0.10	NA	NA	0.22	0.22	0.22	0.21
2023-4-23	0.14	0.23	0.14	0.12	0.09	NA	NA	NA	NA	0.19	0.16	0.01	NA
2023-4-26	0.08	0.13	0.15	0.17	0.19	0.11	0.13	NA	NA	0.34	0.33	0.30	0.29
2023-4-29	0.06	0.05	0.07	0.11	0.12	0.13	0.14	0.15	0.13	0.27	0.27	0.27	0.24
2023-5-2	0.07	0.10	0.10	0.07	0.01	0.00	0.02	0.03	0.05	0.41	0.31	0.22	0.08
2023-5-5	0.04	0.13	0.09	0.07	0.02	0.00	NA	NA	NA	0.11	0.11	0.12	0.09
2023-5-8	0.07	0.04	0.06	0.10	0.09	0.07	0.08	0.07	0.06	0.24	0.23	0.22	0.19
2023-5-11	0.02	0.05	0.04	0.03	0.09	0.25	NA	NA	NA	0.30	0.28	0.24	0.22
2023-5-14	0.07	0.08	0.09	0.08	0.05	0.05	0.05	0.05	NA	0.29	0.27	0.24	0.18
2023-5-17	0.04	0.05	0.01	0.09	0.11	0.11	0.24	NA	NA	0.18	0.18	0.16	0.13
2023-5-20	0.03	0.10	0.05	0.03	0.06	0.00	NA	NA	NA	0.23	0.21	0.17	0.06
2023-5-23	0.02	0.08	0.04	0.00	0.05	0.03	0.09	0.09	NA	0.24	0.23	0.21	0.21
2023-5-26	0.06	0.03	0.08	0.11	0.16	0.26	NA	NA	NA	0.24	0.24	0.24	0.23
2023-5-29	0.01	0.16	0.11	0.02	0.02	0.05	0.08	0.06	NA	0.15	0.15	0.15	0.15
2023-6-1	0.02	0.07	0.05	0.02	0.01	0.00	0.05	0.03	NA	0.22	0.22	0.21	0.18
2023-6-4	0.01	0.04	0.05	0.07	0.01	0.01	NA	NA	NA	0.27	0.27	0.25	0.15
2023-6-7	0.03	0.10	0.02	0.09	0.24	0.21	0.17	NA	NA	0.27	0.27	0.25	0.24
2023-6-10	0.00	0.05	0.00	0.03	0.03	0.07	0.07	NA	NA	0.22	0.22	0.21	0.17
2023-6-13	0.02	0.04	0.07	0.09	0.08	0.15	0.29	NA	NA	0.30	0.30	0.28	0.24
2023-6-16	0.06	0.13	0.05	0.02	0.03	0.01	NA	NA	NA	0.20	0.17	0.12	0.10
2023-6-19	0.01	0.04	0.07	0.08	0.10	0.15	NA	NA	NA	0.22	0.22	0.21	0.19
2023-6-22	0.06	0.09	0.08	0.06	0.07	0.04	0.08	NA	NA	0.20	0.13	0.11	0.07
2023-6-25	0.03	0.13	0.15	0.13	0.16	0.29	0.44	NA	NA	0.30	0.28	0.25	0.25

Table B1(1) (continued)

Start date of 3-day interval	Dynamic U-values calculated by data pre-processing methods $[W/(m^2 \cdot K)]$												
	PV4	PV5	PV6	PV7	AV0	AV1	AV2	AV3	AV4	AV5	AV6	AV7	TL
2023-2-4	NA	NA	NA	NA	0.60	0.49	0.47	0.42	0.40	0.42	0.36	0.14	0.44
2023-2-7	NA	NA	NA	NA	0.43	0.24	0.41	NA	NA	NA	NA	NA	0.38
2023-2-10	NA	NA	NA	NA	0.64	0.55	0.55	0.45	0.41	0.38	0.38	0.40	0.40
2023-2-13	0.18	0.19	NA	NA	0.39	0.34	0.28	0.26	0.19	0.26	0.21	0.14	0.35
2023-2-16	0.41	0.34	NA	NA	0.54	0.48	0.42	0.38	0.31	0.27	0.21	0.19	0.37
2023-2-19	0.17	0.18	NA	NA	0.35	0.29	0.23	0.18	0.13	0.18	NA	NA	0.32
2023-2-22	NA	NA	NA	NA	0.45	0.34	0.36	0.40	0.35	0.31	0.25	0.06	0.29
2023-2-25	0.24	0.09	NA	NA	0.50	0.42	0.37	0.33	0.30	0.32	0.40	0.39	0.38
2023-2-28	0.27	0.29	0.26	NA	0.59	0.47	0.41	0.33	0.30	0.31	0.27	0.23	0.42
2023-3-3	0.32	0.31	0.20	NA	0.56	0.51	0.46	0.39	0.31	0.26	0.20	0.21	0.44
2023-3-6	0.29	0.21	0.15	NA	0.51	0.46	0.39	0.35	0.30	0.26	0.22	0.20	0.39
2023-3-9	0.35	0.32	0.25	0.28	0.57	0.50	0.44	0.37	0.31	0.26	0.22	0.20	0.44
2023-3-12	0.19	0.19	0.21	NA	0.39	0.36	0.32	0.25	0.21	0.20	0.22	0.20	0.34
2023-3-15	0.19	0.14	NA	NA	0.33	0.29	0.27	0.27	0.24	0.27	0.30	0.22	0.30
2023-3-18	NA	NA	NA	NA	0.52	0.42	0.38	0.40	0.35	0.49	NA	NA	0.43
2023-3-21	NA	NA	NA	NA	0.53	0.35	0.36	0.41	NA	NA	NA	NA	0.35
2023-3-24	0.40	NA	NA	NA	0.39	0.32	0.32	0.31	0.34	0.23	0.18	0.16	0.38
2023-3-27	0.08	NA	NA	NA	0.52	0.42	0.37	0.31	0.20	0.27	0.25	0.21	0.36
2023-3-30	0.35	NA	NA	NA	0.68	0.57	0.59	0.45	0.35	0.32	0.31	0.32	0.51
2023-4-2	0.21	0.21	0.10	NA	0.46	0.37	0.32	0.29	0.23	0.21	0.18	0.23	0.36
2023-4-5	0.32	0.20	NA	NA	0.34	0.29	0.27	0.30	0.31	0.26	0.36	NA	0.37
2023-4-8	0.24	0.21	0.17	NA	0.36	0.33	0.29	0.24	0.21	0.19	0.18	0.22	0.30
2023-4-11	0.20	0.18	0.15	0.12	0.39	0.32	0.29	0.27	0.24	0.20	0.16	0.14	0.29
2023-4-14	0.25	0.20	0.13	NA	0.37	0.32	0.28	0.25	0.22	0.18	0.19	0.25	0.37
2023-4-17	0.15	0.09	0.06	NA	0.36	0.32	0.27	0.25	0.17	0.08	0.06	NA	0.35
2023-4-20	0.17	0.11	NA	NA	0.41	0.35	0.31	0.23	0.16	0.10	NA	NA	0.45
2023-4-23	NA	NA	NA	NA	0.36	0.23	0.13	0.09	NA	NA	NA	NA	0.38
2023-4-26	0.19	0.14	NA	NA	0.45	0.39	0.35	0.32	0.24	0.20	0.47	NA	0.50
2023-4-29	0.22	0.21	0.18	0.13	0.34	0.30	0.27	0.24	0.23	0.22	0.22	0.27	0.36
2023-5-2	0.08	0.08	0.08	0.08	0.52	0.43	0.38	0.32	0.20	0.15	0.12	0.11	0.40
2023-5-5	0.03	NA	NA	NA	0.24	0.18	0.14	0.09	0.03	NA	NA	NA	0.24
2023-5-8	0.15	0.15	0.10	0.06	0.42	0.37	0.33	0.29	0.24	0.26	0.18	0.20	0.46
2023-5-11	0.25	NA	NA	NA	0.43	0.40	0.34	0.38	0.48	0.57	NA	NA	0.43
2023-5-14	0.16	0.15	0.12	NA	0.42	0.38	0.33	0.29	0.23	0.24	0.26	0.45	0.40
2023-5-17	0.13	0.24	NA	NA	0.44	0.34	0.26	0.12	0.12	0.24	NA	NA	0.55
2023-5-20	0.07	NA	NA	NA	0.31	0.23	0.14	0.09	0.06	NA	NA	NA	0.33
2023-5-23	0.14	0.13	0.09	NA	0.46	0.41	0.36	0.37	0.35	0.33	0.16	NA	0.47
2023-5-26	0.30	NA	NA	NA	0.50	0.40	0.34	0.32	0.49	0.62	NA	NA	0.63

Table B1(1) (continued)

Start date of 3-day interval	Dynamic U-values calculated by data pre-processing methods $[W/(m^2 \cdot K)]$												
	PV4	PV5	PV6	PV7	AV0	AV1	AV2	AV3	AV4	AV5	AV6	AV7	TL
2023-5-29	0.15	0.13	0.07	NA	0.49	0.40	0.27	0.22	0.18	0.12	0.06	NA	0.73
2023-6-1	0.14	0.13	0.06	NA	0.40	0.35	0.29	0.26	0.19	0.10	0.05	NA	0.45
2023-6-4	0.02	NA	NA	NA	0.45	0.30	0.24	0.17	0.23	NA	NA	NA	0.56
2023-6-7	0.21	0.17	NA	NA	0.47	0.38	0.35	0.44	0.42	0.36	0.55	NA	0.59
2023-6-10	0.13	0.09	NA	NA	0.49	0.39	0.29	0.15	0.11	0.08	NA	NA	0.58
2023-6-13	0.20	0.29	NA	NA	0.47	0.40	0.32	0.26	0.17	0.29	NA	NA	0.50
2023-6-16	0.05	NA	NA	NA	0.48	0.34	0.23	0.09	0.06	NA	NA	NA	0.46
2023-6-19	0.16	NA	NA	NA	0.40	0.32	0.26	0.21	0.19	NA	NA	NA	0.51
2023-6-22	0.08	0.08	NA	NA	0.34	0.26	0.22	0.20	0.16	0.08	NA	NA	0.34
2023-6-25	0.30	0.44	NA	NA	0.50	0.42	0.37	0.41	0.36	0.44	NA	NA	0.54

Table B1(2) Dynamic U-values of the CLT tested envelope with 5-day time intervals

Start date of 5-day interval	Dynamic U-values calculated by data pre-processing methods $[W/(m^2 \cdot K)]$												
	ND	TD0	TD1	TD2	TD3	TD4	TD5	TD6	TD7	PV0	PV1	PV2	PV3
2023-2-4	0.03	0.02	0.07	NA	NA	NA	NA	NA	NA	0.41	0.26	NA	NA
2023-2-9	0.13	0.14	0.14	0.12	0.04	0.04	0.05	NA	NA	0.32	0.25	0.18	0.08
2023-2-14	0.24	0.47	0.44	0.40	0.43	0.37	0.33	NA	NA	0.74	0.67	0.60	0.60
2023-2-19	0.11	0.17	0.17	0.19	0.16	0.10	0.18	NA	NA	0.36	0.33	0.29	0.23
2023-2-24	0.13	0.21	0.18	0.19	0.18	0.19	0.09	NA	NA	0.48	0.38	0.32	0.27
2023-3-1	0.24	0.41	0.38	0.36	0.31	0.24	0.23	0.18	NA	0.56	0.51	0.47	0.40
2023-3-6	0.21	0.38	0.33	0.29	0.25	0.24	0.21	0.21	0.28	0.57	0.51	0.44	0.38
2023-3-11	0.17	0.26	0.25	0.22	0.18	0.11	0.11	0.13	NA	0.46	0.42	0.37	0.29
2023-3-16	0.00	0.07	0.03	0.02	0.03	0.06	0.11	NA	NA	0.29	0.23	0.13	0.09
2023-3-21	0.03	0.05	0.03	0.02	0.01	NA	NA	NA	NA	0.27	0.16	0.12	0.07
2023-3-26	0.11	0.16	0.21	0.28	0.21	0.16	NA	NA	NA	0.53	0.46	0.39	0.29
2023-3-31	0.13	0.19	0.22	0.24	0.22	0.15	0.15	0.09	NA	0.47	0.42	0.37	0.34
2023-4-5	0.09	0.09	0.12	0.17	0.18	0.20	0.18	0.13	NA	0.30	0.29	0.28	0.28
2023-4-10	0.06	0.11	0.11	0.11	0.04	0.08	0.09	0.12	0.10	0.36	0.33	0.28	0.18
2023-4-15	0.05	0.03	0.05	0.06	0.08	0.11	0.12	0.08	NA	0.27	0.26	0.24	0.22
2023-4-20	0.01	0.09	0.04	0.03	0.14	0.14	0.10	NA	NA	0.21	0.20	0.21	0.21
2023-4-25	0.03	0.04	0.07	0.13	0.16	0.09	0.13	NA	NA	0.29	0.27	0.26	0.25
2023-4-30	0.08	0.11	0.12	0.12	0.09	0.10	0.09	0.10	0.07	0.36	0.32	0.28	0.22
2023-5-5	0.02	0.07	0.03	0.01	0.05	0.08	0.21	0.16	0.09	0.18	0.18	0.19	0.17
2023-5-10	0.03	0.01	0.01	0.05	0.07	0.08	0.01	0.01	0.05	0.28	0.26	0.23	0.19
2023-5-15	0.05	0.01	0.05	0.08	0.06	0.05	0.07	0.05	NA	0.23	0.23	0.20	0.15
2023-5-20	0.03	0.12	0.07	0.03	0.02	0.02	0.09	0.09	NA	0.20	0.19	0.17	0.14
2023-5-25	0.04	0.02	0.06	0.09	0.14	0.20	0.13	0.07	NA	0.24	0.24	0.23	0.22
2023-5-30	0.02	0.13	0.09	0.03	0.01	0.01	0.06	0.03	NA	0.19	0.19	0.18	0.17
2023-6-4	0.02	0.09	0.00	0.05	0.01	0.01	NA	NA	NA	0.28	0.27	0.25	0.15
2023-6-9	0.00	0.03	0.02	0.06	0.06	0.10	0.14	NA	NA	0.23	0.23	0.22	0.19
2023-6-14	0.01	0.03	0.03	0.05	0.07	0.09	NA	NA	NA	0.27	0.26	0.23	0.20
2023-6-19	0.00	0.01	0.01	0.02	0.05	0.12	0.08	NA	NA	0.20	0.19	0.18	0.16
2023-6-24	0.00	0.10	0.12	0.13	0.16	0.29	0.44	NA	NA	0.32	0.28	0.25	0.25

Table B1(2) (continued)

Start date of 5-day interval	Dynamic U-values calculated by data pre-processing methods $[W/(m^2 \cdot K)]$												
	PV4	PV5	PV6	PV7	AV0	AV1	AV2	AV3	AV4	AV5	AV6	AV7	TL
2023-2-4	NA	NA	NA	NA	0.52	0.34	0.47	0.42	0.40	0.42	0.36	0.14	0.42
2023-2-9	0.06	0.05	NA	NA	0.40	0.33	0.27	0.19	0.18	0.36	0.38	0.40	0.32
2023-2-14	0.43	0.33	NA	NA	0.56	0.49	0.43	0.41	0.33	0.27	0.21	0.18	0.40
2023-2-19	0.17	0.18	NA	NA	0.41	0.34	0.28	0.23	0.19	0.24	0.25	0.06	0.33
2023-2-24	0.22	0.09	NA	NA	0.50	0.40	0.35	0.31	0.29	0.33	0.35	0.32	0.36
2023-3-1	0.31	0.30	0.21	NA	0.56	0.50	0.45	0.38	0.31	0.27	0.20	0.20	0.44
2023-3-6	0.34	0.29	0.23	0.28	0.53	0.48	0.41	0.37	0.32	0.28	0.24	0.20	0.41
2023-3-11	0.19	0.17	0.17	NA	0.44	0.40	0.35	0.28	0.22	0.21	0.21	0.21	0.37
2023-3-16	0.09	0.11	NA	NA	0.37	0.29	0.22	0.22	0.19	0.21	NA	NA	0.32
2023-3-21	NA	NA	NA	NA	0.34	0.22	0.18	0.17	NA	NA	NA	NA	0.29
2023-3-26	0.20	NA	NA	NA	0.57	0.47	0.42	0.37	0.26	0.25	0.22	0.18	0.42
2023-3-31	0.23	0.21	0.10	NA	0.52	0.43	0.39	0.33	0.25	0.23	0.21	0.26	0.40
2023-4-5	0.27	0.23	0.17	NA	0.35	0.31	0.28	0.27	0.24	0.21	0.18	0.21	0.34
2023-4-10	0.17	0.16	0.15	0.12	0.40	0.34	0.31	0.27	0.22	0.18	0.18	0.17	0.31
2023-4-15	0.20	0.18	0.08	NA	0.34	0.30	0.26	0.24	0.19	0.16	0.16	0.25	0.35
2023-4-20	0.17	0.11	NA	NA	0.38	0.30	0.26	0.22	0.16	0.10	NA	NA	0.41
2023-4-25	0.16	0.14	NA	NA	0.41	0.34	0.31	0.29	0.21	0.20	0.47	NA	0.42
2023-4-30	0.19	0.17	0.15	0.09	0.44	0.38	0.33	0.28	0.23	0.20	0.19	0.20	0.42
2023-5-5	0.14	0.21	0.16	0.09	0.34	0.29	0.26	0.23	0.21	0.32	0.25	0.35	0.35
2023-5-10	0.18	0.05	0.04	0.06	0.41	0.37	0.32	0.31	0.32	0.36	0.24	0.27	0.41
2023-5-15	0.14	0.17	0.12	NA	0.43	0.37	0.31	0.24	0.19	0.20	0.21	0.41	0.47
2023-5-20	0.13	0.13	0.09	NA	0.37	0.30	0.23	0.20	0.23	0.20	0.09	NA	0.39
2023-5-25	0.21	0.13	0.07	NA	0.50	0.42	0.36	0.35	0.45	0.39	0.16	NA	0.62
2023-5-30	0.14	0.13	0.06	NA	0.44	0.37	0.27	0.23	0.15	0.10	0.05	NA	0.55
2023-6-4	0.02	NA	NA	NA	0.42	0.28	0.22	0.17	0.23	NA	NA	NA	0.49
2023-6-9	0.16	0.16	NA	NA	0.48	0.40	0.31	0.21	0.21	0.24	0.55	NA	0.59
2023-6-14	0.16	NA	NA	NA	0.50	0.39	0.32	0.25	0.14	NA	NA	NA	0.51
2023-6-19	0.14	0.08	NA	NA	0.34	0.27	0.22	0.18	0.16	0.08	NA	NA	0.42
2023-6-24	0.30	0.44	NA	NA	0.52	0.44	0.40	0.43	0.39	0.44	NA	NA	0.51

Table B1(3) Dynamic U-values of the CLT tested envelope with 7-day time intervals

Start date of 7-day interval	Dynamic U-values calculated by data pre-processing methods $[W/(m^2 \cdot K)]$												
	ND	TD0	TD1	TD2	TD3	TD4	TD5	TD6	TD7	PV0	PV1	PV2	PV3
2023-2-4	0.04	0.00	0.12	NA	NA	NA	NA	NA	NA	0.41	0.29	NA	NA
2023-2-11	0.21	0.35	0.33	0.30	0.27	0.22	0.32	NA	NA	0.60	0.53	0.46	0.42
2023-2-18	0.12	0.17	0.18	0.21	0.21	0.12	0.18	NA	NA	0.39	0.36	0.33	0.29
2023-2-25	0.19	0.36	0.31	0.29	0.24	0.19	0.15	0.11	NA	0.55	0.47	0.41	0.33
2023-3-4	0.23	0.38	0.34	0.31	0.27	0.26	0.24	0.22	0.28	0.55	0.50	0.44	0.39
2023-3-11	0.14	0.18	0.18	0.18	0.17	0.11	0.11	0.13	NA	0.40	0.36	0.33	0.27
2023-3-18	0.02	0.02	0.00	0.01	0.01	NA	NA	NA	NA	0.43	0.29	0.15	0.07
2023-3-25	0.08	0.12	0.18	0.28	0.21	0.16	NA	NA	NA	0.51	0.44	0.39	0.29
2023-4-1	0.10	0.12	0.16	0.20	0.22	0.17	0.16	0.09	NA	0.39	0.36	0.32	0.32
2023-4-8	0.09	0.12	0.13	0.14	0.11	0.13	0.13	0.12	0.10	0.34	0.32	0.29	0.24
2023-4-15	0.05	0.03	0.05	0.08	0.11	0.13	0.13	0.08	NA	0.28	0.27	0.25	0.24
2023-4-22	0.02	0.02	0.02	0.08	0.14	0.09	0.08	NA	NA	0.27	0.25	0.24	0.23
2023-4-29	0.07	0.06	0.08	0.10	0.09	0.09	0.09	0.10	0.07	0.30	0.27	0.24	0.20
2023-5-6	0.00	0.06	0.04	0.00	0.03	0.06	0.08	0.07	0.06	0.21	0.20	0.19	0.16
2023-5-13	0.06	0.03	0.06	0.09	0.08	0.08	0.07	0.05	NA	0.25	0.24	0.22	0.18
2023-5-20	0.01	0.08	0.03	0.01	0.03	0.02	0.09	0.09	NA	0.24	0.24	0.22	0.19
2023-5-27	0.00	0.11	0.06	0.00	0.05	0.06	0.10	0.07	NA	0.19	0.19	0.19	0.18
2023-6-3	0.00	0.05	0.03	0.07	0.05	0.05	0.04	0.01	NA	0.26	0.26	0.24	0.18
2023-6-10	0.00	0.03	0.02	0.05	0.05	0.08	0.13	NA	NA	0.24	0.23	0.22	0.18
2023-6-17	0.02	0.03	0.00	0.02	0.05	0.12	0.08	NA	NA	0.22	0.21	0.18	0.16
2023-6-24	0.00	0.10	0.12	0.13	0.16	0.29	0.44	NA	NA	0.32	0.28	0.25	0.25

Table B1(3) (continued)

Start date of 7-day interval	Dynamic U-values calculated by data pre-processing methods $[W/(m^2 \cdot K)]$												
	PV4	PV5	PV6	PV7	AV0	AV1	AV2	AV3	AV4	AV5	AV6	AV7	TL
2023-2-4	NA	NA	NA	NA	0.52	0.37	0.48	0.42	0.40	0.42	0.36	0.14	0.39
2023-2-11	0.28	0.32	NA	NA	0.50	0.43	0.37	0.33	0.27	0.29	0.25	0.23	0.38
2023-2-18	0.19	0.18	NA	NA	0.42	0.35	0.32	0.29	0.24	0.26	0.24	0.20	0.32
2023-2-25	0.23	0.19	0.14	NA	0.56	0.46	0.41	0.34	0.28	0.27	0.25	0.28	0.41
2023-3-4	0.35	0.32	0.23	0.28	0.53	0.48	0.42	0.37	0.33	0.29	0.24	0.20	0.42
2023-3-11	0.18	0.16	0.17	NA	0.40	0.36	0.32	0.27	0.21	0.21	0.21	0.21	0.34
2023-3-18	NA	NA	NA	NA	0.42	0.31	0.25	0.25	0.35	0.49	NA	NA	0.34
2023-3-25	0.20	NA	NA	NA	0.56	0.45	0.43	0.37	0.26	0.25	0.22	0.18	0.44
2023-4-1	0.25	0.21	0.10	NA	0.45	0.38	0.34	0.32	0.26	0.23	0.22	0.26	0.38
2023-4-8	0.22	0.20	0.16	0.12	0.39	0.34	0.30	0.26	0.22	0.19	0.17	0.18	0.31
2023-4-15	0.21	0.18	0.08	NA	0.36	0.31	0.27	0.25	0.20	0.16	0.16	0.25	0.37
2023-4-22	0.14	0.10	NA	NA	0.41	0.34	0.30	0.26	0.18	0.13	0.47	NA	0.45
2023-4-29	0.18	0.17	0.15	0.09	0.41	0.35	0.30	0.26	0.22	0.20	0.19	0.20	0.39
2023-5-6	0.13	0.15	0.10	0.06	0.35	0.31	0.27	0.25	0.25	0.28	0.18	0.20	0.35
2023-5-13	0.16	0.17	0.12	NA	0.43	0.38	0.33	0.28	0.24	0.28	0.26	0.45	0.46
2023-5-20	0.13	0.13	0.09	NA	0.42	0.36	0.32	0.31	0.37	0.37	0.16	NA	0.45
2023-5-27	0.18	0.14	0.08	NA	0.46	0.37	0.28	0.25	0.23	0.13	0.07	NA	0.62
2023-6-3	0.12	0.12	0.03	NA	0.45	0.34	0.29	0.25	0.25	0.21	0.10	NA	0.53
2023-6-10	0.15	0.15	NA	NA	0.45	0.36	0.28	0.19	0.12	0.13	NA	NA	0.51
2023-6-17	0.14	0.08	NA	NA	0.41	0.32	0.24	0.18	0.16	0.08	NA	NA	0.45
2023-6-24	0.30	0.44	NA	NA	0.52	0.44	0.40	0.43	0.39	0.44	NA	NA	0.51

Table B1(4) Dynamic U-values of the CLT tested envelope with 10-day time intervals

Start date of 10-day interval	Dynamic U-values calculated by data pre-processing methods $[W/(m^2 \cdot K)]$											
	ND	TD0	TD1	TD2	TD3	TD4	TD5	TD6	TD7	PV0	PV1	PV2	PV3
2023-2-4	0.08	0.09	0.13	0.12	0.04	0.04	0.05	NA	NA	0.34	0.25	0.18	0.08
2023-2-14	0.18	0.32	0.31	0.30	0.31	0.24	0.27	NA	NA	0.56	0.50	0.46	0.44
2023-2-24	0.20	0.33	0.30	0.30	0.27	0.23	0.22	0.18	NA	0.53	0.47	0.42	0.36
2023-3-6	0.19	0.32	0.29	0.26	0.22	0.19	0.17	0.18	0.28	0.52	0.47	0.41	0.34
2023-3-16	0.02	0.06	0.03	0.00	0.01	0.06	0.11	NA	NA	0.28	0.20	0.13	0.08
2023-3-26	0.12	0.17	0.21	0.26	0.22	0.15	0.15	0.09	NA	0.50	0.44	0.38	0.32
2023-4-5	0.08	0.10	0.11	0.14	0.12	0.15	0.13	0.12	0.10	0.33	0.31	0.28	0.24
2023-4-15	0.03	0.02	0.01	0.05	0.10	0.11	0.11	0.08	NA	0.25	0.24	0.23	0.22
2023-4-25	0.06	0.08	0.10	0.12	0.12	0.10	0.10	0.10	0.07	0.33	0.30	0.27	0.23
2023-5-5	0.02	0.03	0.01	0.03	0.06	0.08	0.08	0.07	0.06	0.23	0.22	0.21	0.18
2023-5-15	0.02	0.05	0.01	0.03	0.02	0.04	0.07	0.06	NA	0.22	0.21	0.19	0.14
2023-5-25	0.01	0.07	0.03	0.02	0.06	0.05	0.07	0.04	NA	0.22	0.22	0.21	0.19
2023-6-4	0.01	0.06	0.01	0.06	0.05	0.10	0.14	NA	NA	0.25	0.24	0.23	0.18
2023-6-14	0.00	0.02	0.02	0.03	0.06	0.11	0.08	NA	NA	0.23	0.22	0.20	0.18
2023-6-24	0.00	0.10	0.12	0.13	0.16	0.29	0.44	NA	NA	0.32	0.28	0.25	0.25

Table B1(4) (continued)

Start date of 10-day interval	Dynamic U-values calculated by data pre-processing methods $[W/(m^2 \cdot K)]$											
	PV4	PV5	PV6	PV7	AV0	AV1	AV2	AV3	AV4	AV5	AV6	AV7	TL
2023-2-4	0.06	0.05	NA	NA	0.44	0.33	0.30	0.22	0.22	0.38	0.37	0.37	0.35
2023-2-14	0.32	0.27	NA	NA	0.50	0.43	0.37	0.35	0.28	0.26	0.21	0.18	0.37
2023-2-24	0.28	0.28	0.21	NA	0.54	0.46	0.42	0.36	0.31	0.28	0.24	0.25	0.41
2023-3-6	0.28	0.25	0.21	0.28	0.49	0.44	0.39	0.33	0.28	0.26	0.23	0.20	0.39
2023-3-16	0.09	0.11	NA	NA	0.36	0.26	0.20	0.20	0.19	0.21	NA	NA	0.30
2023-3-26	0.22	0.21	0.10	NA	0.54	0.45	0.40	0.34	0.25	0.24	0.21	0.22	0.41
2023-4-5	0.23	0.20	0.16	0.12	0.38	0.33	0.30	0.27	0.23	0.20	0.18	0.18	0.32
2023-4-15	0.19	0.15	0.08	NA	0.36	0.30	0.26	0.23	0.18	0.14	0.16	0.25	0.37
2023-4-25	0.18	0.16	0.15	0.09	0.43	0.37	0.32	0.28	0.23	0.20	0.19	0.20	0.42
2023-5-5	0.16	0.15	0.10	0.06	0.38	0.33	0.29	0.28	0.28	0.35	0.24	0.29	0.38
2023-5-15	0.14	0.15	0.10	NA	0.40	0.34	0.28	0.22	0.20	0.20	0.19	0.41	0.43
2023-5-25	0.16	0.13	0.06	NA	0.47	0.39	0.32	0.29	0.26	0.19	0.09	NA	0.58
2023-6-4	0.15	0.16	NA	NA	0.46	0.35	0.28	0.20	0.21	0.24	0.55	NA	0.55
2023-6-14	0.15	0.08	NA	NA	0.41	0.33	0.27	0.21	0.15	0.08	NA	NA	0.47
2023-6-24	0.30	0.44	NA	NA	0.52	0.44	0.40	0.43	0.39	0.44	NA	NA	0.51

Table B1(5) Dynamic U-values of the CLT tested envelope with 14-day time intervals

Start date of 14-day interval	Dynamic U-values calculated by data pre-processing methods $[W/(m^2 \cdot K)]$												
	ND	TD0	TD1	TD2	TD3	TD4	TD5	TD6	TD7	PV0	PV1	PV2	PV3
2023-2-4	0.16	0.28	0.29	0.30	0.27	0.22	0.32	NA	NA	0.57	0.50	0.46	0.42
2023-2-18	0.16	0.27	0.25	0.26	0.23	0.17	0.15	0.11	NA	0.49	0.42	0.38	0.32
2023-3-4	0.19	0.28	0.26	0.25	0.23	0.20	0.20	0.19	0.28	0.48	0.44	0.40	0.34
2023-3-18	0.04	0.05	0.09	0.16	0.13	0.16	NA	NA	NA	0.48	0.38	0.32	0.25
2023-4-1	0.09	0.12	0.14	0.17	0.15	0.15	0.14	0.12	0.10	0.36	0.34	0.31	0.27
2023-4-15	0.03	0.00	0.04	0.08	0.12	0.11	0.11	0.08	NA	0.27	0.26	0.25	0.23
2023-4-29	0.03	0.01	0.01	0.05	0.06	0.08	0.09	0.09	0.07	0.26	0.24	0.22	0.18
2023-5-13	0.03	0.02	0.02	0.05	0.06	0.06	0.07	0.06	NA	0.25	0.24	0.22	0.18
2023-5-27	0.00	0.08	0.02	0.03	0.05	0.06	0.08	0.04	NA	0.22	0.22	0.21	0.18
2023-6-10	0.01	0.03	0.01	0.04	0.05	0.10	0.11	NA	NA	0.23	0.22	0.20	0.18
2023-6-24	0.00	0.10	0.12	0.13	0.16	0.29	0.44	NA	NA	0.32	0.28	0.25	0.25

Table B1(5) (continued)

Start date of 14-day interval	Dynamic U-values calculated by data pre-processing methods $[W/(m^2 \cdot K)]$												
	PV4	PV5	PV6	PV7	AV0	AV1	AV2	AV3	AV4	AV5	AV6	AV7	TL
2023-2-4	0.28	0.32	NA	NA	0.50	0.42	0.38	0.33	0.28	0.30	0.26	0.23	0.38
2023-2-18	0.22	0.18	0.14	NA	0.50	0.42	0.37	0.32	0.27	0.27	0.25	0.25	0.37
2023-3-4	0.29	0.27	0.22	0.28	0.48	0.43	0.38	0.33	0.29	0.26	0.23	0.20	0.39
2023-3-18	0.20	NA	NA	NA	0.50	0.39	0.36	0.33	0.28	0.28	0.22	0.18	0.39
2023-4-1	0.23	0.20	0.15	0.12	0.41	0.35	0.32	0.29	0.24	0.21	0.19	0.20	0.34
2023-4-15	0.19	0.15	0.08	NA	0.38	0.32	0.28	0.25	0.19	0.15	0.18	0.25	0.40
2023-4-29	0.16	0.16	0.13	0.09	0.38	0.33	0.29	0.26	0.24	0.23	0.19	0.20	0.37
2023-5-13	0.16	0.15	0.10	NA	0.43	0.37	0.32	0.29	0.28	0.31	0.24	0.45	0.46
2023-5-27	0.17	0.14	0.06	NA	0.45	0.36	0.28	0.25	0.23	0.16	0.09	NA	0.58
2023-6-10	0.15	0.13	NA	NA	0.43	0.34	0.27	0.19	0.14	0.12	NA	NA	0.49
2023-6-24	0.30	0.44	NA	NA	0.52	0.44	0.40	0.43	0.39	0.44	NA	NA	0.51

Table B1(6) Dynamic U-values of the CLT tested envelope with 20-day time intervals

Start date of 20-day interval	Dynamic U-values calculated by data pre-processing methods $[W/(m^2 \cdot K)]$												
	ND	TD0	TD1	TD2	TD3	TD4	TD5	TD6	TD7	PV0	PV1	PV2	PV3
2023-2-4	0.15	0.25	0.26	0.27	0.25	0.19	0.26	NA	NA	0.50	0.44	0.40	0.37
2023-2-24	0.19	0.33	0.30	0.28	0.24	0.20	0.19	0.18	0.28	0.52	0.47	0.41	0.35
2023-3-16	0.06	0.06	0.10	0.16	0.16	0.13	0.14	0.09	NA	0.42	0.36	0.31	0.27
2023-4-5	0.05	0.04	0.06	0.10	0.11	0.13	0.13	0.12	0.10	0.29	0.27	0.26	0.23
2023-4-25	0.04	0.02	0.04	0.07	0.09	0.09	0.10	0.09	0.07	0.28	0.26	0.24	0.21
2023-5-15	0.01	0.06	0.02	0.03	0.04	0.05	0.07	0.06	NA	0.22	0.21	0.20	0.17
2023-6-4	0.01	0.04	0.01	0.05	0.05	0.10	0.13	NA	NA	0.24	0.23	0.22	0.18
2023-6-24	0.00	0.10	0.12	0.13	0.16	0.29	0.44	NA	NA	0.32	0.28	0.25	0.25

Table B1(6) (continued)

Start date of 20-day interval	Dynamic U-values calculated by data pre-processing methods $[W/(m^2 \cdot K)]$												
	PV4	PV5	PV6	PV7	AV0	AV1	AV2	AV3	AV4	AV5	AV6	AV7	TL
2023-2-4	0.25	0.26	NA	NA	0.48	0.40	0.36	0.32	0.26	0.29	0.25	0.22	0.36
2023-2-24	0.28	0.26	0.21	0.28	0.51	0.45	0.40	0.34	0.29	0.27	0.23	0.22	0.40
2023-3-16	0.20	0.18	0.10	NA	0.47	0.37	0.34	0.31	0.24	0.23	0.21	0.22	0.37
2023-4-5	0.21	0.18	0.15	0.12	0.37	0.32	0.28	0.25	0.21	0.18	0.17	0.19	0.34
2023-4-25	0.17	0.16	0.13	0.09	0.40	0.35	0.31	0.28	0.25	0.26	0.21	0.22	0.40
2023-5-15	0.15	0.14	0.09	NA	0.44	0.37	0.30	0.26	0.24	0.20	0.16	0.41	0.51
2023-6-4	0.15	0.14	NA	NA	0.44	0.34	0.27	0.21	0.18	0.21	0.55	NA	0.51
2023-6-24	0.30	0.44	NA	NA	0.52	0.44	0.40	0.43	0.39	0.44	NA	NA	0.51

Table B1(7) Dynamic U-values of the CLT tested envelope with 30-day time intervals

Start date of 40-day interval	Dynamic U-values calculated by data pre-processing methods $[W/(m^2 \cdot K)]$												
	ND	TD0	TD1	TD2	TD3	TD4	TD5	TD6	TD7	PV0	PV1	PV2	PV3
2023-2-4	0.17	0.29	0.28	0.28	0.26	0.21	0.23	0.18	NA	0.52	0.45	0.41	0.36
2023-3-6	0.13	0.19	0.20	0.22	0.20	0.17	0.17	0.17	0.28	0.48	0.42	0.37	0.32
2023-4-5	0.05	0.05	0.07	0.10	0.11	0.12	0.12	0.11	0.09	0.30	0.28	0.26	0.23
2023-5-5	0.01	0.05	0.01	0.03	0.05	0.06	0.07	0.06	0.06	0.22	0.22	0.20	0.18
2023-6-4	0.01	0.02	0.03	0.05	0.06	0.12	0.18	NA	NA	0.25	0.24	0.22	0.19

Table B1(7) (continued)

Start date of 40-day interval	Dynamic U-values calculated by data pre-processing methods [W/(m^2 · K)]											
	PV4	PV5	PV6	PV7	AV0	AV1	AV2	AV3	AV4	AV5	AV6	AV7	TL
2023-2-4	0.27	0.27	0.21	NA	0.51	0.43	0.38	0.34	0.29	0.29	0.25	0.23	0.38
2023-3-6	0.25	0.23	0.20	0.28	0.48	0.41	0.37	0.32	0.27	0.25	0.23	0.21	0.38
2023-4-5	0.20	0.17	0.15	0.11	0.39	0.33	0.29	0.26	0.22	0.19	0.18	0.19	0.37
2023-5-5	0.16	0.14	0.09	0.06	0.42	0.36	0.30	0.27	0.25	0.24	0.19	0.35	0.46
2023-6-4	0.17	0.19	NA	NA	0.45	0.35	0.29	0.24	0.21	0.25	0.55	NA	0.51

Table B1(8) Dynamic U-values of the CLT tested envelope with 40-day time intervals

Start date of 40-day interval	Dynamic U-values calculated by data pre-processing methods [W/(m^2 · K)]											
	ND	TD0	TD1	TD2	TD3	TD4	TD5	TD6	TD7	PV0	PV1	PV2	PV3
2023-2-4	0.18	0.30	0.28	0.27	0.24	0.20	0.20	0.18	0.28	0.52	0.46	0.41	0.35
2023-3-16	0.06	0.05	0.08	0.12	0.12	0.13	0.13	0.12	0.10	0.34	0.30	0.28	0.24
2023-4-25	0.03	0.02	0.01	0.05	0.06	0.07	0.08	0.08	0.07	0.25	0.24	0.22	0.19
2023-6-4	0.01	0.02	0.03	0.05	0.06	0.12	0.18	NA	NA	0.25	0.24	0.22	0.19

Table B1(8) (continued)

Start date of 40-day interval	Dynamic U-values calculated by data pre-processing methods [W/(m^2 · K)]											
	PV4	PV5	PV6	PV7	AV0	AV1	AV2	AV3	AV4	AV5	AV6	AV7	TL
2023-2-4	0.27	0.26	0.21	0.28	0.50	0.43	0.38	0.33	0.28	0.27	0.24	0.22	0.39
2023-3-16	0.21	0.18	0.15	0.12	0.41	0.34	0.30	0.27	0.22	0.19	0.19	0.20	0.35
2023-4-25	0.16	0.15	0.11	0.09	0.42	0.36	0.30	0.27	0.24	0.23	0.19	0.26	0.45
2023-6-4	0.17	0.19	NA	NA	0.45	0.35	0.29	0.24	0.21	0.25	0.55	NA	0.51

Table B1(9) Dynamic U-values of the CLT tested envelope with 50-day time intervals

Start date of 50-day interval	Dynamic U-values calculated by data pre-processing methods [W/(m^2 · K)]											
	ND	TD0	TD1	TD2	TD3	TD4	TD5	TD6	TD7	PV0	PV1	PV2	PV3
2023-2-4	0.16	0.25	0.24	0.25	0.23	0.19	0.19	0.18	0.28	0.50	0.44	0.39	0.34
2023-3-26	0.06	0.05	0.07	0.11	0.12	0.12	0.12	0.10	0.08	0.32	0.30	0.27	0.24
2023-5-15	0.00	0.04	0.00	0.04	0.05	0.08	0.10	0.06	NA	0.24	0.23	0.21	0.18

Table B1(9) (continued)

Start date of 50-day interval	Dynamic U-values calculated by data pre-processing methods [W/(m² · K)]												
	PV4	PV5	PV6	PV7	AV0	AV1	AV2	AV3	AV4	AV5	AV6	AV7	TL
2023-2-4	0.27	0.25	0.21	0.28	0.48	0.41	0.37	0.33	0.28	0.27	0.24	0.22	0.38
2023-3-26	0.20	0.17	0.14	0.10	0.41	0.35	0.31	0.28	0.23	0.22	0.20	0.21	0.38
2023-5-15	0.16	0.16	0.09	NA	0.44	0.36	0.29	0.25	0.22	0.21	0.17	0.41	0.51

Table B2(1) Dynamic U-values of the masonry cavity tested envelope with 3-day time intervals

Start date of 3-day interval	Dynamic U-values calculated by data pre-processing methods [W/(m² · K)]												
	ND	TD0	TD1	TD2	TD3	TD4	TD5	TD6	TD7	TD8	TD9	TD 10	TD 11
2022-7-17	0.69	0.66	0.63	0.59	0.55	0.44	0.35	0.33	0.31	0.28	NA	NA	NA
2022-7-20	0.45	0.45	0.44	0.44	0.44	0.43	0.40	0.38	0.39	0.51	0.49	NA	NA
2022-7-23	0.00	0.18	0.15	0.09	0.03	0.00	0.04	0.07	0.10	0.10	NA	NA	NA
2022-7-26	0.09	0.04	0.06	0.07	0.09	0.10	0.11	0.13	0.14	0.15	0.13	NA	NA
2022-7-29	0.06	0.16	0.11	0.06	0.04	0.00	0.04	0.06	NA	NA	NA	NA	NA
2022-8-1	0.12	0.08	0.11	0.13	0.14	0.12	0.13	0.13	0.11	NA	NA	NA	NA
2022-8-4	0.26	0.17	0.20	0.23	0.26	0.26	0.27	0.27	0.28	0.30	0.28	0.27	NA
2022-8-7	0.27	0.28	0.28	0.28	0.28	0.28	0.28	0.29	0.28	0.30	0.33	0.36	NA
2022-8-10	0.72	0.80	0.78	0.75	0.73	0.71	0.69	0.68	0.66	0.70	0.74	NA	NA
2022-8-13	0.77	0.88	0.85	0.82	0.80	0.79	0.79	0.78	0.76	0.75	0.74	NA	NA
2022-8-16	0.22	0.16	0.18	0.19	0.20	0.21	0.25	0.27	0.34	0.33	0.34	NA	NA
2022-8-19	0.07	0.04	0.00	0.03	0.06	0.07	0.08	0.10	0.11	0.10	NA	NA	NA
2022-8-22	0.19	0.13	0.15	0.17	0.19	0.20	0.22	0.24	0.28	0.27	0.28	NA	NA
2022-8-25	0.20	0.18	0.19	0.21	0.21	0.21	0.22	0.22	0.21	0.21	0.22	0.22	NA
2022-8-28	0.05	0.08	0.07	0.05	0.01	0.02	0.01	0.05	0.05	0.02	0.14	0.16	NA
2022-8-31	0.10	0.28	0.24	0.20	0.15	0.13	0.11	0.09	0.09	0.14	0.24	NA	NA
2022-9-3	0.10	0.22	0.18	0.15	0.13	0.12	0.10	0.08	0.05	NA	NA	NA	NA
2022-9-6	0.03	0.07	0.06	0.05	0.03	0.02	0.02	0.01	0.01	0.07	0.09	NA	NA
2022-9-9	0.33	0.47	0.46	0.44	0.39	0.36	0.32	0.30	0.29	0.43	0.48	NA	NA
2022-9-12	0.17	0.39	0.37	0.33	0.26	0.23	0.20	0.18	0.11	0.09	0.09	0.07	0.04
2022-9-15	0.15	0.32	0.32	0.30	0.28	0.25	0.22	0.18	0.16	0.15	0.14	0.10	0.12
2022-9-18	0.37	0.53	0.53	0.53	0.52	0.49	0.43	0.40	0.38	0.36	0.33	0.30	NA
2022-9-21	0.33	0.55	0.54	0.53	0.50	0.43	0.39	0.36	0.35	0.33	0.30	0.22	0.13
2022-9-24	0.26	0.40	0.40	0.40	0.40	0.40	0.39	0.38	0.34	0.30	0.26	0.21	0.17
2022-9-27	0.32	0.49	0.49	0.49	0.49	0.48	0.47	0.43	0.38	0.36	0.34	0.29	0.25
2022-9-30	0.46	0.63	0.63	0.63	0.63	0.62	0.60	0.56	0.53	0.50	0.46	0.35	0.26
2022-10-3	0.47	0.58	0.58	0.58	0.57	0.56	0.52	0.49	0.44	0.37	0.30	0.27	0.26
2022-10-6	0.40	0.55	0.55	0.55	0.55	0.54	0.52	0.49	0.46	0.41	0.36	0.33	0.32

Table B2(1) (continued)

Start date of 3-day interval	Dynamic U-values calculated by data pre-processing methods $[W/(m^2 \cdot K)]$												
	ND	TD0	TD1	TD2	TD3	TD4	TD5	TD6	TD7	TD8	TD9	TD 10	TD 11
2022-10-9	0.38	0.57	0.57	0.57	0.57	0.56	0.55	0.51	0.46	0.44	0.40	0.36	0.33
2022-10-12	0.49	0.66	0.66	0.65	0.65	0.64	0.63	0.60	0.56	0.53	0.50	0.47	0.43
2022-10-15	0.49	0.66	0.66	0.65	0.64	0.62	0.61	0.58	0.55	0.52	0.47	0.44	0.40
2022-10-18	0.41	0.51	0.51	0.50	0.50	0.50	0.50	0.48	0.47	0.42	0.29	0.26	0.20
2022-10-21	0.62	0.69	0.69	0.69	0.68	0.68	0.68	0.65	0.61	0.55	0.50	NA	NA
2022-10-24	0.52	0.66	0.66	0.66	0.65	0.65	0.62	0.60	0.56	0.50	0.47	0.41	0.39
2022-10-27	0.51	0.59	0.59	0.59	0.59	0.59	0.58	0.56	0.53	0.48	0.39	0.36	NA
2022-10-30	0.52	0.60	0.60	0.60	0.60	0.60	0.60	0.59	0.56	0.54	0.51	0.43	0.38
2022-11-2	0.53	0.63	0.63	0.63	0.63	0.63	0.63	0.62	0.61	0.59	0.54	0.52	0.49
2022-11-5	0.79	0.91	0.91	0.91	0.91	0.91	0.91	0.91	0.91	0.89	0.82	0.77	0.75
2022-11-8	0.81	0.87	0.87	0.87	0.87	0.87	0.87	0.87	0.85	0.84	0.81	0.78	0.77
2022-11-11	0.68	0.72	0.72	0.72	0.72	0.72	0.72	0.72	0.70	0.68	0.63	0.58	0.54
2022-11-14	0.74	0.77	0.77	0.77	0.77	0.77	0.77	0.77	0.77	0.77	0.77	0.76	0.74
2022-11-17	0.79	0.81	0.81	0.81	0.81	0.81	0.81	0.81	0.81	0.81	0.81	0.81	0.80
2022-11-20	0.75	0.81	0.81	0.81	0.81	0.81	0.81	0.81	0.81	0.81	0.81	0.81	0.79
2022-11-23	0.85	0.92	0.92	0.92	0.92	0.92	0.92	0.92	0.92	0.92	0.92	0.90	0.88
2022-11-26	0.85	0.89	0.89	0.89	0.89	0.89	0.89	0.89	0.89	0.89	0.89	0.88	0.82
2022-11-29	0.77	0.79	0.79	0.79	0.79	0.79	0.79	0.79	0.79	0.79	0.79	0.79	0.79
2022-12-2	0.82	0.88	0.88	0.88	0.88	0.88	0.88	0.88	0.88	0.88	0.88	0.88	0.88
2022-12-5	0.81	0.86	0.86	0.86	0.86	0.86	0.86	0.86	0.86	0.86	0.86	0.86	0.86
2022-12-8	0.89	0.94	0.94	0.94	0.94	0.94	0.94	0.94	0.94	0.94	0.94	0.94	0.94
2022-12-11	0.85	0.86	0.86	0.86	0.86	0.86	0.86	0.86	0.86	0.86	0.86	0.86	0.86

Table B2(1) (continued)

Start date of 3-day interval	Dynamic U-values calculated by data pre-processing methods $[W/(m^2 \cdot K)]$												
	TD 12	TD 13	PV0	PV1	PV2	PV3	PV4	PV5	PV6	PV7	PV8	PV9	PV 10
2022-7-17	NA	NA	NA	NA	NA	NA	NA	NA	NA	NA	NA	NA	NA
2022-7-20	NA	NA	NA	NA	NA	NA	NA	NA	NA	NA	NA	NA	NA
2022-7-23	NA	NA	0.42	0.37	0.27	0.18	0.13	0.08	0.03	0.00	NA	NA	NA
2022-7-26	NA	NA	0.25	0.18	0.13	0.07	0.06	0.04	NA	NA	NA	NA	NA
2022-7-29	NA	NA	0.32	0.23	0.16	0.13	0.08	0.02	NA	NA	NA	NA	NA
2022-8-1	NA	NA	0.41	0.21	0.09	0.07	0.05	NA	NA	NA	NA	NA	NA
2022-8-4	NA	NA	0.82	0.49	0.29	0.09	0.04	0.01	0.00	NA	NA	NA	NA
2022-8-7	NA	NA	0.32	0.24	0.15	0.13	0.06	0.02	NA	NA	NA	NA	NA
2022-8-10	NA	NA	NA	NA	NA	NA	NA	NA	NA	NA	NA	NA	NA
2022-8-13	NA	NA	NA	NA	NA	NA	NA	NA	NA	NA	NA	NA	NA
2022-8-16	NA	NA	0.47	0.34	0.23	0.21	0.18	0.07	0.00	NA	NA	NA	NA
2022-8-19	NA	NA	0.42	0.28	0.19	0.11	0.08	0.04	0.02	0.00	NA	NA	NA
2022-8-22	NA	NA	0.42	0.22	0.13	0.06	NA	NA	NA	NA	NA	NA	NA
2022-8-25	NA	NA	0.59	0.34	0.12	0.10	0.07	0.03	NA	NA	NA	NA	NA
2022-8-28	NA	NA	0.54	0.54	0.49	0.40	0.33	0.30	0.27	0.23	0.19	0.20	0.16
2022-8-31	NA	NA	0.44	0.39	0.33	0.26	0.23	0.21	0.21	0.22	0.24	0.28	NA
2022-9-3	NA	NA	0.24	0.19	0.16	0.14	0.12	0.10	0.09	0.06	NA	NA	NA
2022-9-6	NA	NA	0.21	0.19	0.17	0.15	0.14	0.13	0.13	0.10	0.01	NA	NA
2022-9-9	NA	NA	0.47	0.46	0.44	0.39	0.36	0.32	0.30	0.29	0.43	0.48	NA
2022-9-12	NA	NA	0.39	0.37	0.33	0.26	0.23	0.20	0.18	0.11	0.09	0.09	0.07
2022-9-15	0.12	NA	0.32	0.32	0.30	0.28	0.25	0.22	0.18	0.16	0.15	0.14	0.10
2022-9-18	NA	NA	0.53	0.53	0.53	0.52	0.49	0.43	0.40	0.38	0.36	0.33	0.30
2022-9-21	NA	NA	0.55	0.54	0.53	0.50	0.43	0.39	0.36	0.35	0.33	0.30	0.22
2022-9-24	0.17	0.14	0.40	0.40	0.40	0.40	0.40	0.39	0.38	0.34	0.30	0.26	0.21
2022-9-27	0.24	0.21	0.49	0.49	0.49	0.49	0.48	0.47	0.43	0.38	0.36	0.34	0.29
2022-9-30	0.25	0.24	0.63	0.63	0.63	0.63	0.62	0.60	0.56	0.53	0.50	0.46	0.35
2022-10-3	0.24	NA	0.58	0.58	0.58	0.57	0.56	0.52	0.49	0.44	0.37	0.30	0.27
2022-10-6	0.30	0.29	0.55	0.55	0.55	0.55	0.54	0.52	0.49	0.46	0.41	0.36	0.33
2022-10-9	0.31	0.27	0.57	0.57	0.57	0.57	0.56	0.55	0.51	0.46	0.44	0.40	0.36
2022-10-12	0.39	NA	0.66	0.66	0.65	0.65	0.64	0.63	0.60	0.56	0.53	0.50	0.47
2022-10-15	0.28	NA	0.66	0.66	0.65	0.64	0.62	0.61	0.58	0.55	0.52	0.47	0.44
2022-10-18	0.19	0.16	0.51	0.51	0.50	0.50	0.50	0.50	0.48	0.47	0.42	0.29	0.26
2022-10-21	NA	NA	0.69	0.69	0.69	0.68	0.68	0.68	0.65	0.61	0.55	0.50	NA
2022-10-24	NA	NA	0.66	0.66	0.66	0.65	0.65	0.62	0.60	0.56	0.50	0.47	0.41
2022-10-27	NA	NA	0.59	0.59	0.59	0.59	0.59	0.58	0.56	0.53	0.48	0.39	0.36
2022-10-30	NA	NA	0.60	0.60	0.60	0.60	0.60	0.60	0.59	0.56	0.54	0.51	0.43
2022-11-2	0.47	0.48	0.63	0.63	0.63	0.63	0.63	0.63	0.62	0.61	0.59	0.54	0.52
2022-11-5	0.70	0.61	0.91	0.91	0.91	0.91	0.91	0.91	0.91	0.91	0.89	0.82	0.77

Table B2(1) (continued)

Start date of 3-day interval	Dynamic U-values calculated by data pre-processing methods [W/(m^2 · K)]												
	TD 12	TD 13	PV0	PV1	PV2	PV3	PV4	PV5	PV6	PV7	PV8	PV9	PV 10
2022-11-8	0.75	0.74	0.87	0.87	0.87	0.87	0.87	0.87	0.87	0.85	0.84	0.81	0.78
2022-11-11	0.50	NA	0.72	0.72	0.72	0.72	0.72	0.72	0.72	0.70	0.68	0.63	0.58
2022-11-14	0.73	0.70	0.77	0.77	0.77	0.77	0.77	0.77	0.77	0.77	0.77	0.77	0.76
2022-11-17	0.78	0.74	0.81	0.81	0.81	0.81	0.81	0.81	0.81	0.81	0.81	0.81	0.81
2022-11-20	0.76	0.69	0.81	0.81	0.81	0.81	0.81	0.81	0.81	0.81	0.81	0.81	0.81
2022-11-23	0.86	0.82	0.92	0.92	0.92	0.92	0.92	0.92	0.92	0.92	0.92	0.92	0.90
2022-11-26	0.78	0.75	0.89	0.89	0.89	0.89	0.89	0.89	0.89	0.89	0.89	0.89	0.88
2022-11-29	0.79	0.78	0.79	0.79	0.79	0.79	0.79	0.79	0.79	0.79	0.79	0.79	0.79
2022-12-2	0.88	0.85	0.88	0.88	0.88	0.88	0.88	0.88	0.88	0.88	0.88	0.88	0.88
2022-12-5	0.85	0.83	0.86	0.86	0.86	0.86	0.86	0.86	0.86	0.86	0.86	0.86	0.86
2022-12-8	0.94	0.94	0.94	0.94	0.94	0.94	0.94	0.94	0.94	0.94	0.94	0.94	0.94
2022-12-11	0.86	0.86	0.86	0.86	0.86	0.86	0.86	0.86	0.86	0.86	0.86	0.86	0.86

Table B2(1) (continued)

Start date of 3-day interval	Dynamic U-values calculated by data pre-processing methods $[W/(m^2 \cdot K)]$											
	PV 11	PV 12	PV 13	AV0	AV1	AV2	AV3	AV4	AV5	AV6	AV7	AV8
2022-7-17	NA	NA	NA	0.31	0.28	0.26	0.24	0.20	0.17	0.16	0.15	0.14
2022-7-20	NA	NA	NA	0.45	0.44	0.44	0.44	0.43	0.40	0.38	0.39	0.51
2022-7-23	NA	NA	NA	0.26	0.23	0.17	0.12	0.10	0.08	0.08	0.10	0.10
2022-7-26	NA	NA	NA	0.21	0.18	0.15	0.13	0.12	0.12	0.13	0.14	0.15
2022-7-29	NA	NA	NA	0.22	0.15	0.11	0.09	0.06	0.04	0.06	NA	NA
2022-8-1	NA	NA	NA	0.38	0.33	0.30	0.24	0.21	0.20	0.15	0.11	NA
2022-8-4	NA	NA	NA	0.37	0.31	0.28	0.27	0.26	0.27	0.27	0.28	0.30
2022-8-7	NA	NA	NA	0.37	0.36	0.35	0.34	0.33	0.31	0.31	0.30	0.31
2022-8-10	NA	NA	NA	0.49	0.47	0.45	0.44	0.43	0.41	0.40	0.37	0.31
2022-8-13	NA	NA	NA	0.67	0.64	0.62	0.59	0.58	0.57	0.55	0.52	0.46
2022-8-16	NA	NA	NA	0.30	0.27	0.25	0.25	0.25	0.25	0.27	0.34	0.33
2022-8-19	NA	NA	NA	0.32	0.26	0.20	0.16	0.11	0.10	0.10	0.11	0.10
2022-8-22	NA	NA	NA	0.31	0.27	0.24	0.23	0.22	0.23	0.25	0.29	0.27
2022-8-25	NA	NA	NA	0.30	0.29	0.28	0.27	0.27	0.27	0.26	0.24	0.22
2022-8-28	NA	NA	NA	0.42	0.41	0.37	0.34	0.31	0.30	0.29	0.25	0.24
2022-8-31	NA	NA	NA	0.36	0.29	0.23	0.18	0.15	0.14	0.13	0.13	0.16
2022-9-3	NA	NA	NA	0.30	0.24	0.20	0.18	0.16	0.13	0.11	0.05	NA
2022-9-6	NA	NA	NA	0.18	0.16	0.14	0.13	0.12	0.11	0.10	0.08	0.07
2022-9-9	NA	NA	NA	0.48	0.46	0.44	0.39	0.36	0.32	0.30	0.29	0.43
2022-9-12	0.04	NA	NA	0.41	0.37	0.33	0.26	0.23	0.20	0.18	0.11	0.09
2022-9-15	0.12	0.12	NA	0.33	0.32	0.30	0.28	0.25	0.22	0.18	0.16	0.15
2022-9-18	NA	NA	NA	0.53	0.53	0.53	0.52	0.49	0.43	0.40	0.38	0.36
2022-9-21	0.13	NA	NA	0.55	0.54	0.53	0.50	0.43	0.39	0.36	0.35	0.33
2022-9-24	0.17	0.17	0.14	0.40	0.40	0.40	0.40	0.40	0.39	0.38	0.34	0.30
2022-9-27	0.25	0.24	0.21	0.49	0.49	0.49	0.49	0.48	0.47	0.43	0.38	0.36
2022-9-30	0.26	0.25	0.24	0.63	0.63	0.63	0.63	0.62	0.60	0.56	0.53	0.50
2022-10-3	0.26	0.24	NA	0.59	0.58	0.58	0.57	0.56	0.52	0.49	0.44	0.37
2022-10-6	0.32	0.30	0.29	0.55	0.55	0.55	0.55	0.54	0.52	0.49	0.46	0.41
2022-10-9	0.33	0.31	0.27	0.57	0.57	0.57	0.57	0.56	0.55	0.51	0.46	0.44
2022-10-12	0.43	0.39	NA	0.68	0.67	0.65	0.65	0.64	0.63	0.60	0.56	0.53
2022-10-15	0.40	0.28	NA	0.66	0.66	0.65	0.64	0.62	0.61	0.58	0.55	0.52
2022-10-18	0.20	0.19	0.16	0.52	0.51	0.50	0.50	0.50	0.50	0.48	0.47	0.42
2022-10-21	NA	NA	NA	0.69	0.69	0.69	0.68	0.68	0.68	0.65	0.61	0.55
2022-10-24	0.39	NA	NA	0.66	0.66	0.66	0.65	0.65	0.62	0.60	0.56	0.50
2022-10-27	NA	NA	NA	0.59	0.59	0.59	0.59	0.59	0.58	0.56	0.53	0.48
2022-10-30	0.38	NA	NA	0.60	0.60	0.60	0.60	0.60	0.60	0.59	0.56	0.54
2022-11-2	0.49	0.47	0.48	0.63	0.63	0.63	0.63	0.63	0.63	0.62	0.61	0.59
2022-11-5	0.75	0.70	0.61	0.91	0.91	0.91	0.91	0.91	0.91	0.91	0.91	0.89

Table B2(1) (continued)

Start date of 3-day interval	Dynamic U-values calculated by data pre-processing methods [W/(m² · K)]											
	PV 11	PV 12	PV 13	AV0	AV1	AV2	AV3	AV4	AV5	AV6	AV7	AV8
2022-11-8	0.77	0.75	0.74	0.87	0.87	0.87	0.87	0.87	0.87	0.87	0.85	0.84
2022-11-11	0.54	0.50	NA	0.72	0.72	0.72	0.72	0.72	0.72	0.72	0.70	0.68
2022-11-14	0.74	0.73	0.70	0.77	0.77	0.77	0.77	0.77	0.77	0.77	0.77	0.77
2022-11-17	0.80	0.78	0.74	0.81	0.81	0.81	0.81	0.81	0.81	0.81	0.81	0.81
2022-11-20	0.79	0.76	0.69	0.81	0.81	0.81	0.81	0.81	0.81	0.81	0.81	0.81
2022-11-23	0.88	0.86	0.82	0.92	0.92	0.92	0.92	0.92	0.92	0.92	0.92	0.92
2022-11-26	0.82	0.78	0.75	0.89	0.89	0.89	0.89	0.89	0.89	0.89	0.89	0.89
2022-11-29	0.79	0.79	0.78	0.79	0.79	0.79	0.79	0.79	0.79	0.79	0.79	0.79
2022-12-2	0.88	0.88	0.85	0.88	0.88	0.88	0.88	0.88	0.88	0.88	0.88	0.88
2022-12-5	0.86	0.85	0.83	0.86	0.86	0.86	0.86	0.86	0.86	0.86	0.86	0.86
2022-12-8	0.94	0.94	0.94	0.94	0.94	0.94	0.94	0.94	0.94	0.94	0.94	0.94
2022-12-11	0.86	0.86	0.86	0.86	0.86	0.86	0.86	0.86	0.86	0.86	0.86	0.86

Table B2(1) (continued)

Start date of 3-day interval	Dynamic U-values calculated by data pre-processing methods [$W/(m^2 \cdot K)$]					
	AV9	AV10	AV11	AV12	AV13	TL
2022-7-17	0.12	0.12	0.12	0.12	0.11	0.19
2022-7-20	0.49	NA	NA	NA	NA	0.44
2022-7-23	NA	NA	NA	NA	NA	0.26
2022-7-26	0.13	NA	NA	NA	NA	0.19
2022-7-29	NA	NA	NA	NA	NA	0.18
2022-8-1	NA	NA	NA	NA	NA	0.23
2022-8-4	0.28	0.27	NA	NA	NA	0.34
2022-8-7	0.34	0.34	0.32	0.35	NA	0.22
2022-8-10	0.24	0.22	0.22	0.21	0.25	0.33
2022-8-13	0.33	0.16	0.14	NA	NA	0.43
2022-8-16	0.34	NA	NA	NA	NA	0.29
2022-8-19	NA	NA	NA	NA	NA	0.26
2022-8-22	0.28	NA	NA	NA	NA	0.20
2022-8-25	0.22	0.22	NA	NA	NA	0.22
2022-8-28	0.22	0.16	NA	NA	NA	0.35
2022-8-31	0.25	NA	NA	NA	NA	0.36
2022-9-3	NA	NA	NA	NA	NA	0.28
2022-9-6	0.09	NA	NA	NA	NA	0.19
2022-9-9	0.48	NA	NA	NA	NA	0.58
2022-9-12	0.09	0.07	0.04	NA	NA	0.41
2022-9-15	0.14	0.10	0.12	0.12	NA	0.38
2022-9-18	0.33	0.30	NA	NA	NA	0.61
2022-9-21	0.30	0.22	0.13	NA	NA	0.67
2022-9-24	0.26	0.21	0.17	0.17	0.14	0.43
2022-9-27	0.34	0.29	0.25	0.24	0.21	0.55
2022-9-30	0.46	0.35	0.26	0.25	0.24	0.68
2022-10-3	0.30	0.27	0.26	0.24	NA	0.61
2022-10-6	0.36	0.33	0.32	0.30	0.29	0.59
2022-10-9	0.40	0.36	0.33	0.31	0.27	0.64
2022-10-12	0.50	0.47	0.43	0.39	NA	0.82
2022-10-15	0.47	0.44	0.40	0.28	NA	0.77
2022-10-18	0.29	0.26	0.20	0.19	0.16	0.57
2022-10-21	0.50	NA	NA	NA	NA	0.75
2022-10-24	0.47	0.41	0.39	NA	NA	0.68
2022-10-27	0.39	0.36	NA	NA	NA	0.61
2022-10-30	0.51	0.43	0.38	NA	NA	0.64
2022-11-2	0.54	0.52	0.49	0.47	0.48	0.63
2022-11-5	0.82	0.77	0.75	0.70	0.61	0.88
2022-11-8	0.81	0.78	0.77	0.75	0.74	0.90

Table B2(1) (continued)

Start date of 3-day interval	Dynamic U-values calculated by data pre-processing methods $[W/(m^2 \cdot K)]$					
	AV9	AV10	AV11	AV12	AV13	TL
2022-11-11	0.63	0.58	0.54	0.50	NA	0.69
2022-11-14	0.77	0.76	0.74	0.73	0.70	0.76
2022-11-17	0.81	0.81	0.80	0.78	0.74	0.81
2022-11-20	0.81	0.81	0.79	0.76	0.69	0.80
2022-11-23	0.92	0.90	0.88	0.86	0.82	0.95
2022-11-26	0.89	0.88	0.82	0.78	0.75	0.87
2022-11-29	0.79	0.79	0.79	0.79	0.78	0.76
2022-12-2	0.88	0.88	0.88	0.88	0.85	0.87
2022-12-5	0.86	0.86	0.86	0.85	0.83	0.87
2022-12-8	0.94	0.94	0.94	0.94	0.94	0.93
2022-12-11	0.86	0.86	0.86	0.86	0.86	0.84

Table B2(2) Dynamic U-values of the masonry cavity tested envelope with 5-day time intervals

Start date of 5-day interval	Dynamic U-values calculated by data pre-processing methods [W/(m^2 · K)]												
	ND	TD0	TD1	TD2	TD3	TD4	TD5	TD6	TD7	TD8	TD9	TD 10	TD 11
2022-7-17	0.62	0.61	0.59	0.58	0.57	0.54	0.51	0.48	0.47	0.46	0.49	NA	NA
2022-7-22	0.07	0.02	0.01	0.03	0.07	0.09	0.12	0.14	0.16	0.13	NA	NA	NA
2022-7-27	0.00	0.08	0.04	0.00	0.02	0.05	0.08	0.12	0.13	0.13	0.13	NA	NA
2022-8-1	0.21	0.14	0.18	0.21	0.22	0.23	0.25	0.25	0.28	0.31	0.35	NA	NA
2022-8-6	0.31	0.29	0.29	0.30	0.30	0.30	0.30	0.31	0.31	0.29	0.30	0.31	NA
2022-8-11	0.77	0.88	0.85	0.82	0.80	0.79	0.78	0.77	0.75	0.73	0.74	NA	NA
2022-8-16	0.15	0.08	0.11	0.13	0.15	0.16	0.18	0.20	0.25	0.29	0.34	NA	NA
2022-8-21	0.18	0.14	0.15	0.17	0.18	0.19	0.21	0.22	0.21	0.23	0.21	0.20	NA
2022-8-26	0.11	0.00	0.01	0.03	0.06	0.08	0.08	0.06	0.06	0.08	0.05	0.01	NA
2022-8-31	0.11	0.28	0.24	0.19	0.16	0.13	0.11	0.09	0.09	0.14	0.24	NA	NA
2022-9-5	0.02	0.12	0.11	0.10	0.09	0.07	0.07	0.05	0.02	0.07	0.09	NA	NA
2022-9-10	0.26	0.46	0.44	0.41	0.35	0.31	0.27	0.25	0.21	0.18	0.16	0.07	0.04
2022-9-15	0.22	0.39	0.39	0.37	0.36	0.34	0.30	0.26	0.24	0.23	0.21	0.14	0.12
2022-9-20	0.30	0.49	0.49	0.48	0.46	0.41	0.36	0.33	0.31	0.29	0.25	0.15	0.11
2022-9-25	0.33	0.48	0.48	0.48	0.48	0.48	0.47	0.44	0.40	0.37	0.34	0.28	0.24
2022-9-30	0.46	0.64	0.64	0.64	0.64	0.63	0.59	0.54	0.51	0.47	0.42	0.31	0.26
2022-10-5	0.41	0.56	0.56	0.56	0.56	0.54	0.53	0.49	0.45	0.40	0.37	0.32	0.30
2022-10-10	0.44	0.61	0.60	0.60	0.60	0.59	0.58	0.56	0.51	0.49	0.46	0.43	0.39
2022-10-15	0.43	0.57	0.57	0.56	0.56	0.55	0.54	0.51	0.48	0.45	0.40	0.37	0.29
2022-10-20	0.59	0.66	0.66	0.66	0.65	0.65	0.65	0.63	0.60	0.55	0.51	0.43	NA
2022-10-25	0.52	0.63	0.63	0.63	0.63	0.63	0.60	0.57	0.54	0.48	0.40	0.40	0.39
2022-10-30	0.52	0.59	0.59	0.59	0.59	0.59	0.59	0.59	0.56	0.53	0.50	0.45	0.42
2022-11-4	0.75	0.86	0.86	0.86	0.86	0.86	0.86	0.86	0.86	0.84	0.79	0.75	0.72
2022-11-9	0.72	0.78	0.78	0.78	0.78	0.78	0.78	0.78	0.76	0.74	0.69	0.65	0.63
2022-11-14	0.77	0.80	0.80	0.80	0.80	0.80	0.80	0.80	0.80	0.80	0.80	0.79	0.78
2022-11-19	0.76	0.81	0.81	0.81	0.81	0.81	0.81	0.81	0.81	0.81	0.81	0.81	0.80
2022-11-24	0.87	0.91	0.91	0.91	0.91	0.91	0.91	0.91	0.91	0.91	0.91	0.90	0.85
2022-11-29	0.79	0.83	0.83	0.83	0.83	0.83	0.83	0.83	0.83	0.83	0.83	0.83	0.83
2022-12-4	0.82	0.86	0.86	0.86	0.86	0.86	0.86	0.86	0.86	0.86	0.86	0.86	0.86
2022-12-9	0.88	0.90	0.90	0.90	0.90	0.90	0.90	0.90	0.90	0.90	0.90	0.90	0.90

Table B2(2) (continued)

Start date of 5-day interval	Dynamic U-values calculated by data pre-processing methods $[W/(m^2 \cdot K)]$												
	TD 12	TD 13	PV0	PV1	PV2	PV3	PV4	PV5	PV6	PV7	PV8	PV9	PV 10
2022-7-17	NA	NA	NA	NA	NA	NA	NA	NA	NA	NA	NA	NA	NA
2022-7-22	NA	NA	0.40	0.35	0.25	0.17	0.12	0.07	0.03	0.00	NA	NA	NA
2022-7-27	NA	NA	0.30	0.21	0.15	0.11	0.07	0.03	NA	NA	NA	NA	NA
2022-8-1	NA	NA	0.75	0.36	0.21	0.05	0.04	0.01	0.00	NA	NA	NA	NA
2022-8-6	NA	NA	0.40	0.36	0.21	0.13	0.05	0.02	NA	NA	NA	NA	NA
2022-8-11	NA	NA	NA	NA	NA	NA	NA	NA	NA	NA	NA	NA	NA
2022-8-16	NA	NA	0.42	0.28	0.19	0.14	0.12	0.05	0.02	0.00	NA	NA	NA
2022-8-21	NA	NA	0.46	0.31	0.21	0.14	0.12	0.04	NA	NA	NA	NA	NA
2022-8-26	NA	NA	0.55	0.52	0.47	0.39	0.32	0.30	0.27	0.23	0.19	0.20	0.16
2022-8-31	NA	NA	0.37	0.31	0.26	0.21	0.19	0.17	0.16	0.19	0.24	0.28	NA
2022-9-5	NA	NA	0.22	0.20	0.19	0.17	0.16	0.15	0.14	0.11	0.01	NA	NA
2022-9-10	NA	NA	0.46	0.44	0.41	0.35	0.31	0.27	0.25	0.21	0.18	0.16	0.07
2022-9-15	0.12	NA	0.39	0.39	0.37	0.36	0.34	0.30	0.26	0.24	0.23	0.21	0.14
2022-9-20	0.07	0.05	0.49	0.49	0.48	0.46	0.41	0.36	0.33	0.31	0.29	0.25	0.15
2022-9-25	0.23	0.21	0.48	0.48	0.48	0.48	0.48	0.47	0.44	0.40	0.37	0.34	0.28
2022-9-30	0.24	0.24	0.64	0.64	0.64	0.64	0.63	0.59	0.54	0.51	0.47	0.42	0.31
2022-10-5	0.29	0.27	0.56	0.56	0.56	0.56	0.54	0.53	0.49	0.45	0.40	0.37	0.32
2022-10-10	0.34	0.27	0.61	0.60	0.60	0.60	0.59	0.58	0.56	0.51	0.49	0.46	0.43
2022-10-15	0.20	0.16	0.57	0.57	0.56	0.56	0.55	0.54	0.51	0.48	0.45	0.40	0.37
2022-10-20	NA	NA	0.66	0.66	0.66	0.65	0.65	0.65	0.63	0.60	0.55	0.51	0.43
2022-10-25	NA	NA	0.63	0.63	0.63	0.63	0.63	0.60	0.57	0.54	0.48	0.40	0.40
2022-10-30	0.44	0.48	0.59	0.59	0.59	0.59	0.59	0.59	0.59	0.56	0.53	0.50	0.45
2022-11-4	0.66	0.54	0.86	0.86	0.86	0.86	0.86	0.86	0.86	0.86	0.84	0.79	0.75
2022-11-9	0.68	NA	0.78	0.78	0.78	0.78	0.78	0.78	0.78	0.76	0.74	0.69	0.65
2022-11-14	0.76	0.70	0.80	0.80	0.80	0.80	0.80	0.80	0.80	0.80	0.80	0.80	0.79
2022-11-19	0.77	0.72	0.81	0.81	0.81	0.81	0.81	0.81	0.81	0.81	0.81	0.81	0.81
2022-11-24	0.83	0.78	0.91	0.91	0.91	0.91	0.91	0.91	0.91	0.91	0.91	0.91	0.90
2022-11-29	0.83	0.81	0.83	0.83	0.83	0.83	0.83	0.83	0.83	0.83	0.83	0.83	0.83
2022-12-4	0.86	0.84	0.86	0.86	0.86	0.86	0.86	0.86	0.86	0.86	0.86	0.86	0.86
2022-12-9	0.90	0.90	0.90	0.90	0.90	0.90	0.90	0.90	0.90	0.90	0.90	0.90	0.90

Table B2(2) (continued)

Start date of 5-day interval	Dynamic U-values calculated by data pre-processing methods $[W/(m^2 \cdot K)]$										
	PV 11	PV 12	PV 13	AV0	AV1	AV2	AV3	AV4	AV5	AV6	AV7	AV8
2022-7-17	NA	NA	NA	0.42	0.41	0.39	0.38	0.36	0.33	0.29	0.27	0.23
2022-7-22	NA	NA	NA	0.22	0.20	0.17	0.15	0.14	0.13	0.14	0.16	0.13
2022-7-27	NA	NA	NA	0.23	0.18	0.14	0.11	0.09	0.09	0.12	0.13	0.13
2022-8-1	NA	NA	NA	0.39	0.32	0.29	0.27	0.26	0.26	0.25	0.28	0.31
2022-8-6	NA	NA	NA	0.36	0.35	0.34	0.32	0.31	0.30	0.30	0.29	0.28
2022-8-11	NA	NA	NA	0.61	0.59	0.57	0.55	0.53	0.52	0.50	0.46	0.40
2022-8-16	NA	NA	NA	0.31	0.26	0.23	0.21	0.20	0.19	0.20	0.25	0.29
2022-8-21	NA	NA	NA	0.30	0.27	0.24	0.22	0.21	0.21	0.22	0.22	0.23
2022-8-26	NA	NA	NA	0.39	0.37	0.34	0.32	0.30	0.29	0.28	0.25	0.24
2022-8-31	NA	NA	NA	0.33	0.26	0.21	0.17	0.15	0.13	0.12	0.12	0.16
2022-9-5	NA	NA	NA	0.23	0.20	0.19	0.17	0.15	0.14	0.12	0.09	0.07
2022-9-10	0.04	NA	NA	0.48	0.44	0.41	0.35	0.31	0.27	0.25	0.21	0.18
2022-9-15	0.12	0.12	NA	0.39	0.39	0.37	0.36	0.34	0.30	0.26	0.24	0.23
2022-9-20	0.11	0.07	0.05	0.50	0.49	0.48	0.46	0.41	0.36	0.33	0.31	0.29
2022-9-25	0.24	0.23	0.21	0.48	0.48	0.48	0.48	0.48	0.47	0.44	0.40	0.37
2022-9-30	0.26	0.24	0.24	0.65	0.64	0.64	0.64	0.63	0.59	0.54	0.51	0.47
2022-10-5	0.30	0.29	0.27	0.56	0.56	0.56	0.56	0.54	0.53	0.49	0.45	0.40
2022-10-10	0.39	0.34	0.27	0.62	0.61	0.60	0.60	0.59	0.58	0.56	0.51	0.49
2022-10-15	0.29	0.20	0.16	0.58	0.57	0.56	0.56	0.55	0.54	0.51	0.48	0.45
2022-10-20	NA	NA	NA	0.66	0.66	0.66	0.65	0.65	0.65	0.63	0.60	0.55
2022-10-25	0.39	NA	NA	0.63	0.63	0.63	0.63	0.63	0.60	0.57	0.54	0.48
2022-10-30	0.42	0.44	0.48	0.59	0.59	0.59	0.59	0.59	0.59	0.59	0.56	0.53
2022-11-4	0.72	0.66	0.54	0.86	0.86	0.86	0.86	0.86	0.86	0.86	0.86	0.84
2022-11-9	0.63	0.68	NA	0.78	0.78	0.78	0.78	0.78	0.78	0.78	0.76	0.74
2022-11-14	0.78	0.76	0.70	0.80	0.80	0.80	0.80	0.80	0.80	0.80	0.80	0.80
2022-11-19	0.80	0.77	0.72	0.81	0.81	0.81	0.81	0.81	0.81	0.81	0.81	0.81
2022-11-24	0.85	0.83	0.78	0.91	0.91	0.91	0.91	0.91	0.91	0.91	0.91	0.91
2022-11-29	0.83	0.83	0.81	0.83	0.83	0.83	0.83	0.83	0.83	0.83	0.83	0.83
2022-12-4	0.86	0.86	0.84	0.86	0.86	0.86	0.86	0.86	0.86	0.86	0.86	0.86
2022-12-9	0.90	0.90	0.90	0.90	0.90	0.90	0.90	0.90	0.90	0.90	0.90	0.90

Table B2(2) (continued)

Start date of 5-day interval	Dynamic U-values calculated by data pre-processing methods $[W/(m^2 \cdot K)]$					
	AV9	AV10	AV11	AV12	AV13	TL
2022-7-17	0.17	0.12	0.12	0.12	0.11	0.31
2022-7-22	NA	NA	NA	NA	NA	0.23
2022-7-27	0.13	NA	NA	NA	NA	0.19
2022-8-1	0.35	NA	NA	NA	NA	0.29
2022-8-6	0.28	0.26	0.25	0.23	0.24	0.25
2022-8-11	0.28	0.20	0.20	0.20	0.25	0.41
2022-8-16	0.34	NA	NA	NA	NA	0.26
2022-8-21	0.21	0.20	NA	NA	NA	0.21
2022-8-26	0.22	0.19	NA	NA	NA	0.35
2022-8-31	0.25	NA	NA	NA	NA	0.27
2022-9-5	0.09	NA	NA	NA	NA	0.28
2022-9-10	0.16	0.07	0.04	NA	NA	0.45
2022-9-15	0.21	0.14	0.12	0.12	NA	0.53
2022-9-20	0.25	0.15	0.11	0.07	0.05	0.54
2022-9-25	0.34	0.28	0.24	0.23	0.21	0.52
2022-9-30	0.42	0.31	0.26	0.24	0.24	0.70
2022-10-5	0.37	0.32	0.30	0.29	0.27	0.64
2022-10-10	0.46	0.43	0.39	0.34	0.27	0.73
2022-10-15	0.40	0.37	0.29	0.20	0.16	0.66
2022-10-20	0.51	0.43	NA	NA	NA	0.69
2022-10-25	0.40	0.40	0.39	NA	NA	0.66
2022-10-30	0.50	0.45	0.42	0.44	0.48	0.63
2022-11-4	0.79	0.75	0.72	0.66	0.54	0.88
2022-11-9	0.69	0.65	0.63	0.68	NA	0.76
2022-11-14	0.80	0.79	0.78	0.76	0.70	0.79
2022-11-19	0.81	0.81	0.80	0.77	0.72	0.84
2022-11-24	0.91	0.90	0.85	0.83	0.78	0.84
2022-11-29	0.83	0.83	0.83	0.83	0.81	0.86
2022-12-4	0.86	0.86	0.86	0.86	0.84	0.88
2022-12-9	0.90	0.90	0.90	0.90	0.90	0.88

Table B2(3) Dynamic U-values of the masonry cavity tested envelope with 7-day time intervals

Start date of 7-day interval	Dynamic U-values calculated by data pre-processing methods [W/(m^2 · K)]												
	ND	TD0	TD1	TD2	TD3	TD4	TD5	TD6	TD7	TD8	TD9	TD 10	TD 11
2022-7-17	0.44	0.40	0.40	0.41	0.41	0.39	0.37	0.34	0.34	0.40	0.49	NA	NA
2022-7-24	0.03	0.07	0.05	0.01	0.03	0.05	0.07	0.10	0.13	0.13	0.13	NA	NA
2022-7-31	0.18	0.10	0.13	0.16	0.18	0.20	0.23	0.24	0.27	0.30	0.28	0.27	NA
2022-8-7	0.53	0.57	0.56	0.55	0.54	0.53	0.52	0.52	0.51	0.53	0.53	0.36	NA
2022-8-14	0.31	0.27	0.28	0.29	0.29	0.29	0.32	0.33	0.38	0.35	0.34	NA	NA
2022-8-21	0.18	0.14	0.16	0.17	0.18	0.19	0.21	0.21	0.21	0.22	0.22	0.22	NA
2022-8-28	0.04	0.20	0.17	0.13	0.09	0.06	0.06	0.08	0.07	0.08	0.20	0.16	NA
2022-9-4	0.06	0.18	0.17	0.15	0.14	0.12	0.10	0.09	0.05	0.06	0.09	NA	NA
2022-9-11	0.21	0.40	0.39	0.36	0.31	0.28	0.24	0.21	0.18	0.16	0.15	0.09	0.10
2022-9-18	0.31	0.49	0.49	0.48	0.46	0.42	0.37	0.35	0.33	0.31	0.27	0.18	0.11
2022-9-25	0.37	0.52	0.52	0.52	0.52	0.52	0.51	0.48	0.44	0.41	0.37	0.30	0.24
2022-10-2	0.43	0.58	0.58	0.57	0.57	0.56	0.53	0.49	0.45	0.40	0.36	0.31	0.30
2022-10-9	0.44	0.62	0.61	0.61	0.61	0.60	0.59	0.56	0.51	0.49	0.46	0.42	0.37
2022-10-16	0.50	0.61	0.61	0.60	0.60	0.59	0.59	0.56	0.52	0.47	0.38	0.32	0.25
2022-10-23	0.53	0.63	0.63	0.63	0.62	0.62	0.61	0.59	0.55	0.50	0.43	0.40	0.39
2022-10-30	0.56	0.65	0.65	0.65	0.65	0.65	0.65	0.64	0.62	0.61	0.57	0.54	0.52
2022-11-6	0.79	0.86	0.86	0.86	0.86	0.86	0.86	0.86	0.85	0.83	0.78	0.75	0.74
2022-11-13	0.75	0.77	0.77	0.77	0.77	0.77	0.77	0.77	0.77	0.77	0.77	0.77	0.76
2022-11-20	0.82	0.88	0.88	0.88	0.88	0.88	0.88	0.88	0.88	0.88	0.88	0.87	0.84
2022-11-27	0.79	0.83	0.83	0.83	0.83	0.83	0.83	0.83	0.83	0.83	0.83	0.83	0.82
2022-12-4	0.85	0.90	0.90	0.90	0.90	0.90	0.90	0.90	0.90	0.90	0.90	0.90	0.90
2022-12-11	0.85	0.86	0.86	0.86	0.86	0.86	0.86	0.86	0.86	0.86	0.86	0.86	0.86

Table B2(3) (continued)

Start date of 7-day interval	Dynamic U-values calculated by data pre-processing methods $[W/(m^2 \cdot K)]$												
	TD 12	TD 13	PV0	PV1	PV2	PV3	PV4	PV5	PV6	PV7	PV8	PV9	PV 10
2022-7-17	NA	NA	0.81	0.59	0.39	0.31	0.25	NA	NA	NA	NA	NA	NA
2022-7-24	NA	NA	0.32	0.27	0.20	0.13	0.10	0.06	0.03	0.00	NA	NA	NA
2022-7-31	NA	NA	0.46	0.28	0.18	0.13	0.09	0.01	0.00	NA	NA	NA	NA
2022-8-7	NA	NA	0.32	0.24	0.15	0.13	0.06	0.02	NA	NA	NA	NA	NA
2022-8-14	NA	NA	0.42	0.28	0.19	0.14	0.12	0.05	0.02	0.00	NA	NA	NA
2022-8-21	NA	NA	0.50	0.32	0.19	0.13	0.10	0.04	NA	NA	NA	NA	NA
2022-8-28	NA	NA	0.45	0.40	0.35	0.29	0.24	0.22	0.21	0.21	0.21	0.25	0.16
2022-9-4	NA	NA	0.26	0.24	0.23	0.21	0.19	0.17	0.16	0.13	0.05	NA	NA
2022-9-11	0.12	NA	0.40	0.39	0.36	0.31	0.28	0.24	0.21	0.18	0.16	0.15	0.09
2022-9-18	0.07	0.05	0.49	0.49	0.48	0.46	0.42	0.37	0.35	0.33	0.31	0.27	0.18
2022-9-25	0.24	0.23	0.52	0.52	0.52	0.52	0.52	0.51	0.48	0.44	0.41	0.37	0.30
2022-10-2	0.29	0.29	0.58	0.58	0.57	0.57	0.56	0.53	0.49	0.45	0.40	0.36	0.31
2022-10-9	0.32	0.27	0.62	0.61	0.61	0.61	0.60	0.59	0.56	0.51	0.49	0.46	0.42
2022-10-16	0.20	0.16	0.61	0.61	0.60	0.60	0.59	0.59	0.56	0.52	0.47	0.38	0.32
2022-10-23	NA	NA	0.63	0.63	0.63	0.62	0.62	0.61	0.59	0.55	0.50	0.43	0.40
2022-10-30	0.49	0.49	0.65	0.65	0.65	0.65	0.65	0.65	0.64	0.62	0.61	0.57	0.54
2022-11-6	0.74	0.62	0.86	0.86	0.86	0.86	0.86	0.86	0.86	0.85	0.83	0.78	0.75
2022-11-13	0.75	0.71	0.77	0.77	0.77	0.77	0.77	0.77	0.77	0.77	0.77	0.77	0.77
2022-11-20	0.81	0.75	0.88	0.88	0.88	0.88	0.88	0.88	0.88	0.88	0.88	0.88	0.87
2022-11-27	0.81	0.80	0.83	0.83	0.83	0.83	0.83	0.83	0.83	0.83	0.83	0.83	0.83
2022-12-4	0.89	0.88	0.90	0.90	0.90	0.90	0.90	0.90	0.90	0.90	0.90	0.90	0.90
2022-12-11	0.86	0.86	0.86	0.86	0.86	0.86	0.86	0.86	0.86	0.86	0.86	0.86	0.86

Table B2(3) (continued)

Start date of 7-day interval	Dynamic U-values calculated by data pre-processing methods $[W/(m^2 \cdot K)]$											
	PV 11	PV 12	PV 13	AV0	AV1	AV2	AV3	AV4	AV5	AV6	AV7	AV8
2022-7-17	NA	NA	NA	0.38	0.36	0.34	0.33	0.31	0.29	0.26	0.25	0.23
2022-7-24	NA	NA	NA	0.21	0.18	0.15	0.11	0.10	0.09	0.11	0.13	0.13
2022-7-31	NA	NA	NA	0.36	0.30	0.27	0.24	0.24	0.24	0.24	0.27	0.30
2022-8-7	NA	NA	NA	0.46	0.45	0.44	0.42	0.41	0.40	0.39	0.37	0.35
2022-8-14	NA	NA	NA	0.42	0.38	0.35	0.33	0.31	0.31	0.31	0.34	0.31
2022-8-21	NA	NA	NA	0.31	0.28	0.26	0.25	0.24	0.24	0.24	0.23	0.23
2022-8-28	NA	NA	NA	0.38	0.33	0.29	0.25	0.22	0.21	0.19	0.17	0.20
2022-9-4	NA	NA	NA	0.26	0.23	0.21	0.20	0.18	0.16	0.14	0.11	0.07
2022-9-11	0.10	0.12	NA	0.41	0.39	0.36	0.31	0.28	0.24	0.21	0.18	0.16
2022-9-18	0.11	0.07	0.05	0.49	0.49	0.48	0.46	0.42	0.37	0.35	0.33	0.31
2022-9-25	0.24	0.24	0.23	0.52	0.52	0.52	0.52	0.52	0.51	0.48	0.44	0.41
2022-10-2	0.30	0.29	0.29	0.58	0.58	0.57	0.57	0.56	0.53	0.49	0.45	0.40
2022-10-9	0.37	0.32	0.27	0.62	0.62	0.61	0.61	0.60	0.59	0.56	0.51	0.49
2022-10-16	0.25	0.20	0.16	0.62	0.61	0.60	0.60	0.59	0.59	0.56	0.52	0.47
2022-10-23	0.39	NA	NA	0.63	0.63	0.63	0.62	0.62	0.61	0.59	0.55	0.50
2022-10-30	0.52	0.49	0.49	0.65	0.65	0.65	0.65	0.65	0.65	0.64	0.62	0.61
2022-11-6	0.74	0.74	0.62	0.86	0.86	0.86	0.86	0.86	0.86	0.86	0.85	0.83
2022-11-13	0.76	0.75	0.71	0.77	0.77	0.77	0.77	0.77	0.77	0.77	0.77	0.77
2022-11-20	0.84	0.81	0.75	0.88	0.88	0.88	0.88	0.88	0.88	0.88	0.88	0.88
2022-11-27	0.82	0.81	0.80	0.83	0.83	0.83	0.83	0.83	0.83	0.83	0.83	0.83
2022-12-4	0.90	0.89	0.88	0.90	0.90	0.90	0.90	0.90	0.90	0.90	0.90	0.90
2022-12-11	0.86	0.86	0.86	0.86	0.86	0.86	0.86	0.86	0.86	0.86	0.86	0.86

Table B2(3) (continued)

Start date of 7-day interval	Dynamic U-values calculated by data pre-processing methods $[W/(m^2 \cdot K)]$					
	AV9	AV10	AV11	AV12	AV13	TL
2022-7-17	0.17	0.12	0.12	0.12	0.11	0.30
2022-7-24	0.13	NA	NA	NA	NA	0.19
2022-7-31	0.28	0.27	NA	NA	NA	0.27
2022-8-7	0.30	0.24	0.23	0.21	0.25	0.31
2022-8-14	0.25	0.15	0.13	NA	NA	0.32
2022-8-21	0.22	0.22	NA	NA	NA	0.21
2022-8-28	0.24	0.16	NA	NA	NA	0.38
2022-9-4	0.09	NA	NA	NA	NA	0.34
2022-9-11	0.15	0.09	0.10	0.12	NA	0.42
2022-9-18	0.27	0.18	0.11	0.07	0.05	0.56
2022-9-25	0.37	0.30	0.24	0.24	0.23	0.60
2022-10-2	0.36	0.31	0.30	0.29	0.29	0.62
2022-10-9	0.46	0.42	0.37	0.32	0.27	0.73
2022-10-16	0.38	0.32	0.25	0.20	0.16	0.67
2022-10-23	0.43	0.40	0.39	NA	NA	0.64
2022-10-30	0.57	0.54	0.52	0.49	0.49	0.69
2022-11-6	0.78	0.75	0.74	0.74	0.62	0.83
2022-11-13	0.77	0.77	0.76	0.75	0.71	0.79
2022-11-20	0.88	0.87	0.84	0.81	0.75	0.89
2022-11-27	0.83	0.83	0.82	0.81	0.80	0.81
2022-12-4	0.90	0.90	0.90	0.89	0.88	0.89
2022-12-11	0.86	0.86	0.86	0.86	0.86	0.85

Table B2(4) Dynamic U-values of the masonry cavity tested envelope with 10-day time intervals

Start date of 10-day interval	Dynamic U-values calculated by data pre-processing methods [W/(m² · K)]											
	ND	TD0	TD1	TD2	TD3	TD4	TD5	TD6	TD7	TD8	TD9	TD 10	TD 11
2022-7-17	0.30	0.23	0.23	0.25	0.27	0.27	0.27	0.26	0.28	0.29	0.49	NA	NA
2022-7-27	0.11	0.03	0.08	0.11	0.13	0.15	0.17	0.21	0.23	0.28	0.26	NA	NA
2022-8-6	0.53	0.58	0.56	0.56	0.54	0.54	0.53	0.53	0.51	0.50	0.44	0.31	NA
2022-8-16	0.17	0.11	0.13	0.15	0.16	0.17	0.19	0.21	0.24	0.27	0.31	0.20	NA
2022-8-26	0.00	0.14	0.12	0.08	0.05	0.03	0.02	0.02	0.01	0.01	0.06	0.01	NA
2022-9-5	0.14	0.29	0.28	0.26	0.22	0.19	0.17	0.15	0.11	0.08	0.10	0.07	0.04
2022-9-15	0.26	0.44	0.44	0.42	0.41	0.37	0.33	0.30	0.28	0.26	0.23	0.15	0.12
2022-9-25	0.39	0.56	0.56	0.55	0.55	0.55	0.52	0.49	0.45	0.41	0.37	0.29	0.25
2022-10-5	0.43	0.58	0.58	0.58	0.58	0.57	0.56	0.53	0.48	0.45	0.42	0.38	0.35
2022-10-15	0.50	0.61	0.61	0.61	0.60	0.60	0.59	0.57	0.54	0.49	0.43	0.37	0.29
2022-10-25	0.52	0.61	0.61	0.61	0.61	0.61	0.60	0.58	0.55	0.51	0.47	0.44	0.41
2022-11-4	0.74	0.82	0.82	0.82	0.82	0.82	0.82	0.82	0.81	0.79	0.74	0.71	0.69
2022-11-14	0.76	0.80	0.80	0.80	0.80	0.80	0.80	0.80	0.80	0.80	0.80	0.80	0.79
2022-11-24	0.82	0.87	0.87	0.87	0.87	0.87	0.87	0.87	0.87	0.87	0.86	0.86	0.84
2022-12-4	0.85	0.88	0.88	0.88	0.88	0.88	0.88	0.88	0.88	0.88	0.88	0.88	0.88

Table B2(4) (continued)

Start date of 10-day interval	Dynamic U-values calculated by data pre-processing methods [W/(m² · K)]											
	TD 12	TD 13	PV0	PV1	PV2	PV3	PV4	PV5	PV6	PV7	PV8	PV9	PV 10
2022-7-17	NA	NA	0.40	0.35	0.25	0.17	0.12	0.07	0.03	0.00	NA	NA	NA
2022-7-27	NA	NA	0.38	0.24	0.15	0.11	0.07	0.03	0.00	NA	NA	NA	NA
2022-8-6	NA	NA	0.40	0.36	0.21	0.13	0.05	0.02	NA	NA	NA	NA	NA
2022-8-16	NA	NA	0.43	0.29	0.20	0.14	0.12	0.05	0.02	0.00	NA	NA	NA
2022-8-26	NA	NA	0.42	0.37	0.32	0.26	0.22	0.21	0.19	0.21	0.21	0.25	0.16
2022-9-5	NA	NA	0.37	0.35	0.33	0.28	0.25	0.22	0.20	0.17	0.17	0.16	0.07
2022-9-15	0.11	0.05	0.44	0.44	0.42	0.41	0.37	0.33	0.30	0.28	0.26	0.23	0.15
2022-9-25	0.24	0.23	0.56	0.56	0.55	0.55	0.55	0.52	0.49	0.45	0.41	0.37	0.29
2022-10-5	0.31	0.27	0.58	0.58	0.58	0.58	0.57	0.56	0.53	0.48	0.45	0.42	0.38
2022-10-15	0.20	0.16	0.61	0.61	0.61	0.60	0.60	0.59	0.57	0.54	0.49	0.43	0.37
2022-10-25	0.44	0.48	0.61	0.61	0.61	0.61	0.61	0.60	0.58	0.55	0.51	0.47	0.44
2022-11-4	0.67	0.54	0.82	0.82	0.82	0.82	0.82	0.82	0.82	0.81	0.79	0.74	0.71
2022-11-14	0.77	0.72	0.80	0.80	0.80	0.80	0.80	0.80	0.80	0.80	0.80	0.80	0.80
2022-11-24	0.83	0.80	0.87	0.87	0.87	0.87	0.87	0.87	0.87	0.87	0.87	0.86	0.86
2022-12-4	0.88	0.88	0.88	0.88	0.88	0.88	0.88	0.88	0.88	0.88	0.88	0.88	0.88

Table B2(4) (continued)

Start date of 10-day interval	Dynamic U-values calculated by data pre-processing methods $[W/(m^2 \cdot K)]$											
	PV 11	PV 12	PV 13	AV0	AV1	AV2	AV3	AV4	AV5	AV6	AV7	AV8
2022-7-17	NA	NA	NA	0.33	0.31	0.29	0.28	0.26	0.24	0.22	0.23	0.21
2022-7-27	NA	NA	NA	0.31	0.25	0.22	0.19	0.18	0.19	0.21	0.23	0.28
2022-8-6	NA	NA	NA	0.49	0.47	0.46	0.44	0.43	0.41	0.40	0.38	0.34
2022-8-16	NA	NA	NA	0.30	0.26	0.23	0.22	0.20	0.20	0.21	0.24	0.27
2022-8-26	NA	NA	NA	0.36	0.32	0.28	0.25	0.23	0.22	0.20	0.19	0.21
2022-9-5	0.04	NA	NA	0.35	0.32	0.30	0.26	0.23	0.20	0.18	0.15	0.13
2022-9-15	0.12	0.11	0.05	0.44	0.44	0.42	0.41	0.37	0.33	0.30	0.28	0.26
2022-9-25	0.25	0.24	0.23	0.56	0.56	0.55	0.55	0.55	0.52	0.49	0.45	0.41
2022-10-5	0.35	0.31	0.27	0.59	0.58	0.58	0.58	0.57	0.56	0.53	0.48	0.45
2022-10-15	0.29	0.20	0.16	0.62	0.61	0.61	0.60	0.60	0.59	0.57	0.54	0.49
2022-10-25	0.41	0.44	0.48	0.61	0.61	0.61	0.61	0.61	0.60	0.58	0.55	0.51
2022-11-4	0.69	0.67	0.54	0.82	0.82	0.82	0.82	0.82	0.82	0.82	0.81	0.79
2022-11-14	0.79	0.77	0.72	0.80	0.80	0.80	0.80	0.80	0.80	0.80	0.80	0.80
2022-11-24	0.84	0.83	0.80	0.87	0.87	0.87	0.87	0.87	0.87	0.87	0.87	0.87
2022-12-4	0.88	0.88	0.88	0.88	0.88	0.88	0.88	0.88	0.88	0.88	0.88	0.88

Table B2(4) (continued)

Start date of 10-day interval	Dynamic U-values calculated by data pre-processing methods $[W/(m^2 \cdot K)]$					
	AV9	AV10	AV11	AV12	AV13	TL
2022-7-17	0.17	0.12	0.12	0.12	0.11	0.28
2022-7-27	0.26	NA	NA	NA	NA	0.25
2022-8-6	0.28	0.23	0.22	0.21	0.25	0.32
2022-8-16	0.31	0.20	NA	NA	NA	0.23
2022-8-26	0.23	0.19	NA	NA	NA	0.32
2022-9-5	0.14	0.07	0.04	NA	NA	0.37
2022-9-15	0.23	0.15	0.12	0.11	0.05	0.53
2022-9-25	0.37	0.29	0.25	0.24	0.23	0.60
2022-10-5	0.42	0.38	0.35	0.31	0.27	0.68
2022-10-15	0.43	0.37	0.29	0.20	0.16	0.67
2022-10-25	0.47	0.44	0.41	0.44	0.48	0.64
2022-11-4	0.74	0.71	0.69	0.67	0.54	0.82
2022-11-14	0.80	0.80	0.79	0.77	0.72	0.82
2022-11-24	0.86	0.86	0.84	0.83	0.80	0.85
2022-12-4	0.88	0.88	0.88	0.88	0.88	0.88

Table B2(5) Dynamic U-values of the masonry cavity tested envelope with 14-day time intervals

Start date of 14-day interval	Dynamic U-values calculated by data pre-processing methods [W/(m² · K)]											
	ND	TD0	TD1	TD2	TD3	TD4	TD5	TD6	TD7	TD8	TD9	TD 10	TD 11
2022-7-17	0.22	0.16	0.17	0.19	0.22	0.22	0.23	0.23	0.26	0.28	0.45	NA	NA
2022-7-31	0.36	0.32	0.34	0.35	0.35	0.37	0.39	0.39	0.40	0.42	0.43	0.31	NA
2022-8-14	0.25	0.20	0.22	0.23	0.24	0.24	0.26	0.27	0.30	0.29	0.27	0.22	NA
2022-8-28	0.05	0.19	0.17	0.14	0.12	0.09	0.08	0.08	0.06	0.03	0.11	0.16	NA
2022-9-11	0.26	0.45	0.44	0.42	0.39	0.36	0.31	0.28	0.26	0.24	0.21	0.13	0.10
2022-9-25	0.40	0.55	0.55	0.55	0.55	0.54	0.52	0.48	0.45	0.41	0.37	0.30	0.27
2022-10-9	0.46	0.61	0.61	0.61	0.60	0.60	0.59	0.56	0.52	0.48	0.43	0.40	0.35
2022-10-23	0.55	0.64	0.64	0.64	0.64	0.64	0.63	0.62	0.60	0.57	0.53	0.52	0.52
2022-11-6	0.77	0.82	0.82	0.82	0.82	0.82	0.82	0.82	0.81	0.80	0.78	0.76	0.75
2022-11-20	0.81	0.85	0.85	0.85	0.85	0.85	0.85	0.85	0.85	0.85	0.85	0.85	0.83
2022-12-4	0.85	0.88	0.88	0.88	0.88	0.88	0.88	0.88	0.88	0.88	0.88	0.88	0.88

Table B2(5) (continued)

Start date of 14-day interval	Dynamic U-values calculated by data pre-processing methods [W/(m² · K)]											
	TD 12	TD 13	PV0	PV1	PV2	PV3	PV4	PV5	PV6	PV7	PV8	PV9	PV 10
2022-7-17	NA	NA	0.37	0.30	0.21	0.14	0.10	0.06	0.03	0.00	NA	NA	NA
2022-7-31	NA	NA	0.45	0.28	0.18	0.13	0.08	0.01	0.00	NA	NA	NA	NA
2022-8-14	NA	NA	0.45	0.30	0.19	0.14	0.11	0.05	0.02	0.00	NA	NA	NA
2022-8-28	NA	NA	0.34	0.31	0.28	0.24	0.21	0.19	0.18	0.17	0.20	0.25	0.16
2022-9-11	0.11	0.05	0.45	0.44	0.42	0.39	0.36	0.31	0.28	0.26	0.24	0.21	0.13
2022-9-25	0.26	0.25	0.55	0.55	0.55	0.55	0.54	0.52	0.48	0.45	0.41	0.37	0.30
2022-10-9	0.30	0.25	0.61	0.61	0.61	0.60	0.60	0.59	0.56	0.52	0.48	0.43	0.40
2022-10-23	0.49	0.49	0.64	0.64	0.64	0.64	0.64	0.63	0.62	0.60	0.57	0.53	0.52
2022-11-6	0.75	0.69	0.82	0.82	0.82	0.82	0.82	0.82	0.82	0.81	0.80	0.78	0.76
2022-11-20	0.81	0.78	0.85	0.85	0.85	0.85	0.85	0.85	0.85	0.85	0.85	0.85	0.85
2022-12-4	0.88	0.88	0.88	0.88	0.88	0.88	0.88	0.88	0.88	0.88	0.88	0.88	0.88

Table B2(5) (continued)

Start date of 14-day interval	Dynamic U-values calculated by data pre-processing methods $[W/(m^2 \cdot K)]$											
	PV 11	PV 12	PV 13	AV0	AV1	AV2	AV3	AV4	AV5	AV6	AV7	AV8
2022-7-17	NA	NA	NA	0.31	0.28	0.26	0.24	0.22	0.21	0.21	0.21	0.20
2022-7-31	NA	NA	NA	0.42	0.39	0.37	0.36	0.35	0.35	0.34	0.34	0.34
2022-8-14	NA	NA	NA	0.37	0.33	0.30	0.29	0.27	0.28	0.28	0.29	0.28
2022-8-28	NA	NA	NA	0.32	0.28	0.25	0.22	0.20	0.18	0.16	0.14	0.15
2022-9-11	0.10	0.11	0.05	0.46	0.44	0.42	0.39	0.36	0.31	0.28	0.26	0.24
2022-9-25	0.27	0.26	0.25	0.55	0.55	0.55	0.55	0.54	0.52	0.48	0.45	0.41
2022-10-9	0.35	0.30	0.25	0.62	0.62	0.61	0.60	0.60	0.59	0.56	0.52	0.48
2022-10-23	0.52	0.49	0.49	0.64	0.64	0.64	0.64	0.64	0.63	0.62	0.60	0.57
2022-11-6	0.75	0.75	0.69	0.82	0.82	0.82	0.82	0.82	0.82	0.82	0.81	0.80
2022-11-20	0.83	0.81	0.78	0.85	0.85	0.85	0.85	0.85	0.85	0.85	0.85	0.85
2022-12-4	0.88	0.88	0.88	0.88	0.88	0.88	0.88	0.88	0.88	0.88	0.88	0.88

Table B2(5) (continued)

Start date of 14-day interval	Dynamic U-values calculated by data pre-processing methods $[W/(m^2 \cdot K)]$					
	AV9	AV10	AV11	AV12	AV13	TL
2022-7-17	0.17	0.12	0.12	0.12	0.11	0.26
2022-7-31	0.30	0.24	0.23	0.21	0.25	0.30
2022-8-14	0.24	0.17	0.13	NA	NA	0.26
2022-8-28	0.19	0.16	NA	NA	NA	0.36
2022-9-11	0.21	0.13	0.10	0.11	0.05	0.49
2022-9-25	0.37	0.30	0.27	0.26	0.25	0.61
2022-10-9	0.43	0.40	0.35	0.30	0.25	0.70
2022-10-23	0.53	0.52	0.52	0.49	0.49	0.67
2022-11-6	0.78	0.76	0.75	0.75	0.69	0.81
2022-11-20	0.85	0.85	0.83	0.81	0.78	0.85
2022-12-4	0.88	0.88	0.88	0.88	0.88	0.88

Table B2(6) Dynamic U-values of the masonry cavity tested envelope with 20-day time intervals

Start date of 20-day interval	Dynamic U-values calculated by data pre-processing methods [W/(m² · K)]												
	ND	TD0	TD1	TD2	TD3	TD4	TD5	TD6	TD7	TD8	TD9	TD 10	TD 11
2022-7-17	0.21	0.14	0.16	0.18	0.21	0.22	0.23	0.24	0.26	0.29	0.43	NA	NA
2022-8-6	0.35	0.31	0.32	0.33	0.33	0.33	0.35	0.36	0.39	0.40	0.39	0.29	NA
2022-8-26	0.07	0.22	0.20	0.18	0.14	0.12	0.10	0.09	0.07	0.05	0.09	0.06	0.04
2022-9-15	0.33	0.50	0.50	0.49	0.49	0.47	0.44	0.40	0.37	0.34	0.31	0.24	0.20
2022-10-5	0.46	0.60	0.60	0.59	0.59	0.58	0.57	0.55	0.51	0.47	0.42	0.38	0.34
2022-10-25	0.64	0.72	0.72	0.72	0.72	0.72	0.72	0.72	0.70	0.69	0.65	0.64	0.63
2022-11-14	0.80	0.84	0.84	0.84	0.84	0.84	0.84	0.84	0.84	0.84	0.84	0.83	0.81
2022-12-4	0.85	0.88	0.88	0.88	0.88	0.88	0.88	0.88	0.88	0.88	0.88	0.88	0.88

Table B2(6) (continued)

Start date of 20-day interval	Dynamic U-values calculated by data pre-processing methods [W/(m² · K)]												
	TD 12	TD 13	PV0	PV1	PV2	PV3	PV4	PV5	PV6	PV7	PV8	PV9	PV 10
2022-7-17	NA	NA	0.39	0.29	0.20	0.14	0.10	0.06	0.03	0.00	NA	NA	NA
2022-8-6	NA	NA	0.43	0.30	0.20	0.14	0.11	0.05	0.02	0.00	NA	NA	NA
2022-8-26	NA	NA	0.38	0.36	0.32	0.27	0.24	0.22	0.20	0.19	0.19	0.19	0.08
2022-9-15	0.21	0.22	0.50	0.50	0.49	0.49	0.47	0.44	0.40	0.37	0.34	0.31	0.24
2022-10-5	0.30	0.26	0.60	0.60	0.59	0.59	0.58	0.57	0.55	0.51	0.47	0.42	0.38
2022-10-25	0.62	0.53	0.72	0.72	0.72	0.72	0.72	0.72	0.72	0.70	0.69	0.65	0.64
2022-11-14	0.80	0.78	0.84	0.84	0.84	0.84	0.84	0.84	0.84	0.84	0.84	0.84	0.83
2022-12-4	0.88	0.88	0.88	0.88	0.88	0.88	0.88	0.88	0.88	0.88	0.88	0.88	0.88

Table B2(6) (continued)

Start date of 30-day interval	Dynamic U-values calculated by data pre-processing methods [W/(m² · K)]											
	PV 11	PV 12	PV 13	AV0	AV1	AV2	AV3	AV4	AV5	AV6	AV7	AV8
2022-7-17	NA	NA	NA	0.32	0.29	0.26	0.24	0.23	0.22	0.22	0.23	0.23
2022-8-6	NA	NA	NA	0.41	0.38	0.36	0.34	0.33	0.33	0.33	0.34	0.33
2022-8-26	0.04	NA	NA	0.36	0.32	0.29	0.25	0.23	0.21	0.19	0.17	0.17
2022-9-15	0.20	0.21	0.22	0.50	0.50	0.49	0.49	0.47	0.44	0.40	0.37	0.34
2022-10-5	0.34	0.30	0.26	0.60	0.60	0.59	0.59	0.58	0.57	0.55	0.51	0.47
2022-10-25	0.63	0.62	0.53	0.72	0.72	0.72	0.72	0.72	0.72	0.72	0.70	0.69
2022-11-14	0.81	0.80	0.78	0.84	0.84	0.84	0.84	0.84	0.84	0.84	0.84	0.84
2022-12-4	0.88	0.88	0.88	0.88	0.88	0.88	0.88	0.88	0.88	0.88	0.88	0.88

Table B2(6) (continued)

Start date of 20-day interval	Dynamic U-values calculated by data pre-processing methods [W/(m² · K)]					
	AV9	AV10	AV11	AV12	AV13	TL
2022-7-17	0.18	0.12	0.12	0.12	0.11	0.27
2022-8-6	0.28	0.23	0.22	0.21	0.25	0.29
2022-8-26	0.18	0.09	0.04	NA	NA	0.34
2022-9-15	0.31	0.24	0.20	0.21	0.22	0.57
2022-10-5	0.42	0.38	0.34	0.30	0.26	0.68
2022-10-25	0.65	0.64	0.63	0.62	0.53	0.74
2022-11-14	0.84	0.83	0.81	0.80	0.78	0.83
2022-12-4	0.88	0.88	0.88	0.88	0.88	0.88

Table B2(7) Dynamic U-values of the masonry cavity tested envelope with 30-day time intervals

Start date of 30-day interval	Dynamic U-values calculated by data pre-processing methods [W/(m² · K)]												
	ND	TD0	TD1	TD2	TD3	TD4	TD5	TD6	TD7	TD8	TD9	TD 10	TD 11
2022-7-17	0.33	0.28	0.29	0.30	0.32	0.32	0.34	0.35	0.37	0.39	0.44	0.31	NA
2022-8-16	0.00	0.13	0.10	0.08	0.05	0.03	0.02	0.01	0.00	0.02	0.04	0.06	0.04
2022-9-15	0.36	0.53	0.53	0.52	0.52	0.50	0.48	0.45	0.41	0.38	0.35	0.31	0.28
2022-10-15	0.60	0.69	0.69	0.69	0.69	0.69	0.68	0.67	0.65	0.64	0.60	0.59	0.59
2022-11-14	0.82	0.85	0.85	0.85	0.85	0.85	0.85	0.85	0.85	0.85	0.85	0.85	0.84

Table B2(7) (continued)

Start date of 30-day interval	Dynamic U-values calculated by data pre-processing methods [W/(m² · K)]												
	TD 12	TD 13	PV0	PV1	PV2	PV3	PV4	PV5	PV6	PV7	PV8	PV9	PV 10
2022-7-17	NA	NA	0.39	0.29	0.20	0.14	0.10	0.05	0.03	0.00	NA	NA	NA
2022-8-16	NA	NA	0.39	0.35	0.31	0.26	0.23	0.21	0.20	0.18	0.19	0.19	0.08
2022-9-15	0.27	0.26	0.53	0.53	0.52	0.52	0.50	0.48	0.45	0.41	0.38	0.35	0.31
2022-10-15	0.57	0.48	0.69	0.69	0.69	0.69	0.69	0.68	0.67	0.65	0.64	0.60	0.59
2022-11-14	0.84	0.83	0.85	0.85	0.85	0.85	0.85	0.85	0.85	0.85	0.85	0.85	0.85

Table B2(7) (continued)

Start date of 30-day interval	Dynamic U-values calculated by data pre-processing methods $[W/(m^2 \cdot K)]$											
	PV 11	PV 12	PV 13	AV0	AV1	AV2	AV3	AV4	AV5	AV6	AV7	AV8
2022-7-17	NA	NA	NA	0.39	0.36	0.34	0.32	0.31	0.31	0.30	0.31	0.29
2022-8-16	0.04	NA	NA	0.34	0.30	0.27	0.24	0.22	0.21	0.19	0.18	0.19
2022-9-15	0.28	0.27	0.26	0.53	0.53	0.52	0.52	0.50	0.48	0.45	0.41	0.38
2022-10-15	0.59	0.57	0.48	0.69	0.69	0.69	0.69	0.69	0.68	0.67	0.65	0.64
2022-11-14	0.84	0.84	0.83	0.85	0.85	0.85	0.85	0.85	0.85	0.85	0.85	0.85

Table B2(7) (continued)

Start date of 30-day interval	Dynamic U-values calculated by data pre-processing methods $[W/(m^2 \cdot K)]$					
	AV9	AV10	AV11	AV12	AV13	TL
2022-7-17	0.24	0.19	0.17	0.15	0.13	0.29
2022-8-16	0.19	0.09	0.04	NA	NA	0.30
2022-9-15	0.35	0.31	0.28	0.27	0.26	0.61
2022-10-15	0.60	0.59	0.59	0.57	0.48	0.72
2022-11-14	0.85	0.85	0.84	0.84	0.83	0.85

Table B2(8) Dynamic U-values of the masonry cavity tested envelope with 40-day time intervals

Start date of 40-day interval	Dynamic U-values calculated by data pre-processing methods $[W/(m^2 \cdot K)]$												
	ND	TD0	TD1	TD2	TD3	TD4	TD5	TD6	TD7	TD8	TD9	TD 10	TD 11
2022-7-17	0.28	0.23	0.24	0.26	0.27	0.28	0.29	0.31	0.33	0.35	0.40	0.29	NA
2022-8-26	0.22	0.39	0.38	0.37	0.35	0.33	0.31	0.29	0.28	0.27	0.27	0.22	0.19
2022-10-5	0.55	0.66	0.66	0.66	0.66	0.66	0.65	0.64	0.61	0.59	0.55	0.52	0.50
2022-11-14	0.82	0.85	0.85	0.85	0.85	0.85	0.85	0.85	0.85	0.85	0.85	0.85	0.84

Table B2(8) (continued)

Start date of 40-day interval	Dynamic U-values calculated by data pre-processing methods $[W/(m^2 \cdot K)]$												
	TD 12	TD 13	PV0	PV1	PV2	PV3	PV4	PV5	PV6	PV7	PV8	PV9	PV 10
2022-7-17	NA	NA	0.40	0.29	0.20	0.14	0.10	0.05	0.02	0.00	NA	NA	NA
2022-8-26	0.21	0.22	0.46	0.46	0.44	0.42	0.40	0.37	0.35	0.33	0.32	0.29	0.22
2022-10-5	0.47	0.39	0.66	0.66	0.66	0.66	0.66	0.65	0.64	0.61	0.59	0.55	0.52
2022-11-14	0.84	0.83	0.85	0.85	0.85	0.85	0.85	0.85	0.85	0.85	0.85	0.85	0.85

Table B2(8) (continued)

Start date of 40-day interval	Dynamic U-values calculated by data pre-processing methods [W/(m² · K)]											
	PV 11	PV 12	PV 13	AV0	AV1	AV2	AV3	AV4	AV5	AV6	AV7	AV8
2022-7-17	NA	NA	NA	0.37	0.34	0.31	0.30	0.29	0.28	0.28	0.29	0.29
2022-8-26	0.19	0.21	0.22	0.44	0.43	0.41	0.39	0.37	0.35	0.33	0.31	0.30
2022-10-5	0.50	0.47	0.39	0.66	0.66	0.66	0.66	0.66	0.65	0.64	0.61	0.59
2022-11-14	0.84	0.84	0.83	0.85	0.85	0.85	0.85	0.85	0.85	0.85	0.85	0.85

Table B2(8) (continued)

Start date of 40-day interval	Dynamic U-values calculated by data pre-processing methods [W/(m² · K)]					
	AV9	AV10	AV11	AV12	AV13	TL
2022-7-17	0.25	0.19	0.17	0.15	0.13	0.28
2022-8-26	0.28	0.22	0.19	0.21	0.22	0.47
2022-10-5	0.55	0.52	0.50	0.47	0.39	0.71
2022-11-14	0.85	0.85	0.84	0.84	0.83	0.85

Table B2(9) Dynamic U-values of the masonry cavity tested envelope with 50-day time intervals

Start date of 50-day interval	Dynamic U-values calculated by data pre-processing methods [W/(m² · K)]											
	ND	TD0	TD1	TD2	TD3	TD4	TD5	TD6	TD7	TD8	TD9	TD 10	TD 11
2022-7-17	0.22	0.14	0.16	0.18	0.19	0.20	0.21	0.22	0.24	0.24	0.17	0.16	NA
2022-9-5	0.35	0.51	0.51	0.50	0.50	0.48	0.47	0.44	0.41	0.38	0.35	0.31	0.27
2022-10-25	0.76	0.81	0.81	0.81	0.81	0.81	0.81	0.81	0.81	0.81	0.81	0.81	0.81

Table B2(9) (continued)

Start date of 50-day interval	Dynamic U-values calculated by data pre-processing methods [W/(m² · K)]												
	TD 12	TD 13	PV0	PV1	PV2	PV3	PV4	PV5	PV6	PV7	PV8	PV9	PV 10
2022-7-17	NA	NA	0.41	0.33	0.27	0.21	0.18	0.17	0.18	0.21	0.21	0.25	0.16
2022-9-5	0.26	0.25	0.53	0.53	0.52	0.51	0.50	0.48	0.45	0.42	0.40	0.36	0.31
2022-10-25	0.82	0.82	0.81	0.81	0.81	0.81	0.81	0.81	0.81	0.81	0.81	0.81	0.81

Table B2(9) (continued)

Start date of 50-day interval	Dynamic U-values calculated by data pre-processing methods $[W/(m^2 \cdot K)]$											
	PV 11	PV 12	PV 13	AV0	AV1	AV2	AV3	AV4	AV5	AV6	AV7	AV8
2022-7-17	NA	NA	NA	0.37	0.33	0.31	0.29	0.27	0.27	0.26	0.27	0.27
2022-9-5	0.27	0.26	0.25	0.52	0.52	0.51	0.50	0.49	0.47	0.44	0.41	0.39
2022-10-25	0.81	0.82	0.82	0.81	0.81	0.81	0.81	0.81	0.81	0.81	0.81	0.81

Table B2(9) (continued)

Start date of 50-day interval	Dynamic U-values calculated by data pre-processing methods $[W/(m^2 \cdot K)]$					
	AV9	AV10	AV11	AV12	AV13	TL
2022-7-17	0.25	0.19	0.17	0.15	0.13	0.29
2022-9-5	0.35	0.31	0.27	0.26	0.25	0.59
2022-10-25	0.81	0.81	0.81	0.82	0.82	0.81

Table B3(1) Dynamic U-values of the RC tested envelope with 3-day time intervals

Start date of 3-day interval	Dynamic U-values calculated by data pre-processing methods $[W/(m^2 \cdot K)]$												
	ND	TD0	TD1	TD2	TD3	TD4	TD5	TD6	TD7	TD8	TD9	TD10	TD11
2023-2-2	0.32	0.36	0.36	0.36	0.36	0.36	0.36	0.36	0.36	0.36	0.36	0.36	0.36
2023-2-5	0.32	0.36	0.36	0.36	0.36	0.36	0.36	0.36	0.36	0.36	0.36	0.36	0.36
2023-2-8	0.34	0.38	0.38	0.38	0.38	0.38	0.38	0.38	0.38	0.38	0.38	0.38	0.38
2023-2-11	0.28	0.31	0.31	0.31	0.31	0.31	0.31	0.31	0.31	0.31	0.31	0.31	0.31
2023-3-3	0.26	0.34	0.34	0.34	0.34	0.34	0.34	0.34	0.34	0.34	0.34	0.34	0.33
2023-3-6	0.25	0.31	0.31	0.31	0.31	0.31	0.31	0.31	0.31	0.31	0.31	0.31	0.31
2023-3-9	0.26	0.34	0.34	0.34	0.34	0.34	0.34	0.34	0.34	0.34	0.33	0.32	0.32
2023-3-12	0.24	0.29	0.29	0.29	0.29	0.29	0.29	0.29	0.29	0.29	0.29	0.29	0.29
2023-4-3	0.17	0.23	0.23	0.23	0.23	0.23	0.23	0.23	0.23	0.23	0.22	0.22	0.22
2023-4-6	0.21	0.28	0.28	0.28	0.28	0.28	0.28	0.28	0.28	0.28	0.28	0.28	0.28
2023-4-9	0.33	0.43	0.43	0.43	0.41	0.38	0.38	0.35	0.33	0.30	0.29	0.28	0.27
2023-4-12	0.24	0.34	0.34	0.34	0.34	0.34	0.34	0.34	0.34	0.34	0.34	0.34	0.32
2023-5-1	0.27	0.47	0.45	0.43	0.40	0.35	0.32	0.30	0.28	0.28	0.27	0.26	0.26
2023-5-4	0.20	0.38	0.38	0.38	0.35	0.33	0.28	0.25	0.22	0.20	0.18	0.17	0.16
2023-5-7	0.19	0.39	0.39	0.37	0.36	0.34	0.31	0.28	0.24	0.22	0.20	0.19	0.18
2023-5-10	0.24	0.44	0.42	0.39	0.36	0.32	0.29	0.27	0.26	0.24	0.22	0.22	0.21
2023-6-2	0.15	0.35	0.31	0.30	0.28	0.25	0.22	0.19	0.16	0.15	0.14	0.13	0.13
2023-6-5	0.20	0.41	0.35	0.29	0.25	0.23	0.22	0.20	0.19	0.17	0.16	NA	NA
2023-6-8	0.11	0.31	0.26	0.19	0.17	0.15	0.14	0.12	0.11	0.10	0.09	0.08	0.07
2023-6-11	0.16	0.38	0.32	0.28	0.24	0.19	0.17	0.15	0.14	0.14	0.13	0.12	NA
2023-7-3	0.03	0.06	0.05	0.03	0.01	0.01	0.01	0.02	0.02	0.06	NA	NA	NA
2023-7-6	0.01	0.10	0.06	0.04	0.04	0.03	0.02	0.01	0.01	0.01	0.01	0.05	NA
2023-7-9	0.03	0.07	0.04	0.01	0.01	0.01	0.02	0.03	0.05	NA	NA	NA	NA
2023-7-12	0.04	0.10	0.10	0.09	0.09	0.09	0.10	0.12	0.09	0.04	0.02	0.02	NA

Table B3(1) (continued)

Start date of 3-day interval	Dynamic U-values calculated by data pre-processing methods $[W/(m^2 \cdot K)]$												
	TD12	TD13	PV0	PV1	PV2	PV3	PV4	PV5	PV6	PV7	PV8	PV9	PV10
2023-2-2	0.36	0.36	0.36	0.36	0.36	0.36	0.36	0.36	0.36	0.36	0.36	0.36	0.36
2023-2-5	0.36	0.36	0.36	0.36	0.36	0.36	0.36	0.36	0.36	0.36	0.36	0.36	0.36
2023-2-8	0.38	0.38	0.38	0.38	0.38	0.38	0.38	0.38	0.38	0.38	0.38	0.38	0.38
2023-2-11	0.31	0.31	0.31	0.31	0.31	0.31	0.31	0.31	0.31	0.31	0.31	0.31	0.31
2023-3-3	0.33	0.32	0.34	0.34	0.34	0.34	0.34	0.34	0.34	0.34	0.34	0.34	0.34
2023-3-6	0.31	0.31	0.31	0.31	0.31	0.31	0.31	0.31	0.31	0.31	0.31	0.31	0.31
2023-3-9	0.31	0.31	0.34	0.34	0.34	0.34	0.34	0.34	0.34	0.34	0.34	0.33	0.32
2023-3-12	0.29	0.29	0.29	0.29	0.29	0.29	0.29	0.29	0.29	0.29	0.29	0.29	0.29
2023-4-3	0.20	0.20	0.23	0.23	0.23	0.23	0.23	0.23	0.23	0.23	0.23	0.22	0.22
2023-4-6	0.28	0.26	0.28	0.28	0.28	0.28	0.28	0.28	0.28	0.28	0.28	0.28	0.28
2023-4-9	0.26	0.24	0.43	0.43	0.43	0.41	0.38	0.38	0.35	0.33	0.30	0.29	0.28
2023-4-12	0.31	0.30	0.34	0.34	0.34	0.34	0.34	0.34	0.34	0.34	0.34	0.34	0.34
2023-5-1	0.27	0.26	0.47	0.45	0.43	0.40	0.35	0.32	0.30	0.28	0.28	0.27	0.26
2023-5-4	0.15	0.15	0.38	0.38	0.38	0.35	0.33	0.28	0.25	0.22	0.20	0.18	0.17
2023-5-7	0.16	0.14	0.39	0.39	0.37	0.36	0.34	0.31	0.28	0.24	0.22	0.20	0.19
2023-5-10	0.20	0.20	0.44	0.42	0.39	0.36	0.32	0.29	0.27	0.26	0.24	0.22	0.22
2023-6-2	0.13	0.11	0.35	0.31	0.30	0.28	0.25	0.22	0.19	0.16	0.15	0.14	0.13
2023-6-5	NA	NA	0.41	0.35	0.29	0.25	0.23	0.22	0.20	0.19	0.17	0.16	NA
2023-6-8	0.08	NA	0.31	0.26	0.19	0.17	0.15	0.14	0.12	0.11	0.10	0.09	0.08
2023-6-11	NA	NA	0.38	0.32	0.28	0.24	0.19	0.17	0.15	0.14	0.14	0.13	0.12
2023-7-3	NA	NA	0.18	0.16	0.12	0.09	0.08	0.07	0.06	0.05	0.06	NA	NA
2023-7-6	NA	NA	0.19	0.12	0.09	0.08	0.07	0.06	0.04	0.04	0.02	0.02	0.05
2023-7-9	NA	NA	0.27	0.19	0.10	0.07	0.06	0.04	0.01	NA	NA	NA	NA
2023-7-12	NA	NA	0.13	0.12	0.12	0.12	0.12	0.12	0.12	0.09	0.04	0.02	0.02

Table B3(1) (continued)

Start date of 3-day interval	Dynamic U-values calculated by data pre-processing methods $[W/(m^2 \cdot K)]$											
	PV11	PV12	PV13	AV0	AV1	AV2	AV3	AV4	AV5	AV6	AV7	AV8
2023-2-2	0.36	0.36	0.36	0.36	0.36	0.36	0.36	0.36	0.36	0.36	0.36	0.36
2023-2-5	0.36	0.36	0.36	0.36	0.36	0.36	0.36	0.36	0.36	0.36	0.36	0.36
2023-2-8	0.38	0.38	0.38	0.38	0.38	0.38	0.38	0.38	0.38	0.38	0.38	0.38
2023-2-11	0.31	0.31	0.31	0.31	0.31	0.31	0.31	0.31	0.31	0.31	0.31	0.31
2023-3-3	0.33	0.33	0.32	0.34	0.34	0.34	0.34	0.34	0.34	0.34	0.34	0.34
2023-3-6	0.31	0.31	0.31	0.31	0.31	0.31	0.31	0.31	0.31	0.31	0.31	0.31
2023-3-9	0.32	0.31	0.31	0.34	0.34	0.34	0.34	0.34	0.34	0.34	0.34	0.34
2023-3-12	0.29	0.29	0.29	0.29	0.29	0.29	0.29	0.29	0.29	0.29	0.29	0.29
2023-4-3	0.22	0.20	0.20	0.23	0.23	0.23	0.23	0.23	0.23	0.23	0.23	0.23
2023-4-6	0.28	0.28	0.26	0.28	0.28	0.28	0.28	0.28	0.28	0.28	0.28	0.28
2023-4-9	0.27	0.26	0.24	0.43	0.43	0.43	0.41	0.38	0.38	0.35	0.33	0.30
2023-4-12	0.32	0.31	0.30	0.34	0.34	0.34	0.34	0.34	0.34	0.34	0.34	0.34
2023-5-1	0.26	0.27	0.26	0.59	0.52	0.47	0.40	0.35	0.32	0.30	0.28	0.28
2023-5-4	0.16	0.15	0.15	0.38	0.38	0.38	0.35	0.33	0.28	0.25	0.22	0.20
2023-5-7	0.18	0.16	0.14	0.39	0.39	0.37	0.36	0.34	0.31	0.28	0.24	0.22
2023-5-10	0.21	0.20	0.20	0.54	0.49	0.42	0.36	0.32	0.29	0.27	0.26	0.24
2023-6-2	0.13	0.13	0.11	0.36	0.31	0.30	0.28	0.25	0.22	0.19	0.16	0.15
2023-6-5	NA	NA	NA	0.50	0.41	0.32	0.26	0.23	0.22	0.20	0.19	0.17
2023-6-8	0.07	0.08	NA	0.35	0.26	0.19	0.17	0.15	0.14	0.12	0.11	0.10
2023-6-11	NA	NA	NA	0.49	0.41	0.35	0.29	0.23	0.19	0.16	0.14	0.14
2023-7-3	NA	NA	NA	0.19	0.16	0.11	0.08	0.06	0.05	0.04	0.03	0.06
2023-7-6	NA	NA	NA	0.25	0.19	0.13	0.10	0.08	0.04	0.03	0.03	0.02
2023-7-9	NA	NA	NA	0.27	0.23	0.16	0.10	0.04	0.03	0.03	0.05	NA
2023-7-12	NA	NA	NA	0.19	0.18	0.17	0.16	0.12	0.12	0.12	0.09	0.04

Table B3(1) (continued)

Start date of 3-day interval	Dynamic U-values calculated by data pre-processing methods $[W/(m^2 \cdot K)]$					
	AV9	AV10	AV11	AV12	AV13	TL
2023-2-2	0.36	0.36	0.36	0.36	0.36	0.36
2023-2-5	0.36	0.36	0.36	0.36	0.36	0.35
2023-2-8	0.38	0.38	0.38	0.38	0.38	0.38
2023-2-11	0.31	0.31	0.31	0.31	0.31	0.31
2023-3-3	0.34	0.34	0.33	0.33	0.32	0.34
2023-3-6	0.31	0.31	0.31	0.31	0.31	0.32
2023-3-9	0.33	0.32	0.32	0.31	0.31	0.33
2023-3-12	0.29	0.29	0.29	0.29	0.29	0.30
2023-4-3	0.22	0.22	0.22	0.20	0.20	0.24
2023-4-6	0.28	0.28	0.28	0.28	0.26	0.29
2023-4-9	0.29	0.28	0.27	0.26	0.24	0.41
2023-4-12	0.34	0.34	0.32	0.31	0.30	0.34
2023-5-1	0.27	0.26	0.26	0.27	0.26	0.49
2023-5-4	0.18	0.17	0.16	0.15	0.15	0.38
2023-5-7	0.20	0.19	0.18	0.16	0.14	0.37
2023-5-10	0.22	0.22	0.21	0.20	0.20	0.45
2023-6-2	0.14	0.13	0.13	0.13	0.11	0.36
2023-6-5	0.16	NA	NA	NA	NA	0.44
2023-6-8	0.09	0.08	0.07	0.08	NA	0.33
2023-6-11	0.13	0.12	NA	NA	NA	0.37
2023-7-3	NA	NA	NA	NA	NA	0.15
2023-7-6	0.01	0.05	NA	NA	NA	0.18
2023-7-9	NA	NA	NA	NA	NA	0.20
2023-7-12	0.02	0.02	NA	NA	NA	0.16

Table B3(2) Dynamic U-values of the RC tested envelope with 5-day time intervals

Start date of 5-day interval	Dynamic U-values calculated by data pre-processing methods $[W/(m^2 \cdot K)]$												
	ND	TD0	TD1	TD2	TD3	TD4	TD5	TD6	TD7	TD8	TD9	TD10	TD11
2023-2-2	0.32	0.35	0.35	0.35	0.35	0.35	0.35	0.35	0.35	0.35	0.35	0.35	0.35
2023-2-7	0.31	0.35	0.35	0.35	0.35	0.35	0.35	0.35	0.35	0.35	0.35	0.35	0.35
2023-3-3	0.26	0.33	0.33	0.33	0.33	0.33	0.33	0.33	0.33	0.33	0.33	0.33	0.33
2023-3-8	0.25	0.31	0.31	0.31	0.31	0.31	0.31	0.31	0.31	0.31	0.31	0.30	0.30
2023-4-3	0.18	0.24	0.24	0.24	0.24	0.24	0.24	0.24	0.24	0.24	0.24	0.24	0.23
2023-4-8	0.27	0.37	0.37	0.37	0.37	0.36	0.36	0.35	0.34	0.33	0.33	0.32	0.31
2023-5-1	0.24	0.42	0.40	0.39	0.37	0.35	0.31	0.28	0.26	0.25	0.24	0.24	0.26
2023-5-6	0.20	0.40	0.40	0.39	0.37	0.34	0.31	0.28	0.25	0.23	0.21	0.20	0.19
2023-5-11	0.24	0.46	0.42	0.38	0.33	0.30	0.28	0.25	0.24	0.22	0.21	0.20	0.20
2023-6-2	0.17	0.37	0.33	0.30	0.27	0.25	0.22	0.20	0.17	0.16	0.14	0.13	0.13
2023-6-7	0.13	0.33	0.29	0.23	0.21	0.17	0.15	0.14	0.12	0.11	0.09	0.08	0.07
2023-6-12	0.17	0.38	0.28	0.23	0.20	0.18	0.16	0.15	0.14	0.14	0.13	0.12	NA
2023-7-3	0.01	0.09	0.06	0.04	0.03	0.03	0.02	0.02	0.02	0.01	0.01	0.05	NA
2023-7-8	0.02	0.06	0.03	0.01	0.01	0.01	0.02	0.02	0.03	0.01	NA	NA	NA
2023-7-13	0.05	0.11	0.10	0.10	0.10	0.10	0.11	0.12	0.09	0.04	0.02	0.02	NA

Table B3(2) (continued)

Start date of 5-day interval	Dynamic U-values calculated by data pre-processing methods $[W/(m^2 \cdot K)]$												
	TD12	TD13	PV0	PV1	PV2	PV3	PV4	PV5	PV6	PV7	PV8	PV9	PV10
2023-2-2	0.35	0.35	0.35	0.35	0.35	0.35	0.35	0.35	0.35	0.35	0.35	0.35	0.35
2023-2-7	0.35	0.35	0.35	0.35	0.35	0.35	0.35	0.35	0.35	0.35	0.35	0.35	0.35
2023-3-3	0.32	0.32	0.33	0.33	0.33	0.33	0.33	0.33	0.33	0.33	0.33	0.33	0.33
2023-3-8	0.30	0.30	0.31	0.31	0.31	0.31	0.31	0.31	0.31	0.31	0.31	0.31	0.30
2023-4-3	0.22	0.21	0.24	0.24	0.24	0.24	0.24	0.24	0.24	0.24	0.24	0.24	0.24
2023-4-8	0.30	0.29	0.37	0.37	0.37	0.37	0.36	0.36	0.35	0.34	0.33	0.33	0.32
2023-5-1	0.27	0.26	0.42	0.40	0.39	0.37	0.35	0.31	0.28	0.26	0.25	0.24	0.24
2023-5-6	0.18	0.18	0.40	0.40	0.39	0.37	0.34	0.31	0.28	0.25	0.23	0.21	0.20
2023-5-11	0.20	0.21	0.46	0.42	0.38	0.33	0.30	0.28	0.25	0.24	0.22	0.21	0.20
2023-6-2	0.13	0.11	0.37	0.33	0.30	0.27	0.25	0.22	0.20	0.17	0.16	0.14	0.13
2023-6-7	0.08	NA	0.33	0.29	0.23	0.21	0.17	0.15	0.14	0.12	0.11	0.09	0.08
2023-6-12	NA	NA	0.38	0.28	0.23	0.20	0.18	0.16	0.15	0.14	0.14	0.13	0.12
2023-7-3	NA	NA	0.19	0.14	0.11	0.09	0.08	0.07	0.05	0.04	0.03	0.02	0.05
2023-7-8	NA	NA	0.25	0.17	0.10	0.07	0.06	0.04	0.02	0.05	0.03	NA	NA
2023-7-13	NA	NA	0.13	0.12	0.12	0.12	0.12	0.12	0.12	0.09	0.04	0.02	0.02

Table B3(2) (continued)

Start date of 5-day interval	Dynamic U-values calculated by data pre-processing methods $[W/(m^2 \cdot K)]$											
	PV11	PV12	PV13	AV0	AV1	AV2	AV3	AV4	AV5	AV6	AV7	AV8
2023-2-2	0.35	0.35	0.35	0.35	0.35	0.35	0.35	0.35	0.35	0.35	0.35	0.35
2023-2-7	0.35	0.35	0.35	0.35	0.35	0.35	0.35	0.35	0.35	0.35	0.35	0.35
2023-3-3	0.33	0.32	0.32	0.33	0.33	0.33	0.33	0.33	0.33	0.33	0.33	0.33
2023-3-8	0.30	0.30	0.30	0.31	0.31	0.31	0.31	0.31	0.31	0.31	0.31	0.31
2023-4-3	0.23	0.22	0.21	0.24	0.24	0.24	0.24	0.24	0.24	0.24	0.24	0.24
2023-4-8	0.31	0.30	0.29	0.37	0.37	0.37	0.37	0.36	0.36	0.35	0.34	0.33
2023-5-1	0.26	0.27	0.26	0.48	0.44	0.41	0.37	0.35	0.31	0.28	0.26	0.25
2023-5-6	0.19	0.18	0.18	0.40	0.40	0.39	0.37	0.34	0.31	0.28	0.25	0.23
2023-5-11	0.20	0.20	0.21	0.59	0.53	0.42	0.33	0.30	0.28	0.25	0.24	0.22
2023-6-2	0.13	0.13	0.11	0.39	0.34	0.31	0.27	0.25	0.22	0.20	0.17	0.16
2023-6-7	0.07	0.08	NA	0.39	0.31	0.25	0.21	0.17	0.15	0.14	0.12	0.11
2023-6-12	NA	NA	NA	0.55	0.43	0.35	0.28	0.23	0.19	0.16	0.14	0.14
2023-7-3	NA	NA	NA	0.21	0.16	0.10	0.07	0.05	0.04	0.03	0.02	0.02
2023-7-8	NA	NA	NA	0.28	0.25	0.19	0.15	0.08	0.04	0.03	0.05	0.02
2023-7-13	NA	NA	NA	0.16	0.16	0.16	0.15	0.13	0.12	0.12	0.09	0.04

Table B3(2) (continued)

Start date of 5-day interval	Dynamic U-values calculated by data pre-processing methods $[W/(m^2 \cdot K)]$					
	AV9	AV10	AV11	AV12	AV13	TL
2023-2-2	0.35	0.35	0.35	0.35	0.35	0.36
2023-2-7	0.35	0.35	0.35	0.35	0.35	0.35
2023-3-3	0.33	0.33	0.33	0.32	0.32	0.34
2023-3-8	0.31	0.30	0.30	0.30	0.30	0.31
2023-4-3	0.24	0.24	0.23	0.22	0.21	0.25
2023-4-8	0.33	0.32	0.31	0.30	0.29	0.36
2023-5-1	0.24	0.24	0.26	0.27	0.26	0.45
2023-5-6	0.21	0.20	0.19	0.18	0.18	0.38
2023-5-11	0.21	0.20	0.20	0.20	0.21	0.48
2023-6-2	0.14	0.13	0.13	0.13	0.11	0.39
2023-6-7	0.09	0.08	0.07	0.08	NA	0.36
2023-6-12	0.13	0.12	NA	NA	NA	0.36
2023-7-3	0.01	0.05	NA	NA	NA	0.16
2023-7-8	NA	NA	NA	NA	NA	0.20
2023-7-13	0.02	0.02	NA	NA	NA	0.15

Table B3(3) Dynamic U-values of the RC tested envelope with 7-day time intervals

Start date of 7-day interval	Dynamic U-values calculated by data pre-processing methods [$W/(m^2 \cdot K)$]												
	ND	TD0	TD1	TD2	TD3	TD4	TD5	TD6	TD7	TD8	TD9	TD10	TD11
2023-2-2	0.32	0.36	0.36	0.36	0.36	0.36	0.36	0.36	0.36	0.36	0.36	0.36	0.36
2023-2-9	0.31	0.34	0.34	0.34	0.34	0.34	0.34	0.34	0.34	0.34	0.34	0.34	0.34
2023-3-3	0.26	0.33	0.33	0.33	0.33	0.33	0.33	0.33	0.33	0.33	0.33	0.33	0.33
2023-3-10	0.24	0.30	0.30	0.30	0.30	0.30	0.30	0.30	0.30	0.30	0.30	0.29	0.29
2023-4-3	0.21	0.29	0.29	0.29	0.29	0.28	0.28	0.27	0.27	0.27	0.26	0.26	0.26
2023-4-10	0.26	0.34	0.34	0.34	0.34	0.34	0.34	0.33	0.33	0.32	0.32	0.31	0.30
2023-5-1	0.22	0.42	0.41	0.40	0.36	0.33	0.29	0.26	0.24	0.23	0.22	0.21	0.21
2023-5-8	0.23	0.42	0.40	0.38	0.36	0.34	0.31	0.28	0.26	0.24	0.22	0.21	0.20
2023-6-2	0.16	0.37	0.33	0.28	0.26	0.23	0.21	0.19	0.17	0.15	0.14	0.13	0.12
2023-6-9	0.14	0.33	0.28	0.23	0.21	0.17	0.15	0.13	0.12	0.11	0.09	0.08	0.07
2023-7-3	0.01	0.07	0.05	0.03	0.02	0.02	0.01	0.01	0.01	0.01	0.01	0.05	NA
2023-7-10	0.02	0.10	0.09	0.08	0.07	0.07	0.08	0.11	0.09	0.04	0.02	0.02	NA

Table B3(3) (continued)

Start date of 7-day interval	Dynamic U-values calculated by data pre-processing methods $[W/(m^2 \cdot K)]$												
	TD12	TD13	PV0	PV1	PV2	PV3	PV4	PV5	PV6	PV7	PV8	PV9	PV10
2023-2-2	0.36	0.36	0.36	0.36	0.36	0.36	0.36	0.36	0.36	0.36	0.36	0.36	0.36
2023-2-9	0.34	0.34	0.34	0.34	0.34	0.34	0.34	0.34	0.34	0.34	0.34	0.34	0.34
2023-3-3	0.33	0.32	0.33	0.33	0.33	0.33	0.33	0.33	0.33	0.33	0.33	0.33	0.33
2023-3-10	0.29	0.29	0.30	0.30	0.30	0.30	0.30	0.30	0.30	0.30	0.30	0.30	0.29
2023-4-3	0.25	0.24	0.29	0.29	0.29	0.29	0.28	0.28	0.27	0.27	0.27	0.26	0.26
2023-4-10	0.28	0.27	0.34	0.34	0.34	0.34	0.34	0.34	0.33	0.33	0.32	0.32	0.31
2023-5-1	0.20	0.21	0.42	0.41	0.40	0.36	0.33	0.29	0.26	0.24	0.23	0.22	0.21
2023-5-8	0.20	0.20	0.42	0.40	0.38	0.36	0.34	0.31	0.28	0.26	0.24	0.22	0.21
2023-6-2	0.13	0.11	0.37	0.33	0.28	0.26	0.23	0.21	0.19	0.17	0.15	0.14	0.13
2023-6-9	0.08	NA	0.33	0.28	0.23	0.21	0.17	0.15	0.13	0.12	0.11	0.09	0.08
2023-7-3	NA	NA	0.19	0.14	0.11	0.08	0.07	0.06	0.05	0.04	0.03	0.02	0.05
2023-7-10	NA	NA	0.15	0.14	0.12	0.11	0.11	0.12	0.12	0.09	0.04	0.02	0.02

Table B3(3) (continued)

Start date of 7-day interval	Dynamic U-values calculated by data pre-processing methods $[W/(m^2 \cdot K)]$											
	PV11	PV12	PV13	AV0	AV1	AV2	AV3	AV4	AV5	AV6	AV7	AV8
2023-2-2	0.36	0.36	0.36	0.36	0.36	0.36	0.36	0.36	0.36	0.36	0.36	0.36
2023-2-9	0.34	0.34	0.34	0.34	0.34	0.34	0.34	0.34	0.34	0.34	0.34	0.34
2023-3-3	0.33	0.33	0.32	0.33	0.33	0.33	0.33	0.33	0.33	0.33	0.33	0.33
2023-3-10	0.29	0.29	0.29	0.30	0.30	0.30	0.30	0.30	0.30	0.30	0.30	0.30
2023-4-3	0.26	0.25	0.24	0.29	0.29	0.29	0.29	0.28	0.28	0.27	0.27	0.27
2023-4-10	0.30	0.28	0.27	0.34	0.34	0.34	0.34	0.34	0.34	0.33	0.33	0.32
2023-5-1	0.21	0.20	0.21	0.47	0.44	0.41	0.36	0.33	0.29	0.26	0.24	0.23
2023-5-8	0.20	0.20	0.20	0.48	0.45	0.40	0.36	0.34	0.31	0.28	0.26	0.24
2023-6-2	0.12	0.13	0.11	0.41	0.35	0.29	0.26	0.23	0.21	0.19	0.17	0.15
2023-6-9	0.07	0.08	NA	0.43	0.33	0.28	0.23	0.19	0.16	0.14	0.12	0.11
2023-7-3	NA	NA	NA	0.22	0.18	0.13	0.10	0.07	0.05	0.03	0.03	0.02
2023-7-10	NA	NA	NA	0.21	0.20	0.17	0.14	0.10	0.10	0.11	0.09	0.04

Table B3(3) (continued)

Start date of 7-day interval	Dynamic U-values calculated by data pre-processing methods $[W/(m^2 \cdot K)]$					
	AV9	AV10	AV11	AV12	AV13	TL
2023-2-2	0.36	0.36	0.36	0.36	0.36	0.36
2023-2-9	0.34	0.34	0.34	0.34	0.34	0.34
2023-3-3	0.33	0.33	0.33	0.33	0.32	0.34
2023-3-10	0.30	0.29	0.29	0.29	0.29	0.30
2023-4-3	0.26	0.26	0.26	0.25	0.24	0.30
2023-4-10	0.32	0.31	0.30	0.28	0.27	0.34
2023-5-1	0.22	0.21	0.21	0.20	0.21	0.43
2023-5-8	0.22	0.21	0.20	0.20	0.20	0.43
2023-6-2	0.14	0.13	0.12	0.13	0.11	0.39
2023-6-9	0.09	0.08	0.07	0.08	NA	0.35
2023-7-3	0.01	0.05	NA	NA	NA	0.17
2023-7-10	0.02	0.02	NA	NA	NA	0.17

Table B3(4) Dynamic U-values of the RC tested envelope with 14-day time intervals

Start date of 14-day interval	Dynamic U-values calculated by data pre-processing methods $[W/(m^2 \cdot K)]$												
	ND	TD0	TD1	TD2	TD3	TD4	TD5	TD6	TD7	TD8	TD9	TD10	TD11
2023-2-2	0.32	0.35	0.35	0.35	0.35	0.35	0.35	0.35	0.35	0.35	0.35	0.35	0.35
2023-3-3	0.25	0.32	0.32	0.32	0.32	0.32	0.32	0.32	0.32	0.32	0.32	0.31	0.31
2023-4-3	0.23	0.31	0.31	0.31	0.31	0.31	0.30	0.30	0.29	0.29	0.29	0.28	0.27
2023-5-1	0.23	0.42	0.41	0.39	0.36	0.33	0.30	0.27	0.25	0.23	0.22	0.21	0.21
2023-6-2	0.15	0.36	0.31	0.26	0.24	0.21	0.19	0.17	0.15	0.13	0.12	0.11	0.10
2023-7-3	0.00	0.09	0.07	0.05	0.04	0.04	0.05	0.05	0.05	0.03	0.02	0.02	NA

Table B3(4) (continued)

Start date of 14-day interval	Dynamic U-values calculated by data pre-processing methods $[W/(m^2 \cdot K)]$												
	TD12	TD13	PV0	PV1	PV2	PV3	PV4	PV5	PV6	PV7	PV8	PV9	PV10
2023-2-2	0.35	0.35	0.35	0.35	0.35	0.35	0.35	0.35	0.35	0.35	0.35	0.35	0.35
2023-3-3	0.31	0.30	0.32	0.32	0.32	0.32	0.32	0.32	0.32	0.32	0.32	0.32	0.31
2023-4-3	0.26	0.25	0.31	0.31	0.31	0.31	0.31	0.30	0.30	0.29	0.29	0.29	0.28
2023-5-1	0.20	0.21	0.42	0.41	0.39	0.36	0.33	0.30	0.27	0.25	0.23	0.22	0.21
2023-6-2	0.10	0.11	0.36	0.31	0.26	0.24	0.21	0.19	0.17	0.15	0.13	0.12	0.11
2023-7-3	NA	NA	0.17	0.14	0.11	0.10	0.10	0.09	0.09	0.07	0.04	0.02	0.02

Table B3(4) (continued)

Start date of 14-day interval	Dynamic U-values calculated by data pre-processing methods $[W/(m^2 \cdot K)]$											
	PV11	PV12	PV13	AV0	AV1	AV2	AV3	AV4	AV5	AV6	AV7	AV8
2023-2-2	0.35	0.35	0.35	0.35	0.35	0.35	0.35	0.35	0.35	0.35	0.35	0.35
2023-3-3	0.31	0.31	0.30	0.32	0.32	0.32	0.32	0.32	0.32	0.32	0.32	0.32
2023-4-3	0.27	0.26	0.25	0.31	0.31	0.31	0.31	0.31	0.30	0.30	0.29	0.29
2023-5-1	0.21	0.20	0.21	0.47	0.45	0.41	0.36	0.33	0.30	0.27	0.25	0.23
2023-6-2	0.10	0.10	0.11	0.42	0.34	0.29	0.25	0.21	0.19	0.17	0.15	0.13
2023-7-3	NA	NA	NA	0.22	0.19	0.15	0.12	0.09	0.07	0.07	0.06	0.03

Table B3(4) (continued)

Start date of 14-day interval	Dynamic U-values calculated by data pre-processing methods $[W/(m^2 \cdot K)]$					
	AV9	AV10	AV11	AV12	AV13	TL
2023-2-2	0.35	0.35	0.35	0.35	0.35	0.37
2023-3-3	0.32	0.31	0.31	0.31	0.30	0.34
2023-4-3	0.29	0.28	0.27	0.26	0.25	0.34
2023-5-1	0.22	0.21	0.21	0.20	0.21	0.44
2023-6-2	0.12	0.11	0.10	0.10	0.11	0.38
2023-7-3	0.02	0.02	NA	NA	NA	0.18

Table B4(1) Dynamic U-values of the brick tested envelope with 3-day time intervals

Start date of 3-day interval	Dynamic U-values calculated by data pre-processing methods $[W/(m^2 \cdot K)]$												
	ND	TD0	TD1	TD2	TD3	TD4	TD5	TD6	TD7	TD8	TD9	TD10	TD11
2023-1-16	0.50	0.54	0.54	0.54	0.54	0.54	0.54	0.54	0.54	0.54	0.54	0.54	0.54
2023-1-19	0.47	0.50	0.50	0.50	0.50	0.50	0.50	0.50	0.50	0.50	0.50	0.50	0.50
2023-1-22	0.46	0.48	0.48	0.48	0.48	0.48	0.48	0.48	0.48	0.48	0.48	0.48	0.48
2023-1-25	0.53	0.57	0.57	0.57	0.57	0.57	0.57	0.57	0.57	0.57	0.57	0.57	0.57
2023-2-15	0.56	0.63	0.63	0.63	0.63	0.63	0.63	0.63	0.63	0.63	0.63	0.63	0.63
2023-2-18	0.47	0.55	0.55	0.55	0.55	0.55	0.55	0.55	0.55	0.55	0.55	0.55	0.55
2023-2-21	0.49	0.60	0.60	0.60	0.60	0.60	0.60	0.60	0.60	0.60	0.60	0.60	0.60
2023-2-24	0.50	0.63	0.63	0.63	0.63	0.63	0.63	0.63	0.63	0.63	0.63	0.63	0.62
2023-2-27	0.56	0.63	0.63	0.63	0.63	0.63	0.63	0.63	0.63	0.63	0.62	0.61	0.59
2023-3-16	0.44	0.57	0.57	0.57	0.57	0.57	0.57	0.57	0.57	0.57	0.57	0.57	0.57
2023-3-19	0.54	0.79	0.79	0.79	0.79	0.79	0.79	0.78	0.74	0.72	0.70	0.69	0.67
2023-3-22	0.40	0.48	0.48	0.48	0.48	0.48	0.48	0.48	0.48	0.48	0.48	0.48	0.48
2023-3-25	0.39	0.52	0.52	0.52	0.52	0.52	0.52	0.52	0.52	0.52	0.52	0.52	0.51
2023-3-28	0.36	0.61	0.61	0.60	0.60	0.58	0.57	0.56	0.55	0.54	0.53	0.52	0.50
2023-4-16	0.33	0.52	0.52	0.52	0.51	0.49	0.48	0.47	0.44	0.42	0.40	0.38	0.36
2023-4-19	0.33	0.47	0.47	0.47	0.46	0.46	0.44	0.43	0.42	0.41	0.41	0.40	0.39
2023-4-22	0.17	0.35	0.35	0.35	0.35	0.35	0.35	0.34	0.34	0.34	0.33	0.33	0.33
2023-4-25	0.21	0.34	0.34	0.33	0.33	0.33	0.32	0.31	0.30	0.29	0.27	0.26	0.25
2023-5-16	0.12	0.26	0.23	0.21	0.19	0.18	0.17	0.16	0.15	0.14	0.14	0.15	0.14
2023-5-19	0.07	0.19	0.19	0.18	0.17	0.15	0.13	0.12	0.12	0.12	0.12	0.11	0.08
2023-5-22	0.04	0.35	0.30	0.26	0.23	0.20	0.21	0.20	0.20	0.16	0.14	0.09	0.04
2023-5-25	0.07	0.11	0.07	0.06	0.04	0.03	0.05	0.02	0.03	0.04	0.05	0.05	NA
2023-5-28	0.07	0.15	0.15	0.14	0.12	0.11	0.09	0.08	0.06	0.03	0.02	0.02	0.01
2023-6-16	0.14	0.04	0.01	0.03	0.07	0.07	0.08	0.10	0.08	NA	NA	NA	NA
2023-6-19	0.04	0.03	0.01	0.00	0.00	0.02	0.03	0.04	0.04	0.05	NA	NA	NA
2023-6-22	0.02	0.21	0.15	0.12	0.11	0.07	0.05	0.05	0.06	0.06	NA	NA	NA
2023-6-25	0.25	0.18	0.18	0.17	0.17	0.18	0.15	0.12	0.11	NA	NA	NA	NA
2023-6-28	0.07	0.04	0.01	0.01	0.02	0.03	0.04	0.05	0.05	0.07	0.08	0.09	0.09

Table B4(1) (continued)

Start date of 3-day interval	Dynamic U-values calculated by data pre-processing methods $[W/(m^2 \cdot K)]$												
	TD12	TD13	PV0	PV1	PV2	PV3	PV4	PV5	PV6	PV7	PV8	PV9	PV10
2023-1-16	0.54	0.54	0.54	0.54	0.54	0.54	0.54	0.54	0.54	0.54	0.54	0.54	0.54
2023-1-19	0.50	0.50	0.50	0.50	0.50	0.50	0.50	0.50	0.50	0.50	0.50	0.50	0.50
2023-1-22	0.48	0.48	0.48	0.48	0.48	0.48	0.48	0.48	0.48	0.48	0.48	0.48	0.48
2023-1-25	0.57	0.57	0.57	0.57	0.57	0.57	0.57	0.57	0.57	0.57	0.57	0.57	0.57
2023-2-15	0.63	0.63	0.63	0.63	0.63	0.63	0.63	0.63	0.63	0.63	0.63	0.63	0.63
2023-2-18	0.55	0.55	0.55	0.55	0.55	0.55	0.55	0.55	0.55	0.55	0.55	0.55	0.55
2023-2-21	0.60	0.60	0.60	0.60	0.60	0.60	0.60	0.60	0.60	0.60	0.60	0.60	0.60
2023-2-24	0.62	0.61	0.63	0.63	0.63	0.63	0.63	0.63	0.63	0.63	0.63	0.63	0.63
2023-2-27	0.58	0.57	0.63	0.63	0.63	0.63	0.63	0.63	0.63	0.63	0.63	0.62	0.61
2023-3-16	0.57	0.56	0.57	0.57	0.57	0.57	0.57	0.57	0.57	0.57	0.57	0.57	0.57
2023-3-19	0.64	0.62	0.79	0.79	0.79	0.79	0.79	0.79	0.78	0.74	0.72	0.70	0.69
2023-3-22	0.47	0.46	0.48	0.48	0.48	0.48	0.48	0.48	0.48	0.48	0.48	0.48	0.48
2023-3-25	0.51	0.50	0.52	0.52	0.52	0.52	0.52	0.52	0.52	0.52	0.52	0.52	0.52
2023-3-28	0.48	0.45	0.61	0.61	0.60	0.60	0.58	0.57	0.56	0.55	0.54	0.53	0.52
2023-4-16	0.32	0.29	0.52	0.52	0.52	0.51	0.49	0.48	0.47	0.44	0.42	0.40	0.38
2023-4-19	0.36	0.35	0.47	0.47	0.47	0.46	0.46	0.44	0.43	0.42	0.41	0.41	0.40
2023-4-22	0.32	0.32	0.35	0.35	0.35	0.35	0.35	0.35	0.34	0.34	0.34	0.33	0.33
2023-4-25	0.25	0.23	0.34	0.34	0.33	0.33	0.33	0.32	0.31	0.30	0.29	0.27	0.26
2023-5-16	0.13	0.20	0.26	0.23	0.21	0.19	0.18	0.17	0.16	0.15	0.14	0.14	0.15
2023-5-19	NA	NA	0.21	0.21	0.19	0.18	0.16	0.15	0.14	0.14	0.13	0.12	0.11
2023-5-22	NA	NA	0.49	0.43	0.37	0.31	0.28	0.25	0.23	0.20	0.16	0.14	0.09
2023-5-25	NA	NA	0.56	0.46	0.43	0.40	0.38	0.37	0.28	0.12	0.23	NA	NA
2023-5-28	0.19	0.19	0.56	0.54	0.53	0.53	0.53	0.51	0.46	0.41	0.34	0.27	0.22
2023-6-16	NA	NA	0.83	0.68	0.51	0.38	0.40	0.33	NA	NA	NA	NA	NA
2023-6-19	NA	NA	0.23	0.18	0.15	0.13	0.09	0.07	0.05	0.04	0.02	NA	NA
2023-6-22	NA	NA	0.30	0.22	0.19	0.16	0.12	0.08	0.05	0.06	0.06	NA	NA
2023-6-25	NA	NA	1.09	0.73	0.71	0.68	NA	NA	NA	NA	NA	NA	NA
2023-6-28	0.07	NA	0.36	0.26	0.20	0.17	0.13	0.13	0.15	0.24	0.01	0.01	NA

Table B4(1) (continued)

Start date of 3-day interval	Dynamic U-values calculated by data pre-processing methods $[W/(m^2 \cdot K)]$											
	PV11	PV12	PV13	AV0	AV1	AV2	AV3	AV4	AV5	AV6	AV7	AV8
2023-1-16	0.54	0.54	0.54	0.54	0.54	0.54	0.54	0.54	0.54	0.54	0.54	0.54
2023-1-19	0.50	0.50	0.50	0.50	0.50	0.50	0.50	0.50	0.50	0.50	0.50	0.50
2023-1-22	0.48	0.48	0.48	0.48	0.48	0.48	0.48	0.48	0.48	0.48	0.48	0.48
2023-1-25	0.57	0.57	0.57	0.57	0.57	0.57	0.57	0.57	0.57	0.57	0.57	0.57
2023-2-15	0.63	0.63	0.63	0.63	0.63	0.63	0.63	0.63	0.63	0.63	0.63	0.63
2023-2-18	0.55	0.55	0.55	0.55	0.55	0.55	0.55	0.55	0.55	0.55	0.55	0.55
2023-2-21	0.60	0.60	0.60	0.60	0.60	0.60	0.60	0.60	0.60	0.60	0.60	0.60
2023-2-24	0.62	0.62	0.61	0.63	0.63	0.63	0.63	0.63	0.63	0.63	0.63	0.63
2023-2-27	0.59	0.58	0.57	0.63	0.63	0.63	0.63	0.63	0.63	0.63	0.63	0.63
2023-3-16	0.57	0.57	0.56	0.57	0.57	0.57	0.57	0.57	0.57	0.57	0.57	0.57
2023-3-19	0.67	0.64	0.62	0.79	0.79	0.79	0.79	0.79	0.79	0.78	0.74	0.72
2023-3-22	0.48	0.47	0.46	0.48	0.48	0.48	0.48	0.48	0.48	0.48	0.48	0.48
2023-3-25	0.51	0.51	0.50	0.52	0.52	0.52	0.52	0.52	0.52	0.52	0.52	0.52
2023-3-28	0.50	0.48	0.45	0.61	0.61	0.60	0.60	0.58	0.57	0.56	0.55	0.54
2023-4-16	0.36	0.32	0.29	0.52	0.52	0.52	0.51	0.49	0.48	0.47	0.44	0.42
2023-4-19	0.39	0.36	0.35	0.47	0.47	0.47	0.46	0.46	0.44	0.43	0.42	0.41
2023-4-22	0.33	0.32	0.32	0.35	0.35	0.35	0.35	0.35	0.35	0.34	0.34	0.34
2023-4-25	0.25	0.25	0.23	0.34	0.34	0.33	0.33	0.33	0.32	0.31	0.30	0.29
2023-5-16	0.14	0.13	0.20	0.31	0.25	0.22	0.19	0.18	0.17	0.16	0.15	0.14
2023-5-19	0.08	NA	NA	0.24	0.23	0.22	0.20	0.17	0.14	0.13	0.13	0.12
2023-5-22	0.04	NA	NA	0.50	0.41	0.35	0.29	0.26	0.24	0.22	0.20	0.16
2023-5-25	NA	NA	NA	0.31	0.23	0.19	0.17	0.14	0.13	0.10	0.06	0.06
2023-5-28	0.21	0.19	0.19	0.27	0.26	0.25	0.23	0.22	0.21	0.19	0.18	0.15
2023-6-16	NA	NA	NA	0.36	0.30	0.25	0.19	0.15	0.14	0.10	0.08	NA
2023-6-19	NA	NA	NA	0.17	0.15	0.13	0.12	0.10	0.10	0.08	0.06	0.05
2023-6-22	NA	NA	NA	0.40	0.32	0.23	0.19	0.16	0.13	0.05	0.06	0.06
2023-6-25	NA	NA	NA	0.30	0.27	0.25	0.22	0.18	0.15	0.13	0.16	NA
2023-6-28	NA	NA	NA	0.19	0.14	0.11	0.10	0.09	0.09	0.08	0.08	0.07

Table B4(1) (continued)

Start date of 3-day interval	Dynamic U-values calculated by data pre-processing methods $[W/(m^2 \cdot K)]$					
	AV9	AV10	AV11	AV12	AV13	TL
2023-1-16	0.54	0.54	0.54	0.54	0.54	0.53
2023-1-19	0.50	0.50	0.50	0.50	0.50	0.50
2023-1-22	0.48	0.48	0.48	0.48	0.48	0.48
2023-1-25	0.57	0.57	0.57	0.57	0.57	0.57
2023-2-15	0.63	0.63	0.63	0.63	0.63	0.62
2023-2-18	0.55	0.55	0.55	0.55	0.55	0.55
2023-2-21	0.60	0.60	0.60	0.60	0.60	0.61
2023-2-24	0.63	0.63	0.62	0.62	0.61	0.62
2023-2-27	0.62	0.61	0.59	0.58	0.57	0.63
2023-3-16	0.57	0.57	0.57	0.57	0.56	0.55
2023-3-19	0.70	0.69	0.67	0.64	0.62	0.78
2023-3-22	0.48	0.48	0.48	0.47	0.46	0.46
2023-3-25	0.52	0.52	0.51	0.51	0.50	0.51
2023-3-28	0.53	0.52	0.50	0.48	0.45	0.59
2023-4-16	0.40	0.38	0.36	0.32	0.29	0.53
2023-4-19	0.41	0.40	0.39	0.36	0.35	0.43
2023-4-22	0.33	0.33	0.33	0.32	0.32	0.32
2023-4-25	0.27	0.26	0.25	0.25	0.23	0.35
2023-5-16	0.14	0.15	0.14	0.13	0.20	0.27
2023-5-19	0.12	0.11	0.08	NA	NA	0.25
2023-5-22	0.14	0.09	0.04	NA	NA	0.39
2023-5-25	0.05	0.05	NA	NA	NA	0.21
2023-5-28	0.14	0.11	0.12	0.19	0.19	0.23
2023-6-16	NA	NA	NA	NA	NA	0.27
2023-6-19	NA	NA	NA	NA	NA	0.16
2023-6-22	NA	NA	NA	NA	NA	0.28
2023-6-25	NA	NA	NA	NA	NA	0.23
2023-6-28	0.08	0.09	0.09	0.07	NA	0.17

Table B4(2) Dynamic U-values of the brick tested envelope with 5-day time intervals

Start date of 5-day interval	Dynamic U-values calculated by data pre-processing methods $[W/(m^2 \cdot K)]$												
	ND	TD0	TD1	TD2	TD3	TD4	TD5	TD6	TD7	TD8	TD9	TD10	TD11
2023-1-16	0.50	0.52	0.52	0.52	0.52	0.52	0.52	0.52	0.52	0.52	0.52	0.52	0.52
2023-1-21	0.47	0.50	0.50	0.50	0.50	0.50	0.50	0.50	0.50	0.50	0.50	0.50	0.50
2023-1-26	0.53	0.57	0.57	0.57	0.57	0.57	0.57	0.57	0.57	0.57	0.57	0.57	0.57
2023-2-15	0.53	0.61	0.61	0.61	0.61	0.61	0.61	0.61	0.61	0.61	0.61	0.61	0.61
2023-2-20	0.47	0.58	0.58	0.58	0.58	0.58	0.58	0.58	0.58	0.58	0.58	0.58	0.58
2023-2-25	0.55	0.65	0.65	0.65	0.65	0.65	0.65	0.65	0.65	0.65	0.64	0.64	0.63
2023-3-16	0.47	0.64	0.64	0.64	0.64	0.64	0.64	0.63	0.62	0.61	0.61	0.60	0.60
2023-3-21	0.41	0.51	0.51	0.51	0.51	0.51	0.51	0.51	0.50	0.50	0.50	0.49	0.49
2023-3-26	0.38	0.59	0.59	0.58	0.57	0.56	0.56	0.55	0.55	0.54	0.54	0.53	0.52
2023-4-16	0.36	0.53	0.53	0.53	0.52	0.50	0.48	0.47	0.45	0.44	0.42	0.40	0.38
2023-4-21	0.18	0.32	0.32	0.32	0.32	0.32	0.32	0.32	0.31	0.31	0.31	0.31	0.31
2023-4-26	0.22	0.39	0.39	0.38	0.37	0.37	0.36	0.35	0.34	0.33	0.31	0.31	0.29
2023-5-16	0.10	0.24	0.21	0.19	0.17	0.16	0.15	0.13	0.13	0.12	0.14	0.15	0.14
2023-5-21	0.03	0.22	0.20	0.18	0.17	0.17	0.18	0.18	0.17	0.15	0.13	0.11	0.06
2023-5-26	0.06	0.16	0.15	0.14	0.12	0.10	0.09	0.07	0.05	0.02	0.01	0.02	0.01
2023-6-16	0.11	0.01	0.01	0.03	0.05	0.06	0.06	0.07	0.06	0.06	NA	NA	NA
2023-6-21	0.00	0.14	0.10	0.09	0.08	0.05	0.04	0.02	0.01	0.02	NA	NA	NA
2023-6-26	0.11	0.01	0.03	0.04	0.05	0.06	0.05	0.06	0.05	0.07	0.08	0.09	0.09

Table B4(2) (continued)

Start date of 5-day interval	Dynamic U-values calculated by data pre-processing methods $[W/(m^2 \cdot K)]$												
	TD12	TD13	PV0	PV1	PV2	PV3	PV4	PV5	PV6	PV7	PV8	PV9	PV10
2023-1-16	0.52	0.52	0.52	0.52	0.52	0.52	0.52	0.52	0.52	0.52	0.52	0.52	0.52
2023-1-21	0.50	0.50	0.50	0.50	0.50	0.50	0.50	0.50	0.50	0.50	0.50	0.50	0.50
2023-1-26	0.57	0.57	0.57	0.57	0.57	0.57	0.57	0.57	0.57	0.57	0.57	0.57	0.57
2023-2-15	0.61	0.61	0.61	0.61	0.61	0.61	0.61	0.61	0.61	0.61	0.61	0.61	0.61
2023-2-20	0.58	0.58	0.58	0.58	0.58	0.58	0.58	0.58	0.58	0.58	0.58	0.58	0.58
2023-2-25	0.62	0.61	0.65	0.65	0.65	0.65	0.65	0.65	0.65	0.65	0.65	0.64	0.64
2023-3-16	0.59	0.58	0.64	0.64	0.64	0.64	0.64	0.64	0.63	0.62	0.61	0.61	0.60
2023-3-21	0.48	0.46	0.51	0.51	0.51	0.51	0.51	0.51	0.51	0.50	0.50	0.50	0.49
2023-3-26	0.51	0.49	0.59	0.59	0.58	0.57	0.56	0.56	0.55	0.55	0.54	0.54	0.53
2023-4-16	0.33	0.31	0.53	0.53	0.53	0.52	0.50	0.48	0.47	0.45	0.44	0.42	0.40
2023-4-21	0.30	0.30	0.32	0.32	0.32	0.32	0.32	0.32	0.32	0.31	0.31	0.31	0.31
2023-4-26	0.30	0.28	0.39	0.39	0.38	0.37	0.37	0.36	0.35	0.34	0.33	0.31	0.31
2023-5-16	0.13	0.20	0.25	0.22	0.20	0.18	0.17	0.16	0.14	0.14	0.13	0.14	0.15
2023-5-21	NA	NA	0.33	0.30	0.28	0.25	0.23	0.21	0.19	0.18	0.16	0.13	0.11
2023-5-26	0.19	0.19	0.56	0.53	0.51	0.50	0.49	0.48	0.43	0.39	0.33	0.27	0.22
2023-6-16	NA	NA	0.60	0.47	0.35	0.26	0.21	0.13	0.03	0.03	0.02	NA	NA
2023-6-21	NA	NA	0.27	0.20	0.17	0.15	0.11	0.08	0.05	0.06	0.06	NA	NA
2023-6-26	0.07	NA	0.40	0.29	0.22	0.19	0.13	0.13	0.15	0.24	0.01	0.01	NA

Table B4(2) (continued)

Start date of 5-day interval	Dynamic U-values calculated by data pre-processing methods [W/(m$^2 \cdot$ K)]											
	PV11	PV12	PV13	AV0	AV1	AV2	AV3	AV4	AV5	AV6	AV7	AV8
2023-1-16	0.52	0.52	0.52	0.52	0.52	0.52	0.52	0.52	0.52	0.52	0.52	0.52
2023-1-21	0.50	0.50	0.50	0.50	0.50	0.50	0.50	0.50	0.50	0.50	0.50	0.50
2023-1-26	0.57	0.57	0.57	0.57	0.57	0.57	0.57	0.57	0.57	0.57	0.57	0.57
2023-2-15	0.61	0.61	0.61	0.61	0.61	0.61	0.61	0.61	0.61	0.61	0.61	0.61
2023-2-20	0.58	0.58	0.58	0.58	0.58	0.58	0.58	0.58	0.58	0.58	0.58	0.58
2023-2-25	0.63	0.62	0.61	0.65	0.65	0.65	0.65	0.65	0.65	0.65	0.65	0.65
2023-3-16	0.60	0.59	0.58	0.64	0.64	0.64	0.64	0.64	0.64	0.63	0.62	0.61
2023-3-21	0.49	0.48	0.46	0.51	0.51	0.51	0.51	0.51	0.51	0.51	0.50	0.50
2023-3-26	0.52	0.51	0.49	0.59	0.59	0.58	0.57	0.56	0.56	0.55	0.55	0.54
2023-4-16	0.38	0.33	0.31	0.53	0.53	0.53	0.52	0.50	0.48	0.47	0.45	0.44
2023-4-21	0.31	0.30	0.30	0.32	0.32	0.32	0.32	0.32	0.32	0.32	0.31	0.31
2023-4-26	0.29	0.30	0.28	0.39	0.39	0.38	0.37	0.37	0.36	0.35	0.34	0.33
2023-5-16	0.14	0.13	0.20	0.30	0.26	0.23	0.20	0.17	0.15	0.14	0.13	0.13
2023-5-21	0.06	NA	NA	0.37	0.31	0.28	0.25	0.22	0.21	0.19	0.18	0.15
2023-5-26	0.21	0.19	0.19	0.29	0.25	0.23	0.22	0.20	0.19	0.18	0.16	0.14
2023-6-16	NA	NA	NA	0.27	0.23	0.20	0.16	0.13	0.12	0.10	0.08	0.06
2023-6-21	NA	NA	NA	0.31	0.25	0.20	0.16	0.13	0.10	0.06	0.05	0.04
2023-6-26	NA	NA	NA	0.23	0.17	0.15	0.13	0.11	0.10	0.09	0.09	0.07

Table B4(2) (continued)

Start date of 5-day interval	Dynamic U-values calculated by data pre-processing methods $[W/(m^2 \cdot K)]$					
	AV9	AV10	AV11	AV12	AV13	TL
2023-1-16	0.52	0.52	0.52	0.52	0.52	0.52
2023-1-21	0.50	0.50	0.50	0.50	0.50	0.50
2023-1-26	0.57	0.57	0.57	0.57	0.57	0.56
2023-2-15	0.61	0.61	0.61	0.61	0.61	0.60
2023-2-20	0.58	0.58	0.58	0.58	0.58	0.58
2023-2-25	0.64	0.64	0.63	0.62	0.61	0.65
2023-3-16	0.61	0.60	0.60	0.59	0.58	0.61
2023-3-21	0.50	0.49	0.49	0.48	0.46	0.51
2023-3-26	0.54	0.53	0.52	0.51	0.49	0.56
2023-4-16	0.42	0.40	0.38	0.33	0.31	0.52
2023-4-21	0.31	0.31	0.31	0.30	0.30	0.31
2023-4-26	0.31	0.31	0.29	0.30	0.28	0.38
2023-5-16	0.14	0.15	0.14	0.13	0.20	0.26
2023-5-21	0.13	0.11	0.06	NA	NA	0.31
2023-5-26	0.12	0.11	0.12	0.19	0.19	0.24
2023-6-16	NA	NA	NA	NA	NA	0.22
2023-6-21	NA	NA	NA	NA	NA	0.23
2023-6-26	0.08	0.09	0.09	0.07	NA	0.20

Table B4(3) Dynamic U-values of the brick tested envelope with 7-day time intervals

Start date of 7-day interval	Dynamic U-values calculated by data pre-processing methods $[W/(m^2 \cdot K)]$												
	ND	TD0	TD1	TD2	TD3	TD4	TD5	TD6	TD7	TD8	TD9	TD10	TD11
2023-1-16	0.48	0.51	0.51	0.51	0.51	0.51	0.51	0.51	0.51	0.51	0.51	0.51	0.51
2023-1-23	0.51	0.54	0.54	0.54	0.54	0.54	0.54	0.54	0.54	0.54	0.54	0.54	0.54
2023-2-15	0.51	0.59	0.59	0.59	0.59	0.59	0.59	0.59	0.59	0.59	0.59	0.59	0.59
2023-2-22	0.52	0.62	0.62	0.62	0.62	0.62	0.62	0.62	0.62	0.62	0.62	0.62	0.61
2023-3-16	0.49	0.65	0.65	0.65	0.65	0.65	0.65	0.64	0.63	0.62	0.61	0.61	0.60
2023-3-23	0.37	0.52	0.52	0.52	0.52	0.51	0.51	0.51	0.50	0.50	0.50	0.49	0.49
2023-4-16	0.31	0.47	0.47	0.47	0.46	0.45	0.44	0.43	0.42	0.40	0.39	0.38	0.37
2023-4-23	0.20	0.35	0.35	0.34	0.34	0.33	0.33	0.32	0.31	0.30	0.29	0.28	0.28
2023-5-16	0.11	0.26	0.23	0.22	0.20	0.18	0.17	0.16	0.15	0.14	0.14	0.14	0.14
2023-5-23	0.07	0.15	0.13	0.11	0.10	0.09	0.08	0.07	0.05	0.03	0.02	0.00	0.02
2023-6-16	0.06	0.07	0.04	0.01	0.00	0.01	0.02	0.03	0.03	0.04	NA	NA	NA
2023-6-23	0.10	0.01	0.01	0.03	0.04	0.04	0.04	0.05	0.05	0.07	0.08	0.09	0.09

Table B4(3) (continued)

Start date of 7-day interval	Dynamic U-values calculated by data pre-processing methods $[W/(m^2 \cdot K)]$												
	TD12	TD13	PV0	PV1	PV2	PV3	PV4	PV5	PV6	PV7	PV8	PV9	PV10
2023-1-16	0.51	0.51	0.51	0.51	0.51	0.51	0.51	0.51	0.51	0.51	0.51	0.51	0.51
2023-1-23	0.54	0.54	0.54	0.54	0.54	0.54	0.54	0.54	0.54	0.54	0.54	0.54	0.54
2023-2-15	0.59	0.59	0.59	0.59	0.59	0.59	0.59	0.59	0.59	0.59	0.59	0.59	0.59
2023-2-22	0.61	0.60	0.62	0.62	0.62	0.62	0.62	0.62	0.62	0.62	0.62	0.62	0.62
2023-3-16	0.59	0.57	0.65	0.65	0.65	0.65	0.65	0.65	0.64	0.63	0.62	0.61	0.61
2023-3-23	0.48	0.47	0.52	0.52	0.52	0.52	0.51	0.51	0.51	0.50	0.50	0.50	0.49
2023-4-16	0.34	0.33	0.47	0.47	0.47	0.46	0.45	0.44	0.43	0.42	0.40	0.39	0.38
2023-4-23	0.27	0.26	0.35	0.35	0.34	0.34	0.33	0.33	0.32	0.31	0.30	0.29	0.28
2023-5-16	0.13	0.20	0.27	0.24	0.22	0.21	0.19	0.18	0.16	0.16	0.14	0.14	0.14
2023-5-23	0.19	0.19	0.55	0.49	0.46	0.43	0.42	0.39	0.35	0.31	0.26	0.20	0.15
2023-6-16	NA	NA	0.34	0.26	0.20	0.16	0.12	0.09	0.06	0.05	0.04	NA	NA
2023-6-23	0.07	NA	0.38	0.28	0.22	0.19	0.13	0.12	0.10	0.24	0.01	0.01	NA

Table B4(3) (continued)

Start date of 7-day interval	Dynamic U-values calculated by data pre-processing methods $[W/(m^2 \cdot K)]$											
	PV11	PV12	PV13	AV0	AV1	AV2	AV3	AV4	AV5	AV6	AV7	AV8
2023-1-16	0.51	0.51	0.51	0.51	0.51	0.51	0.51	0.51	0.51	0.51	0.51	0.51
2023-1-23	0.54	0.54	0.54	0.54	0.54	0.54	0.54	0.54	0.54	0.54	0.54	0.54
2023-2-15	0.59	0.59	0.59	0.59	0.59	0.59	0.59	0.59	0.59	0.59	0.59	0.59
2023-2-22	0.61	0.61	0.60	0.62	0.62	0.62	0.62	0.62	0.62	0.62	0.62	0.62
2023-3-16	0.60	0.59	0.57	0.65	0.65	0.65	0.65	0.65	0.65	0.64	0.63	0.62
2023-3-23	0.49	0.48	0.47	0.52	0.52	0.52	0.52	0.51	0.51	0.51	0.50	0.50
2023-4-16	0.37	0.34	0.33	0.47	0.47	0.47	0.46	0.45	0.44	0.43	0.42	0.40
2023-4-23	0.28	0.27	0.26	0.35	0.35	0.34	0.34	0.33	0.33	0.32	0.31	0.30
2023-5-16	0.14	0.13	0.20	0.31	0.27	0.24	0.21	0.19	0.17	0.16	0.15	0.14
2023-5-23	0.13	0.19	0.19	0.31	0.27	0.24	0.22	0.20	0.19	0.17	0.16	0.13
2023-6-16	NA	NA	NA	0.27	0.22	0.18	0.14	0.12	0.10	0.08	0.06	0.05
2023-6-23	NA	NA	NA	0.26	0.21	0.17	0.15	0.12	0.11	0.09	0.09	0.07

Table B4(3) (continued)

Start date of 7-day interval	Dynamic U-values calculated by data pre-processing methods [W/(m^2·K)]					
	AV9	AV10	AV11	AV12	AV13	TL
2023-1-16	0.51	0.51	0.51	0.51	0.51	0.51
2023-1-23	0.54	0.54	0.54	0.54	0.54	0.54
2023-2-15	0.59	0.59	0.59	0.59	0.59	0.58
2023-2-22	0.62	0.62	0.61	0.61	0.60	0.63
2023-3-16	0.61	0.61	0.60	0.59	0.57	0.62
2023-3-23	0.50	0.49	0.49	0.48	0.47	0.51
2023-4-16	0.39	0.38	0.37	0.34	0.33	0.45
2023-4-23	0.29	0.28	0.28	0.27	0.26	0.34
2023-5-16	0.14	0.14	0.14	0.13	0.20	0.29
2023-5-23	0.12	0.10	0.10	0.19	0.19	0.24
2023-6-16	NA	NA	NA	NA	NA	0.22
2023-6-23	0.08	0.09	0.09	0.07	NA	0.21

Table B4(4) Dynamic U-values of the brick tested envelope with 14-day time intervals

Start date of 14-day interval	Dynamic U-values calculated by data pre-processing methods [W/(m^2·K)]												
	ND	TD0	TD1	TD2	TD3	TD4	TD5	TD6	TD7	TD8	TD9	TD10	TD11
2023-1-16	0.49	0.53	0.53	0.53	0.53	0.53	0.53	0.53	0.53	0.53	0.53	0.53	0.53
2023-2-15	0.51	0.61	0.61	0.61	0.61	0.61	0.61	0.61	0.61	0.61	0.61	0.60	0.60
2023-3-16	0.42	0.57	0.57	0.57	0.57	0.57	0.57	0.56	0.56	0.55	0.55	0.54	0.53
2023-4-16	0.25	0.41	0.41	0.41	0.40	0.39	0.38	0.38	0.36	0.35	0.34	0.34	0.33
2023-5-16	0.02	0.21	0.19	0.17	0.15	0.14	0.13	0.12	0.11	0.10	0.10	0.09	0.11
2023-6-16	0.08	0.04	0.01	0.01	0.02	0.03	0.03	0.04	0.04	0.06	0.08	0.09	0.09

Table B4(4) (continued)

Start date of 14-day interval	Dynamic U-values calculated by data pre-processing methods $[W/(m^2 \cdot K)]$												
	TD12	TD13	PV0	PV1	PV2	PV3	PV4	PV5	PV6	PV7	PV8	PV9	PV10
2023-1-16	0.53	0.53	0.53	0.53	0.53	0.53	0.53	0.53	0.53	0.53	0.53	0.53	0.53
2023-2-15	0.60	0.60	0.61	0.61	0.61	0.61	0.61	0.61	0.61	0.61	0.61	0.61	0.60
2023-3-16	0.52	0.51	0.57	0.57	0.57	0.57	0.57	0.57	0.56	0.56	0.55	0.55	0.54
2023-4-16	0.31	0.30	0.41	0.41	0.41	0.40	0.39	0.38	0.38	0.36	0.35	0.34	0.34
2023-5-16	0.14	0.19	0.34	0.31	0.28	0.26	0.24	0.22	0.20	0.18	0.16	0.15	0.14
2023-6-16	0.07	NA	0.36	0.27	0.21	0.17	0.13	0.10	0.07	0.07	0.04	0.01	NA

Table B4(4) (continued)

Start date of 14-day interval	Dynamic U-values calculated by data pre-processing methods $[W/(m^2 \cdot K)]$											
	PV11	PV12	PV13	AV0	AV1	AV2	AV3	AV4	AV5	AV6	AV7	AV8
2023-1-16	0.53	0.53	0.53	0.53	0.53	0.53	0.53	0.53	0.53	0.53	0.53	0.53
2023-2-15	0.60	0.60	0.60	0.61	0.61	0.61	0.61	0.61	0.61	0.61	0.61	0.61
2023-3-16	0.53	0.52	0.51	0.57	0.57	0.57	0.57	0.57	0.57	0.56	0.56	0.55
2023-4-16	0.33	0.31	0.30	0.41	0.41	0.41	0.40	0.39	0.38	0.38	0.36	0.35
2023-5-16	0.14	0.14	0.19	0.31	0.27	0.24	0.22	0.20	0.18	0.16	0.15	0.14
2023-6-16	NA	NA	NA	0.26	0.21	0.18	0.15	0.12	0.11	0.09	0.08	0.06

Table B4(4) (continued)

Start date of 14-day interval	Dynamic U-values calculated by data pre-processing methods $[W/(m^2 \cdot K)]$					
	AV9	AV10	AV11	AV12	AV13	TL
2023-1-16	0.53	0.53	0.53	0.53	0.53	0.53
2023-2-15	0.61	0.60	0.60	0.60	0.60	0.61
2023-3-16	0.55	0.54	0.53	0.52	0.51	0.58
2023-4-16	0.34	0.34	0.33	0.31	0.30	0.41
2023-5-16	0.13	0.13	0.13	0.14	0.19	0.28
2023-6-16	0.08	0.07	0.07	0.07	NA	0.22

Table B5 Average U-values of four tested envelopes

Data pre-processing methods	Average U-value $[W/(m^2 \cdot K)]$			
	CLT	Masonry cavity	RC	Brick
ND	0.07	0.40	0.24	0.39
TD0	0.09	0.55	0.33	0.50
TD1	0.11	0.55	0.32	0.50
TD2	0.13	0.55	0.32	0.50
TD3	0.14	0.55	0.31	0.50
TD4	0.14	0.55	0.31	0.50
TD5	0.14	0.56	0.31	0.50
TD6	0.13	0.57	0.31	0.51
TD7	0.10	0.59	0.31	0.51
TD8		0.62	0.31	0.51
TD9		0.66	0.31	0.52
TD10		0.70	0.32	0.52
TD11		0.73	0.32	0.52
TD12		0.76	0.32	0.53
TD13		0.79	0.31	0.53
PV0	0.37	0.69	0.34	0.53
PV1	0.33	0.68	0.32	0.53
PV2	0.30	0.68	0.33	0.53
PV3	0.26	0.68	0.32	0.53
PV4	0.22	0.67	0.32	0.53
PV5	0.20	0.67	0.31	0.52
PV6	0.16	0.67	0.31	0.52
PV7	0.12	0.67	0.31	0.52
PV8		0.68	0.31	0.52
PV9		0.68	0.31	0.52
PV10		0.71	0.32	0.53
PV11		0.73	0.32	0.53
PV12		0.76	0.32	0.53
PV13		0.79	0.31	0.53
AV0	0.45	0.63	0.34	0.52
AV1	0.38	0.62	0.34	0.51
AV2	0.33	0.62	0.33	0.51
AV3	0.29	0.61	0.32	0.51
AV4	0.25	0.61	0.31	0.51
AV5	0.24	0.61	0.31	0.51
AV6	0.22	0.62	0.31	0.51
AV7	0.22	0.63	0.31	0.51
AV8		0.64	0.31	0.51
AV9		0.66	0.31	0.52

Table B5 (continued)

Data pre-processing methods	Average U-value $[W/(m^2 \cdot K)]$			
	CLT	Masonry cavity	RC	Brick
AV10		0.69	0.32	0.52
AV11		0.71	0.32	0.52
AV12		0.74	0.32	0.53
AV13		0.77	0.31	0.53
TL	0.41	0.61	0.34	0.43

Appendix (C) Hourly Temperature and Relative Humidity in 2023 and Average Hourly Temperature and Relative Humidity from 2013 to 2022 in 11 Case Cities

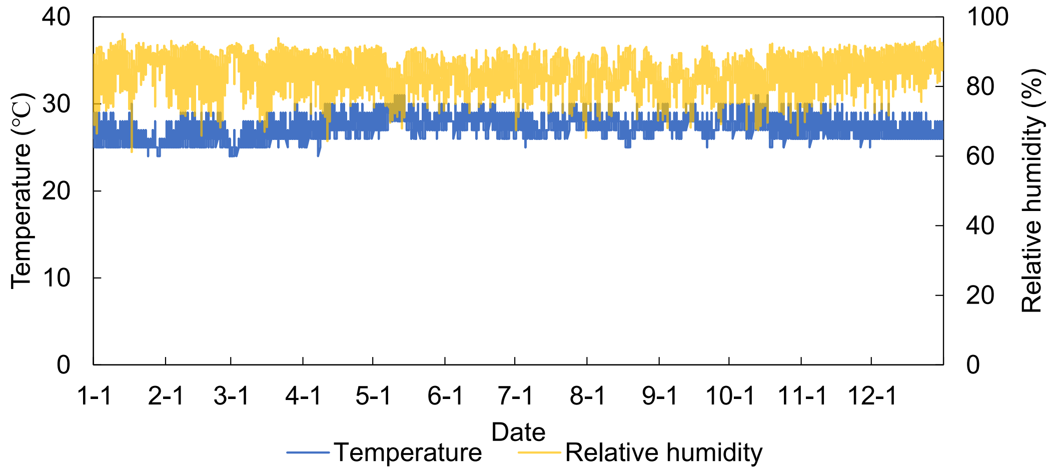

Figure C1 Hourly temperature in Singapore in 2023

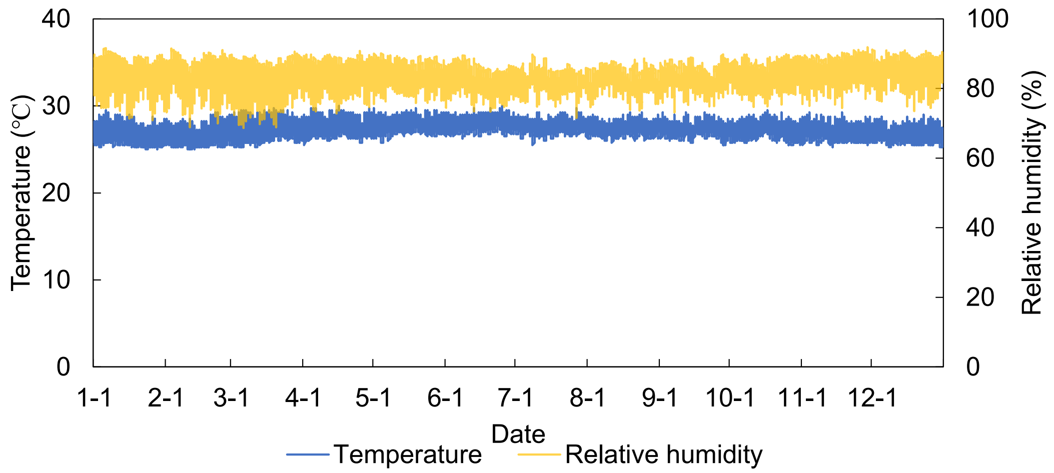

Figure C2 Average hourly temperature in Singapore from 2013 to 2022

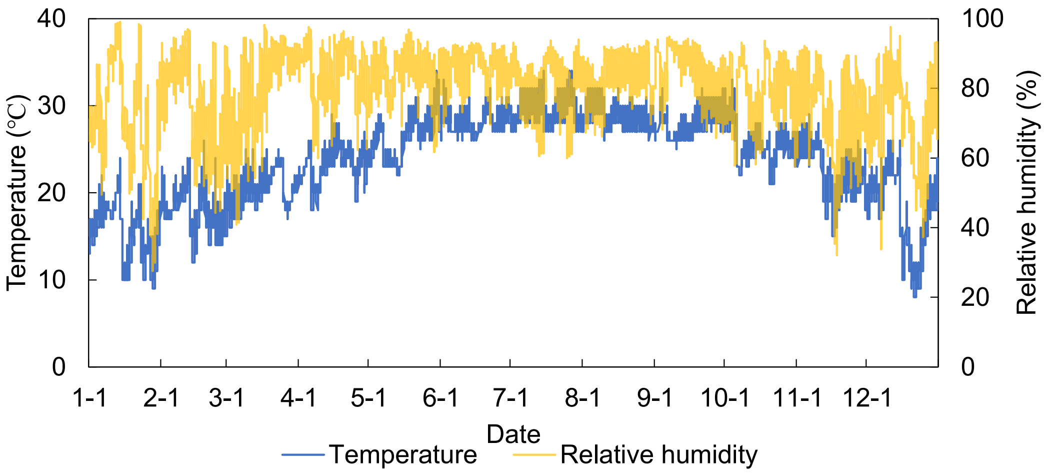

Figure C3 Hourly temperature in Bangkok in 2023

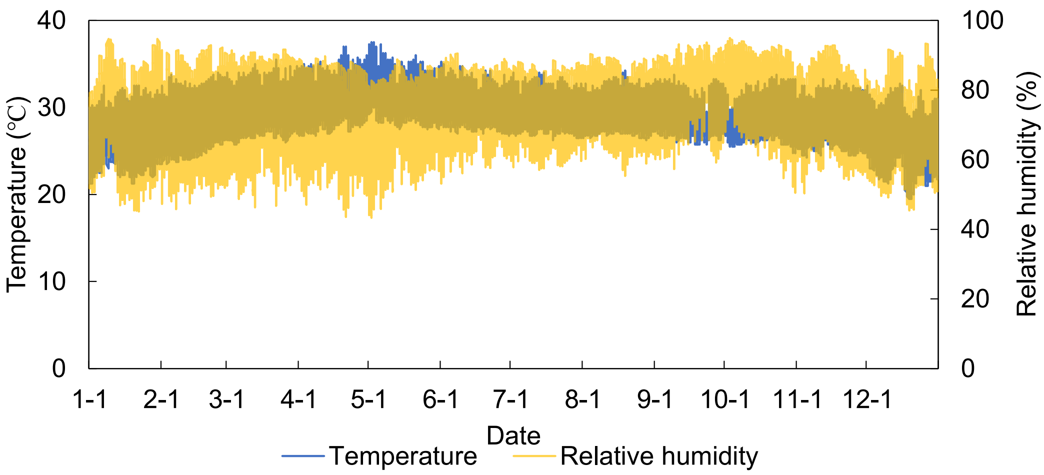

Figure C4 Average hourly temperature in Bangkok from 2013 to 2022

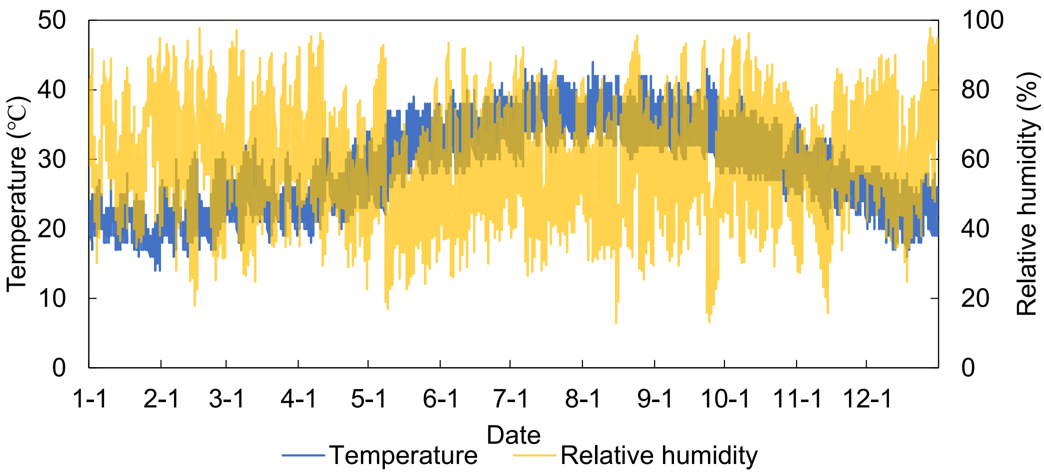

Figure C5 Hourly temperature in Dubai in 2023

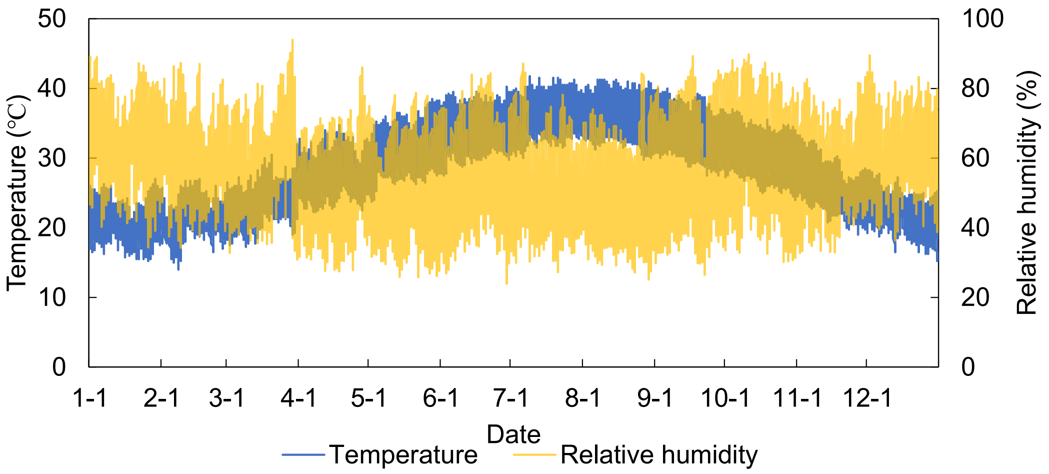

Figure C6 Average hourly temperature in Dubai from 2013 to 2022

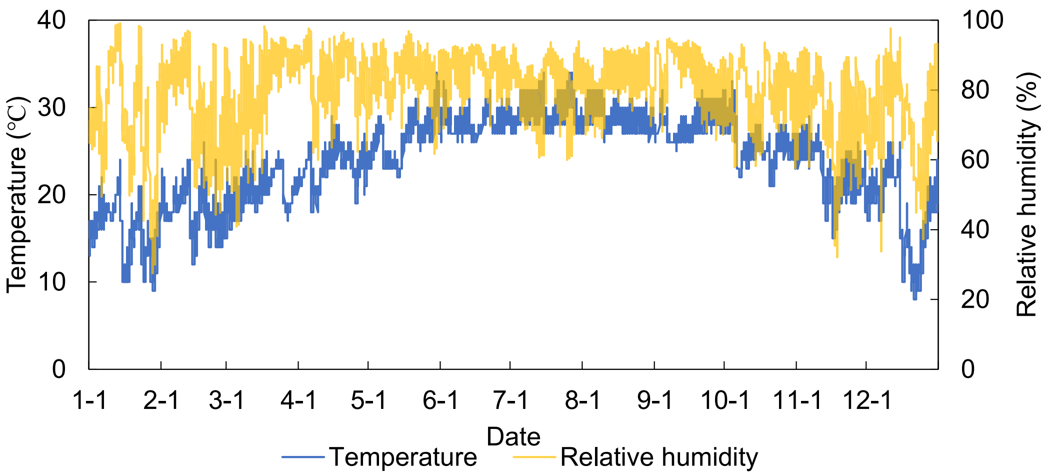

Figure C7 Hourly temperature in Hong Kong in 2023

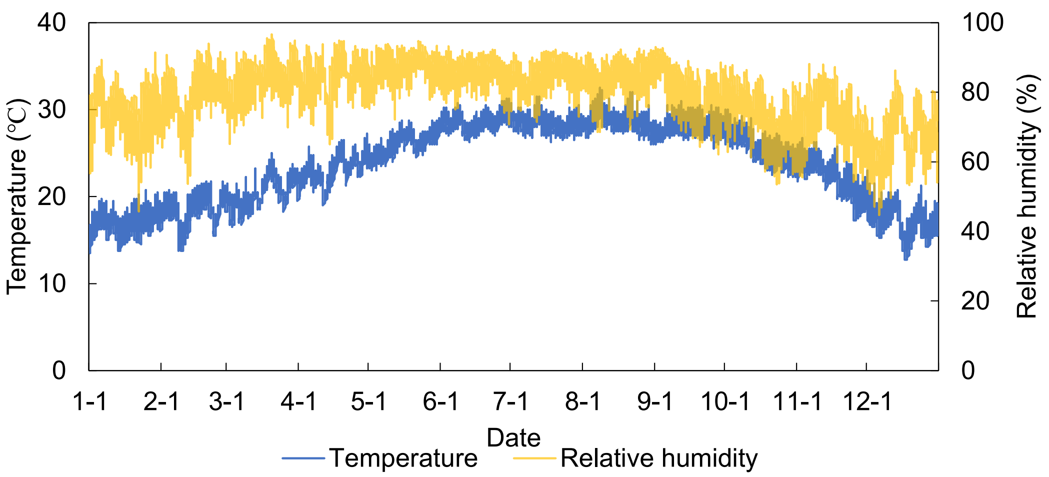

Figure C8 Average hourly temperature in Hong Kong from 2013 to 2022

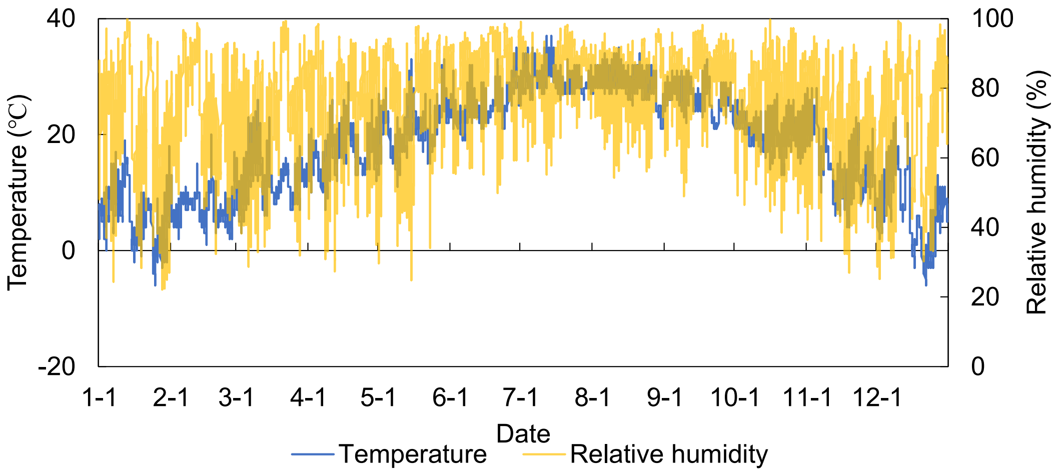

Figure C9 Hourly temperature in Shanghai in 2023

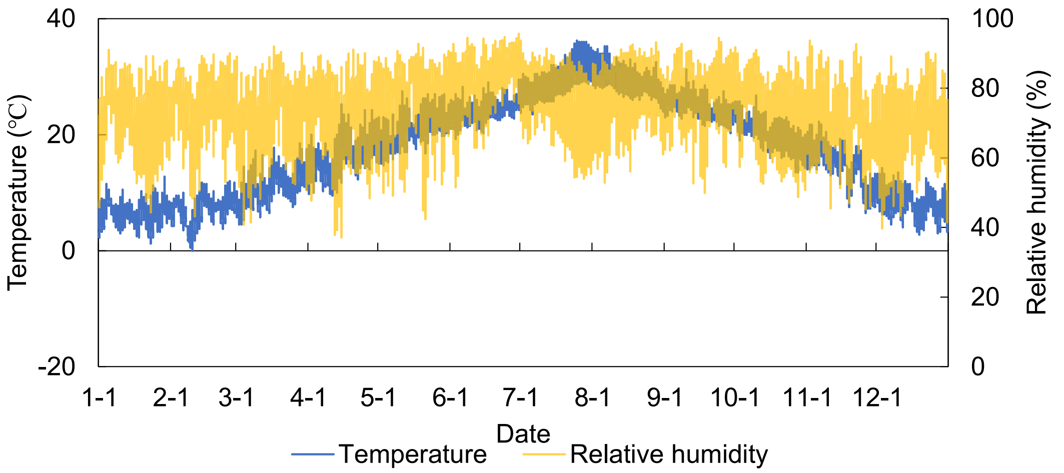

Figure C10 Average hourly temperature in Shanghai from 2013 to 2022

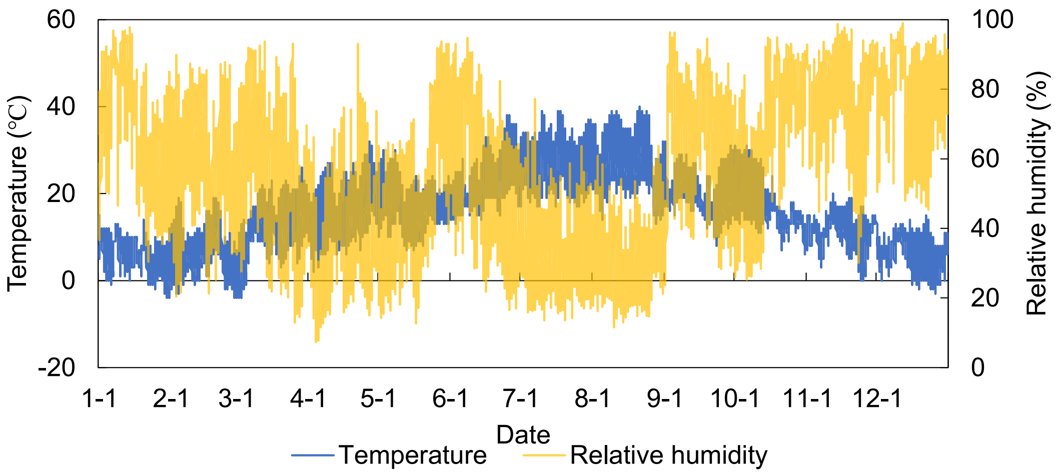

Figure C11 Hourly temperature in Madrid in 2023

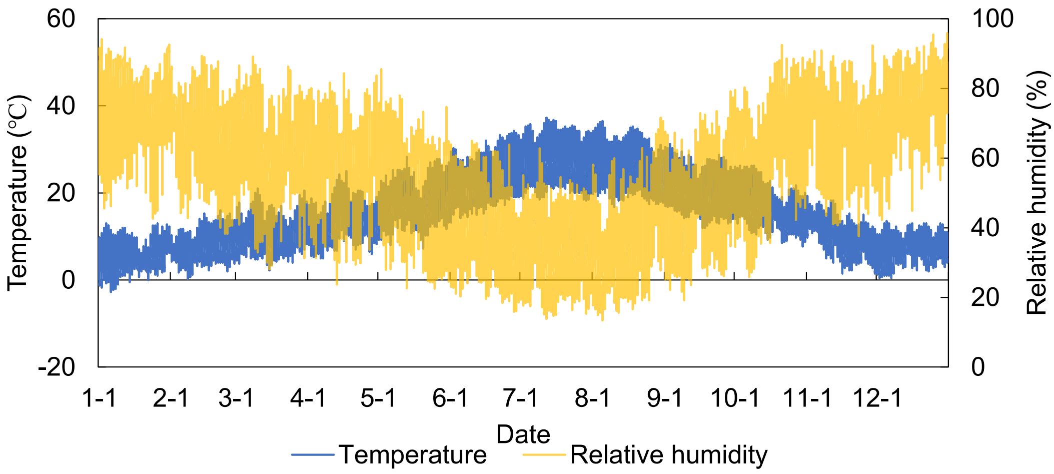

Figure C12 Average hourly temperature in Madrid from 2013 to 2022

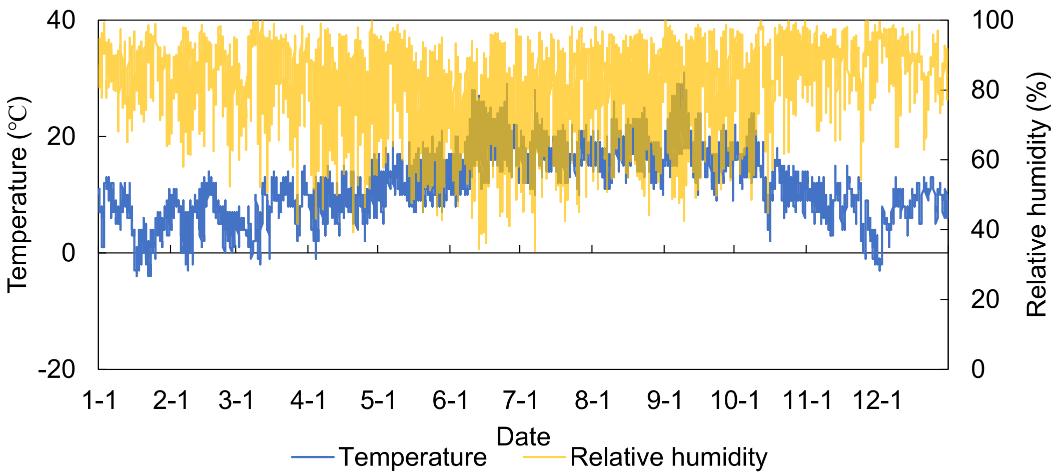

Figure C13 Hourly temperature in London in 2023

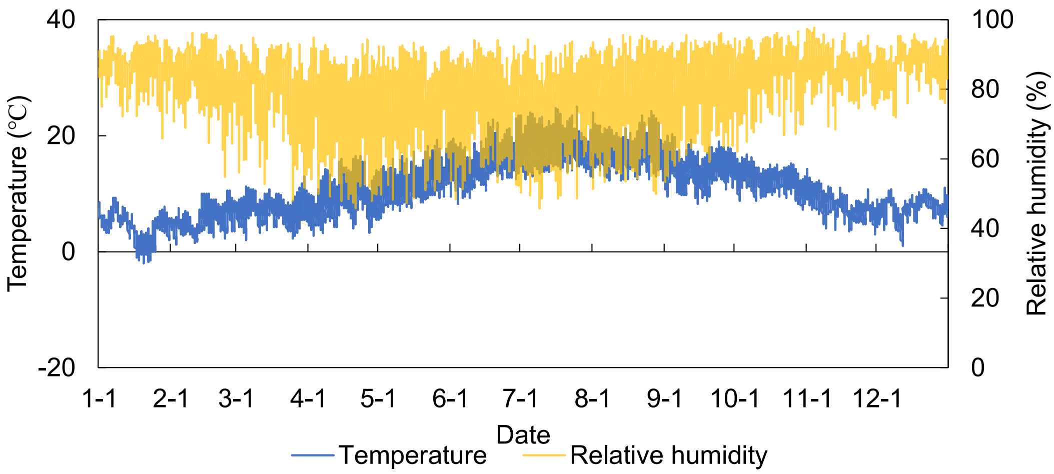

Figure C14 Average hourly temperature in London from 2013 to 2022

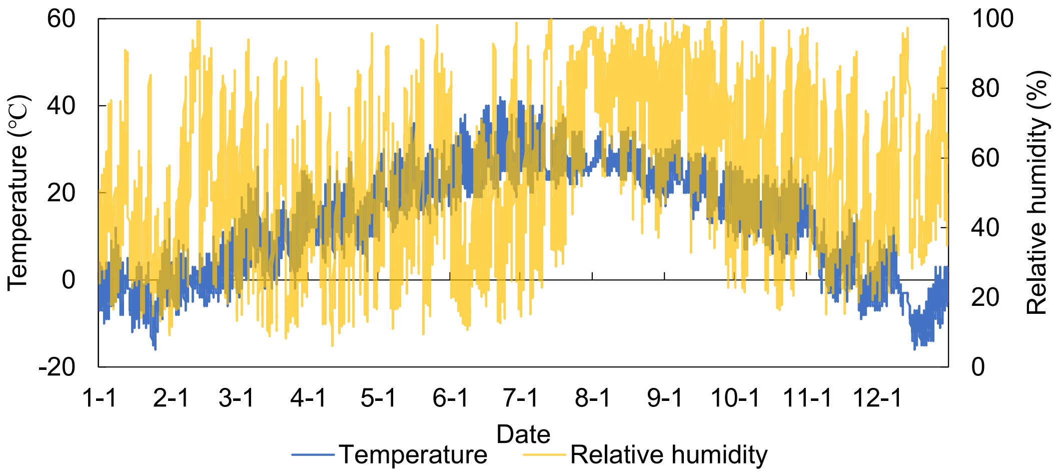

Figure C15 Hourly temperature in Beijing in 2023

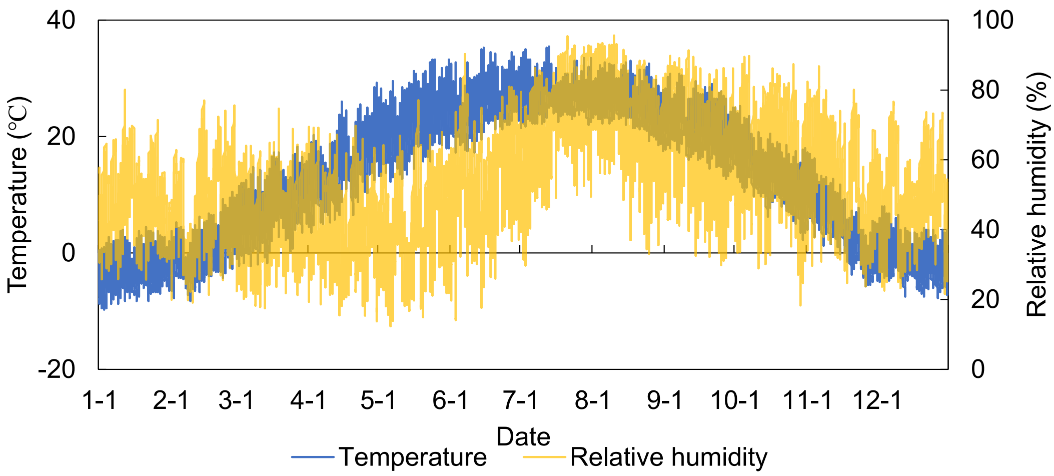

Figure C16 Average hourly temperature in Beijing from 2013 to 2022

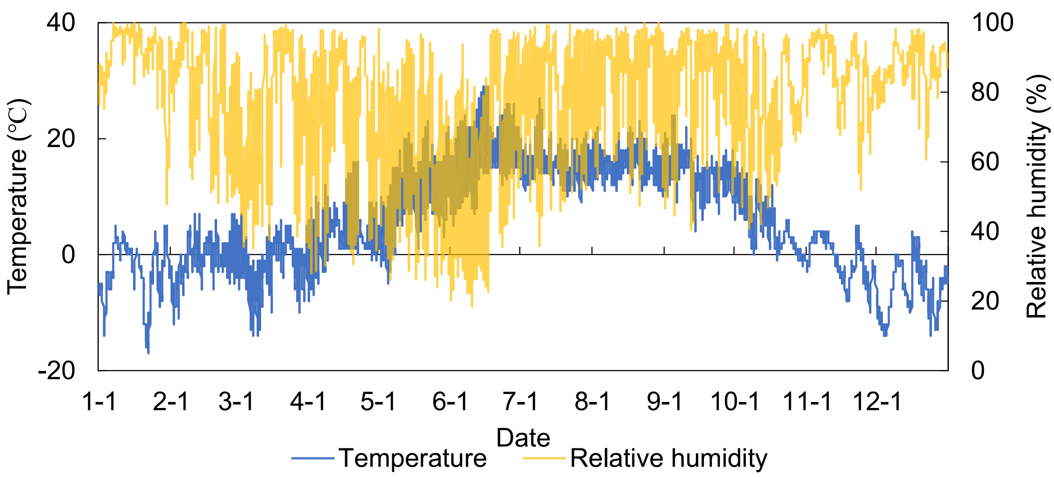

Figure C17 Hourly temperature in Oslo in 2023

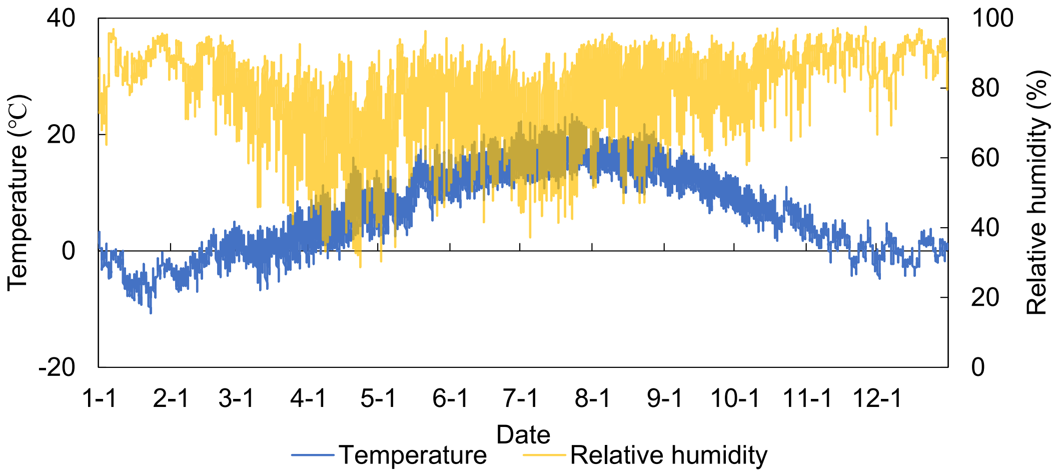

Figure C18 Average hourly temperature in Oslo from 2013 to 2022

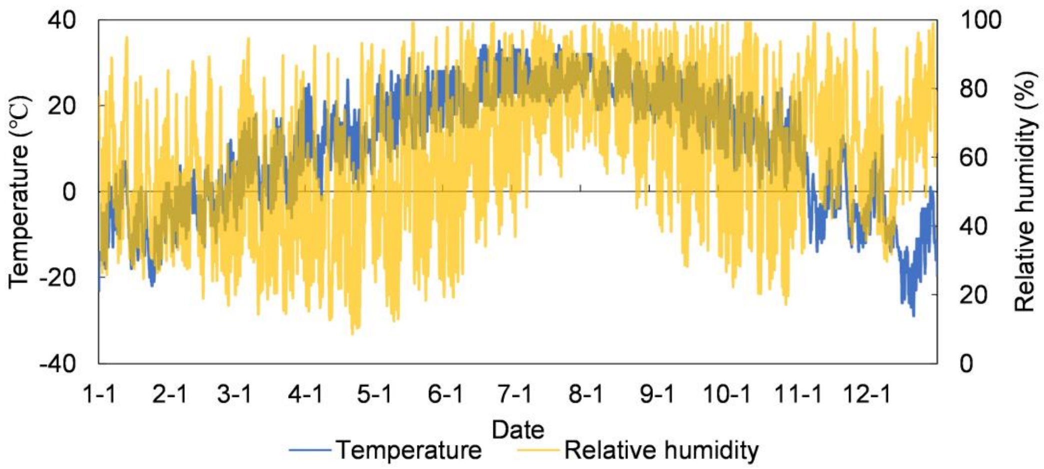

Figure C19 Hourly temperature in Shenyang in 2023

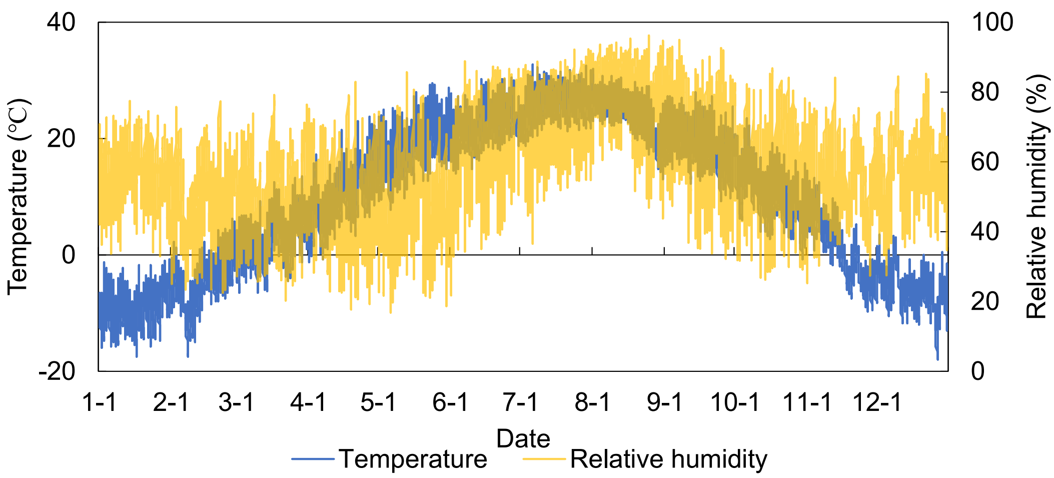

Figure C20 Average hourly temperature in Shenyang from 2013 to 2022

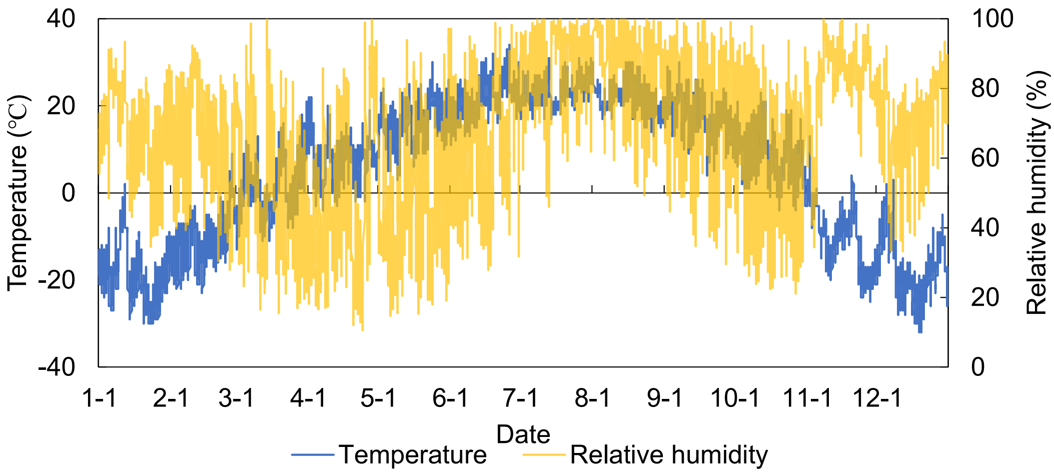

Figure C21 Hourly temperature in Harbin in 2023

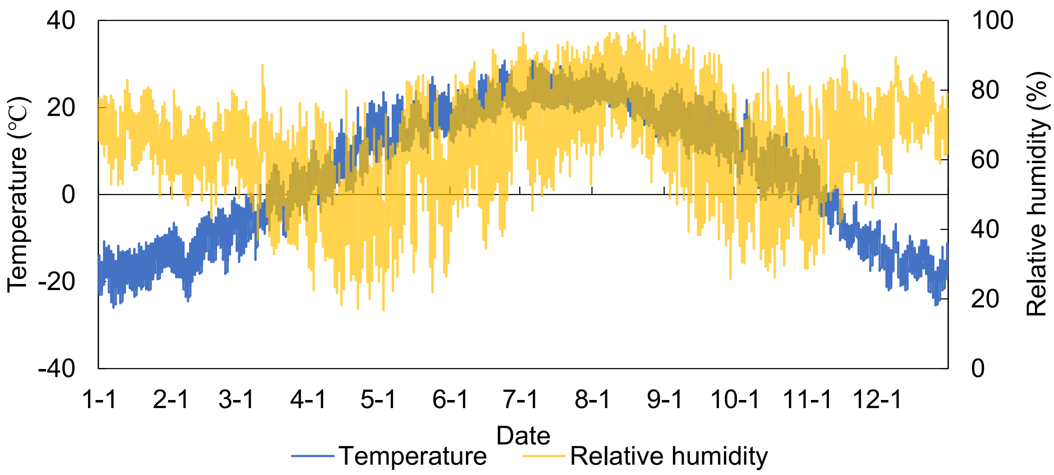

Figure C22 Average hourly temperature in Harbin from 2013 to 2022